UNIVERSITY OF OKLAHOMA

GRADUATE COLLEGE

PERFORMANCE-DECLINE CURVE ANALYSIS OF VERTICAL AND HORIZONTAL WELLS IN ANISOTROPIC AND NATURALLY FRACTURED RESERVOIRS

A Dissertation

SUBMITTED TO THE GRADUATE FACULTY

in partial fulfillment of the requirements for the

degree of

Doctor of Philosophy

By

SCOTT BRADLEY CLINE
Norman, Oklahoma
1999

UMI Number: 9952411

Bell & Howell Information and Learning Company
300 North Zeeb Road
P.O. Box 1346
Ann Arbor, MI 48106-1346

PERFORMANCE-DECLINE CURVE ANALYSIS OF VERTICAL AND HORIZONTAL WELLS IN ANISOTROPIC AND NATURALLY FRACTURED RESERVOIRS

A Dissertation APPROVED FOR THE SCHOOL OF PETROLEUM AND GEOLOGICAL ENGINEERING

BY

Acknowledgements

I thank all faculty committee members for their various individual contributions during my tenure in the Petroleum Engineering Department and for putting up with a part time student for all these years. Foremost I thank Dr. Tiab for not only his challenging classes but for encouraging me to continue this project when, after unexpectedly leaving the petroleum industry, I could have easily given up. His persistent reminder to register each semester is the only reason I kept working. Thanks to Dr. Roy Knapp, who introduced me to simulation, who always stressed attention to detail and who may have finally succeeded in teaching me when to use the plural of "data". Thanks to Dr. John Pigott for hopefully transferring some of his keen ability to see the "big picture" when presented with seeming chaos. I have never met anyone else that could so clearly see the important concepts in the midst of overwhelming data. Thanks to Dr. Wiggins for his great production class which introduced me to Muskat, Fetkovich and VanEverdingen and Hurst. Those class notes have been invaluable to me. Thanks to Dr. Osisanya whose teaching style made learning so fun and who set a great example by his hard work ethic. Each of you influenced my life in a positive way and for that I am eternally grateful. Thank you.

I also thank my daughter Charlotte Anne Cline, now a freshman at the University of Rochester, and my son Thomas Ansley Cline, a 10th grade student in Rushville, New York. Thank you both for sacrificing many of our precious moments together over these past few years and occasionally, but not often enough, convincing me to take a break from this project to see what was happening in your own lives. Thank you Cindy Stewart for encouraging me to continue the project, for helping with the daily routines so that I could keep going, and for your general love and support. And thanks to all the rest of my family and friends who put up with my bad moods, understood or at least tolerated it when I gave up family functions to work on this project and gave me moral support.

I tried my best to keep a balance between family, friends and work despite the difficult circumstances of the past few years but I took too much from all of you. I did not however take your help for granted and therefore I hope now that through the grace of God and his Son Jesus Christ that I can pass on to others some of what you have all given me. Thank you and God bless you all.

Table of Contents

List of Tables

List of Figures

Abstract

This research extends previously developed dimensionless decline type curve concepts and techniques to more general cases of varying reservoir shapes, well locations and anisotropic permeability conditions. The research also introduces some novel approaches to estimating, from field production data, the simulation reservoir properties such as oil-water and gas-oil relative permeability relationships, PVT properties, and capillary pressure in the absence of laboratory measurements. Semi-analytical two-phase analytic equations are then developed that approximate the two phase flow in solution gas reservoirs for use as a "quick-look" tool to validate simulation model design by comparing expected and actual simulation output. Techniques and correlation curves based on simulation experiments are then generated to aid in proper simulation model design in cases where directional permeability is highly anisotropic. The last part of the research explores anisotropic and fracture permeability conditions for both vertical and horizontal wells where anisotropic and fractured reservoirs are modeled and studied in an effort to characterize fracture-matrix characteristics based on rate-time decline curve character.

It is not generally known that the "Fetkovich" decline type curves were developed for only single-phase radial systems with centrally located wells. This research derives the dimensionless decline rate and time relationships for the cases of more general reservoir geometry and well location. These relationships are then used to construct new type curves for various reservoir shapes and well locations. The data are then tabulated and

combined with "Arp's" depletion stems to form more general dimensionless decline curves and tabular data. A set of derivative curves is also generated, tabulated and plotted. These generalized decline curves are then modified for use with horizontal wells by incorporation of the equivalent well bore radius concept into the decline curve construction and display.

Extensive simulation experiments then demonstrate the effects of horizontal permeability anisotropy on well performance. The experiments confirmed the hypothesis that there are problems in properly simulating horizontal wells in horizontally anisotropic reservoirs. It is shown that unless the reservoir is extremely large in comparison to the length of the horizontal well, deviation from permeability isotropy in the principal x and y directions will yield results that deviate from that predicted by commonly accepted traditional geometric mean averaging. All analytical flow equations use the geometric mean permeability. Extensive experiments show however that as the contrast in x and y permeability increases, while maintaining a constant geometric mean horizontal permeability, the simulated horizontal flow rates deviate increasingly from one another. This deviation does not occur when simulating vertical wells. Graphical relationships showing the effect of permeability anisotropy as a function of dimensionless well length, grid block spacing etc. are presented based on the results of extensive simulation experiments.

Finally, the production rate decline characteristics of fractured reservoirs intersected by horizontal wells are studied through simulation experiments. Tables and charts are produced that help classify each of four different fracture types through characteristic rate-time decline patterns. Pressure data is purposely ignored in an effort to utilize only data that would be typically available to the practicing engineer.

CHAPTER ONE

Introduction and Objectives

The two quantities one usually wishes to determine from decline curve analysis are remaining oil reserves and remaining productive life of the well or reservoir. The forecasts of reserves and future production are the most important items in a reservoir evaluation. Other desirable but normally difficult to determine reservoir parameters include permeability, drainage area, drainage shape and fracture characteristics. Reserve estimating methods are usually categorized into three families: analogy, volumetric, and performance techniques. Performance technique methods are usually further subdivided into simulation studies, material balance and decline-trend analysis.

Special problems occur with well prediction in anisotropic reservoirs particularly with well performance prediction in fractured reservoirs. The end of the infinite acting period is often abrupt and unpredictable. Post infinite acting flow is also quite variable depending on matrix supply support and micro fractures. Therefore decline curve analysis may give insight into fracture nature and type.

This research is primarily concerned with developing methods for better reservoir modeling and interpretation of decline curves using both analytical and empirical decline curve concepts for both vertical and horizontal wells in irregular shaped, anisotropic and fractured reservoirs. Specific attention is focused on reservoirs that in general exhibit anisotropy in directional permeability. Recognition of fracture type from decline curves is also addressed. Inflow performance relations (IPR) and material balance concepts will also be addressed. Type curves, which combine 1) the rate and 2) rate derivative functions, or a group of terms involving these functions, with respect to time, or a group of terms involving time, will also be constructed for various reservoir systems. Adaptation to both vertical and horizontal wells will be addressed. Emphasis will be placed on developing equations and methods to forecast future performance, to calculate reserve estimates and ultimate recovery, classify fracture types and to identify permeability anisotropy. Both naturally fractured and heterogeneous media with vertical and horizontal wells will be examined.

CHAPTER TWO

Decline Curve Background

2.1 History of Decline Curve Theory

Decline curves are the most common means of forecasting production and estimating the value of oil and gas wells. The earliest literature reference to a mathematical decline analysis approach was by Arnold and Anderson in 1908. [1] The various methods used to interpret decline curves have generally been regarded as empirical and not reliable. However, in 1980 Fetkovich demonstrated that decline curve analysis not only has a solid fundamental base but also provides a tool with more diagnostic power than had been previously suspected. Fetkovich constructed log-log type curves, which combine all the standard exponential, hyperbolic and harmonic decline equations developed by Arps with the analytical constant-pressure infinite and finite reservoir solutions.[2,3] He showed that log-log type curves could be analyzed by the type curve matching technique. His type curves were developed for radial reservoirs only. This research will extend these curves to all reservoir shapes and well positions.

2.2 Review of Decline Curve Methods

Decline curve analysis adds the time dimension to the analysis of well performance. Traditional decline curve analysis considers particular cases of production decline in wells producing with constant wellhead pressure that can be treated without explicit material balance calculations. Constant pressure production implies a continuous drop of production rate with time. Production with constant wellhead pressure of a separator or a pipeline without the restriction of a choke is typical of low productivity wells and old high rate wells when wellhead pressure has already reached the minimum delivery pressure required to maintain flow. The constant flowing wellhead pressure that exists in practical problems does not correspond rigorously to a constant flowing bottomhole pressure, which is assumed in developing traditional decline curve analysis. In fact, bottomhole pressure does change if the flow rate declines gradually and wellhead pressure is maintained constant. In many cases this is not a serious restriction as the changes are small and result in only minor losses of accuracy. However in many cases there is loss of accuracy and other methods must be developed to predict decline, ultimate recoveries and reserves in place.

From a practical standpoint, transient decline is only observed in wells with low permeability or during the early life of well production. Depletion decline, also known as pseudo steady state (PSS) decline, is observed for all wells producing by expansion, solution gas, gravity drainage or partial water drive. PSS decline occurs after the radius of drainage has reached the outer boundaries and the well is draining a constant reservoir volume.

Decline curve analysis assumes a tank type model. Important to the use of tank type models is the interpretation of a reservoir pressure or rate and production history to determine the oil in place and whether or not the reservoir has water influx. Tank type models assume the 1) reservoir pore volume is constant, 2) the reservoir temperature is constant, 3) the reservoir has uniform porosity and relative permeability, 4) equilibrium conditions exist at all times in the reservoir. Pressure is assumed to be uniform throughout the reservoir. Deviations of decline or production performance curves from the homogeneous models may yield reservoir information.

It was first assumed that where water drive was absent, the pressure is proportional to the amount of remaining oil and that the productivity indices were constant throughout the well life. In such a hypothetical case, the relationship between cumulative oil produced and pressure would have to be linear and consequently, also the relationship between production rate and cumulative production. This linear relationship between rate and cumulative is typical of exponential or semi-log decline as will be shown later.

In most reservoirs, however, the aforementioned idealized conditions do not occur. Pressures usually are not proportional to the remaining oil, but seem to decline at gradually slower rates as the amount of remaining oil diminishes. At the same time the productivity indices are generally not constant, but show a tendency to decline as the reservoir is being depleted and the gas-oil ratios increase. The combined result of these two tendencies is a rate-cumulative relationship, which, instead of being a straight line on coordinate paper, shows up as a gentle curve, convex toward the origin.

2.3 Characteristics of Decline Analysis

Cumulative production and/or time are normally the independent variable (x) and production rate is the dependent variable (y). Figures 2.1-2.4 show the typical Cartesian and log-log plots of rate–cumulative and rate-time plots. The two most commonly used curves are rate-time and rate-cumulative production curves.

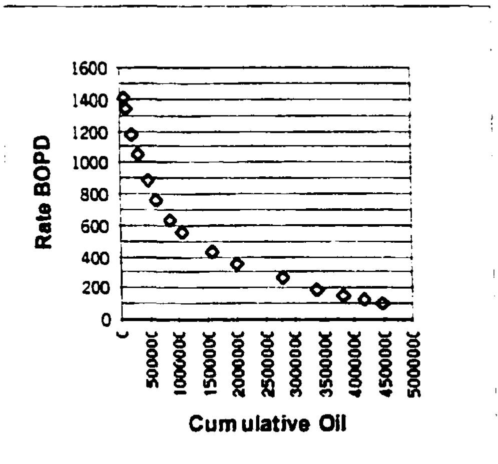

Figure 2.1 Cartesian Rate versus Cumulative

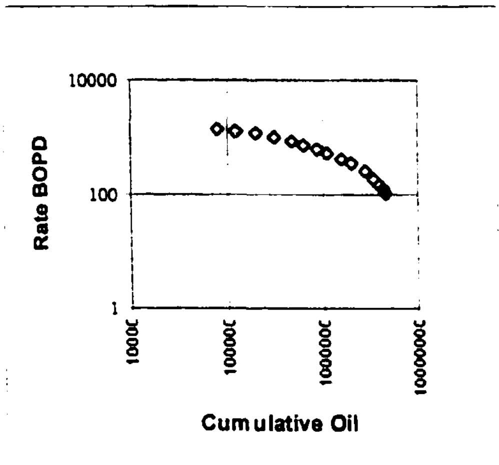

Figure 2.2 Log-Log Rate versus Cumulative

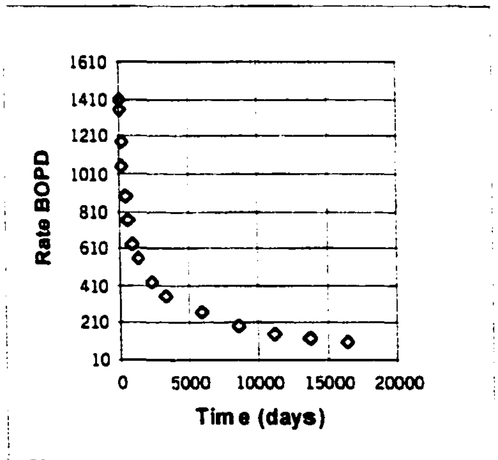

Figure 2.3 Cartesian Rate versus Time

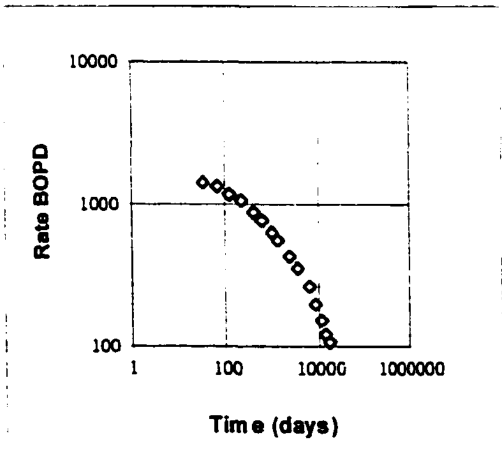

Figure 2.4 Log-Log Rate versus Time

Decline curve analysis is normally done by extrapolation of a performance trend that follows a certain pattern. For extrapolation purposes, this variable has to be 1) more or less a continuous function of the independent variable and 2) it must have a known endpoint. By plotting the continuously changing dependent variable (i.e. rate) vs. the independent variable (cumulative production or time) and extrapolating the trend until the known endpoint, an estimate of the remaining reserves, remaining life and future performance in time can be estimated. The method assumes that whatever caused the controlled trend of the curve in the past will continue in the future. This by nature then is empirical and mathematical expressions of the trend curve based on physical considerations are difficult and applicable in only a few simple cases.

Gradual changes in the production rate of a well may be caused by the 1) decreasing efficiency or effectiveness of the lifting equipment, 2) reduction of the productive index or increase in skin as a result of physical changes in the near well bore environment, 3) changes in bottomhole pressure, GOR, water percentage, or other reservoir conditions 4) Discontinuities in the outlying reservoir.

Production decline, caused by reservoir conditions, must be distinguished from that caused by wellbore conditions or failure of lifting equipment to be used for reserve estimation. When lifting equipment is operating properly and wellbore conditions are satisfactory, a declining production trend must reflect changing reservoir conditions and the extrapolation of such a trend can then be a reliable guide to prediction of remaining reserves.

2.4 Special Case of Solution Gas Drive Reservoirs

A solution gas drive reservoir is an oil reservoir that undergoes primary depletion with the main reservoir energy supplied by 1) the release of gas from the oil and 2) the expansion of the in-place fluids as the reservoir pressure drops. This excludes reservoirs that have significant water influx, oil and gas segregation and gravity assistance. Solution gas drive is also called dispersed gas drive or internal gas drive because the gas come out of solution throughout the portion of the oil zone that has a pressure below the bubblepoint. Initially, pore space contains interstitial water plus oil that contains gas in solution because of pressure. No free gas is assumed to be present in the oil zone. As production continues, the reservoir pressure drops below the bubblepoint, the oil shrinks, the gas that comes out of solution fills part of the pore space and there is minor water expansion. The drive mechanism (gas evolution and expansion) is dispersed or scattered throughout the oil zone.

The evolved gas, less any produced gas, fills the pore space vacated by the produced oil and by shrinkage of the remaining oil. The amount of oil recovered depends on the amount of pore space occupied by gas (S_g) and the oil shrinkage (B_o vs. pressure). Gas-oil relative permeability characteristics and viscosity of oil and gas are important because they determine the flowing GOR at a given S_g and thus the amount of free gas produced along with the oil.

Solution gas drive reservoir performance is characterized by 1) relatively rapid pressure decline, 2) low initial producing GOR rising to a much higher GOR, 3) oil production rates declining because of both 1 and 2, 4) little or no water production, 5) relatively low oil recovery. These reservoirs are ideal secondary waterflood candidates and thus merit considerable research.

CHAPTER THREE

Extending Analytical Solutions to Two Phase for Comparison with Reservoir Simulation Output

3.1 Introduction

As mentioned previously, pseudosteady state, where pressure and thus well performance decreases with time, is the most common reservoir condition. Reservoir simulation is an important tool in reservoir modeling. However blindly jumping into simulation without accurately establishing reservoir and model parameters can lead to erroneous results. It is therefore desirable to develop and use simplified multi-phase analytical methods to estimate reasonable ranges of simulation results. In other words if the simulation yields performance data that deviate significantly from the basic multi-phase analytical methods presented in this paper then the model should be scrutinized for possible errors or simulation instabilities.

This chapter will demonstrate that pseudosteady state, multi-phase analytical approximations to vertical well fluid flow in both isotropic and anisotropic media closely match simulated results without the use of Muskat's pressure integral analysis.[4] The modification of single phase analytical fluid flow equations to include pressure dependant relative permeability, viscosity and formation volume factor at arithmetically averaged reservoir pressure and phase saturation (presented in this research) give results close to those when using more complicated methods. Thus a "quick-check" method is provided for use in verifying simulation parameters such as proper grid spacing, grid size and reservoir parameters.

It will also be demonstrated that, for vertical wells, the use of this effective horizontal permeability, k_h, as the geometric average, results in simulated rate versus pressure data that match analytical results quite well in both isotropic and highly anisotropic conditions. Simulation experiments with Boast-VHS simulation software indicate that vertical well inflow performance predictions match those predicted with analytical equations quite well no matter what the contrast in k_x and k_y as long as the geometric average is the same in each case compared. The match is also excellent between various simulation experiments in which the geometric average is the same but the components k_x and k_y vary widely. This match is good both above and below the bubble point.

Experiments with horizontal wells indicate that the match is often not good with horizontal wells unless the simulation model is closely monitored. This may be a result of either a lack of sufficient grid blocks near the well bore or other misconceptions as to what constitutes effective permeability to a lateral well. The horizontal well aspects will be explored in more detail in chapters six and seven.

3.2 Two Phase Background and Theory

This simplified analysis incorporates the effects of pressure-saturation dependant variables such as relative permeability, formation volume factor and viscosity. Relative permeability is indirectly related to pressure through the saturation-pressure function. The equation for single-phase pseudosteady state flow of a vertical well in a rectangular drainage area is given by the following equation.:

$$q = \frac{0.007078\, k_h h(\overline{P_R} - P_{wf})}{\mu_o B_o \left(\ln \frac{r_e}{r_w} - 0.738 \right)} \tag{3.1}$$

P_R is the average reservoir pressure. Craft and Hawkins showed that for pseudosteady state conditions, the volumetric average reservoir pressure occurs at about one half the distance to the external radius (0.42R).[6] It is very desirable to easily compute oil flow analytically, above and below the bubble point, for use in a "quick-check" comparison with simulated results since much of pseudosteady state flow occurs below the bubble point. In order to represent saturated oil flow in analytic equations it is necessary to begin with the pressure integral concept. Figure 3.1 shows that for solution gas drive reservoirs, viscosity and formation volume factors are pressure dependent properties.[4]

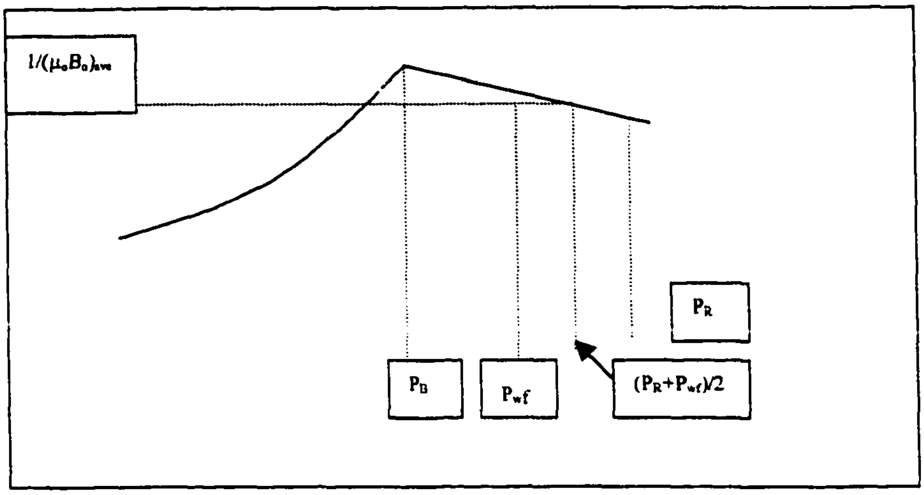

Figure 3.1 Viscosity and Formation Volume Factor as a Function of Pressure

For undersaturated conditions, the combined variation of viscosity and formation volume factor decreases approximately linearly with pressure. The above equation would then be modified above the bubble point as:

$$q = \frac{0.007078\, k_h h}{\left(\ln \frac{r_e}{r_w} - 0.738\right)} \int \frac{dp}{\mu_o B_o} \qquad 3.2$$

The integral is evaluated from P_{wf} to P_e (the pressure at the external boundary). Since $1/\mu_o B_o$ is a straight line, the area is a trapezoid (fig 3.1), so the integral can be represented by:

$$\int \frac{dp}{\mu_o B_o} = \frac{P_e - P_{wf}}{(\mu_o B_o)_{\bar{P}_R}} \qquad 3.3$$

Where, $\frac{1}{(\mu_o B_o)_{\bar{P}_R}}$ is the value at an average pressure $P_R = (P_e + P_{wf})/2$. The resulting inflow equation, at average reservoir pressure for pseudosteady state conditions becomes:

$$q = \frac{0.007078\, k_h h(\overline{P_R} - P_{wf})}{(\mu_o B_o)_{\bar{P}R}\left(\ln\frac{r_e}{r_w} - 0.738\right)} \qquad 3.4$$

Golan[4] (166) and Muskat et al[7] note that below the bubble point, (i.e. saturated reservoir conditions) equation 3 would become (neglecting skin and turbulence effects):

$$q = \frac{0.007078h\, k_h}{\left(\ln\frac{r_e}{r_w} - 0.738\right)} \int \frac{k_{ro}}{\mu_o B_o} dp \qquad 3.5$$

The integral is evaluated from P_{wf} to P_{Rave}.

As noted in the literature, solving the pressure integral is not a trivial procedure.[4] Evinger and Muskat[7] (1942) and later Vogel[8] et al noted however that the pressure function could be accurately represented versus pressure by a straight line ranging from $k_{ro}/\mu_o B_o$ at reservoir pressure (up to the bubble point) to the origin. (Fig 3.2) However, if this is the case, there is no need to evaluate the integral this way. If the straight-line assumption is valid, the problem reduces to expressing the area under the trapezoid situation again, as in the above bubble point region. Appendix A shows the derivation and proof of the use of this approximation. It is shown in Appendix A that this method is equivalent to using the straight-line IPR relationship. Extensions to more complex curvature can be made.

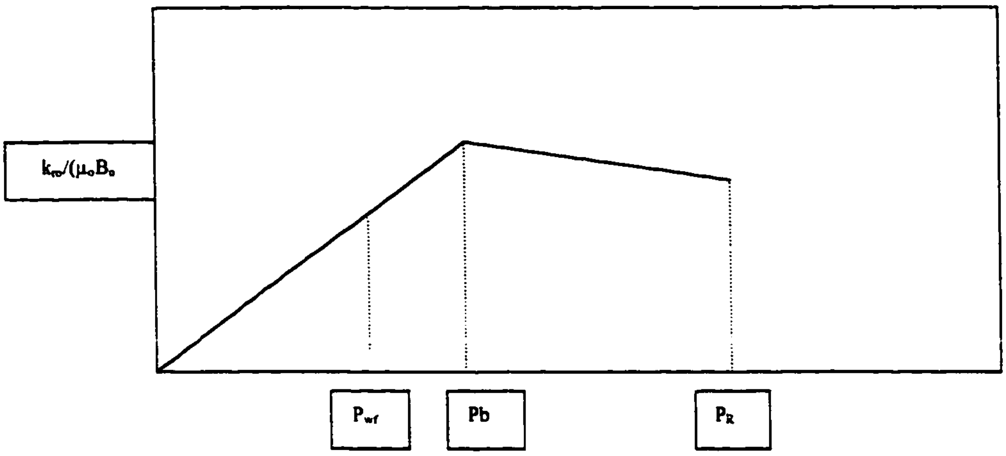

Figure 3.2 Mobility Factor as a Function of Pressure

It is then only necessary to evaluate the $k_{ro}/\mu_o B_o$ at the average reservoir pressure at any given time. It will be shown that this method will give a good approximation. Two phase flow can then be described above and below the bubble point by equation 3.6 if one substitutes $(k_{ro}/\mu_o B_o)_{ave}$ evaluated at average reservoir pressure.

$$q = \frac{0.007078 h k_h (\overline{P_R} - P_{wf})}{\left(\ln \frac{r_e}{r_w} - 0.738 \right)} \left[\frac{k_{ro}}{(\mu_o B_o)} \right]_{S_o, \overline{P_R}} \qquad 3.6$$

Therefore since one knows or assumes the mobility as a function of pressure and saturation that is input to simulators one can use the same function to analytically check against simulation output. Actually it seems to that k_{ro} should be computed at the average oil saturation at any given average pressure situation rather than at the average pressure as proposed in Muskat. Muskat never mentions this in his paper but the integral of k_{ro} should not be from P_{wf} to P_e but from S_{oi} to S_{oe} since k_{ro} is only indirectly related to pressure through the saturation function.

In other words, the pressure integral in equation 3.5 can be approximated by $(k_{ro}/B_o\mu_o)_{ave}$ where k_{ro} is taken as the relative permeability at the arithmetically averaged oil saturation across the simulation grid and $B_o\mu_o$ is the value at average reservoir pressure over the entire simulation grid at any given time step as long as the straight line assumption is valid. Since a relative permeability function that is a function of fluid saturation is input to the simulator, knowing the average grid-block saturation yields the average relative permeability across the model to use in the equation for calculation purposes.

The averaging process is desirable because it is so easy to evaluate tabular simulation output in a spreadsheet. Typical simulators like Boastvhs provide tabular output that can be imported to spreadsheets and averaged over gridblocks in a single operation.[5] Then the data can be input into the analytical equations and compared to simulator calculations. The main question then is whether or not the straight-line assumption is really valid. As a test, equation 3.6 was tested against the simulation output of some real field examples of relative permeability, viscosity and formation volume factor values.

3.3 Comparing Analytical Solutions with Two Phase Simulations

An 11 by 13 block model (Table 1) was tested using real field data as shown in figures 3.3-3.6. Figure 3.5 shows (k_{ro}/μ_oB_o) as a function of average reservoir pressure where k_{ro} is derived from the simulation relative permeability function (defined in terms of fluid saturation) at the grid averaged oil saturation indicated in figure 3.6. Appendix B provides the reader with the algorithm to compute PVT properties.

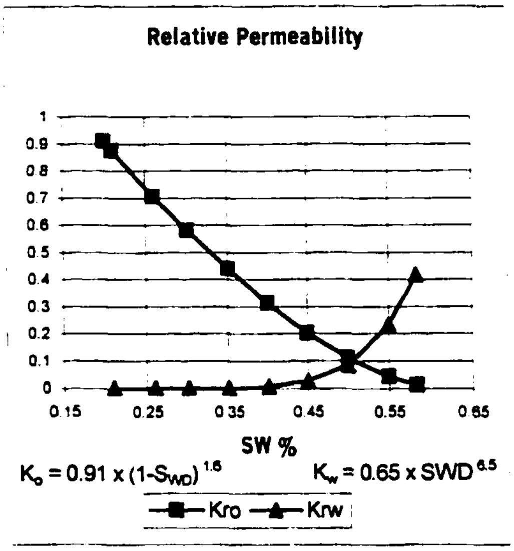

Figure 3.3 Relative Permeability versus Phase Saturation

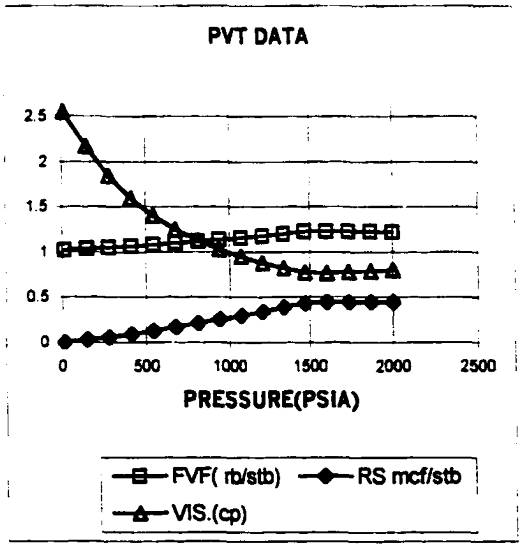

Figure 3.4 PVT Data as a Function of Pressure

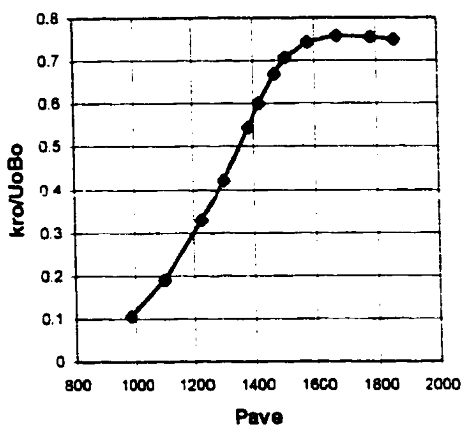

Figure 3.5 Relative Permeability-Viscosity-Formation Volume Factor Function versus Pressure

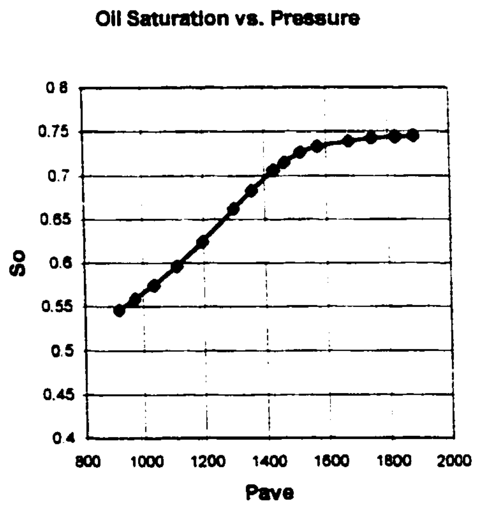

Figure 3.6 Oil Saturation versus Pressure

and Appendix C provides a good guide that has been developed for estimating, from oil-field data, all the necessary simulation inputs such as relative permeability, capillary pressure, etc. Tables 3.2 and 3.3 detail the typical simulation output from Boastvhs utilized to evaluate average saturation and pressures at any given time. Table 3.4 tabulates the actual simulation output values and the calculated analytical values. Figure 3.7 illustrates graphically the comparison of simulated oil rate vs. average reservoir pressure with analytical oil rates versus average pressure for the various models using the case of a vertical well. Average horizontal absolute permeability, k_h is 3.1 md in all cases although contrasts in directional permeability are varied in the simulation. Therefore using the values of $(k_{ro}/\mu_o B_o)_{ave}$ at the grid-wide average reservoir pressure and saturation conditions seems to match actual simulated results very well thus confirming that the straight line assumption is reasonably a good approximation.

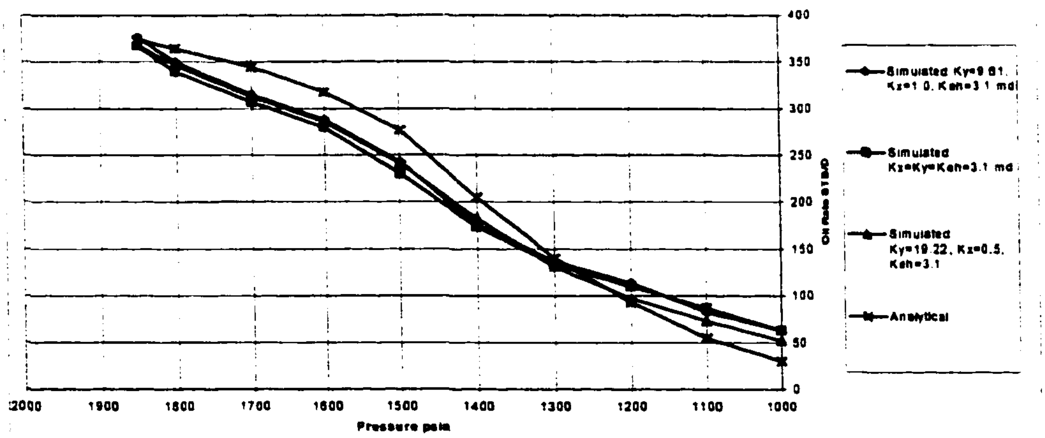

Figure 3.7 Rate versus Pressure for Vertical Well Case of Permeability Anisotropy but Constant Geometric Average Permeability

Table 3.2 and 3.3 Saturation and Pressure Profiles –Tabular Output with Graphics from import to Excel Spreadsheet

day 11188

oil saturation　　average So= 0.574722

0.646	0.646	0.646	0.646	0.646	0.646	0.646	0.646	0.646	0.646	0.646	0.65	0.65	0.646	0.646
0.64	0.64	0.64	0.64	0.64	0.64	0.64	0.64	0.64	0.64	0.64	0.64	0.64	0.64	0.64
0.627	0.627	0.627	0.627	0.627	0.626	0.626	0.626	0.626	0.626	0.627	0.63	0.63	0.627	0.627
0.606	0.606	0.605	0.604	0.603	0.602	0.602	0.601	0.602	0.602	0.603	0.6	0.61	0.606	0.606
0.586	0.585	0.583	0.569	0.555	0.55	0.546	0.544	0.546	0.55	0.555	0.56	0.56	0.585	0.586
0.535	0.536	0.536	0.536	0.536	0.536	0.536	0.531	0.535	0.536	0.536	0.54	0.54	0.535	0.535
0.523	0.524	0.524	0.524	0.525	0.524	0.521	0.512	0.521	0.524	0.525	0.52	0.52	0.524	0.523
0.513	0.513	0.512	0.511	0.51	0.509	0.502	0.493	0.502	0.509	0.51	0.51	0.51	0.513	0.513
0.495	0.494	0.493	0.492	0.491	0.49	0.482	0.475	0.482	0.49	0.491	0.49	0.49	0.494	0.495
0.513	0.512	0.512	0.511	0.51	0.509	0.502	0.493	0.502	0.509	0.51	0.51	0.51	0.512	0.513
0.523	0.523	0.524	0.524	0.525	0.524	0.521	0.512	0.521	0.524	0.525	0.52	0.52	0.523	0.523
0.536	0.535	0.535	0.536	0.536	0.536	0.536	0.531	0.535	0.536	0.536	0.54	0.54	0.536	0.535
0.567	u.565	0.563	0.55	0.554	0.549	0.546	0.544	0.546	0.549	0.554	0.56	0.56	0.566	0.567
0.607	0.607	0.606	0.605	0.604	0.604	0.603	0.603	0.603	0.604	0.604	0.61	0.61	0.607	0.607
0.627	0.627	0.627	0.627	0.627	0.627	0.627	0.626	0.627	0.627	0.627	0.63	0.63	0.627	0.627
0.64	0.64	0.64	0.64	0.64	0.64	0.64	0.64	0.64	0.64	0.64	0.64	0.64	0.64	0.64
0.646	0.646	0.646	0.646	0.645	0.646	0.645	0.645	0.645	0.646	0.646	0.65	0.65	0.646	0.646

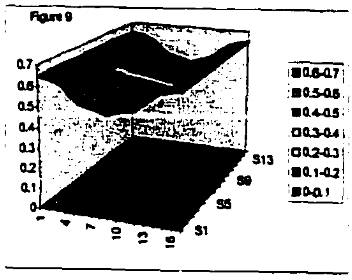

pressure distribution　　Paver 1033.408

1256	1256	1255	1256	1256	1255	1256	1256	1255	1256	1256	1256	1256	1256	1255
1244	1244	1244	1244	1244	1244	1244	1244	1244	1244	1244	1244	1244	1244	1244
1220	1220	1220	1220	1220	1220	1219	1219	1219	1220	1220	1220	1220	1220	1220
1181	1181	1180	1180	1179	1178	1178	1178	1178	1178	1179	1180	1180	1181	1181
1118	1117	1115	1113	1110	1107	1104	1103	1104	1107	1110	1113	1115	1117	1118
998	994	987	977	964	950	938	931	938	950	964	977	987	994	998
878	870	854	829	794	743	684	488	684	743	794	829	854	870	878
791	782	763	734	694	639	563	419	563	639	694	734	763	782	791
759	750	731	702	682	610	539	407	539	610	682	702	731	750	759
791	782	763	734	694	639	563	419	563	639	694	734	763	782	791
878	870	854	830	794	743	684	488	684	743	794	830	854	870	878
998	994	987	977	964	950	938	931	938	950	964	977	987	994	998
1118	1117	1115	1113	1111	1108	1104	1103	1104	1108	1111	1113	1115	1117	1118
1181	1181	1180	1180	1179	1178	1178	1178	1178	1178	1179	1180	1180	1181	1181
1220	1220	1220	1220	1220	1220	1219	1219	1219	1220	1220	1220	1220	1220	1220
1244	1244	1244	1244	1244	1244	1244	1244	1244	1244	1244	1244	1244	1244	1244
1256	1256	1256	1256	1256	1256	1256	1256	1256	1256	1256	1256	1256	1256	1256

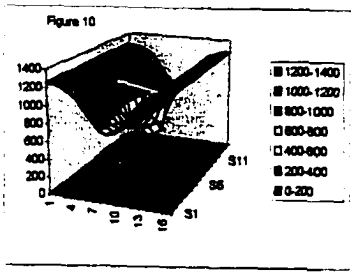

Same Ke but different distribution　　rw 0.5

	vertcon=Ky=9.61, Kx=1			vertxy Kx=Ky=3.1			vertxy Ky=19.22, Kx=0.			Analytical Rates			Muo	Bo	Kro	So
Day	Rate	Pressure	cum oil	Rate	Pressure	cum oil	Rate	Pressure	cum oil	vertcon	vertxy	verthgh				vertcx
31	383	1862	22.1	376	1867	21.6	380	1860	22.9	377.18	378	377	0.7862	1.2231	0.72	0.75
62	333	1768	32.2	322	1769	31.2	339	1784	33.4	358.3	359	362	0.7803	1.2239	0.72	0.75
123	299	1634	51.3	288	1625	49.7	307	1676	52.9	328.88	327	339	0.7689	1.2258	0.71	0.75
214	273	1551	77.1	261	1550	74.5	282	1580	79.6	304.28	304	311	0.7635	1.2266	0.7	0.74
395	243	1499	123.5	229	1500	118.6	248	1508	127.1	277.98	278	280	0.76	1.2273	0.66	0.73
576	219	1466	165	208	1467	157.6	221	1473	169.4	256.44	257	258	0.77	1.2216	0.63	0.72
942	179	1418	236.7	185	1420	228.7	196	1420	241.8	221.48	222	222	0.7877	1.2136	0.57	0.7
1308	169	1379	300.7	163	1384	291.6	170	1382	305.3	194.15	195	195	0.8031	1.2066	0.53	0.69
2304	137	1296	453.9	136	1303	438.7	131	1300	449.9	139.96	141	140	0.8361	1.1919	0.42	0.65
3400	121	1225	596.5	119	1232	578	104	1228	578.4	102.13	103	102	0.8722	1.1792	0.34	0.62
5996	86	1097	859.5	90	1109	843.7	76	1102	811.7	51.597	52.3	51.9	0.9388	1.1578	0.21	0.57
8582	59	986	1043	67	1013	1046	47	985	953.9	25.3	28.2	25.3	1.15	1.1112	0.14	0.53

Table 3.3 Vertical Comparison Output

3.4 Evaluation of Effective Horizontal Permeability Assumptions - Vertical Well Case

Notice also that three cases of directional permeability distributions were simulated and compared in simulation illustrated in Figure 3.7. Figure 3.7 shows that they each match each other very well no matter what the contrast in k_x and k_y as long as the geometric average of k_x and k_y is constant. Overall the vertical simulations match both one another and the analytical results in both isotropic and anisotropic media. It is significant that the match is good for both isotopic and anisotropic media. This also indicates that the common assumption that the geometric mean of permeability (k_h= sqrt ($k_x k_y$) is a valid assumption for a vertical well and that the simulator accurately describes this relationship.

3.5 Evaluation of Effective Horizontal Permeability Assumptions - Horizontal Well Case

Figure 3.8 however shows that the simulated results of horizontal wells do no not match each other for anisotropic media even when the geometric mean is the same. It will be shown through simulation experiments, that published analytical solutions to horizontal well inflow at least track simulated results in cases of isotropic permeability (again above and below the bubble point) but they do not match simulated horizontal results as well in cases of horizontally anisotropic permeability (figures 3.9,3.10,3.11). This phenomenon may result from 1) the difficulty in properly modeling a horizontal well in a simple simulator like Boast and 2) the fact that if the well length is not small in comparison to the size of the reservoir, the geometric mean will not approximate the actual effective horizontal permeability. For instance if the reservoir is semi-infinite, no other wells compete for drainage area, the reservoir is thick, and the well length is short compared to the reservoir dimensions then the geometric average of permeability may work well. The horizontal well would then appear small compared to the reservoir as a whole and the geometric average would give proper results. This is almost never the case in reality. The discrepancy in flow predictions seems to be related to well length, degree of penetration, permeability contrast and distance to the reservoir boundaries. If the simulator allows a large number of grid blocks then grouping smaller blocks near the horizontal wellbore may minimize problem. However in a simulator with grid block limitations such as Boastvhs, it does not appear that the horizontal well can be accurately modeled in cases of direction permeability anisotropy when the wellbore is long compared to the reservoir dimensions. This will be dealt with in more detail in chapters seven and eight.

Nevertheless equation 3.6 provides a framework to calibrate simulator parameters and resulting output for a test of "reasonableness". This equation can be extended to use in horizontal wells, as will be demonstrated in chapter 6 and 7.

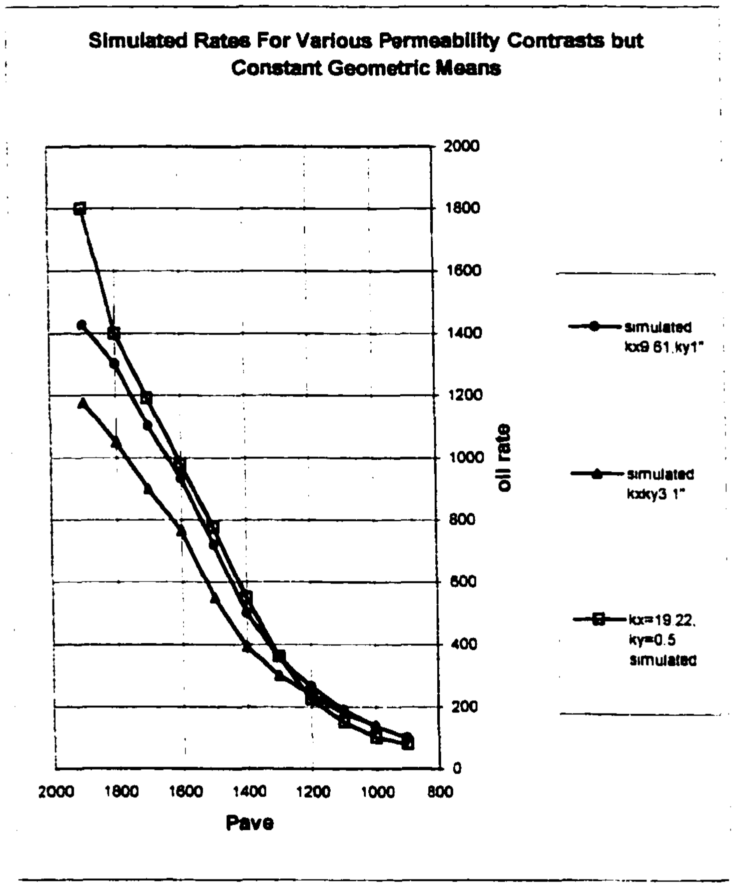

Figure 3.8 Comparison of Simulated Rate versus Pressure for Cases of Anisotropic Horizontal Permeability but Constant Geometric Mean Permeability

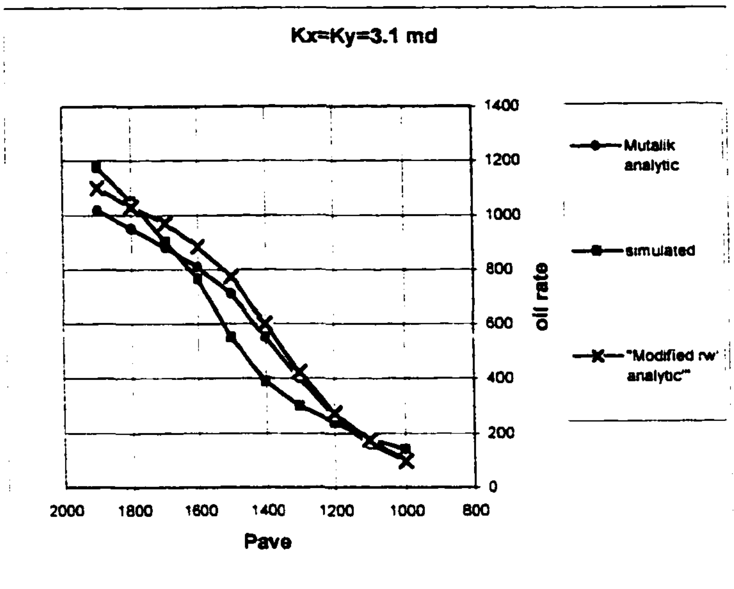

Figure 3.9 Comparison of Simulated with Analytical for Isotopic Permeability

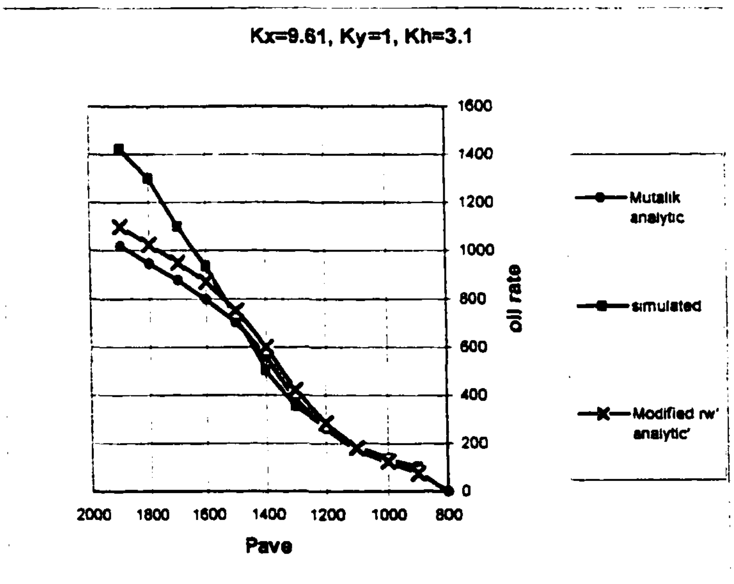

Figure 3.10 Comparison of Simulated and Analytical with Anisotropic Permeability

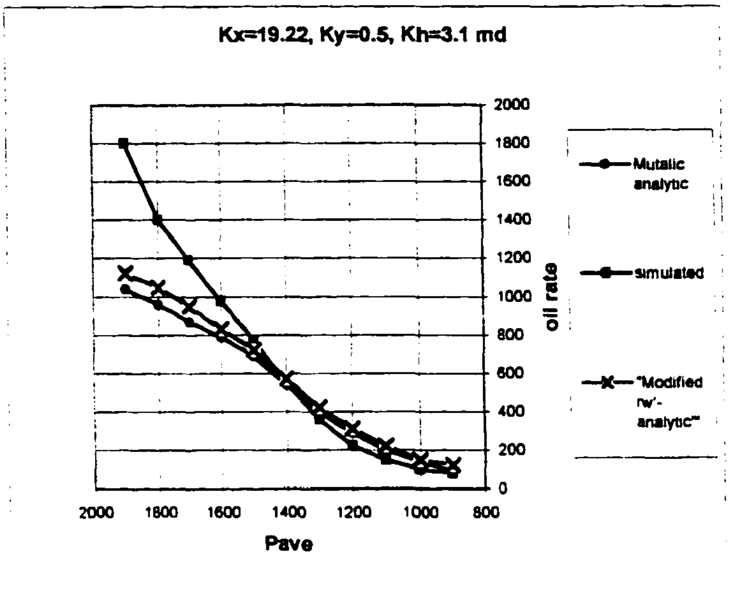

Figure 3.11 Comparison of Simulated and Analytical with Anisotropic Permeability

CHAPTER FOUR

Decline Curve Theory

4.1 Depletion Rate Decline (Pseudosteady State-PSS)

Pressure decreases according to the following relation in the case of constant rate depletion for undersaturated reservoirs with no flow boundaries:

$$P_R = P_i - \frac{q_p B_o}{Ah\phi c_t} t \qquad 4.1$$

In cases of constant pressure depletion, the expression for undersaturated reservoir rate decline is expressed as:

$$q_o(t) = \frac{kh[p_e(t) - p_{wf}]}{141.2\, \mu_o B_o [\ln(r_e / r_{wa})]} \qquad 4.2$$

The material balance equation relates the cumulative production N_p to the pressure $P_e(t)$ at the external boundary of the reservoir. It expresses the cumulative production as a function of the apparent total compressibility of the system c_{ta}, the hydrocarbon pore volume $V_p(1-S_w)$, and the pressure drop in the reservoir p_i-$p_e(t)$. Where c_{ta} is the apparent total compressibility of the system which varies with $p_e(t)$

$$N_p = V_p(1 - S_w) c_{ta} [p_i - p_e(t)] \qquad 4.3$$

More complicated expressions can be constructed for saturated oil reservoirs. Tracy[9](1955) and Tarner [10](1944).

Rate time behavior during depletion has been treated rigorously by mathematicians who solve the flow equations analytically for particular boundary conditions of no flow at the outer boundary and constant pressure at the inner boundary (wellbore). Fetkovich[3] (1980) presented a useful form of the solution of Tsarevich and Kuranov[11] (1966) to prepare type curves of dimensionless rate versus dimensionless time (Figure 4.1). Observation of the type curves shows that transition from the infinite acting transient to the PSS is instantaneous at t_{pss} at least for the radial case. Irregular outer geometry will affect the infinite acting period and may accelaerate true pseudo-steady state production. In contrast to Fetkovich's purely radial form, this research will show how to construct type curves to illustrate this irregular boundary phenomenon for various reservoir shape factors and well positions within the reservoir.

Fetkovich[3] prepared a type curve of dimensionless rate versus dimensionless time using the following relationship (figure 4.1):

$$q_D = \frac{141.5 q \mu B}{kh(P_i - P_{wf})} \qquad 4.4$$

$$t_D = \frac{0.00634 kt}{\phi \mu c_t r_{wa}^2} \qquad 4.5$$

$$r_{wa} = r_w e^{-S}$$ 4.6

$$r_{wa} = \frac{x_f}{2}$$ 4.7

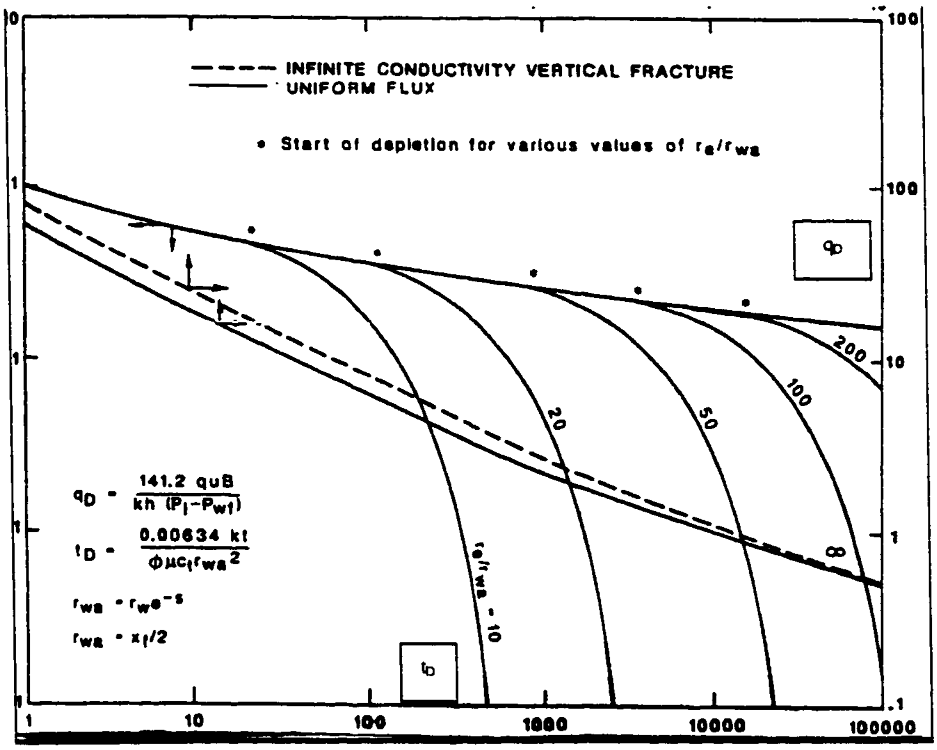

Figure 4.1 Dimensionless Rate versus Time[3]

An irregular outer geometry or off center well location can create a period of transition between transient and PSS production. This transition zone has not been the focus of much research but it may provide valuable information about the reservoir shape. Deviations from Fetkovich curves in the transition zone may indicate non-radial system geometry. The non-radial relationships will be derived in chapter 5 and incorporated into a generalized decline curve system.

A general expression for PSS decline for constant pressure according to the analytical solution is:

$$q_D = Ae^{-Bt_D} \tag{4.8}$$

Where A and B are constants defined by the ratio r_e/r_{wa}. Fetkovich developed expressions for A and B which reflect different ratios of r_e/r_{wa}. The higher the ratio the larger is the time to pseudosteady state t_{Dpss}.

$$A = \frac{1}{\ln(r_e / r_{wa}) - 0.5} \tag{4.9}$$

$$B = \frac{2A}{(r_e / r_{wa})^2 - 1} \tag{4.10}$$

The expressions for A and B reflect the observation that different ratios of r_e/r_{wa} give different depletion stems. The higher the ratio of r_e/r_{wa}, the larger the time to pseudosteady state t_{Dpss} and the lower is q_D at the start of depletion.

Exponential decline, according to the analytical solution, is substantiated by many field observations. The primary observation in Arp's[2] work (1945) suggested that three types of decline could express all conventional depletion declines: hyperbolic, exponential and harmonic. The effective decline rate D_e, or D_{ei} at initial conditions, for the three types of production-decline curves is related to the nominal decline rate D or D_i for initial conditions as follows.

$$D_e = 1 - e^{-D} \qquad \textbf{4.11}$$

The nominal decline rate is the negative slope of the natural log of q vs. time plot. The effective decline D_e is a stepwise function whereas D is a continuous function.

For hyperbolic decline

$$D_{ei} = 1 - (1 + bD_i)^{-1/b} \qquad \textbf{4.12}$$

and for harmonic:

$$D_{ei} = \frac{D_i}{1 - D_i} \qquad \textbf{4.13}$$

Arps[2] classifies three types of decline:

A.

Hyperbolic decline where the decline D is proportional to a fractional power b of the production rate.

$$D = \frac{\frac{dq}{dt}}{q} = \left(\frac{D_i}{q_i^b}\right) q^b \qquad \textbf{4.14}$$

which upon integration becomes:

$$q_o = \frac{q_{oi}}{(1 + bDt)^{\frac{1}{b}}} \qquad 4.15$$

Where q_{oi}= initial oil rate neglecting transient decline

q_o= rate at time t

D= decline constant (Nominal decline rate = negative slope of ln q vs. time)

b= decline exponent

Subscript i denotes initial conditions.

On second integration the rate cumulative expression becomes:

$$N_p = \frac{q_i^b}{(1-b)D_i}\left(q_i^{(1-b)} - q^{(1-b)}\right) \qquad 4.16$$

and the time to abandonment becomes:

$$t_a = \frac{\left(\frac{q_i}{q_a}\right)^b - 1}{b\,D_i} \qquad 4.17$$

and eliminating D_i :

$$t_a = \frac{\left[\left(\frac{q_i}{q_a}\right)^b - 1\right]}{b\left[\frac{q_i^b}{(1-b)N_{pa}}\left(q_i^{1-b} - q^{1-b}\right)\right]} \qquad 4.18$$

B. Exponential b=0

Exponential decline exhibits a straight line on semi log plot of rate versus time. It is also called constant percentage decline since it is characterized by the fact that the drop in production rate per unit of time is proportional to the production rate.

Constant percentage decline (exponential) the nominal decline rate D is constant of

$$D = -\frac{dq / dt}{q} \qquad 4.19$$

which after integration yields:

$$q_o = q_{oi} e^{-Dt} \qquad 4.20$$

After a second integration the rate-cumulative expression for cumulative production at any time t is:

$$N_p = \frac{q_i - q}{D} \qquad 4.21$$

And the remaining life to abandonment time may be obtained by:

$$t_a = \frac{\ln(\frac{q_i}{q_a})}{D} \qquad 4.22$$

or after eliminating D:

$$t_a = \frac{N_{pa}}{q_i}\left(\frac{\frac{q_i}{q_a}\ln\frac{q_i}{q_a}}{\frac{q_i}{q_a} - 1}\right) \qquad 4.23$$

C. Harmonic b=1

For harmonic decline where b= 1 the nominal decline rate D is proportional to the production rate or:

$$D = \frac{\frac{dq}{dt}}{t} = \frac{D_i}{q_i} q \qquad 4.24$$

or after integration:

$$q_o = q_{oi} \frac{1}{(1 + Dt)} \qquad 4.25$$

After a second integration the rate cumulative relationship becomes:

$$N_p = \frac{q_i}{D_i} \ln \frac{q_i}{q} \qquad 4.26$$

And time to abandonment t_a is:

$$t_a = \frac{N_{pa}}{q_i} \left(\frac{\frac{q_i}{q_a} - 1}{\ln \frac{q_i}{q_a}} \right) \qquad 4.27$$

4.2 Solution Gas Drive Meaning

Arps[2] did not give physical reasons for the three observed declines but he indicated that exponential b=0 was common and that b usually ranges from 0 to 0.5 in solution gas reservoirs. It has been observed that the b value in typical solution gas drive reservoirs averages about 0.3 while a 0.5 value indicates water drive or gravity drainage. Exponential is the most rapid decline observed and thus exponential is used for the most conservative estimates for reserves. Recall that exponential decline implies that the total compressibility of the rock and fluid is the only mechanism providing pressure support for the system. Departure from exponential decline in solution gas reservoirs should then be useful in estimating the mobility function shown if figure 3.1. This will be explored further in chapters 5 and 6.

4.3 Physical Meaning to Decline Analysis

Fetkovich[3] expressed Arp's[2] exponential decline equation in terms of reservoir variables and thus gave physical meaning to Arp's observations. He obtained the following expressions for the Arps empirical constants q_{oi} and D.

$$q_{oi} = \frac{kh(p_i - p_{wf})}{141.2\,\mu_o B_o[\ln(r_e / r_{wa}) - 0.5]} \qquad 4.28$$

$$D = \frac{2(0.000264)k}{\phi\,\mu_i c_{ti}(r_e^2 - r_{wa}^2)[\ln(r_e / r_{wa}) - 0.5]} \qquad 4.29$$

These expressions can be used to forecast rate decline if production data are not available to identify the actual decline trend.

Since the transition from infinite to PSS is practically instantaneous in the radial system, a natural extension of the decline type curve is to combine transient and depletion relations onto a single graph. Fetkovich did this and used the unit variable t_{Dd} and q_{Dd} to define the type curves. (Figure 4.2 Combined Fetkovich-Arps analysis)

Hyperbolic decline (1< b >0) results from natural and artificial driving energies that slow down the pressure depletion compared with the depletion caused by pure expansion of a slightly compressible oil. Hyperbolic decline is exhibited if the reservoir drive mechanism is solution gas drive, gas cap expansion, or water drive. It is also exhibited when the natural drive mechanism is supplemented by water or gas injection. The presence of these driving energies implies that total compressibility increases and recovery is improved compared with the pure oil expansion drive mechanism.

When plotted on semi-log paper (rate vs. time) data showing hyperbolic declines tend to curve upward while exponential decline is a straight line of unit slope. The hyperbolic upward curvature is illustrated on figures 2.1 and 2.3.

$$D = -\frac{\ln[q_o(t^*)/q_{oi}]}{t^*} = -2.302\frac{\log[q_o(t^*)/q_{oi}]}{t^*} \qquad 4.30$$

Where t^*, $q_o(t^*)$ is any rate-time point on the semi-log straight line and an intercept of:

$q_{oi} = q_o\ (t=0)$.

4.3.1 Derivation of Fetkovich Type Decline Curves

Arps equation for hyperbolic decline can also be expressed in terms of dimensionless variables and the coefficients of the analytical decline equation (4.4) to yield:

$$q_{Dd} = \frac{A}{(1 + bBt_D)^{\frac{1}{b}}} \qquad 4.31$$

To plot as a single type curve that exhibits exponential harmonic and hyperbolic declines, Fetkovich defined new dimensionless unit variable q_{Dd} and t_{Dd} where:

$$q_{Dd} = \frac{q_o}{q_{oi}} = \frac{q_D}{A} \qquad 4.32$$

and

$$t_{Dd} = Dt = B\,t_D \qquad 4.33$$

Where A and B have been previously defined.

In terms of the unit variable for exponential decline:

$$q_{Dd} = e^{-t_{Dd}} \qquad 4.34$$

and for hyperbolic decline:

$$q_{Dd} = \frac{1}{(1 + bt_{Dd})^{1/b}} \qquad 4.35$$

Fetkovich plotted these equations as type curves with unit dimensionless variable for b= 0 up to b=1. (See Figure 4.2) Since the transition from infinite acting to PSS is practically instantaneous in a radial system, a natural extension is to combine transient with PSS onto a single graph.

When the unit variable $q_{Dd}=q_D/A$ and $t_{Dd}=Bt_D$ are expressed with previously defined A and B definitions then the units are related to the ratio r_e/r_{wa} by:

$$q_{Dd} = [\ln(r_e/r_{wa}) - 0.5]\, q_D = \left[\ln\left(\frac{r_e}{r_{wa}}\right) - 0.5\right]\frac{141.2\,\mu Bq(t)}{kh(p_i - p_{wf})} \tag{4.36}$$

and

$$t_{Dd} = \frac{2}{[(r_e/r_{wa})^2 - 1][\ln(r_e/r_{wa}) - 0.5]}\, t_D = \frac{\dfrac{0.00634kt}{\phi\mu c_t r_{wa}^2}}{0.5\left[\left(\dfrac{r_e}{r_{wa}}\right)^2 - 1\right]\left[\ln\left(\dfrac{r_e}{r_{wa}}\right) - 0.5\right]} \tag{4.37}$$

Combining these expressions with those of Arps for the depletion period resulted in a general type curve for transient and depletion periods as in Fig 4.2.

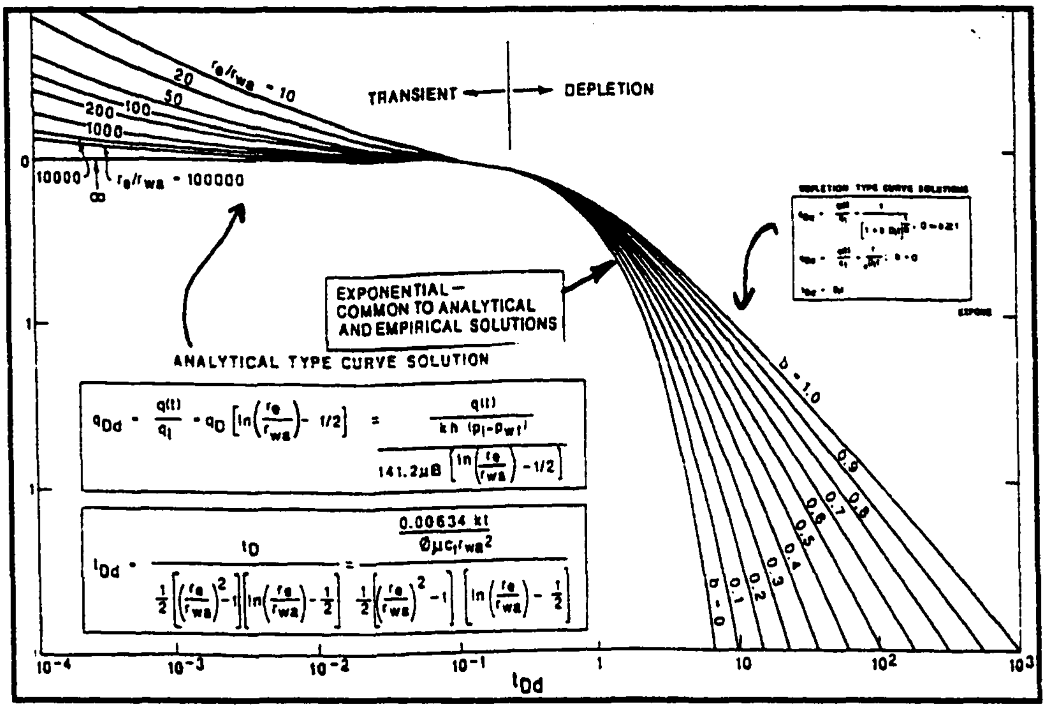

Figure 4.2 Generalized Arps-Fetkovich Dimensionless Decline Curve [3]

4.3.2 Reservoir Parameters From Type Curves

Type curve match points can then be used be used to calculate permeability, skin and drainage radius which yields initial oil in place. Using r_e/r_{wa} from the match, the transmissibility is determined from the match point by:

$$q_D = \frac{141.2\mu B q(t)}{kh(P_i - P_{wf})} \tag{4.38}$$

$$q_{Dd} = q_D\left[\ln\frac{r_e}{r_w} - \frac{1}{2}\right] \tag{4.39}$$

and combining yields:

$$kh = \frac{141.2\,\mu B}{(P_i - P_{wf})}\left(\ln\frac{r_e}{r_w} - \frac{1}{2}\right)\left(\frac{q_t}{q_{dD}}\right)_{match} \qquad \mathbf{4.40}$$

While the apparent wellbore radius is calculated from the following expressions:

$$t_D = \frac{0.00634kt}{\phi\mu c_t r_w^2} \qquad \mathbf{4.41}$$

$$t_{Dd} = \frac{t_D}{\frac{1}{2}\left[\left(\frac{r_e}{r_w}\right)^2 - 1\right]\left[\ln\left(\frac{r_e}{r_w}\right) - \frac{1}{2}\right]} \qquad \mathbf{4.42}$$

and combining to yield:

$$r_{wa}^2 = \frac{0.00634k}{\phi\mu c_t \frac{1}{2}\left[\left(\frac{r_e}{r_{wa}}\right)^2 - 1\right]\left[\ln\left(\frac{r_e}{r_{wa}}\right) - \frac{1}{2}\right]}\left(\frac{t(days)}{t_{dD}}\right)_{match} \qquad \mathbf{4.43}$$

from which $s = -\ln(r_{wa}/r_w)$ and drainage radius is calculated as :

$$r_e = r_{wa}\left(\frac{r_e}{r_{wa}}\right)_{match} \qquad \mathbf{4.44}$$

By knowing the drainage radius then N reserves in place can be calculated from:

$$N(well) = \frac{\pi r_e^2 h\phi(1 - S_w)}{5.615\, B_{oi}} \qquad \textbf{4.45}$$

An example of this calculation is shown in Section 5.4.1.

Thus Fetkovich[3] gave physical meaning to decline curves in radial systems and showed that they could be combined with Arps empirical relationships in the pseudosteady state region. Methods to use the deviation from exponential decline to gain information about the fluid properties, relative permeability and pore volume are explored as part of Appendix C. These concepts will be extended to non-radial geometry and horizontal well analysis in chapters 5 and 6. This should further enhance the decline curve matching process in non-radial reservoirs.

According to Mathews[21], during pseudo steady state, the drainage volumes in a bounded reservoir are proportional to the rates of withdrawal from each drainage volume. Therefore the ratio q_i/N_{pi} will be identical for each well and, thus, the sum of the results from each well should give the same results as from analyzing the total lease or field production rate. Field experience often demonstrates how rapidly readjustments in drainage volumes can take place by changes in the production rate or depletion by offset wells. This of course assumes that the field is not stratified or separated by a fault or drastic anisotropy. The effect compartmentalization by permeability or stratification would be interesting to experiment with in the future.

It is not well known that the Fetkovich Type Curves are based on a strictly radial system operating above the bubble point with the well centrally located. It is obviously desirable to derive a more general case that would apply to any particular reservoir drainage shape such as rectangular, triangular, and reservoirs in which the well is displaced from the reservoir center. It would also be desirable to modify the curves for cases below the bubble point and extract information from that deviation from the strictly exponential case. In the radial case, the transition from infinite acting to pseudosteady state is almost instantaneous.

However in a non-radial reservoir the transition from infinite to pseudosteady state is prolonged. Significant error in type curve matching may result from using the radial form. In low permeability formations rapidly declining transient production can be confused with depletion and an attempt to fit the transient data to the depletion portion of the type curve will result in Arps "b" values that are unrealistically high. It is therefore desirable to properly define the full shape of the type curve over the transient and depletion period properly apply the techniques and analysis.

This method, shown in this section and fully derived in Appendix E utilizes shape factors derived for these various conditions such as shown in Earlouger's Table C-1 *in Advances in Well Testing*[22]. Application of these factors to the Fetkovich system is neither direct nor straightforward. A system was derived that will incorporate all reservoir shapes, positions and later will be applied to vertically fractured and horizontal wells using an equivalent well bore radius concept. The complete derivation is shown in Appendix E and applications to actual field production data is detailed in Chapter 5.

CHAPTER FIVE

Decline Curve Construction, Analysis and Use

5.1 – Introduction

In chapters one and four it was shown that Fetkovich[3] combined the transient analytical solution with the pseudo-steady state (boundary-dominated flow) to develop a single type curve system. In that work, Fetkovich developed the dimensionless terms, q_{dD}, the dimensionless flow rate and t_{dD} the dimensionless time based on the initial flow rate and initial decline. Fetkovich developed his decline curves for radial geometry only. That derivation will be extended to a more general geometry and well position application. Reservoir parameters such as permeability, pore volume, skin etc were then extracted from the transient portion. Fetkovich indicated that reservoir parameters such as pore volume should not be computed until the onset of depletion when an approximation of the Arps[1] decline exponent b could be made. Reservoir and fluid properties can affect the value of the decline exponent b. Solution gas increases the value of b so that the production tail is extended in time. Fractured reservoirs with matrix support also show extended tails.

5.2 Theoretical Background for Dimensionless Solutions

In 1949, Van Everdingen and Hurst[17], first developed the equations used to generate the dimensionless pressure and time values that were later used in decline curves as shown in subsequent section 5.3. These were later extended by Fetkovich[3] to define dimensionless decline parameters. The theory began with the diffusivity equation, the application of certain boundary equations and the application of the Laplace transformation solution. The basic diffusivity equation is:

$$\frac{1}{r}\frac{\partial}{\partial r}\left(r\frac{\partial P}{\partial r}\right) = \frac{\phi\mu\, c}{k}\frac{\partial P}{\partial t} \qquad 5.1$$

The treatment of the diffusivity equation had been essentially the application of the Fourier-Bessel series. VanEverdingen and Hurst[17,18] presented a new approach to the solution in the form of the Laplace transformation since it was recognized that Laplace transformations offered an easier approach. The primary case of interest in decline analysis was the solution to the constant terminal pressure case solved for both the infinite and limited reservoirs. The constant terminal pressure and the constant terminal rate cases are not independent of one another, as knowing the operational form of one, the other can be determined. The initial condition is that at time zero the pressure at all points in the formation is constant and equal to unity. The inner boundary condition is that when the well or reservoir is opened, the pressure at the well or reservoir boundary, $r_D=1$, immediately drops to zero and remains zero for the duration of the production history.

5.2.1 Infinite Case

The outer boundary case for the infinite reservoir is as the reservoir reaches infinity, the pressure drop is zero. This is expressed as:

$$\lim_{(r_{eD} \to \infty)} P_D = 0 \qquad 5.2$$

VanEverdingen and Hurst[17] gave the solution in Laplace space:

$$\bar{Q}_D = \frac{K_1(\sqrt{p})}{z^{3/2} K_o(\sqrt{p})} \qquad 5.3$$

where Q D is the cumulative production, p is the Laplace transform variable and K_o and K_1 are modified Bessel functions of the order zero and one. The application of Mellin's inversion formula to the equation yields the analytical expressions for Q D:

$$Q_D = \frac{4}{\pi^2} \int_0^\infty \frac{1 - e^{-u^2 t_D}}{u^3 \left[J_0^2(u) + Y_0^2(u) \right]} du \qquad 5.4$$

where Jo and Yo are Besel functions of the first and second kind, respectively of order zero.

Since cumulative production Q D is defined as :

$$Q_D = \int_0^t q_D(t)dt \qquad 5.5$$

the Laplace equivalent of q_D is:

$$\bar{q}_D = \frac{K_1(\sqrt{p})}{z^{1/2}K_0(\sqrt{p})} \qquad 5.6$$

This equation is inverted numerically by the Stehfest[19] method to obtain the variation of q_D with t_D. The corresponding analytical expression is:

$$q_D = \frac{4}{\pi^2}\int_0^\infty \frac{e^{-u^2 t_D}}{u\left[J_0^2(u) + Y_0^2(u)\right]}du \qquad 5.7$$

The dimensionless flow rate q_D in field units is of course:

$$q_D = \frac{141.2\mu B q(t)}{kh\left(P_i - P_{wf}\right)} \qquad 5.8$$

and the dimensionless time in field units is:

$$t_D = \frac{0.000634kt}{\phi\mu c_t r_w} \qquad 5.9$$

After considerable work a program was used to invert these equations numerically using the Stehfest numerical Laplace algorithm. The results of this inversion yield values for infinite q_D versus t_D that are tabulated in the Appendix D and plotted on figure 5.1 as the infinite solutions. Notice the divergence of the solutions from the bounded solutions at increasing reservoir sizes (see limited reservoir theory next section.)

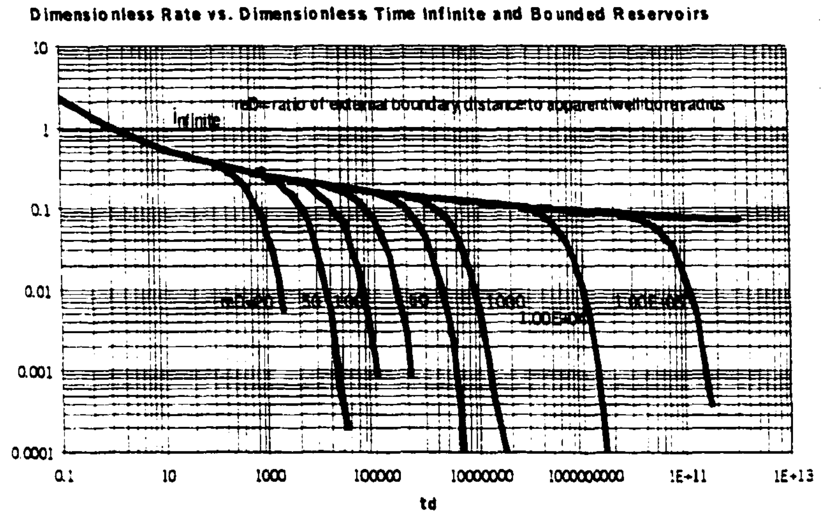

Figure 5.1 Dimensionless Rate versus Dimensionless Time

5.2.2 Solutions in Limited Reservoirs

The Fourier-Bessel type of expansions first developed the solutions for limited reservoirs of radial symmetry. VanEverdingen and Hurst[17] showed how the solutions could be obtained more easily using the Laplace transformation.

5.2.2.1 Conditions

The limited reservoir case is essentially the case of no fluid flow across the exterior boundary where:

$$\left(\frac{\partial P}{\partial r}\right)_{r=r_e} = 0 \qquad \textbf{5.10}$$

The VanEverdingen and Hursts solution to the cumulative production in Laplace space was given by:

$$Q_D = \frac{I_1(r_{eD}\sqrt{p})K_1(r_{eD}\sqrt{p} - K_1(r_{eD}\sqrt{p})I_1\sqrt{p}}{p^{3/2}\left[K_1(r_{eD}\sqrt{p})I_o(\sqrt{p}) + I_1(r_{eD}\sqrt{p})K_o(\sqrt{p})\right]} \qquad \textbf{5.11}$$

In order to apply Mellin's inversion formula, the first consideration is the roots of the denominator of this equation, which indicates the poles. Since the modified Bessel functions for positive real arguments are either increasing or decreasing, the bracketed term in the denominator does not indicate any poles for positive real values for p. An investigation of the integration along the negative real axis both for the upper and lower portions reveals that the above equation is an even function for which the integration along the paths is zero. However poles are indicated along the negative real axis and these residuals help make up the solution for the constant terminal pressure case for the limited radial system. The analytical solution reduces to:

$$Q_D = \frac{r^2{}_{eD} - 1}{2} - 2\sum_{a_1, a_2, etc}^{\infty}\left\{\frac{e^{-a^2{}_n t_D} J_1^2(a_n, r_{eD})}{a_n^2\left[J_0^2(a_n) - J_1^2(a_n, r_{eD})\right]}\right\} \qquad \textbf{5.12}$$

As with the infinite solution, differentiation of cumulative production yields the Laplace and analytical solutions for dimensionless flow rate:

$$q_D = \frac{I_1(r_{eD}\sqrt{p})K_1(r_{eD}\sqrt{p} - K_1(r_{eD}\sqrt{p})I_1\sqrt{p}}{\sqrt{p}\left[K_1(r_{eD}\sqrt{p})I_o(\sqrt{p}) + I_1(r_{eD}\sqrt{p})K_o(\sqrt{p})\right]} \qquad 5.13$$

$$q_D = 2\sum_{a_1,a_2,etc}^{\infty}\left\{\frac{e^{-a^2{}_n t_D}J_1^2(a_n,r_{eD})}{\left[J_0^2(a_n) - J_1^2(a_n,r_{eD})\right]}\right\} \qquad 5.14$$

Where the values of a1, a2 etc are determined as multiple roots of the equation :

$$\left[J_1(a_n r_{eD})Y_0(a_n) - Y_1(a_n r_{eD})J_0(a_n)\right] = 0 \qquad 5.15$$

Once the roots are found the summation is done for the various roots until convergence is obtained. The above two expressions are used to generate the solution for the closed boundary case for various distances to the external boundary. These are also shown in Figure 5.1.

5.3 Generation of Fetkovich Type Curves.

The method of generating the Fetkovich type curves is not a trivial process and is not widely known. The method must be understood and duplicated in order to extend the method to other shapes and well positions. The methodology of duplicating the Fetkovich curves is summarized as follows:

1. Generate the transient solutions for both infinite and closed reservoir systems by the methods of VanEverdingen and Hurst. Lee[20] in his Appendix C Table C-5 published the tabular solutions to the finite radial system with closed exterior boundary. Those values are also tabulated in this Appendix D along with all the solutions needed for finite and infinite cases generated with the Stehfest algorithm and extensions to the general cases. Figure 5.1 showed a graph of the dimensionless rate vs. dimensionless time for the infinite and bounded reservoirs using the tabular results of Lee and those generated from the program. Notice that the finite reservoir solutions for increasingly large reservoirs (i.e. r_{eD} increasing) converge into the infinite solution at increasing dimensionless time values and decreasing dimensionless rate values. The solutions for the infinite case are common to the bounded case where the outer boundary has not been sensed by the well. As the distance to the outer boundary increases, the time taken to reach the pseudo-steady state flow increases. This construction is specifically for radial cases. This research will extend those solutions to other reservoir shapes.

2. The next step is to convert those dimensionless rates and times from the table into the new Fetkovich type dimensionless decline parameters q_{Dd} and t_{Dd} by multiplying or dividing the dimensionless rate and time values in the table by the appropriate Fetkovich A and B values previously discussed in Chapter 4.

$$q_{Dd} = \frac{q_o}{q_{oi}} = \frac{q_D}{A} \quad 5.16$$

where A is given by:

$$A = \frac{1}{\left[\ln\frac{r_e}{r_{wa}} - \frac{1}{2}\right]} = \frac{1}{c_1} \quad 5.17$$

and the dimensionless time scale

$$t_{Dd} = Dt = Bt_D \quad 5.18$$

where:

$$B = \frac{2A}{\left(\frac{r_e}{r_{wa}}\right)^2 - 1} = \frac{1}{0.5\left[\left(\frac{r_e}{r_{wa}}\right)^2 - 1\right]\left[\ln\frac{r_e}{r_{wa}} - 0.5\right]} = \frac{2}{c_2 c_1} \quad 5.19$$

This was shown in chapter four. The dimensionless rate and time is thus expressed as:

$$q_{Dd} = [\ln(r_e / r_{wa}) - 0.5]\, q_D = \frac{\dfrac{q(t)}{kh(p_i - p_{wf})}}{141.2\mu B\left[\ln\left(\dfrac{r_e}{r_{wa}}\right) - 0.5\right]} \qquad 5.20$$

and

$$t_{Dd} = \frac{2}{[(r_e / r_{wa})^2 - 1][\ln(r_e / r_{wa}) - 0.5]}\, t_D = \frac{\dfrac{0.00634kt}{\phi\mu c_t r_{wa}^2}}{0.5\left[\left(\dfrac{r_e}{r_{wa}}\right)^2 - 1\right]\left[\ln\left(\dfrac{r_e}{r_{wa}}\right) - 0.5\right]} \qquad 5.21$$

The tabular values used in these plots are shown in Appendix D.

3. Calculate the Arps empirical dimensionless time and rate from the expression:

$$q_o = \frac{q_{oi}}{(1 + bDt)^{\frac{1}{b}}} \qquad 5.22$$

or defined in dimensionless decline terms:

$$q_{dD} = \frac{q_t}{q_i} = [1 + bDt_{dD}]^{-1/b} \qquad 5.23$$

The decline D is assumed as unity in the calculation of the terms. These values are also computed in a spreadsheet and tabulated in the appendix D for all b values greater than zero and up to one. The exponential decline with b= 0 is calculated as:

$$q_{dD} = e^{-tdD} \qquad 5.24$$

The results are tabulated in the appendix D and plotted on figure 5.2.

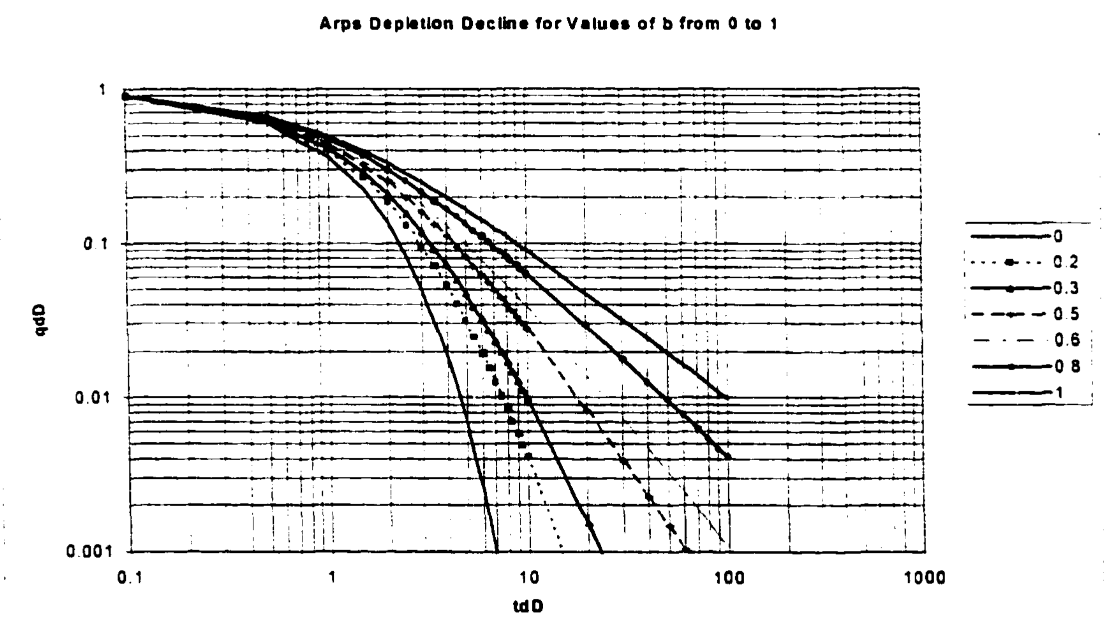

Figure 5.2 Arps Depletion Decline for Values of b from 0 to 1

As discussed before, Fetkovich discovered that the analytical dimensionless rate solution converges with the empirical dimensionless exponential rate solution for pseudo-steady state by defining the dimensionless rate scale.

Combining these expressions from steps one and two with those of Arps for the depletion period resulted in a general type curve for transient and depletion periods (exponential decline only b=0) as reconstructed in Fig 5.3. The transient portion was generated for different sizes of drainage area by r_{eD}. Again the numerical results are shown tabular form in the appendix D. The complete set of tabular results is not available from any other source in the literature. Figure 5.4 shows the final composite curve for the transient and depletion stages.

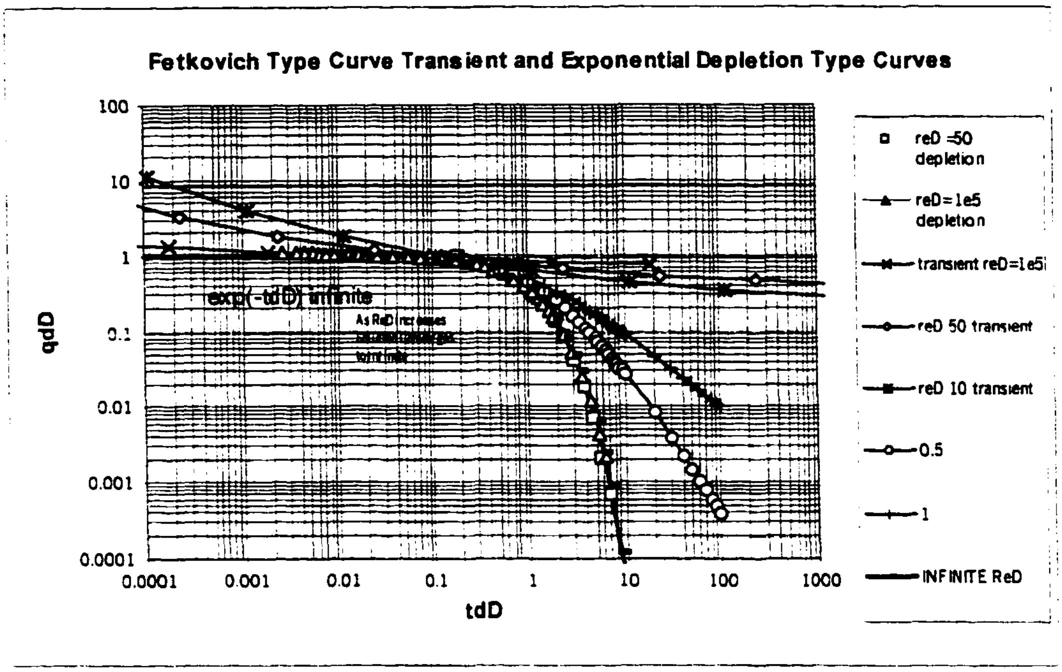

Figure 5.3 Fetkovich Type Curve – Transient and Depletion

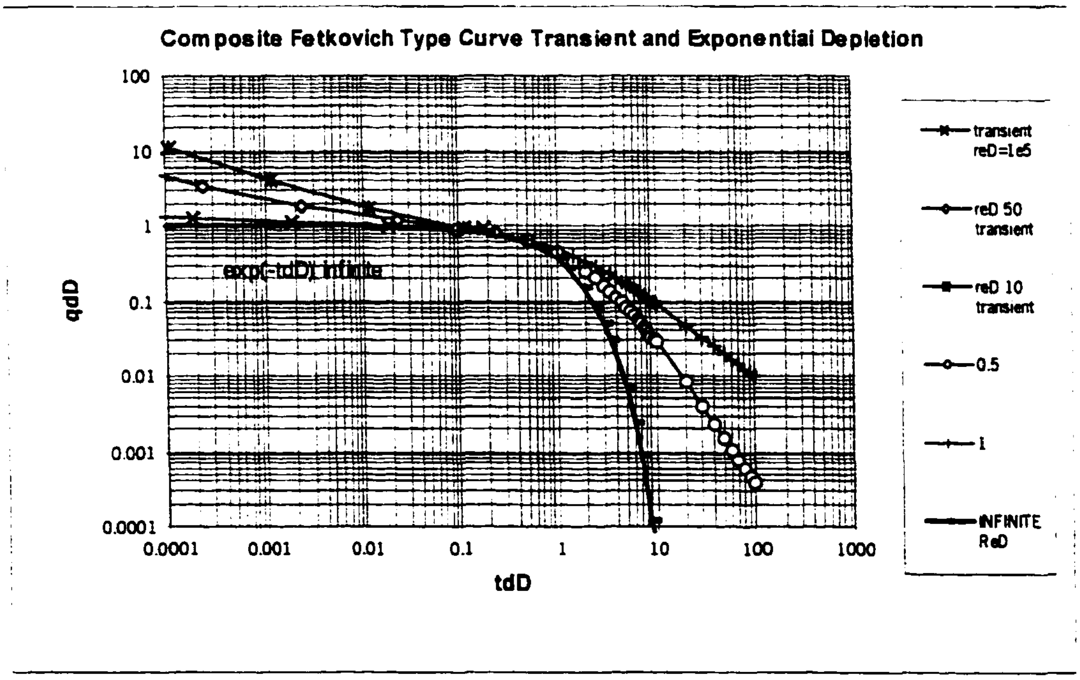

Figure 5.4 Final Composite Fetkovich Type Curve – Transient and Depletion

5.4 Use of Decline Curves in the Calculation of Reservoir Parameters and Future Production Calculations

The type curves can be used to calculate reservoir parameters such as permeability and apparent well bore radius. Data from the infinite acting portion of the type curve is used for these calculations. However points from both the infinite and pseudosteady state portion are needed for the best curve fitting.

5.4.1 Calculation of Transmissibility and Apparent Well Bore Radius

As previously derived:

$$kh = \frac{141.2\mu B}{(P_i - P_{wf})}\left(\ln\frac{r_e}{r_w} - \frac{1}{2}\right)\left(\frac{q_t}{q_{dD}}\right)_{match} \qquad 5.25$$

and apparent well bore radius is expressed as:

$$r_{wa}^{2} = \frac{0.00634k}{\phi\mu c_t \frac{1}{2}\left[\left(\frac{r_e}{r_{wa}}\right)^2 - 1\right]\left[\ln\left(\frac{r_e}{r_{wa}}\right) - \frac{1}{2}\right]}\left(\frac{t(days)}{t_{dD}}\right)_{match} \qquad 5.26$$

In each case $r_{eD} = r_e/r_{wa}$ is read from the type curve match.

For example:

If from the type curve match, r_e/r_{wa} is best represented by 50, q_{Dd} is 0.54, q_t is 10,000 BOPM (333 BOPD) and $\dfrac{(P_i - P_{wf})}{\mu B} = 7259$ from reservoir production data, then from equation above kh is 40.5 md-ft. Then knowing the thickness h, yields k.

Likewise if the corresponding time match points are t=10 months (300 days) and t_{Dd}=1.22 with r_e/r_{wa} = 50, and reservoir characteristics are porosity of 10.1%, viscosity of 1 cp and total compressibility of 20 x 10 -6 , and permeability is 0.33 md then the apparent well bore radius is: 1.042 feet.

5.4.2 Matching the PSS Portion for Calculation of N and Future Flow Rates

The drainage radius can then be calculated from the following expression:

$$r_e = r_{wa}\left(\frac{r_e}{r_{wa}}\right)_{match} \qquad 5.27$$

In the above example, with r_e/r_{wa} = 50 from the match of the transient portion of the curve, r_{wa} from the previous step = 1.042 then the drainage area is r_e = 52 feet.

The reserves in place can then be determined by the expression[4] (399)

$$N(well) = \frac{\pi r_e^2 h\phi(1 - Sw)}{5.615 B_{oi}} \qquad \textbf{5.28}$$

or by:

$$N = \frac{A\phi c_t h P_i}{5.615 B} \qquad \textbf{5.29}$$

5.4.3 Pseudosteady State Type Curve Matching for Reserve Estimates

Fetkovich type expressions can be adapted to determine initial reserves in place and forecast future flow rates. Then if we know the cumulative production, the remaining reserves in place can be calculated. Using a data set from the Fetkovich paper[3], the match (fig 5.5) followed the b=0.5 type curve.

Future producing rates can than be read directly from the real time scale on which the data are plotted. q_i and D_i can be determined from the match points and that data can be used to determine the reserves. The following match points were obtained:

q_t=1000 BOPM, q_{Dd}=0.033

Therefore:

$$q_{Dd} = 0.033 = \frac{q(t)}{qi} = \frac{1000BOPM}{q_i}$$

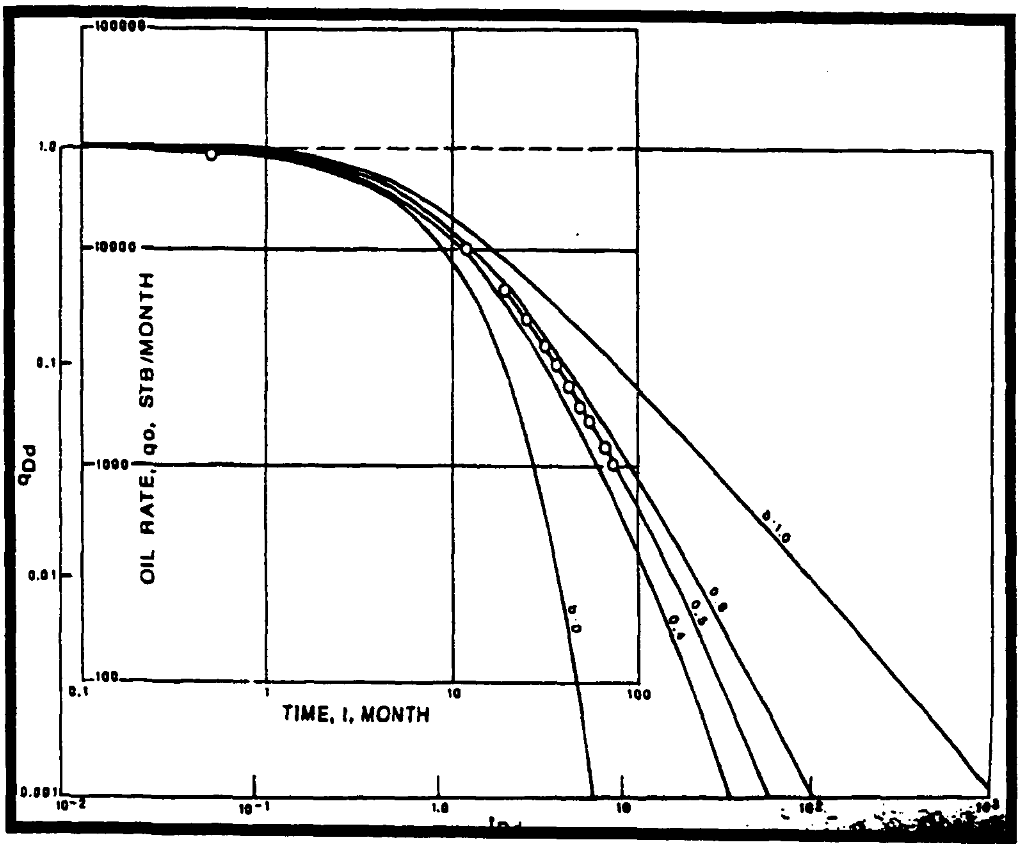

Figure 5.5 Type Curve Matching

therefore the initial production rate is:

$$q_i = 30{,}303 \text{ BOPM}$$

and the time match points were:

$$t_{Dd} = 12,\ t = 100 \text{ months}$$

therefore the initial decline rate is:

$$D_i = \frac{t_{Dd}}{t} = \frac{12}{100 months} = 0.12$$

Once the initial decline rate and initial production rate are known, the initial reserves in place can be calculated since the cumulative oil in place would be the integration of the initial flow rate expression:

$$N_p = \int_0^{t_p} q_t = q_i\left[1 + bD_i t\right]^{-\frac{1}{b}} \tag{5.30}$$

which yields the expression for the hyperbolic (0<b<1) expression for cumulative oil produced.

$$N_p = \frac{q_i^b}{(1-b)D_i}(q_i^{1-b} - q^{1-b}) \tag{5.31}$$

If the initial oil in place is defined as the cumulative oil produced to a reservoir pressure of zero, then the expression reduces to:

$$N_{pi} = \frac{q_i}{(1-b)D_i} \tag{5.32}$$

Therefore using the above match points along the b=0.5 curve we have:

$$N_{pi} = \frac{30{,}303_i}{(1-0.5) * 0.12} = 505{,}050$$

If the decline is exponential then the expression reduces even further. Alternate methods for calculating pore volume and thus reserves with a known initial oil saturation above and below the bubble point are presented in Appendix C. Methods of using the type curve matches for computing oil relative permeability are also presented in Appendix C.

5.4.4 Field Wide Application

According to Mathews[21], during pseudo steady state, the drainage volumes in a bounded reservoir are proportional to the rates of withdrawal from each drainage volume. Therefore the ratio q_i/N_{pi} will be identical for each well and, thus, the sum of the results from each well should give the same results as from analyzing the total lease or field production rate. Field experience often demonstrates how rapidly readjustments in drainage volumes can take place by changes in the production rate or depletion by offset wells. This of course assumes that the field is not stratified or separated by a fault or drastic anisotropy. The effect compartmentalization by permeability or stratification would be interesting to experiment with in the future.

5.5 Extensions of Fetkovich Radial Type Curves to Other Reservoirs Shapes and Well Positions

5.5.1 Introduction

It is not well known that the Fetkovich Type Curves are based on a strictly radial system operating above the bubble point with the well centrally located. It is obviously desirable to derive a more general case that would apply to any particular reservoir drainage shape such as rectangular, triangular, and reservoirs in which the well is displaced from the reservoir center. It would also be desirable to modify the curves for cases below the bubble point and extract information from that deviation from the strictly exponential case. In the radial case, the transition from infinite acting to pseudosteady state is almost instantaneous. However in a non-radial reservoir the transition from infinite to pseudosteady state is prolonged. Significant error in type curve matching may result from using the radial form. In low permeability formations rapidly declining transient production can be confused with depletion and an attempt to fit the transient data to the depletion portion of the type curve will result in Arps "b" values that are unrealistically high. It is therefore desirable to properly define the full shape of the type curve over the transient and depletion period properly apply the techniques and analysis.

This method. shown in this section and fully derived in Appendix E utilizes shape factors derived for these various conditions such as shown in Earlouger's Table C-1 *in Advances in Well Testing*[22]. Application of these factors to the Fetkovich system is neither direct nor straightforward. A system was derived that will incorporate all reservoir shapes, positions and later will be applied to vertically fractured and horizontal wells using an equivalent well bore radius concept. The complete derivation is shown in Appendix E.

5.5.2 Overview of Derivation

Recall that the productivity and decline theory of the previous section Fetkovich defined q_{Dd} as:

$$q_{Dd} = \frac{q(t)}{q_{i\max}} = \frac{141.3\mu Bq(t)}{kh(P_i - P_{wf}}\left[\ln\frac{r_e}{r_w} - \frac{1}{2}\right] = q_D\left[\ln\frac{r_e}{r_w} - \frac{1}{2}\right] = q_D c_1 \qquad 5.33$$

In a similar manner the dimensionless time t_{Dd} was defined as:

$$t_{Dd} = \left[\frac{q_{i\max}}{N_{pi}}\right]t = D_i t = \frac{0.00634kt}{\phi\mu c_t r_w^2}\left[\frac{1}{\frac{1}{2}\left[\left(\frac{r_e}{r_w}\right)^2 - 1\right]\left[\ln\left(\frac{r_e}{r_w}\right) - \frac{1}{2}\right]}\right] = t_D\left[\frac{1}{\frac{1}{2}\left[\left(\frac{r_e}{r_w}\right)^2 - 1\right]\left[\ln\left(\frac{r_e}{r_w}\right) - \frac{1}{2}\right]}\right] \qquad 5.34$$

or:

$$t_{dD} = t_D \frac{2}{c_1 c_2} \qquad 5.35$$

Now instead of using the radial form one begins with a more general equation in terms of the shape factors and drainage area A such as that found on page 243 in Craft and Hawkins[6] so that:

$$q(t) = \frac{kh(\overline{P}_R - P_{wf})}{162.6\mu B}\left[\log\frac{4A}{1.781C_A r_w^2}\right] \qquad 5.36$$

Then applying the Fetkovich definition above and converting constants to Fetkovich's definitions of q_D:

$$q_{Dd} = \frac{q(t)}{q_{i\max}} = q_D\left[1.151\left[\log\frac{4A}{1.781C_A r_w^2}\right]\right] = \frac{141.3\mu Bq(t)}{kh(P_i - P_{wf}}\left[1.151\log\frac{4A}{1.781C_A r_w^2}\right] \qquad 5.37$$

Or condensing notation:

$$q_{Dd} = q_D\left[1.151\left[\log\frac{4A}{1.781C_A r_w^2}\right]\right] = q_D(1.1511c'_1) \qquad \textbf{5.38}$$

where c'_1 is:

$$c'_1 = \log\frac{4A}{1.781C_A r_w^2} \qquad \textbf{5.39}$$

The equivalent Fetkovich form was:

$$q_{Dd} = q_D\left[\ln\frac{r_e}{r_w} - \frac{1}{2}\right] = q_d c_1 \qquad \textbf{5.40}$$

Where c_1 was:

$$c_1 = \left[\ln\frac{r_e}{r_w} - \frac{1}{2}\right] \qquad \textbf{5.41}$$

Likewise the dimensionless time decline can be derived in a manner similar to that of Fetkovich but in terms of the reservoir shape and drainage size factors:

$$t_{Dd} = \left[\frac{q_{i\max}}{N_{pi}}\right]t = D_i t \qquad \textbf{5.42}$$

where :

$$q_{t\max} = \frac{khP_t}{162.6\,\mu B}\left[\frac{1}{\log\dfrac{4A}{1.781C_A r_w^2}}\right] \qquad 5.43$$

and :

$$N_t = \frac{A\phi c_t h P_t}{5.615B} \qquad 5.44$$

and applying the definition of t_{Dd} and converting constants:

$$t_{Dd} = \frac{q_{t\max}}{N_t}t = \frac{0.00634kt}{\phi\mu c_t A}\left[\frac{5.44678}{\log\dfrac{4A}{1.781C_A r_w^2}}\right] \qquad 5.45$$

$$t_{Dd} = \frac{0.00634kt}{\phi\mu c_t r_w^2}\frac{r_w^2}{A}\left[\frac{5.44678}{\log\dfrac{4A}{1.781C_A r_w^2}}\right] = t_D\frac{r_w^2}{A}\left[\frac{5.44678}{\log\dfrac{4A}{1.781C_A r_w^2}}\right] \qquad 5.46$$

or putting in a similar arrangement to that of the Fetkovich radial form:

$$t_{Dd} = \frac{t_D}{\dfrac{A}{r_w^2}\dfrac{\log\dfrac{4A}{1.781C_A r_w^2}}{5.44678}} = \frac{t_D}{\dfrac{0.183594A}{r_w^2}\log\dfrac{4A}{1.781C_A r_w^2}} = \frac{t_D}{0.183594(c_1^{'}c_2^{'})} \qquad 5.47$$

Where $c_2^{'}$ is:

$$c_2^{'} = \frac{A}{r_w^2} \qquad 5.48$$

As compared to c_2 in the Fetkovich radial case:

$$c_2 = \frac{r_e}{r_w^2} - 1 \qquad 5.49$$

And:

$$c_1^{'} = \log \frac{4A}{1.781 C_A r_w^2} \qquad 5.50$$

Again comparing this to the Fetkovich equivalent forms one notes the similarities:

$$c_1 = \ln \frac{r_e}{r_w} - \frac{1}{2} \qquad 5.51$$

The complete derivation of the more general shape and well location case is shown in the Appendix E.

Now if the drainage area can then be expressed in terms of the equivalent radial system $r_{eD}=r_e/r_w$ then the published values of q_D and t_D can be converted directly to decline dimensionless terms for any drainage shape and can also be extended to fractured vertical wells and horizontal wells as will be demonstrated. Therefore define the equivalent drainage area for the radial system as:

$$A=\pi(r_e^2-r_w^2)=\pi r_e^2-\pi r_w^2 \qquad \textbf{5.52}$$

and rearranging:

$$\frac{A}{r_w^2}=\pi\left(\frac{r_e}{r_w}\right)^2-\pi=\pi\left(\left(\frac{r_e}{r_w}\right)^2-1\right) \qquad \textbf{5.53}$$

Therefore using the radial solutions to q_D and t_D at the various $r_{eD}=r_e/r_w$ values and the new constants $c_1^{'}$ and c_2^{1} we can find equivalent expressions in terms of A/r_w^2 and the various shape factors.

Decline curve construction using the shape factor approach has confirmed that when the circular shape factor is used, the above derivation is identical to the Fetkovich radial form. Figure 5.6 is the equivalent radial form using the above derivation with the centrally located circular shape factor A = 31.62. It is identical to the Fetkovich radial solution in figure 5.2. Tabular data for all rectangular comparisons from equations above are provided in the appendix D. Shape Factors are shown in Table 5.1. These shape factors are used for the transition and depletion portions of the type curve. The infinite portion retains the radial form without shape factor adjustment. The change to shape factors is valid for $t_{DA}=\frac{r_w^2}{A}$ greater than 0.025 for a rectangular shape factor of x:y = 2:1 and 0.01 for a rectangular shape factor of x:y = 4:1. This corresponds to a t_{Dd} range from 0.4 to 0.2 on the generalized type curves in the transition and depletion area.

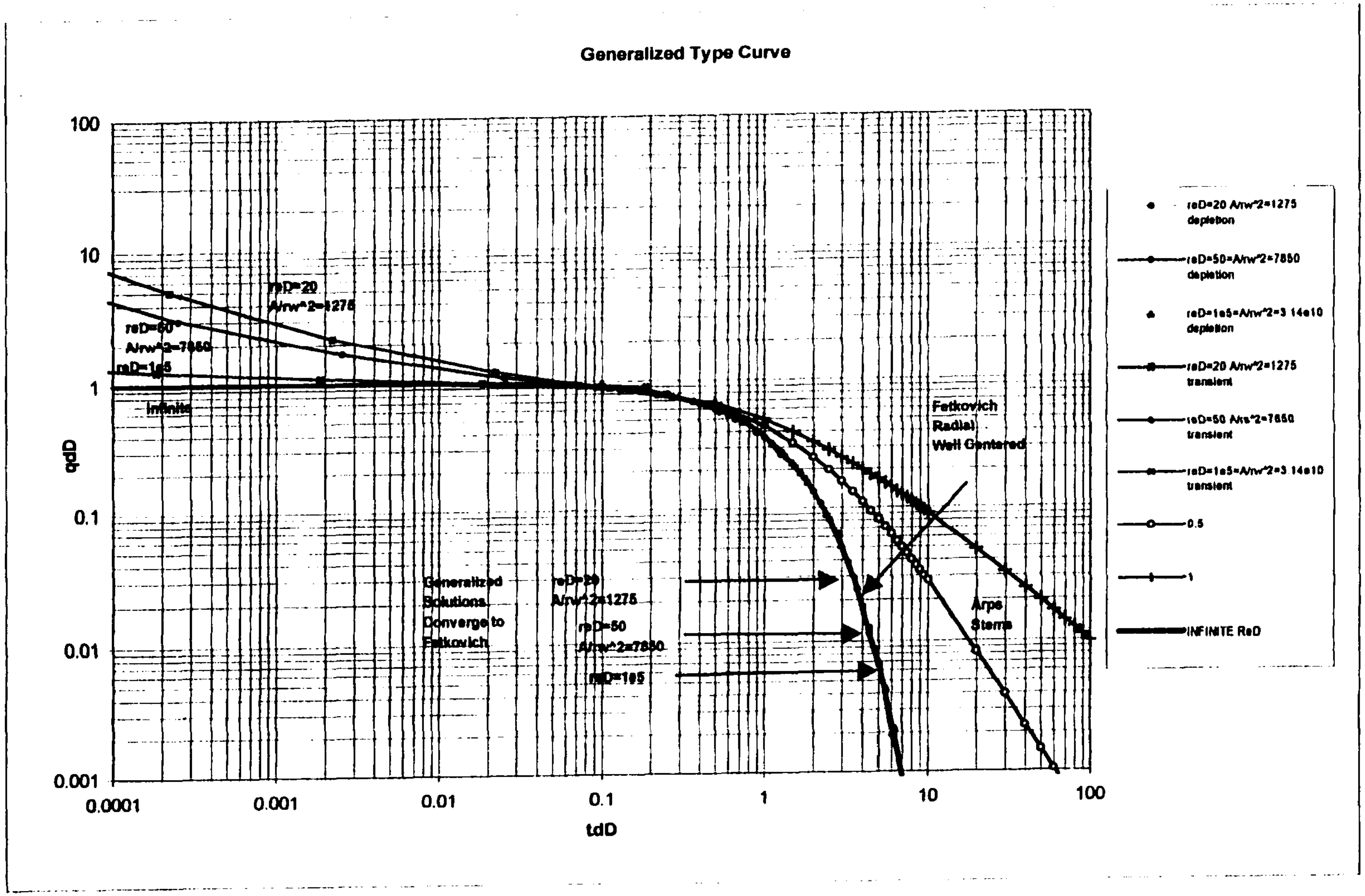

Figure 5.6 Generalized Type Curve -Circular Shape Factor, Well Centered, CA=31.62

N BOUNDED RESERVOIRS	C_A	< 1% error t_{DA} >	
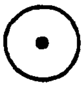	31.62	0.06	0.10
	31.6	0.06	0.10
	27.6	0.07	0.09
	27.1	0.07	0.09
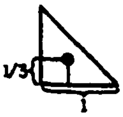	21.9	0.12	0.08
	0.098	0.60	0.015
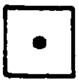	30.8828	0.05	0.09
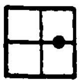	12.9851	0.25	0.03
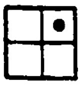	4.5132	0.30	0.025
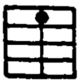	3.3351	0.25	0.01
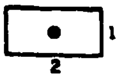	21.8369	0.15	0.025
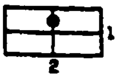	10.8374	0.15	0.025
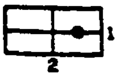	4.5141	0.50	0.06
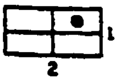	2.0769	0.50	0.02

Table 5.1

Shape Factors for Use in Generalized Decline Curves[22]

Thus the dimensionless decline type curves can now be generated for any drainage shape and well bore position if a shape factor is available. Shape factors are available for a wide range of reservoir situations. For instance the shape factor C_A is 31.62 for a circle, 30.8828 for a square, 21.8369 for a rectangle of dimensions $x_e/y_e=1/2$, and 5.379 for a rectangle of dimensions $x_e/y_e=1/4$. These various shape and well location factors C_A are reproduced in Table 5.1[22].

The decline curves have been presented in terms of A/r_w^2 or alternatively sqrtA/r_w and the equivalent $r_e/r_w=r_{eD}$. A/r_w^2 seems more appropriate for rectangular reservoir shapes. During the transient period the radial solution would still be used as the reservoir boundaries have not yet affected the drainage. However the transient period can be very short with some reservoir shapes with wells near the boundary as will be shown. As the reservoir boundaries are felt a transition period will occur before pseudosteady state is observed. It is this early transition zone that will indicate deviation from radial system and the portion that is most pertinent to this generalized shape method. Theoretically it should be possible to extract reservoir shape information from deviation from radial dimensionless decline curves.

If the well bore radius is small compared to the reservoir size then the area can be approximated by:

$$A \approx \pi r_e^2 \therefore \frac{A}{r_w^2} = \pi \frac{r_e^2}{r_w^2} \quad 5.54$$

or upon rearranging:

$$r_{eD} = \frac{r_e}{r_w} = \frac{\sqrt{A}}{\sqrt{\pi} r_w} \quad 5.55$$

This provides the solution in terms more similar to the Fetkovich type curves. However the more exact solution is necessary when considering horizontal wells since one can define the horizontal well in terms of an apparent well bore radius.

Figures 5.7 and 5.8 show the dimensionless decline curve results of applying the above relationships for a rectangle of dimensions x_e/y_e =0.5 and x_e/y_e =0.25 respectively. Figure 5.9 shows the case where the C_A value is very small in a rectangular reservoir with the well close to the boundary (C_A=10.8374). Notice how the transition zone from infinite to finite acting has shifted to the left as the time to PSS has decreased. Also notice that for small values of r_{eD} such as 50, the infinite and finite solutions do not converge as well. The difference between a rectangle of dimension ration 2 to 1 is not easily distinguished from the radial solution. The method is most useful when the geometry departs significantly from radial or the well is close to a boundary. Reservoir parameters can then be calculated from the type curve match points in the usual way.

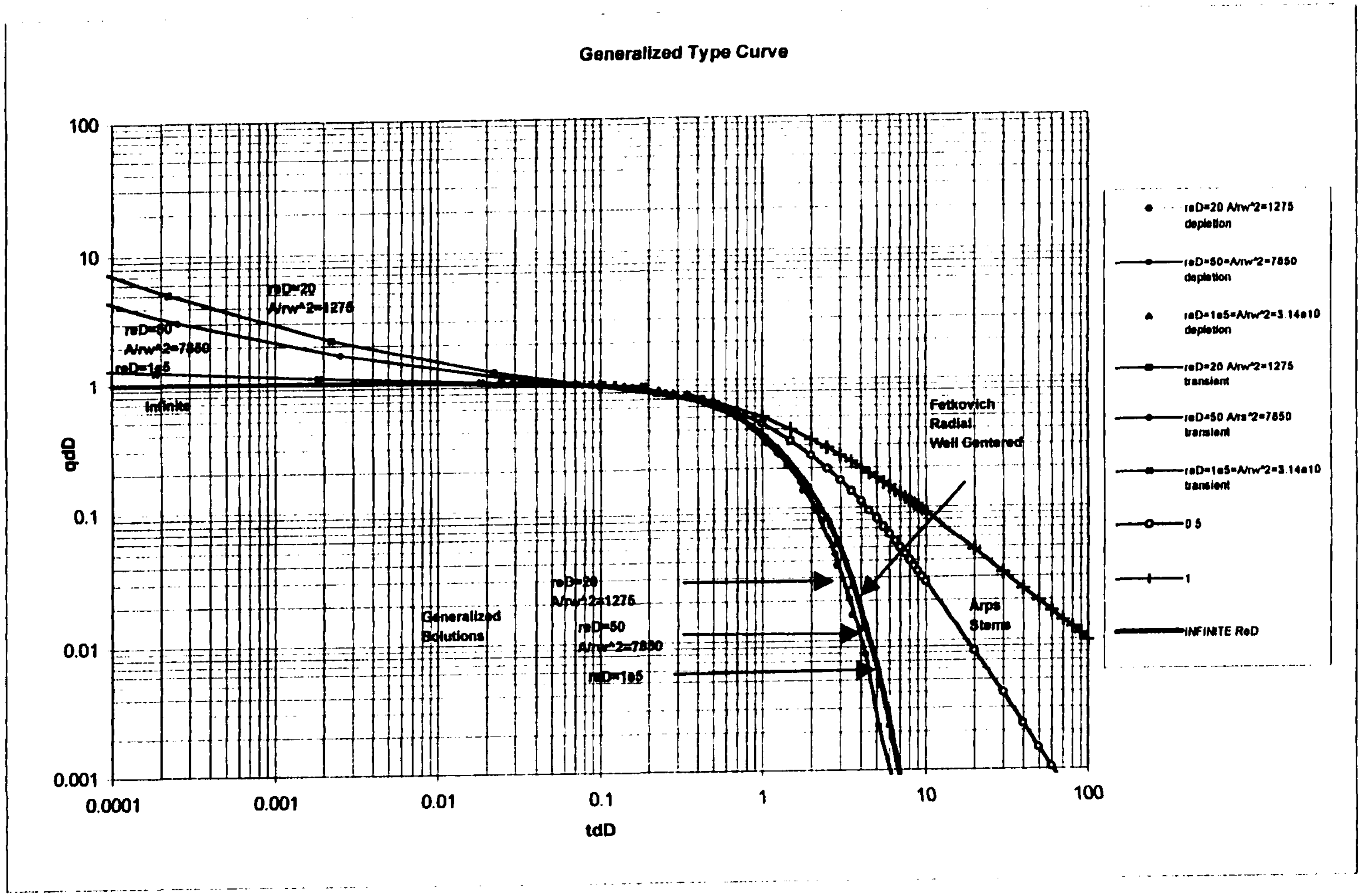

Figure 5.7 Generalized Type Curve -Rectangualar Shape Factor x:y 2:1 Offcenter close to boundary, CA=10.374

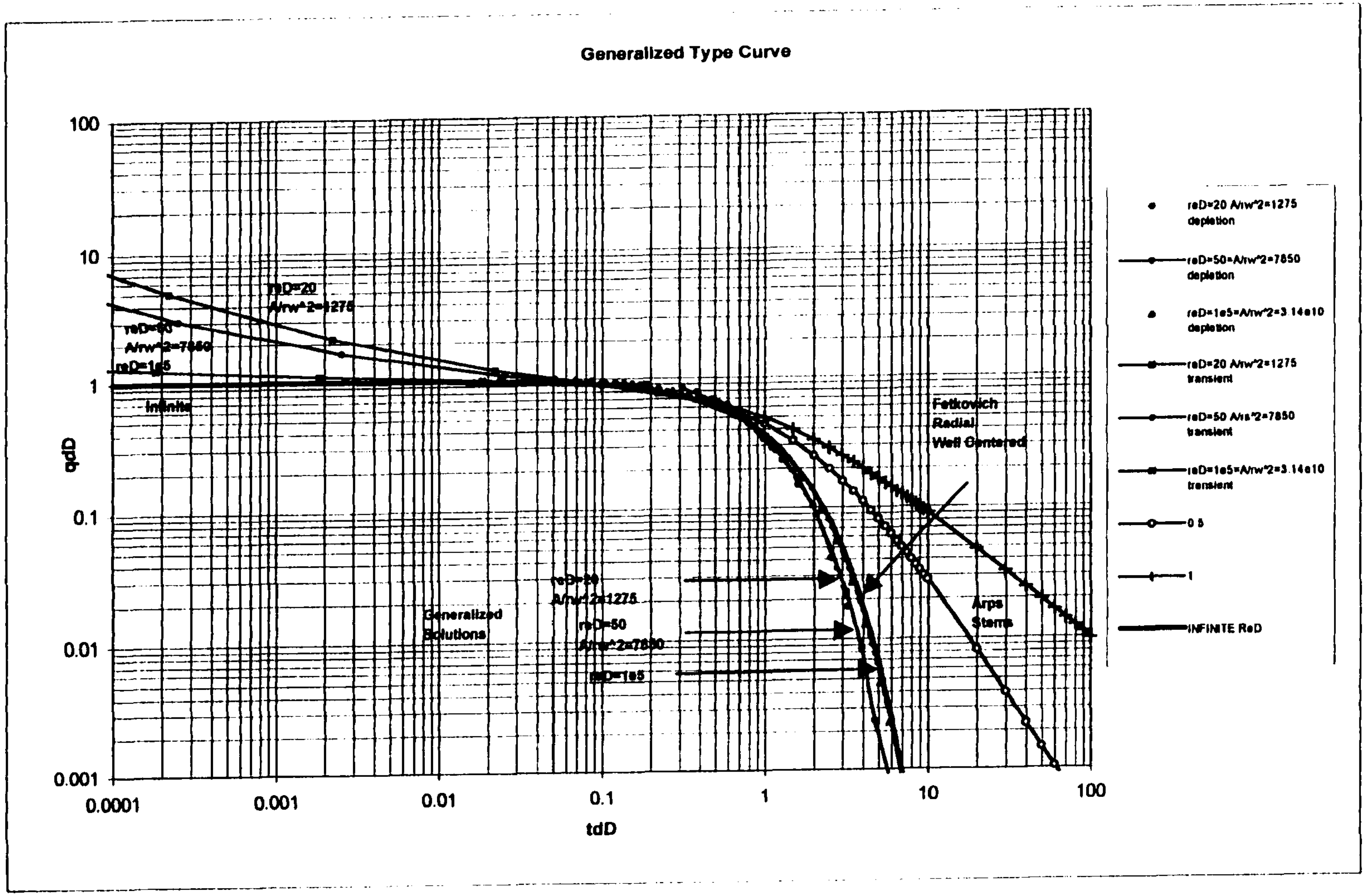

Figure 5.8 Generalized Type Curve -Rectangualar Shape Factor x:y 4:1 Well Centered, CA=5.3790

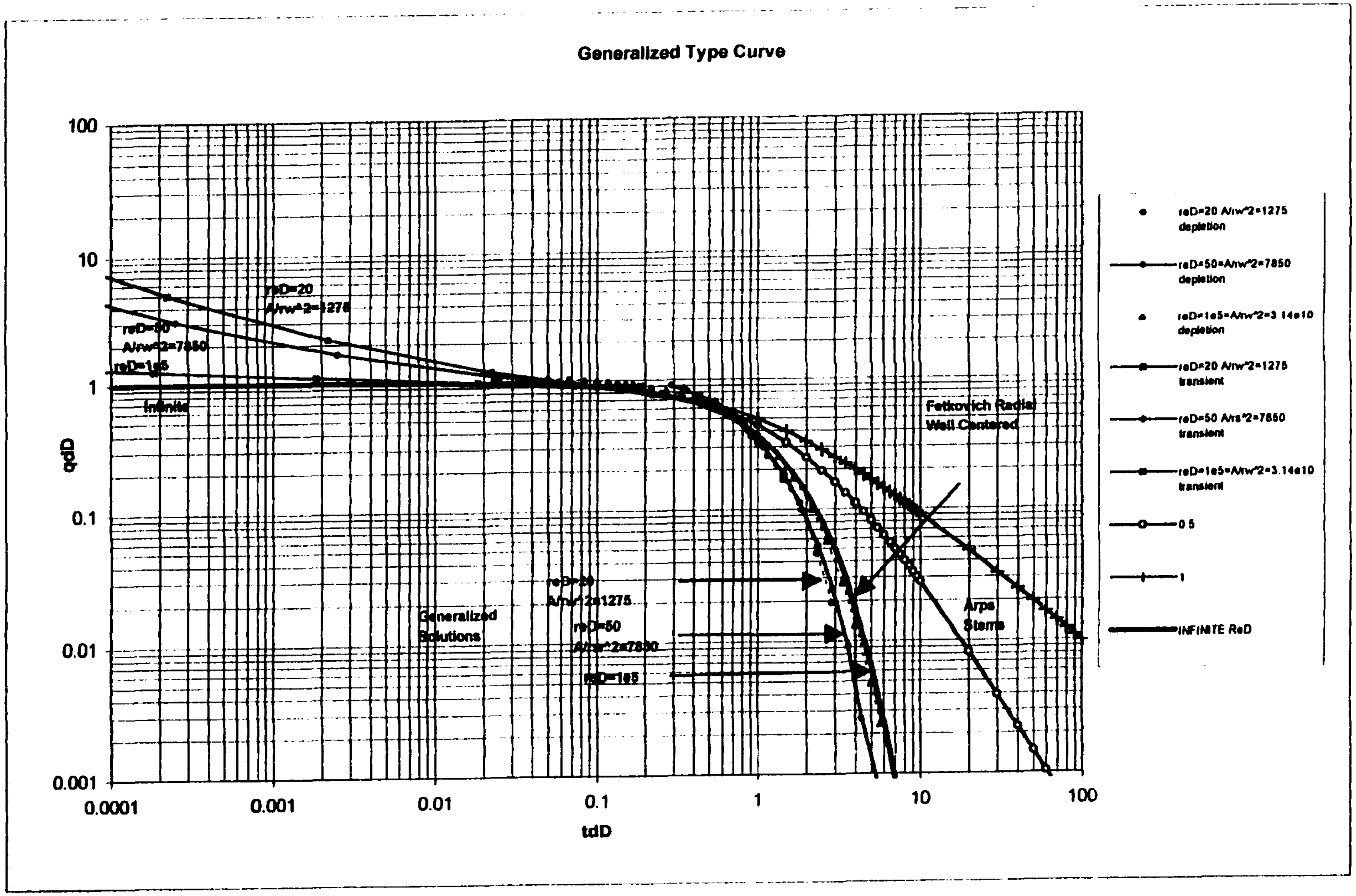

Figure 5.9 Generalized Type Curve -Rectangualar Shape Factor x:y 4:1 Offcenter close to boundary, CA=2.6896

5.5.2.1 Use in Calculating Reserves and Reservoir Parameters

The transmissibility (kh) and permeability (if reservoir thickness is known) can be computed by solving the my dimensionless decline equation for kh and using the match point:

$$q_{Dd} = q_D\left[1.151\log\frac{4A}{1.781C_A r_w^2}\right] = \frac{141.3\mu Bq(t)}{kh(P_i - P_{wf})}1.151\log\frac{4A}{1.781C_A r_w^2} \qquad 5.56$$

and solving for kh:

$$kh = \frac{141.3\mu B}{P_i - P_{wf}}1.151\log\frac{4A}{1.181C_A r_w^2}\left(\frac{q(t)}{q_{Dd}}\right)_{match} \qquad 5.57$$

Since we know A/r_w^2, the match point, and the shape factor we can compute kh for the particular reservoir conditions.

The apparent well bore radius, drainage area and initial reserves can then be computed from the dimensionless decline parameter t_{Dd} and the match points. Ultimate reserves are then computed from the difference between initial reserves and cumulative reserves. r_{wa} is computed from the following relationship derived for the more general shape factor form:

Since t_D is defined before as:

$$t_{Dd} = \frac{t_D}{\dfrac{0.183594A}{r_w^2}\log\dfrac{4A}{1.781C_A r_w^2}} \qquad \textbf{5.58}$$

Now inserting the definition of t_D:

$$t_D = \frac{0.0063kt}{\phi\mu c_t r_{wa}^2} \qquad \textbf{5.59}$$

Solving the dimensionless time equation for r_{wa}^2:

$$r_{wa}^2 = \frac{0.00634k}{\phi\mu c_t \dfrac{A}{r_w^2}\left(\dfrac{\log\dfrac{4A}{1.781C_A r_w^2}}{5.44678}\right)}\left(\frac{t}{t_{Dd}}\right)_{match} \qquad \textbf{5.60}$$

We know the ratio A/r_w^2 and t/t_{Dd} from the type curve match points therefore we can compute the apparent well bore radius, r_{wa}. This apparent well bore radius will be used later.

Now since we know r_{wa} we can calculate the drainage area A since from knowing A/r_w^2 from the type curve match and computing r_w^2 we can solve for the drainage area A by:

$$A = r_{wa}^2 \left(\frac{A}{r_{wa}^2} \right)_{match} \quad \textbf{5.61}$$

This allows for the computation of the original reserves in place from the relationship:

$$N = \frac{A \phi c_t h P_i}{5.615 B} \quad \textbf{5.62}$$

5.5.2.2 Use in Determining Contributions of Solution Gas Energy and Mobility Function

The decline path will be exponential where b=0 and the Fetkovich solutions converge when the only reservoir energy is the compressibility of the rock and fluid. In a solution gas reservoir where water drive is absent the decline path will be more hyperbolic where b values of 0 to 0.5 exist. This deviation from b=0 can give information that can be used in determining the mobility-pressure function that was described in chapter 3 and the appendix C. This concept can be shown in the following figure 5.10.

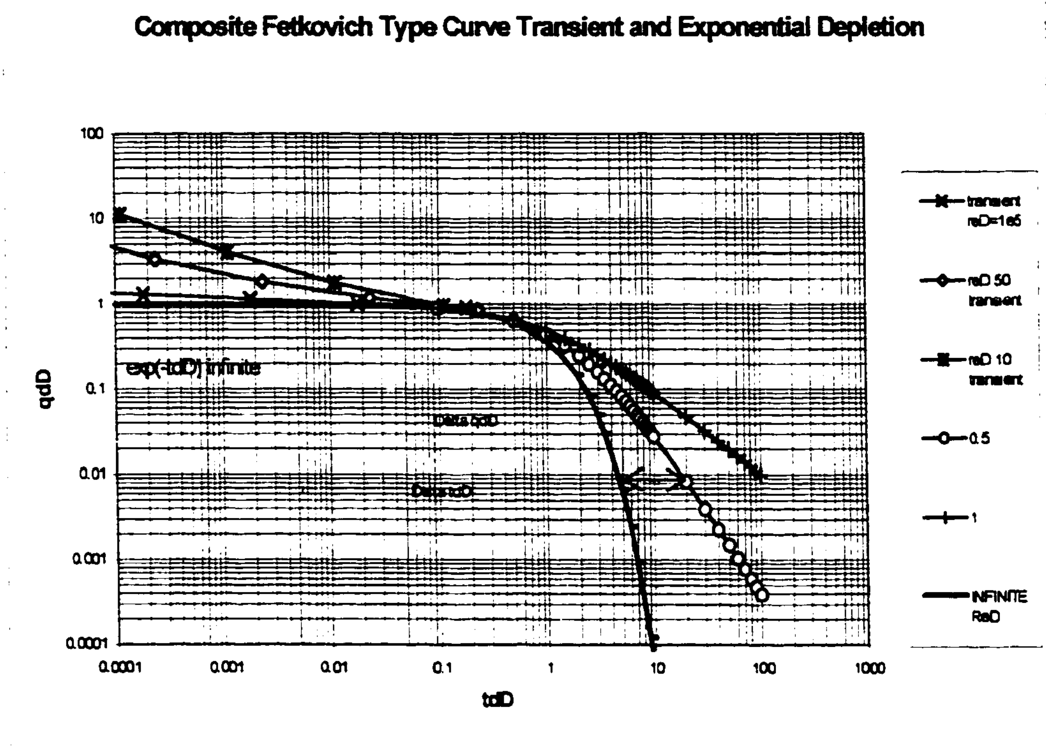

Figure 5.10 Compsite Fetkovich Type Curve

Where Δq_{Dd} represents the difference from the actual path and that predicted with no energy in the system other than the fluid and rock compressibility. The solution gas provides additional pressure support that more than offsets the increased resistance from the reduction in $k_{ro}/(\mu_o B_o)$ with a reduction in pressure and oil saturation. Also with a purely exponential decline with no additional drive energy, the IPR will be constant with declining pressure. Field experience indicates that the IPR does change with depletion since exponential depletion is rare. Once the decline path is known from the above chart, the difference between the decline path and the predicted exponential path should give information about the pressure mobility function and adjustments to IPR over time without the need for well testing techniques.

$$\int \frac{k_{ro}}{\mu_o B_o} dp \cong \frac{(P_R - P_{wf})k_{ro}}{(\mu_o B_o)_{P_{aw}}} \qquad 5.63$$

Some of these ideas as well as some methods for estimating the relative permeability to oil are discussed in more detail in the guide to reservoir parameters in appendix C.

5.5.3 Extension to Fractured Wells

Fetkovich showed an example, which indicated that the "Arps b" value in pseudosteady state condition did not change with a fractured well but the r_{eD}=re/r_{wa} did shift to a smaller match ratio. He used type curves to indicate that the reserves increased as a result of the increase in the effective well bore radius and the resulting shift of the curve to lower values of $r_{eD}=r_e/r_{wa}$. But reserves do not seem to increase in direct proportion to the increase in producing rate as a result of the treatment. He did not derive a relationship to account for these conditions. However if the effective or apparent well bore radius can be calculated after fracture stimulation then the same curves can be used.

As with the dimensionless pressure evaluation of reservoirs that have been fracture stimulated, the A/r_w^2 term can be replaced by x_e^2/x_f^2 or by A/x_f^2 in the equations in the previous section and the same type of analysis could be applied as for the vertical well. Alternatively the fractured well approximations could be used to generate the q_D and t_D terms as follows:

$$q_D = \frac{1}{P_D} = \frac{1}{2\pi t_{DA} + \dfrac{1}{2\left[\ln\left(\dfrac{x_e}{x_f}\right)^2\right] + \dfrac{1}{2}\dfrac{2.2458}{C_A}}} \qquad 5.64$$

for the pseudosteady state portion and :

$$q_D = \frac{1}{P_D} = \frac{1}{\left[2\pi t_{DA} + \left[\dfrac{1}{2\left[\ln\left(\dfrac{x_e}{x_f}\right)^2\right] + 0.80907}\right]\right]} \qquad 5.65$$

for the transient portion. The Fetkovich type curves can then be plotted using the standard relationship adjusted for the differences in t_{DA} and t_D:

$$q_{Dd} = q_D\left[1.15\log\left(\frac{4A}{1.781C_A x_f^2}\right)\right] \qquad 5.66$$

and

$$t_{Dd} = \frac{t_D}{\left(\frac{A}{x_f^2}\right)\frac{\log\frac{4A}{1.781C_A x_f^2}}{5.44678}} \qquad 5.67$$

where t_D is related to t_{DA} by:

$$t_{DA} = t_D\frac{x_f^2}{A} or \frac{x_f^2}{x_e^2} \qquad 5.68$$

Appropriate decline dimensionless graphs can then be easily generated. The following table 5.4 for vertical fractured wells gives the shape factors for variations in reservoir shape and size. These tabular values are a compilation of various experiments, Table C.1 values of Earlougher[22] (modified) and Joshi[23] Table 7-3.

C_f	x_e/y_e					
x_f/x_e	1	2	3	5	10	20
0.1	2.020	1.4100	0.751	0.2110	0.0026	0.000005
0.3	1.820	1.3611	0.836	0.2860	0.0205	0.000140
0.5	1.600	1.2890	0.924	0.6050	0.1179	0.010550
0.7	1.320	1.1100	0.880	0.5960	0.3000	0.122600
1.0	0.791	0.6662	0.528	0.3640	0.2010	0.106300

Table 5.2 Correction Factors for Reservoir Shapes

Therefore the type curves can be generated for any rectangular reservoir shape and fracture penetration ratio using the methods developed in the previous sections. .

5.6 Normalization Techniques

Flowing bottomhole pressure may vary simultaneously with production rate. If the pressure varies in a smooth manner, rate decline can be treated with a constant pressure type curve if the rate used in the curve is normalized by pressure drop according to the relationship:

$$q_n = \frac{q_o(t)}{\left[P_i - P_{wf}\right]} \qquad 5.69$$

Strictly speaking normalization should only be used during the infinite acting period. Golan and experience show that this use after the onset of PSS does not cause a problem since simultaneous pressure and rate decline usually stabilizes to a constant pressure condition before PSS state condition is reached. Normalization can not be used when flowing pressure changes stepwise. Superposition is used then. This normalization process will be extended in the horizontal well technique sections.

5.7 Derivative Methods

In the previous chapter the Fetkovich type curves were generated using the solutions of VanEverdingen and Hurst. This section attempts to derive and use the derivative type curves for both the vertical and horizontal well cases. The use of derivative curves for pressure transient analysis is not new. Tiab[24,25,26] , Bourdet etc presented derivative type curves and direct synthesis techniques for pressure analysis. These methods typically involve the log-log plot of the derivative of a dimensionless pressure or group of terms vs. dimensionless time or a group of terms involving time. The derivative techniques often have more curvature and definition and thus it is easier to obtain unique characteristic type curve matches. However because of the noisy nature of production data derivative curves have had limited usefulness. Nevertheless for the sake of completeness the derivative type curves should be presented.

Decline analysis utilizes flow rate or cumulative production vs. time rather than pressure. Of course the dimensionless pressure P_D is simply the reciprocal of dimensionless rate q_D with a constant applied. Production rate data are much more difficult to uniquely match since conditions are not always ideal. Common data problems are related to such things as well shut-in periods, variations in well bore flowing pressures, mechanical problems, workovers, and erratic daily production recording. It is possible that rate derivative techniques may help in decline analysis using the methods of Fetkovich. Therefore the following methods are presented.

5.7.1 Closed boundary Case

The derivative of VanEverdingen and Hurst's relationships of sections 5.3.1 and 5.3.2 are given as:

$$\frac{\partial q_D}{\partial t_D} = -2 \sum_{a_1, a_2, etc.}^{\infty} \left[\frac{a_n^2 e^{-a_n^2 t_D} J_1^2(a_n, r_{eD}}{J_0^2(a_n) - J_1^2(a_n, r_{eD})} \right] \qquad 5.70$$

Recalling from the previous section that Fetkovich defined the parameters from conversion from dimensionless to type curve dimensionless using the following:

$$A = \frac{1}{\left[\ln\frac{r_e}{r_{wa}} - \frac{1}{2}\right]} \qquad 5.71$$

and :

$$B = \frac{2A}{\left(\frac{r_e}{r_{wa}}\right)^2 - 1} = \frac{1}{0.5\left[\left(\frac{r_e}{r_{wa}}\right)^2 - 1\right]\left[\ln\frac{r_e}{r_{wa}} - 0.5\right]} \qquad 5.72$$

It should be possible to easily convert the derivative of the closed boundary case to type curve dimensionless form since:

$$q_{Dd} = \frac{q_o}{q_{oi}} = \frac{q_D}{A} \qquad 5.73$$

so that :

$$\frac{\partial q_{Dd}}{\partial t_{Dd}} = q'_{Dd} = \frac{\partial q_D}{\partial t_D}\left[\frac{1}{A}\right] = \frac{\partial q_D}{\partial t_D}\left[\ln\frac{r_e}{r_{wa}} - \frac{1}{2}\right] \qquad 5.74$$

Likewise from the previous relationship:

$$t_{Dd} = Dt = Bt_D \qquad 5.75$$

$$t_{Dd} = \frac{t_D}{\frac{1}{2}\left[\left(\frac{r_e}{r_{wa}}\right)^2 - 1\right]\left[\ln\frac{r_e}{r_{wa}} - \frac{1}{2}\right]} \qquad 5.76$$

It is customary to multiply the derivative by t_{Dd} for plotting at the same time scale as the traditional q_{dD} vs. t_{dD} plots for comparison. Therefore the form used in the analysis is:

$$q^{\cdot}_{Dd} * t_{Dd} = -q^{\cdot}_{D} * t_D * \left[\ln \frac{r_e}{r_{wa}} - \frac{1}{2} \right] \quad 5.77$$

5.7.2 Construction of the Derivative Dimensionless Decline Curves

A computer program was written to compute the derivative as well as the q_D values from the VanEverdingen and Hurst relationships. This is done for the radial and then converted to the more general formulation for all reservoir shapes by the application of the appropriate shape and position terms.

Figure 5.11 shows the construction of the transient portion of the curve from the derivative of the radial solutions for various r_{eD} values. Figure 5.12 shows the dimensionless decline rate derivative $q^{\cdot}_{Dd}$ plot. And figure 5.13 shows the dimensionless decline rate derivative $q^{\cdot}_{Dd}$ in the transient region multiplied by t_{Dd} for plotting purposes. Tabular data from the program generated values that are included again in Appendix D.

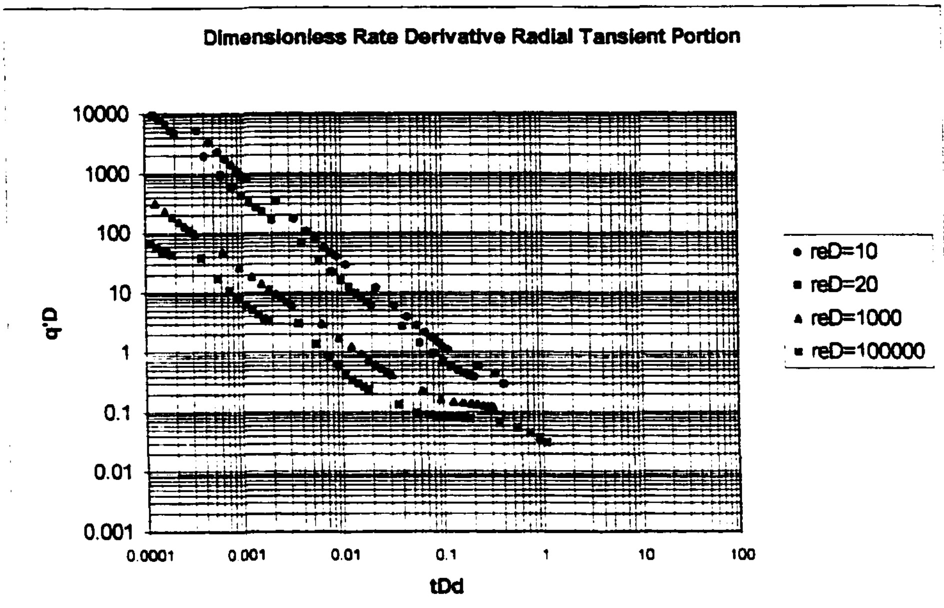

Figure 5.11 Dimensionless Rate Derivative Radial Transient Portion

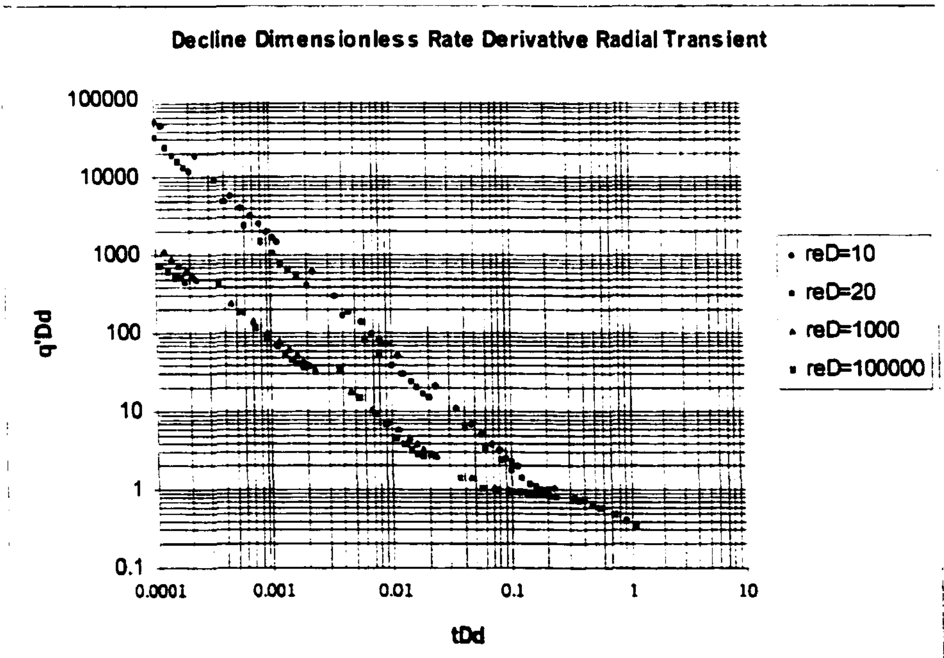

Figure 5.12 Derivative Decline Type Curve Radial Case

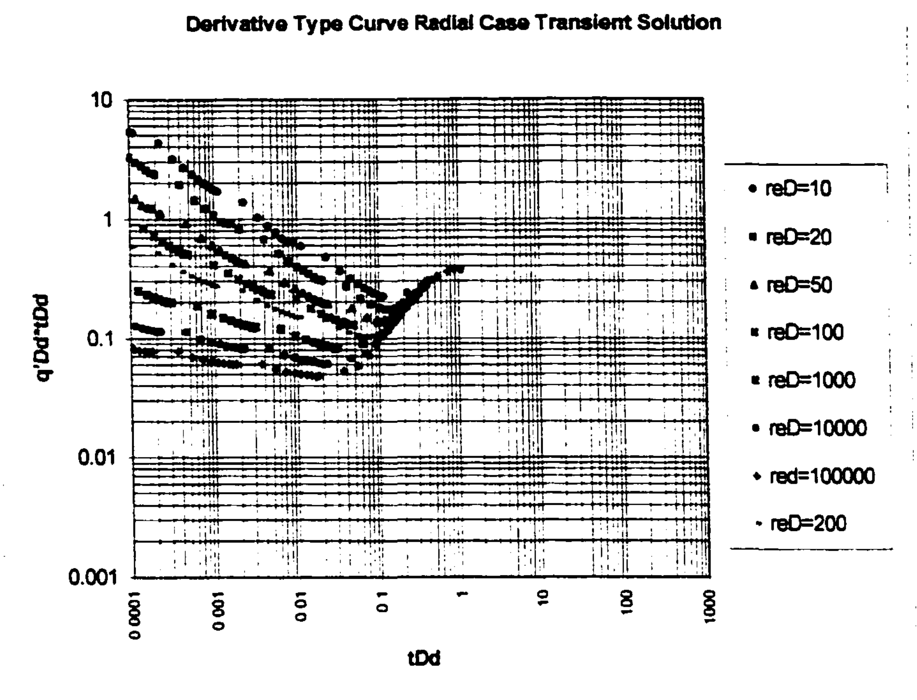

Figure 5.13 Decline Dimensionless Rate Derivative Transient

The depletion portion of the derivative dimensionless decline curve can be constructed by simply differentiating the Arps equations for exponential, hyperbolic and harmonic declines. Therefore the following expressions give the derivatives of the Arps expressions:Exponential:

$$\frac{\partial q_{Dd}}{\partial t_{Dd}} = -\frac{1}{e^{t_D}} \qquad 5.78$$

Hyperbolic:

$$\frac{\partial q_{Dd}}{\partial t_{Dd}} = -\frac{1}{\left(1+bt_{Dd}\right)^{\frac{1}{b}+1}} \qquad 5.79$$

Harmonic:

$$\frac{\partial q_{dD}}{\partial t_{Dd}} = -\frac{1}{\left(1+t_{Dd}\right)^2} \tag{5.80}$$

These expressions are easily computed in a spreadsheet and displayed in figure 5.13 for the depletion portion of the dimensionless derivative decline type curve. The transient and depletion curves are then combined into one graph as shown in figure 5.14. Again notice that the expressions are multiplied by the dimensionless decline time for plotting purposes. Although the data are rather noisy, the depletion and transient portions converge at about time 0.1.

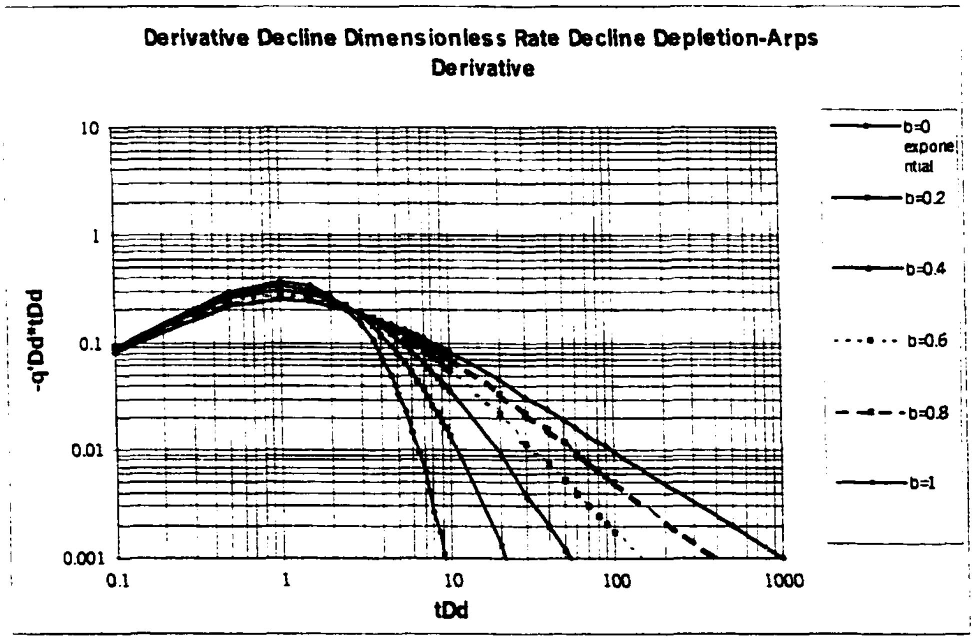

Figure 5.14 Arps Derivative Decline Dimensionless Rate Decline

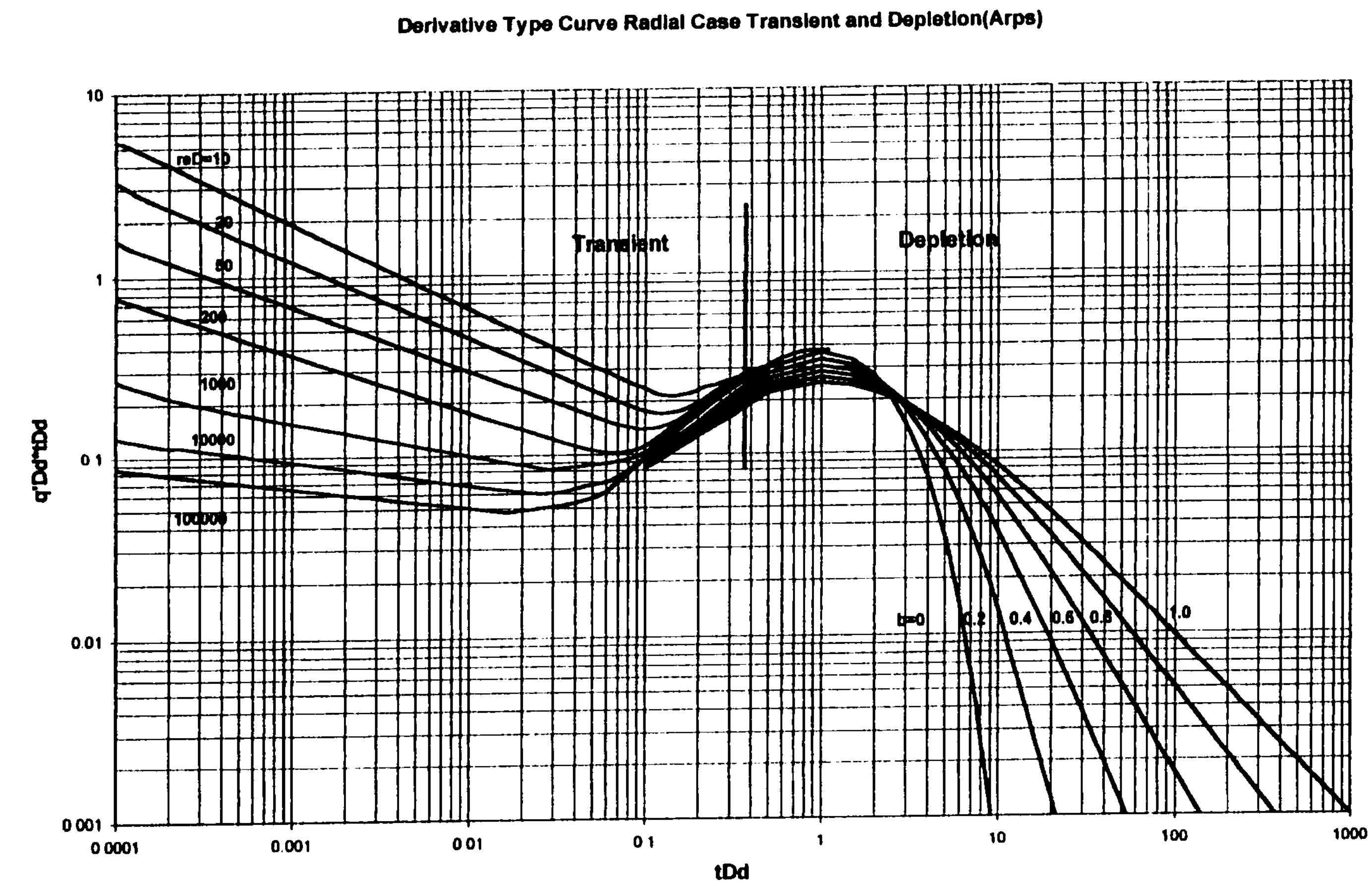

Figure 5.15 Compsosite Dimensionless Decline DerivativeType Curve - Transient and Depletion

5.7.3 Extension to Other Reservoir Shapes

The above construction can be extended to the other reservoir shapes by application of my methods from section 5.6. As the data are so noisy for even the radial case this has not been done in this research. However the extension is straightforward.

5.7.4 Use of the Derivative Curves in Reservoir Analysis

The use of the type curve in reservoir analysis was done in the previous sections. This section will explain the use of the derivative in the analysis. Limited success has been found in using derivatives for decline curve analysis. The derivative type curves primary use as an aid in picking the proper r_{eD} and b curves for decline curve matching. This is done by first converting the field production data to a derivative and then matching to the derivative type curve.

The first step is to compute the numerical derivative of the production data using a derivative approach such as the three-point derivative as follows:

$$t\left[\frac{\partial p}{\partial t}\right]_i = t_i\left[\frac{(t_i - t_{i-1})\Delta P_{i+1}}{(t_{i+1} - t_i)(t_{i+1} - t_{i-1})}\right] + \left[\frac{(t_{i+1} + t_{i-1} - 2t_i)\Delta P_i}{(t_{i+1} - t_i)(t_i - t_{i-1})}\right] - \left[\frac{(t_{i+1} - t_i)\Delta P_{i-1}}{(t_i - t_{i-1})(t_{i+1} - t_{i-1})}\right] \quad \textbf{5.81}$$

This derivative will often give adequate results. If the derivative results in noisy data then certain smoothing techniques can be used.

5.7.5 Data Smoothing Techniques

Data smoothing techniques are varied. For instance one method to reduce noise might include using data points that are separated by at least 0.2 of a log cycle., rather than points that are immediately adjacent and using the natural logarithm of time.

$$t\left[\frac{\partial p}{\partial t}\right]_i = \left[\frac{\partial p}{\partial \ln t}\right]_i \tag{5.82}$$

So that the expression for the numerical differentiation would then be:

$$t\left[\frac{\partial p}{\partial t}\right]_i = \left[\frac{\partial p}{\partial \ln t}\right]_i = \frac{\ln(t_i/t_{i-k})\Delta P_{i+1}}{\ln(t_{i+j}/t_i)\ln(t_{i+j}/t_{i-k})} + \frac{\ln(t_{i+j}t_{i-k}/t_i^2)\Delta P}{\ln(t_{i+j}/t_i)\ln(t_i/t_{i-k})} - \frac{\ln(t_{i+j}/t_i)\Delta P_{i-1}}{\ln(t_i/t_{i-k})\ln(t_{i+j}/t_{i-k})}$$

$$\ln t_{i+j} - \ln t_i >= 0.2$$

$$\ln t_{i+j} - \ln t_{i-k} >= 0.2$$

The value of 0.2 is known as the differentiation interval and could be replaced by smaller or larger values (usually between 0.1 and 0.5) with consequent differences in the smoothing of the noise. The differentiation interval may cause problems in determining the derivative for the last part of the derivative curve, since the data runs out within the last differentiation interval. Therefore some noise is expected at the end of the data string.

The primary benefit of the derivative curve is for an aid in picking the proper r_{eD} and b values with which to match and diagnosing characteristic reservoir types. The calculation of reservoir parameters is identical to the method discussed before. It is difficult to use the derivative type curve unless sufficient data is available in both the transient and depletion portions of the curve.

5.7.6 Example of Derivative Use

The table below is a data set from Golan's book[4] as noted in the table 5.3 below. Applying the above concepts and plotting results in the following graphs in figure 5.16. Figure 5.17 is the derivative type curve developed in the prior sections.

Production Data from Golan page 393 Table E.4.5
b=0.5 considered best match by author

Delta T	Q/mo	Delta q	Q'	Q'alt	t*Q'	t*Q'alt
0	0					
0.5	30000	30000	218.0000			
14	9000	39000	826.1702	1072.949	11566.38	15021.29
19.3	6532	45532	1004.7748	1024.402	19392.15	19770.96
25.1	4621	50153	691.6949	695.1959	17361.54	17449.42
31.1	3541	53694	477.8358	499.0876	14860.69	15521.62
38.5	2862	56556	370.5797	368.052	14267.32	14170
44.9	2252	58808	355.2586	356.0395	15951.11	15986.17
50.1	1869	60677	320.5556	323.3318	16059.83	16198.92
55.7	1593	62270	161.8235	224.2197	9013.571	12489.04
67.1	1158	63428	115.7368	122.8158	7765.942	8240.939
74.7	1041	64469	945.2757	54.7368		

Table 5.3 Derivative of Production Data from Golan Reference

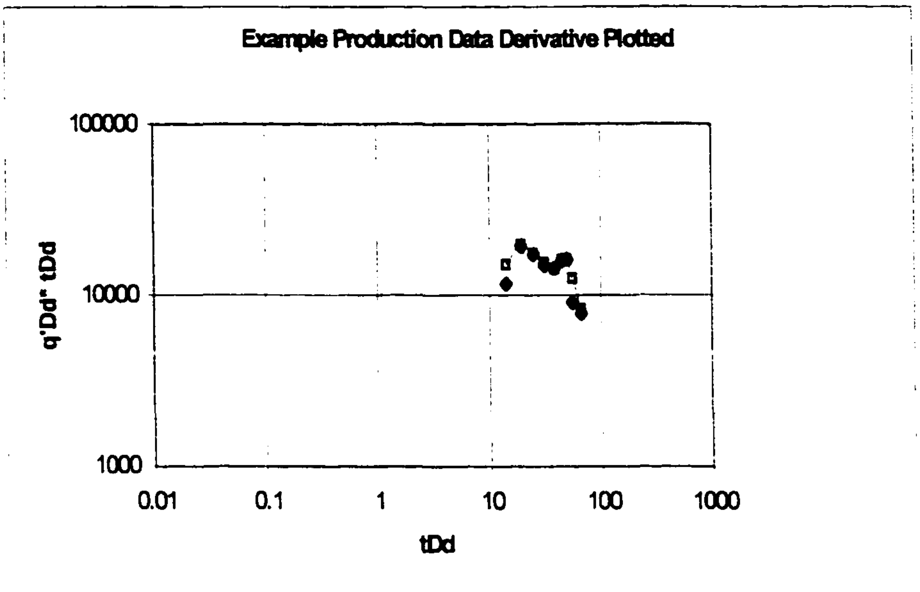

Figure 5.16 Example Production Data-Derivative Method

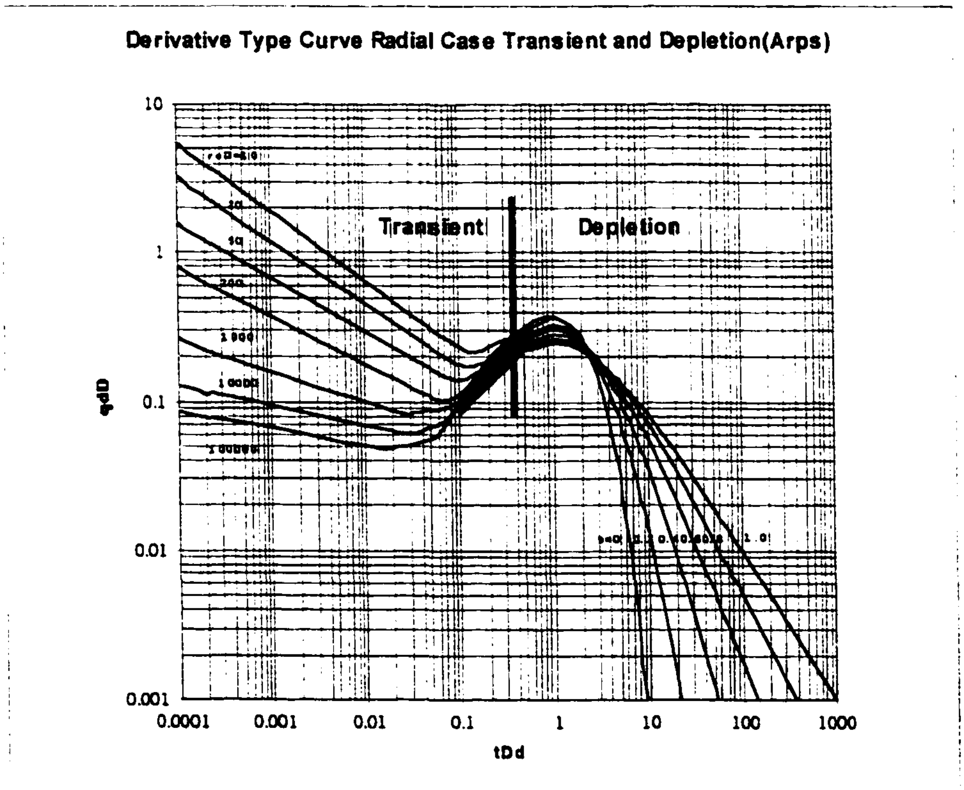

Figure 5.17 Dimensionless Decline Derivative Type Curve

The hope is that the derivative of the production data will help the user pick the appropriate "Arps b" value and the appropriate r_{eD} or A/r_w^2 term to be used in the analysis of reservoir parameters and production forecasting. An examination of the plot of the production derivative shows the same general curvature of the type curve but there is not sufficient data to really help in the transient portion of the curve. Therefore the usefulness in picking the reservoir radius is limited. If early production data can be obtained then this method should help.

5.8 Chapter Summary

This chapter and associated appendices provide one of the most comprehensive treatments of decline curve construction and use available. Compete theory, methodology and tabular data are provided for both Fetkovich type curves construction, extensions of type curve to all reservoir shapes and well positions as well as derivative type curves. These concepts will be extended to the analysis of horizontal wells in the next few chapters.

CHAPTER SIX

Horizontal Wells

6.1 Various Horizontal Well Analytical Equations

There are three popular PSS equations for horizontal well flow. These methods are summarized in the following sub-sections.

6.1.1 Method One: Infinite Conductivity Fracture Method

The method, introduced by Mutalik, Joshi et al[27] assumes that a horizontal well is equivalent to an infinite conductivity fracture. The proposed equation is an extension of fractured vertical well theory. Mutalik et al's equation for flow during pseudosteady state conditions is expressed as:

$$q = \frac{0.007078\, k_h h(\overline{P_R} - P_{wf})}{\mu_o B_o\left(\ln \frac{r_e}{r_w} - A' + s_f + s_m + s_{CA,h} - c' + Dq\right)} \qquad 6.1$$

Where:

$$r_e = \sqrt{\frac{A * 43560}{\pi}} \qquad 6.2$$

and

s_m	=	mechanical skin factor, dimensionless
s_f	=	$-\ln[L/(4r_w)]$= negative skin factor of an infinite conductivity fully penetrating fracture of length L.
$S_{CA,h}$	=	shape related skin factor
c'	=	shape factor conversion constant = 1.386
A'	=	0.75 for circular drainage areas
	=	0.738 for rectangular areas
D_q	=	Near well turbulence factor

The skin factor $S_{CA,h}$ is determined from published charts such as shown in Joshi's Horizontal Well Technology book[23] (figures 7-5 to 7-7) for centrally located wells within drainage areas based on the ratios of $2x_e/2y_e$ for each particular case. The Mutalik method gives the highest flow rates of the three published methods.

Again k_h is always in the formula and is assumed to be represented by the geometric mean of permeability in the principle x and y directions. The analytic equation would thus predict that no matter what the contrast between k_x and k_y, the solution should remain constant as long as the square root of k_xk_y is the same and all other parameters remain constant as shown before. This is probably only the case when the horizontal well is small compared to the reservoir dimensions. The skin factor for shape considerations, $S_{CA,h}$, only accounts for variations in vertical versus horizontal permeability. It does not account for average directional horizontal permeability, k_h, variations.

6.1.2 Method Two – Kuchuk Method

Another method, proposed by Kuchuk et al[28] used the approximate infinite conductivity solution where constant wellbore pressure is obtained by averaging pressure values of the uniform flux solution along the well length. This equation gives the lowest flow rates of the various methods. The term B_o was left off the equation in the literature but it has been added to the equation below to convert the flow to surface conditions for proper comparison. These authors present the following equation to describe single-phase flow in a horizontal

$$q_h = \frac{\left(\overline{P_R} - P_{wf}\right) k_h h}{70.6\, B_o \mu_o \left(F + \frac{h}{0.5L}\sqrt{\frac{k_h}{k_v}}\, s_x \right)} \qquad 6.3$$

well.

Charts such as Table 7-6 in Joshi's book give the F term. F is dependent on $y_w/2y_e$, $x_w/2x_e$, $L/4x_e$, and (y_e/x_e)* sqrt(k_x/k_y). z_w, y_w and x_w are the distances from the center of the horizontal well to the boundaries of the reservoir in the z, y, and x directions respectively. The s_x term is calculated with the following equation.

$$s_x = \ln\left[\left(\frac{\pi r_w}{h}\right)\left(1+\sqrt{\frac{k_v}{k_h}}\right)\sin\left(\frac{\pi z_w}{h}\right)\right] - \sqrt{\frac{k_h}{k_v}}\left(\frac{2h}{L}\right)\left[\frac{1}{3} - \frac{z_w}{h} + \left(\frac{z_w}{h}\right)^2\right] \qquad 6.4$$

Again k_h and k_v are considered but not variations in k_x and k_y other than geometrical averaging of k_x and k_y for k_h. This method seems especially poor at predicting rates above the bubble point for some reason.

6.1.3 Method Three

Another method was presented by Babu and Odeh[29] which is based on a partially penetrating vertical well-turned sideways. This method yields flow rate results in between the Mutalik-Joshi and Kuchuk methods.

Babu and Odeh's[29] equation is expressed as:

$$q = \frac{.007078(2\,X_e)\sqrt{k_y k_v}(P_R - P_{wf})}{B_o\,\mu_o \ln(\sqrt{A}/r_w) + \ln C_H - 0.75 + s_R} \qquad 6.5$$

C_H is the geometric shape factor given as:

$$\ln C_H = 6.28\left(\frac{2y_e}{h}\right)\sqrt{\frac{k_v}{k_y}}\left[\frac{1}{3} - \left(\frac{y_w}{2y_e}\right) + \left(\frac{y_w}{2y_e}\right)\right] - \ln\left[\sin\left(180^\circ\frac{z_w}{h}\right)\right] - 0.5\ln\left[\left(2\frac{y_e}{h}\right)\sqrt{\frac{k_v}{k_y}}\right] - 1.088 \qquad 6.6$$

S_R is the skin factor attributable to partial penetration. S_R will be zero when $L = 2x_e$ i.e. fully penetrating horizontal well. If $L < 2x_e$ then the value depends on the two conditions:

Case1:

$$2\frac{y_e}{\sqrt{k_y}} \geq 1.5\frac{x_e}{\sqrt{k_x}} \ll 0.75\frac{h}{\sqrt{k_v}} \qquad 6.7$$

Case 2:

$$2\frac{x_e}{\sqrt{k_x}} \geq 2.66\frac{y_e}{\sqrt{k_y}} \ll 1.33\frac{h}{\sqrt{k_v}} \qquad \textbf{6.8}$$

Case 1

$$S_R = PXYZ + PXY'$$

PXYZ is given by:

$$PXYZ = \left[2\frac{x_e}{L} - 1\right]\left[\ln\left(\frac{h}{r_w}\right) + 0.25\ln\left(\frac{k_y}{k_v}\right) - \ln\left(\sin\frac{180^\circ z_w}{h}\right) - 1.84\right] \qquad \textbf{6.9}$$

The PXY' component is given by:

$$P'XY = \left(\frac{2(2x_e)^2}{Lh}\sqrt{\frac{k_v}{k_x}}\right)\left[f(x) + 0.5\left[f(y_1) - f(y_2)\right]\right] \qquad \textbf{6.10}$$

x_w is the distance from the horizontal well mid point to the closest boundary in the x direction.

Pressure computations are made at the mid point along the well length.

$$x = \frac{L}{4x_e} \qquad y_1 = \frac{4x_w + L}{4x_e} \qquad y_2 = \frac{4x_w - L}{4x_e}$$

$$f(x) = -x[0.145 + \ln(x) - 0.137(x)^2] \qquad \textbf{6.11}$$

$$f(y) = (2 - y)[0.145 + \ln(2 - y) - 0.137(2 - y)^2] \qquad \textbf{6.12}$$

where y= y1 or y2

Case 2:

$$SR = PXYZ + PY + PXY \qquad \textbf{6.13}$$

PXYZ is calculated as above while PY comes from the relation:

$$PY = 6.28\frac{(2x_e)^2}{2y_e h}\frac{\sqrt{k_y k_v}}{k_x}\left[\left(\frac{1}{3}-\left(\frac{x_w}{2x_e}\right)+\left(\frac{x_w}{2x_e}\right)^2\right)+\frac{L}{48x_e}\left(\frac{L}{2x_e}-3\right)\right] \qquad \textbf{6.14}$$

x_w is the mid-point coordinate of the well. PXY is:

$$PXY = \left(\frac{2x_e}{L}-1\right)\frac{6.28(2y_e)}{h}\sqrt{\frac{k_v}{k_y}}\left[\frac{1}{3}-\left(\frac{y_w}{2y_e}\right)+\left(\frac{y_w}{2y_e}\right)^2\right] \qquad \textbf{6.15}$$

For $[\mathrm{Min}\{y_w, (2y_e - y_w)\}.=0.5y_e$

This method is predicated on the assumption that a "fully penetrating horizontal well should be identical in behavior to a fully penetrating vertical well, provided that the drainage volumes are similar and it is recognized that the horizontal well is parallel in the y direction while the vertical well is parallel to the z direction"[29]. This basic assumption has been bothersome for several reasons as indicated in the following paragraph.

To test the assumption of this method, a comparison was made of the simulated results of a vertical well model to the equivalent horizontal model of the vertical well turned sideways. As suspected the results were not identical. Figure 6.1 illustrates the models used in the validation and comparison experiment. Figure 6.2 shows the comparison of the two cases. In general the equivalent horizontal well gave higher simulated flow results. Variations of pressure with depth were purposely omitted in the experiment, as this would make the difference even larger than observed in thick formations. According to the Babu and Odeh's[29] publication, they only tested the validity of the equivalency of a vertical well turned sideways in the transient regime.

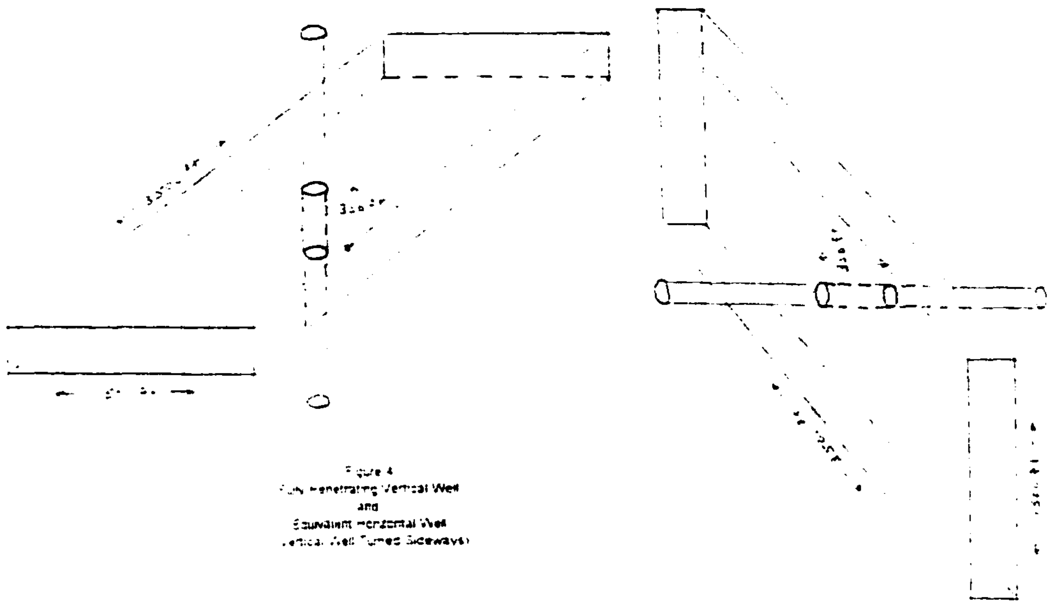

Figure 6.1 Schematic Diagram of Fully Penetrating Vertical Well versus Equivalent Horizontal Well

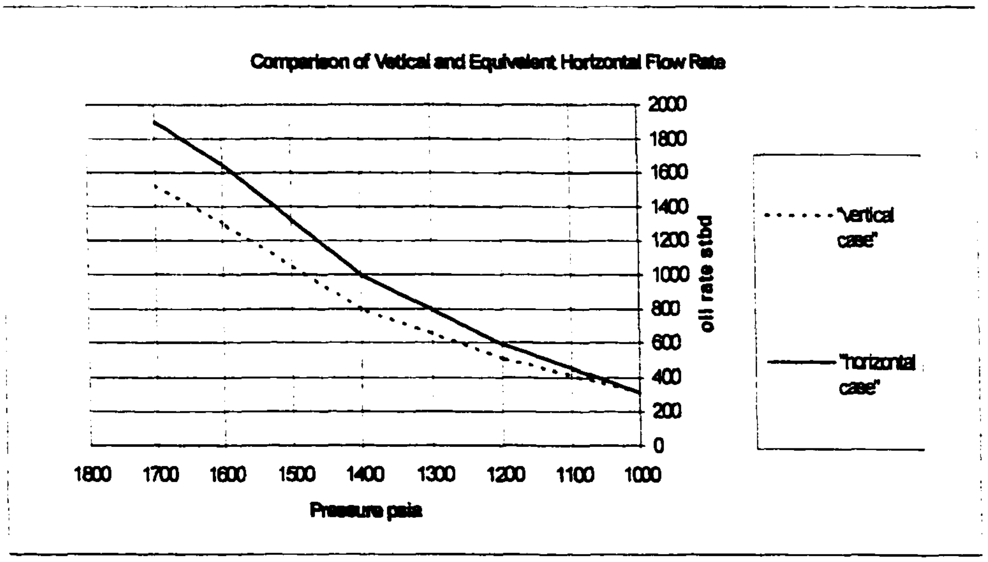

Figure 6.2 Comparison of Simulated Vertical and Equivalent Horizontal Flow Rates

This basic assumption of the Babu and Odeh[29] method may not be valid for several reasons. First, the condition of equal drainage volumes does not seem sufficient. The drainage shape and dimensions would also have to be the same. When a vertical well is turned sideways the reservoir is then very thin horizontally compared to the vertical dimension and severe boundary effects may result. Generally a reservoir is thin compared to its horizontal areal size. If a vertical well is turned sideways then the dimensions in the y and z directions are then distorted compared to the x direction (parallel to the well). Second there are basic pressure differences to take into account. The pressure differences of a vertical versus horizontal slice can be different depending on the formation thickness. Third, there are gravity considerations.

The Babu and Odeh method is also very cumbersome to use. If analytical methods of accounting for horizontal permeability contrasts and situations below the bubble point could be adapted to vertical style methods then a easy and more accurate predictive model might result that could be used to verify, calibrate and validate simulation output.

6.2 Alternative Method Using Effective Wellbore Radius Concept

A horizontal well should be capable of being modeled in terms of familiar vertical equations by the introduction of an equivalent wellbore radius concept. The derivation of the effective radius of a horizontal well as adapted from Joshi[30,32] is shown in appendix F. It will then be shown that the use of the equivalent well bore radius r_w' in vertical style equations, modified for incorporation of solution gas cases below the bubble point, is not only easier to use but is also accurate and thus useful in validating simulation models and simulation output.

The equivalent well bore radius of a horizontal well in comparison to a vertical well is expressed as:

$$r_w' = \frac{0.5 r_{eh} L}{a\left[1+\sqrt{1-\left[\frac{L}{2a}\right]^2}\right]\left[\frac{\beta h}{2r_w}\right]^{\frac{\beta h}{L}}} \qquad 6.16$$

where a is defined as:

$$a = 0.5L\left[0.5+\sqrt{0.25+\left(\frac{2r_{eh}}{L}\right)^4}\right]^{\frac{1}{2}} \qquad 6.17$$

And

$$\beta = \left(\frac{k_h}{k_v}\right)^{\frac{1}{2}}, \quad r_{eh} = \sqrt{\frac{A}{\pi}} \qquad 6.18$$

Where A is in square feet. In a homogeneous reservoir the β term is unity and the apparent well bore radius expression reduces to:

$$r_w' = \frac{0.5 r_{eh} L}{a\left[1+\sqrt{1-\left[\frac{L}{2a}\right]^2}\right]\left[\frac{h}{2r_w}\right]^{\frac{h}{L}}} \qquad 6.19$$

Therefore the equation for the horizontal well would then reduce to:

$$q = \frac{0.007078\ k_h h(\overline{P_R} - P_{wf})}{\mu_o B_o \left(\ln \frac{r_e}{r'_w} - 0.75 \right)} \qquad 6.20$$

Where r'_w is defined above and k_{eh} is as usual the geometric mean of the permeability in the principle x and y directions. As shown in chapter 3 this equation can be converted to a 2-phase flow estimate by estimating and incorporating the mobility as a function of pressure and average saturation. Thus the generalized multi-phase equation approximation for a horizontal flow in terms of equivalent vertical well parameters should be:

$$q = \frac{0.007078\ k_h h(\overline{P_R} - P_{wf})}{\left(\ln \frac{r_e}{r'_w} - 0.75 \right)} \left(\frac{k_{ro}}{\mu_o B_o} \right)_{Pave} \qquad 6.21$$

The other three published methods can also be modified to incorporate the 2 phase flow characteristics. As a validation check of this modification experimental comparisons will be shown as done previously for the vertical well case. The next section will detail validation comparisons for the isotropic results followed by an application to anisotropic cases.

6.3 Demonstration of Validity of 2-phase Horizontal Well Approximations

As a test of the validity and accuracy of these published equations and as a test of the more usable equivalent wellbore radius concept, simulation tests were conducted using horizontal wells in isotropic media compared to the analytical equations. Later anisotropic cases will be presented. Simulated results of each anisotropic model were compared with one another and the 2-phase analytical results were then compared to simulated results. It is important to note that the k_h in the above equations is the absolute horizontal permeability, which must be multiplied by the relative permeability to the desired phase such as oil in this case. Therefore in equations 6.20 and 6.21, for instance, k_h would be multiplied by k_{ro} at each oil saturation point if the flow rate for oil is desired and by $1/(\mu_o B_o)$ and average reservoir pressures as demonstrated previously for the vertical comparisons. This has been done in the analysis but is never presented or addressed in the various papers.

For this project, a test was conducted to see if these saturation and pressure averaged mobility functions would work as well with both vertical and horizontal wells. If the averaging process works as well for horizontal well conditions as it did for vertical wells then it will be easier to perform some other tests on absolute permeability anisotropy and extensions to decline analysis.

6.3.1 Validation Model Results and Discussion

The basic model parameters for horizontal test cases are given in Appendix E. Vertical permeability is 0.1 md in all cases. The average effective horizontal permeability in all cases is 3.1 md. A 15 by 17 by 3-grid block model was used for the horizontal cases. Three models were tested. The first model depicts the isotropic model of constant permeability in both x and y direction ($k_x=k_y=3.1$ md). Models 2 and 3 are the cases in which $k_y=9.61$, $k_x=1.0$ md and $k_y=19.22$, $k_x=0.5$ md but the average horizontal permeability was still 3.1 md ($\sqrt{(k_x k_y)}$) in all cases. The averaging process is desirable because it is so easy to evaluate in a spreadsheet.

Typical simulators give tabular output that can be imported to spreadsheets and averaged over gridblocks in a single operation. Typical simulation output was previously shown in Tables 3.2, 3.3.

Figures 6.3 through 6.5 show the oil rate vs. average pressure plot with the above model. Figure 6.3 is a comparison of the isotropic permeability case (k_x=k_y=3.1md) compared to the various 2-phase analytical equations presented in section 6.2 of this chapter. There are several things to note. First of all the match between the simulated output for the isotropic case of constant x and y permeability and the analytical results is not quite as good as with a vertical well for several of the methods. Note however that the equivalent wellbore radius incorporation using the 2-phase adaptation is one of the best matches to the simulated results. This is very important because it validates the idea that the equivalent wellbore 2-phase analytical equations are reasonable approximations to actual reservoir performance. And because the equivalent wellbore concept is in terms of vertical well terminology and conventions it is immediately applicable to decline analysis as will be shown in chapter 7. In fact the equivalent wellbore radius concept will be shown to also give superior results to the other methods in the case of anisotropic media.

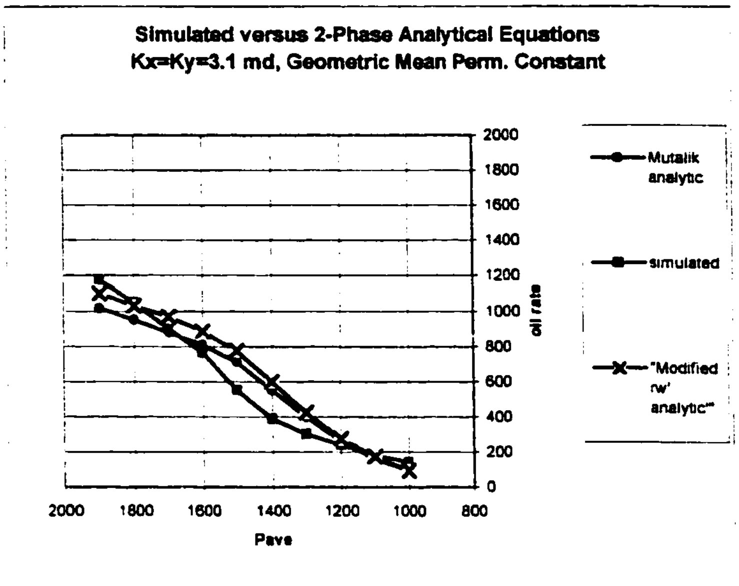

Figure 6.3 Simulated versus 2-Phase Analytical Equations $k_x=k_y=3.1$ md, Geometric Mean Permeability Constant

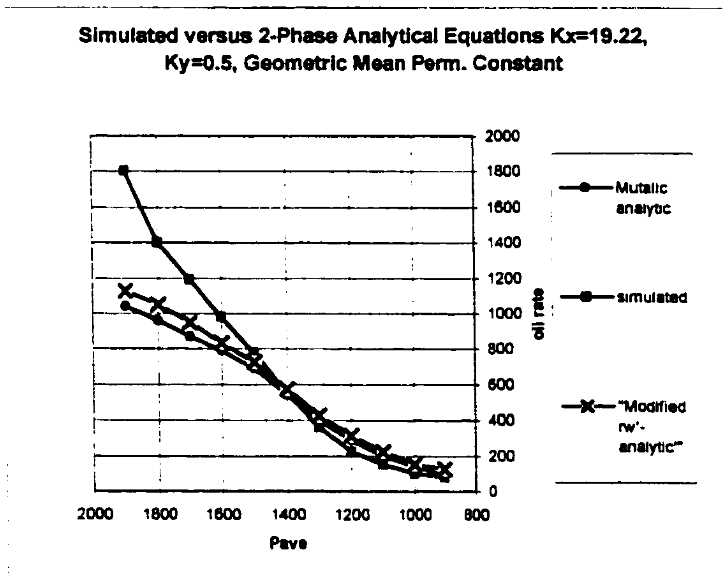

Figure 6.4 Simulated versus 2-Phase Analytical Equations $k_x=19.22$, $k_y=1$,Geometric Mean Permeability Constant

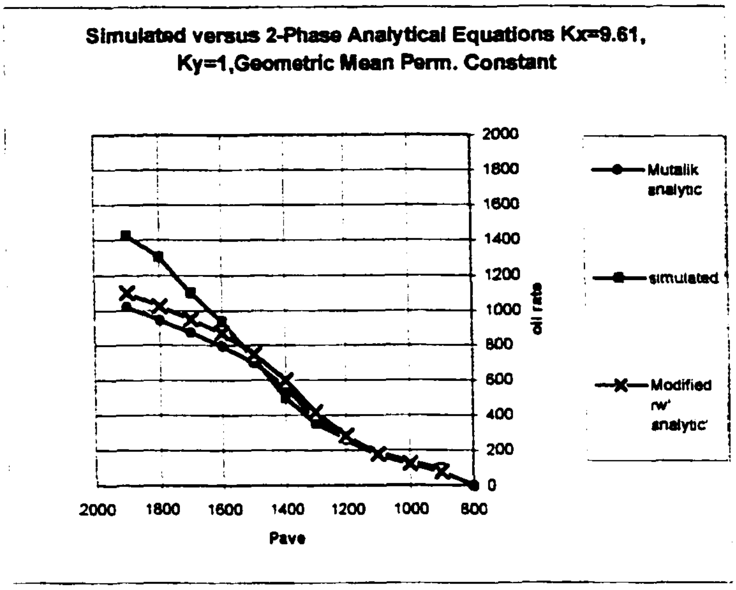

Figure 6.5 Simulated versus 2-Phase Analytical Equations k_x=9.61, k_y=1.0, Geometric Mean Permeability Constant

6.4 Analysis of Analytical and Simulated Pseudosteady State Flow Equations for Horizontal Wells in Anisotropic media.

As mentioned in chapter 3, vertical well-modified 2-phase analytical solutions match simulated results quite well for fluid flow in both isotropic and highly anisotropic media above and below the bubble point. This showed that no matter what the contrast in k_x and k_y, the simulated rate vs. pressure results were essentially identical. Also the analytical computations were shown to be good estimates of simulated results. In contrast, analytical solutions to horizontal well flow generally follow simulated solutions in isotropic media but do not match simulated horizontal results very well in horizontally anisotropic media. The mismatch is especially pronounced above the bubble point. What is the cause of this phenomenon and what can be done to improve the match? Let's first look at the results and see what we can observe.

6.4.1 Anisotropic Experimental Results and Observations

Simulation experiments indicate that published analytical solutions to horizontal well inflow at least track simulated results in cases of isotropic permeability (again above and below the bubble point) (figure 6.3) but they do not match simulated horizontal results as well in cases of horizontally anisotropic permeability. Figures 6.3-6.5 illustrate the comparison of three horizontal permeability cases (single layer model) each with a geometric average of 3.1 m.d. but with varying degrees of anisotropy. Figure 6.4 shows the comparison with simulated k_x=9.61 md, k_y= 1 while figure 6.5 shows output for the case of k_x= 19.22, k_y=0.5. Each case has the same geometric mean permeability. If k_y is set to a constant 9.61 md and k_x to 1.0 md, the match is very poor even though the horizontal average permeability remains at 3.1 md. The deviation between the simulation case and analytical results is even greater if k_y is magnified to 19.22 md vs. k_x=0.5 while keeping k_{eh} equal to 3.1. Therefore the traditional use of a geometric average of k_x and k_y for the effective horizontal permeability is not a good approximation for the horizontal well at least when the wellbore is long in comparison the reservoir dimensions and the maximum grid block number is limited. Since no other parameters have been changed between models, the difference must be in the way k_{eh} is calculated for horizontal wells in the simulation or in some type of numerical or boundary effects due to model design. These are compared with two popular analytic prediction methods discussed earlier in this chapter as well as the modified equivalent wellbore radius method presented in this chapter. Notice also in figure 6.6 that in each case, the simulated horizontal flow rates increase with increasing permeability perpendicular to the well bore despite constant horizontal geometric mean permeability. Theory would predict that anisotropy would not affect results as long and the geometric mean permeability remained constant. There are then two questions to answer. 1) Why do the analytical and simulated results vary and 2) why do the simulated results themselves vary when theory would predict that the permeability contrast would not affect results?

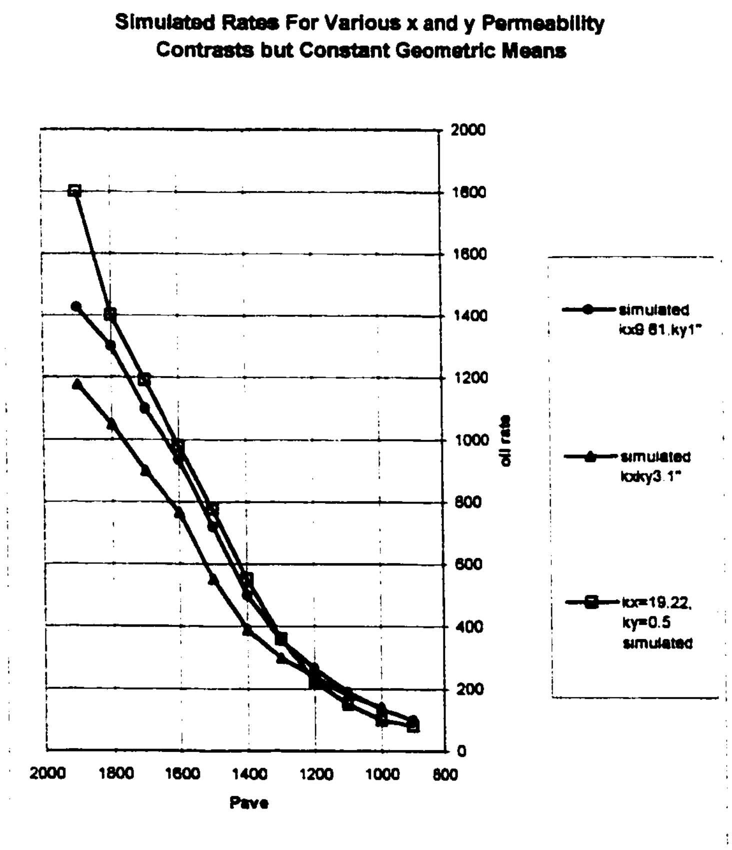

Figure 6.6 Simulated Rates For Various x and y Permeability Contrasts but Constant Geometric Means

6.4.2 Anisotropic Behavior Possibilities

As in the vertical well situation, each horizontal well analytical method requires the use of effective horizontal permeability, k_h, in the calculation. Perhaps one of the problems is a misconception as to what effective horizontal permeability is to a horizontal well. Other possible explanations include the need to include more reservoir blocks in the vicinity of the wellbore and boundary effects when the well is close to the reservoir edge.

If the reservoir is semi-infinite, no other wells compete for drainage area, and the reservoir is thick, then the geometric average of permeability may work satisfactorily. The horizontal well would then appear small compared to the reservoir as a whole and the geometric average would give proper results. This is almost never the case in reality. In practice, reservoirs are limited, compete for drainage area, and are anisotropic. The discrepancy in flow predictions may be a function of well length, degree of penetration, permeability contrast, distance to the reservoir boundaries and number of simulation blocks. This also demonstrates the usefulness of the 2-phase analytical approximations presented in this work as they help to validate simulation model parameters.

All published horizontal well inflow solutions use the geometric average for effective horizontal permeability. If the reservoir is very large compared to the horizontal well length, and the reservoir is isotropic, then the geometric average can be used. In simulation experiments, as the permeability perpendicular to the horizontal well increases over the permeability parallel to the well bore, keeping the square root of $k_x k_y$ constant, the simulated flow rates increase dramatically while the analytical flow rate predictions remain fairly constant depending on the analytical method used. Simulation experiments were conducted to see if this discrepancy appears to be a function of primarily the x, y and z directional permeability contrast, the length of the horizontal well, the distance from the well to the reservoir boundaries and possibly other parameters such as grid size and number of grids in the model.

6.4.3 Background Theory into Effective Horizontal Permeability

In naturally fractured wells, the permeability along the fracture trend is larger than the direction perpendicular to the fractures. As such, a vertical well would drain more length along the fracture trend. Assuming a single phase, steady state flow, one can write the following equation.

$$\frac{\partial}{\partial x}\left(k_x \frac{\partial p}{\partial x}\right)+\frac{\partial}{\partial y}\left(k_y \frac{\partial p}{\partial y}\right)=0 \qquad 6.22$$

Assuming non-variant values of k_x and k_y in the principal x and y directions one can rewrite the equation as:

$$k_x \frac{\partial^2 p}{\partial x^2}+k_y \frac{\partial^2 p}{\partial y^2}=0 \qquad 6.23$$

and multiplying and dividing throughout by $\sqrt{(k_x k_y)}$ the equation can be rewritten as:

$$\sqrt{k_x k_y}\left[\sqrt{\frac{k_x}{k_y}}\frac{\partial^2 p}{\partial x^2}+\sqrt{\frac{k_y}{k_x}}\frac{\partial^2 p}{\partial y^2}\right]=0 \qquad 6.24$$

Which can be rearranged and transformed as follows:

$$\sqrt{k_x k_y}\left[\frac{\partial^2 p}{\partial x^2}+\frac{\partial^2 p}{\partial y'^2}\right]=0 \qquad 6.25$$

where:

$$y' = y\sqrt{\frac{k_x}{k_y}} \qquad 6.26$$

Therefore in an anisotropic reservoir the effective horizontal permeability would be $\sqrt{(k_x k_y)}$ and the drainage length along the high permeability side is $\sqrt{(k_x/k_y)}$ times the length along the low permeability side. Thus if the permeability along the fracture trend is 16 times greater than that perpendicular to the trend then the drainage length along the fracture trend is four times larger than the length perpendicular to the fracture trend.

A horizontal well drilled along the low permeability direction has the potential to drain a significantly larger area than a vertical well, resulting in a larger reserve for horizontal wells versus vertical wells. Now so far the above discussion concerns only a vertical well in anisotropic media. There is limited data for fractured vertical wells with which to calculate the time to reach pseudo-steady state. Horizontal well data are also not extensive.

6.5 Need to Re-Consider Effective Horizontal Permeability in Limited Reservoirs

Due to the longer well length, a horizontal well would drain a larger reservoir area than a vertical well within a given a specific time interval. If a vertical well drains a certain reservoir volume in a given time then that information can be used to calculate a horizontal well drainage area. A horizontal well can be looked at as a number of vertical wells drilled in succession. However unless the reservoir is very large compared to the horizontal well length a distortion may be introduced into the effective horizontal permeability that is not captured in the shape factor alone. As noted in the preceding sections, all horizontal well flow equations assume the square root effective horizontal permeability concept. Various shape and pseudo-skin factors have been developed to account for variations in reservoir shape, well penetration ratios and dimensionless well length but no studies have been performed to investigate the effect of contrasts in k_x and k_y on flow rates versus pressure. This is because it has been assumed that the effective horizontal permeability can be adequately described by the square root of permeability in the principle x and y directions.

This simple geometric average of permeability alone does not appear to work well for horizontal wells in simulation experiments involving Boast reservoir simulator. This is not just related to a shape factor to account for the degree of penetration of the horizontal well relative to the reservoir dimension. For instance Earlougher[22] published shape factors for vertically fractured wells with different ratios of the fracture length x_f relative to the length of the reservoir in the direction parallel to the fracture. If the ratio of x_f to x_e was 0.5 (i.e. the fracture was half as long as the reservoir length parallel to the fracture) then the C_A factor in the equation was 1.662 compared to 2.654 when the fracture was very short and x_f/x_e was 0.1. This would also be the case with the horizontal well where the length varied in comparison to the reservoir x dimension. However given a certain well or fracture length which would still yield a certain shape factor, the equations would all predict a certain constant behavior irrespective of the contrast in k_x and k_y as long as the square root of the product was constant. Likewise Joshi[23] published various shape and skin factors (page 217-219) for use in the traditional horizontal well flow rate equations. However all methods assume horizontal permeability is the square root of x and y permeability.

As previously shown, a reasonable match was obtained between analytical published equations modified by using the modified 2-phase equivalent wellbore radius approximation and simulated results for isotropic permeability. Theoretically equation 6.16 can be used for horizontal wells in both anisotropic and isotropic media. The only difference would be the deletion of the beta term in equation 6.16 for the isotropic case. However inspection of the beta term shows that this term is only introducing variations in the ratio of vertical to horizontal permeability. It does not account for variations in k_x and k_y distributions. As long as the effective horizontal permeability given by the square root of k_xk_y is the same, the analytical results predict no change in flow rate with anisotropy. Clearly this is not always the case in reality. The beta term in the equation and the skin factors in the other methods only address the ratio of vertical and horizontal anisotropy, not the issue of horizontal anisotropy itself. The use of skin factors and Kuchuk's equation yield even worse results.

Simulation results indicate that a simple geometric averaging of x and y permeability does not suffice in the case of a horizontal well.

Notice in the various experiments that as the contrast in x and y permeability was increased (geometric mean constant), the flow rates diverged significantly, especially at higher pressures above the bubble point. This was perplexing and deserved further investigation. Intuition would also indicate that high permeability perpendicular to the horizontal wellbore would yield higher flow rates than equal but lower permeability in both directions. In other words if k_x=9.61 md perpendicular to the wellbore and k_y=1 md parallel to the wellbore one might intuitively expect higher flow rates than if k_x=k_y=3.1 md even though both cases give the same geometric mean k_h of 3.1 md. But analytical equations predict the same productivity no matter what the values of k_x and k_y as long as the square root of the product of $k_x k_y$ is the same.

There were several hypotheses to explain this divergence in flow rate versus average reservoir pressure. First it was thought that perhaps not enough grid blocks were used to define the model. Secondly perhaps distortion was introduced when the well penetration was long compared to the reservoir dimensions. In other words if the well length was insignificant compared to the horizontal dimensions then perhaps the deviation would disappear. Thirdly perhaps the simulator itself is not designed properly to account for such variations. It was not possible to test the third possibility since no access to other simulators was possible but such a comparison should be made to determine if this is a simulator artifact.

6.5 Experimental Results and Observations of Variations in Simulated Output in Cases of Variable Horizontal Permeability Components

This phenomenon was first observed while preparing a class project in 1995. Though a class project paper was written on the subject the paper generated no real interest and it was uncertain what the results really meant. For the past four years the subject has periodically re-surfaced in this research and since no flaws are apparent in the observation, the experimental analysis continued. As a test of the above theory that additional skin factors are needed to account for horizontal anisotropy, scores of simulation experiments were conducted in which the grid blocks, well length and, reservoir size was varied versus contrasts in x and y directional permeability. If the simulated results match analytical results in isotropic media as grids become more numerous then it will be apparent that the explanation lies only in the simulation model itself. The geometric mean would then be validated and discrepancies will be explained by simulation limitations. If this is not the case other explanations must be considered. The "quick-look" 2-phase approximations are used to check results.

6.6.1 Experiments

The first hypothesis tested was the effect of the number and size of the grid blocks used. Boast is limited to 810 grid blocks but this should be sufficient to test the hypothesis. Reservoirs ranging from as small as 0.8 square miles up to 3.6 square miles were tested using various permeability contrasts and well lengths ranging from 400 to 1000 feet ($L/2X_e$ ratios from 10 up to 50, $L/2X_e = 0.02$ to 0.1). Details of the experimental parameters are available from the author. The complete experimental output files are available for inspection and use by the reader however they are too voluminous to include in this document. The following sections summarize some of the findings from those studies.

6.6.2 Effect of Grid Number

The first thing to note is that as the contrast in k_x and k_y becomes more pronounced, the deviation from the isotropic case becomes more pronounced. However the effect of the number of grid blocks is relatively minor. Figures 6.7 through 6.9 show the effect of variations in the # of grid block with increasing contrast in k_x and k_y (geometric mean constant).

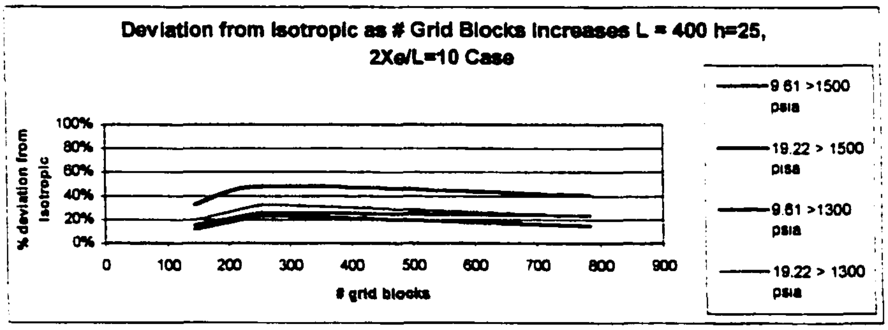

Figure 6.7 Deviation from Isotropic as # Grid Blocks Increases L = 400 h=25, 2Xe/L=10 Case, Geometric Mean $k_x k_y$ Constant

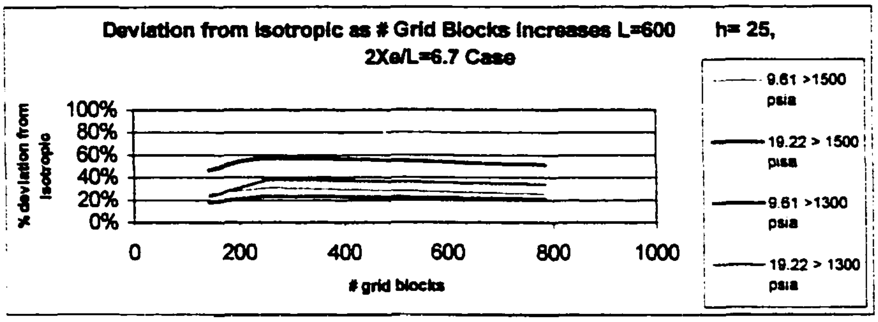

Figure 6.8 Deviation from Isotropic as # Grid Blocks Increases L=600 h= 25, 2Xe/L=6.7 Case Geometric Mean k_xk_y Constant.

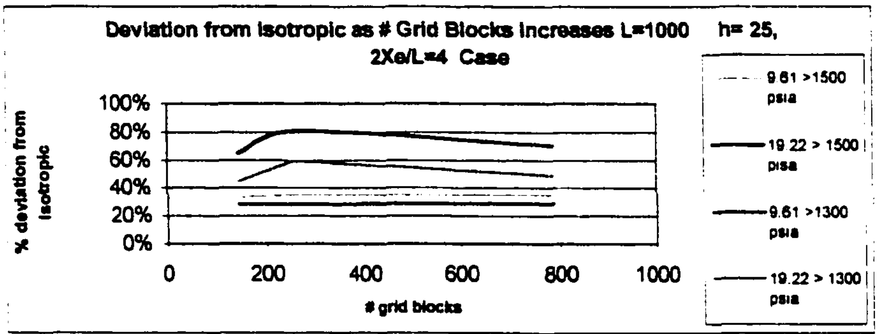

Figure 6.9 Deviation from Isotropic as # Grid Blocks Increases L=1000 h= 25, 2Xe/L=4 Case Geometric Mean k_xk_y Constant.

Note that as the grid blocks increase, keeping the total model size constant, there is relatively little change in the average deviation from the isotropic case. Note also that the average deviation increases with increasing pressure but becomes less noticeable as the reservoir size increases relative to the well length. This can also be shown in the following figures 6.10 and 6.11 from one of the experiments.

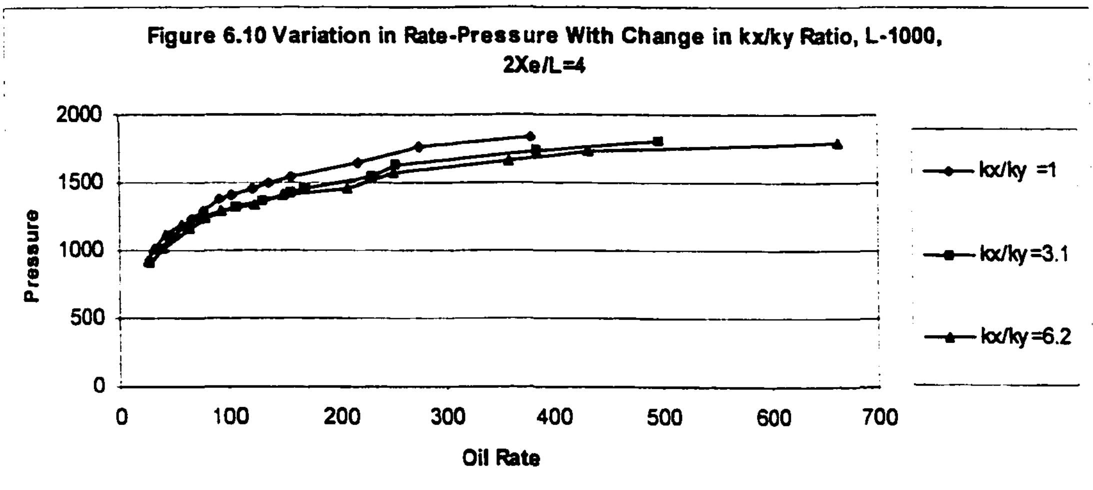

Figure 6.10 Variation in Rate-Pressure With Change in k_x/k_y Ratio, L-1000, 2Xe/L=4

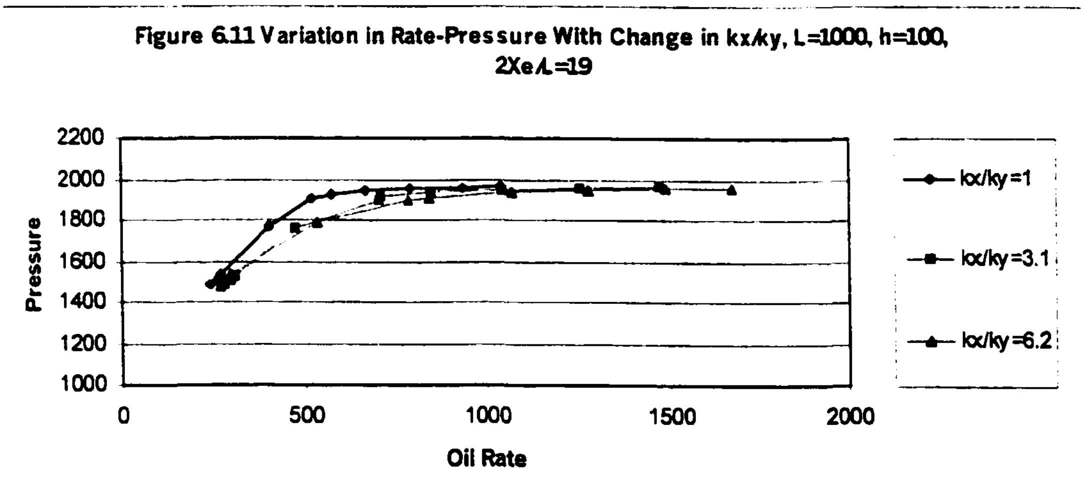

Figure 6.11 Variation in Rate-Pressure With Change in k_x/k_y, L=1000, h=100, 2Xe/L=19

The following plots also show that although the deviation from isotropic increases with increasing well length relative to the reservoir dimensions, the effect of grid size and number is relatively insignificant for any given well length or dimensionless well length.

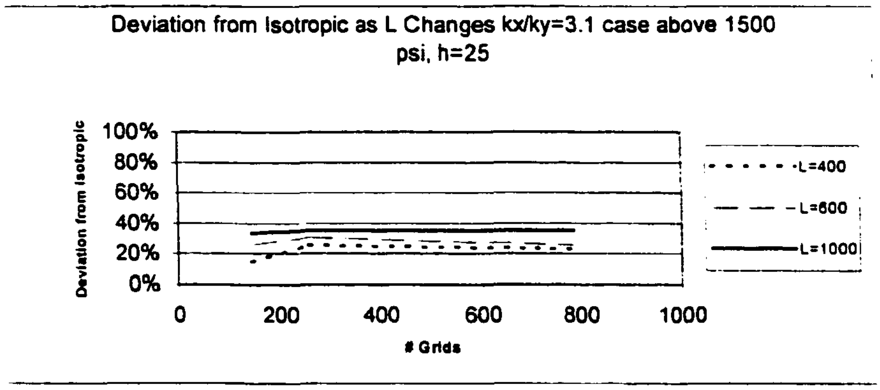

Figure 6.12 Deviation from Isotropic as L Changes k_x/k_y=3.1 case above 1500 psi, h=25

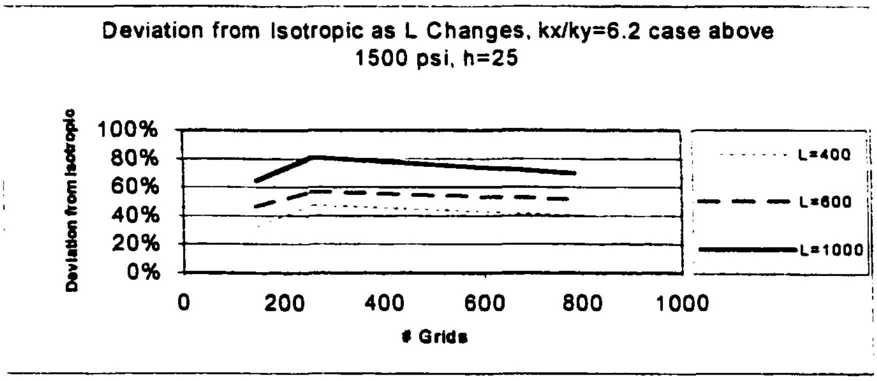

Figure 6.13 Deviation from Isotropic as L Changes, k_x/k_y=6.2 case above 1500 psi, h=25

Similar results can be shown for other cases of larger reservoir to well-length ratios. More complete results are available from the author. Since the effect of grid spacing and number is inconsequential hypothesis one is rejected and the experiments focused on variations in well length and reservoir size.

6.6.3 Effect of Model Size and Penetration Ratios

Dimensionless well length L_D is defined as:

$$L_D = \frac{L}{2h}\sqrt{\frac{k_v}{k_h}} \qquad \textbf{6.27}$$

Where L is the horizontal well length and h is the reservoir thickness in feet.

Figures 6.7 through 6.13 demonstrated that although grid number is not that important, there is a general increase in divergence from the isotropic case as the permeability contrast increases and as the well length increases relative to the reservoir dimensions. This can be further demonstrated graphically by figures 6.14 through 6.15 which collectively show the deviation from isotropic for the smaller model where reservoir thickness is constant but the ratio of horizontal dimension to well length varies. These graphs show that for a given reservoir size, as the well length increases relative to the reservoir dimensions, the deviation in flow rates for a given pressure increasingly deviate from the isotropic case. It also shows the deviation is more pronounced as the anisotropy in k_x and k_y increases.

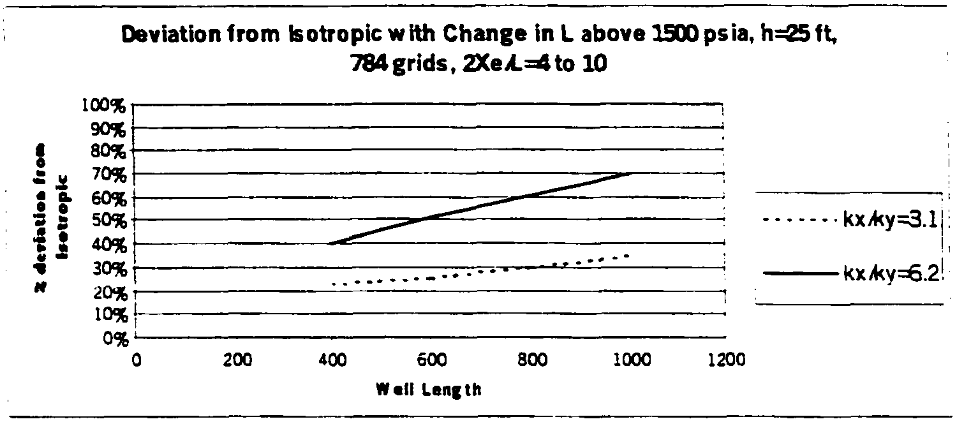

Figure 6.14 Deviation from Isotropic with Change in L above 1500 psia, h=25 ft, 784 grids, 2Xe/L=4 to 10, Small Model

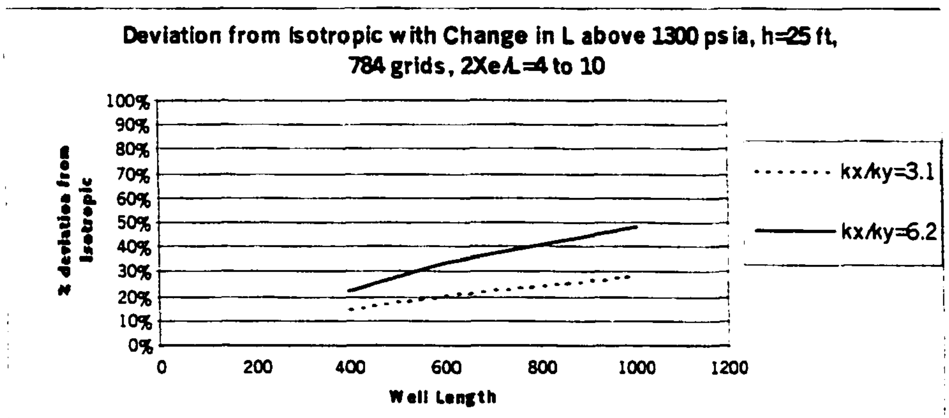

Figure 6.15 Deviation from Isotropic with Change in L above 1300 psia, h=25 ft, 784 grids, 2Xe/L=4 to 10, Small Model

Similarly, figures 6.16 and 6.17 show that as the reservoir thickness increases from 25 ft in the previous figures, keeping other parameters constant, the trend to increasing deviation from the isotropic is the same although the deviation magnitude decreases.

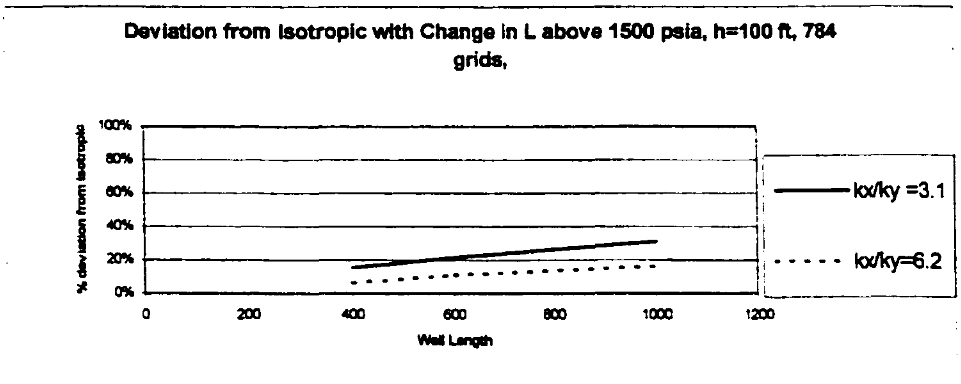

Figure 6.16 Deviation from Isotropic with Change in L above 1500 psia, h=100 ft, 784 grids,2Xe/L= 4 to10, Small Model

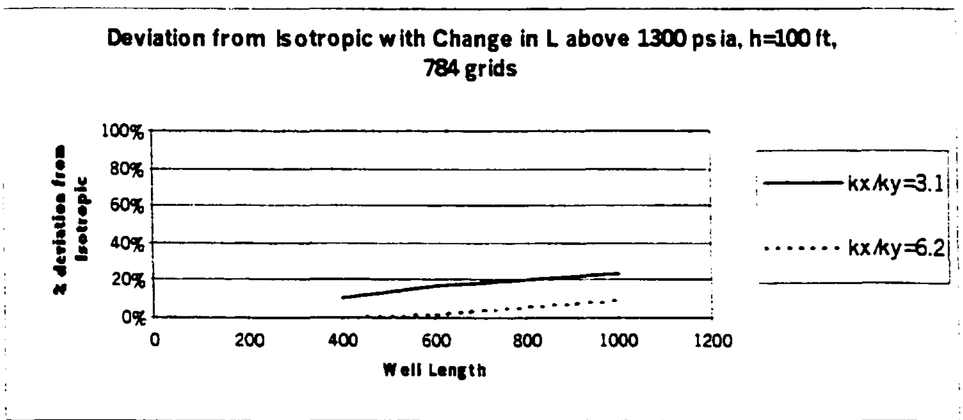

Figure 6.17 Deviation from Isotropic with Change in L above 1300 psia, h=100 f, 784 grids,2Xe/L= 4 to10, Small Model

As the reservoir becomes larger and the ratio of $2X_e/L$ increases, the trend towards increasing deviation from isotropic with increasing well length and reservoir to well length ratio remains the same. However note that the magnitude of the relative deviation from isotropic diminishes. This is shown in figures 6.18 – 6.21.

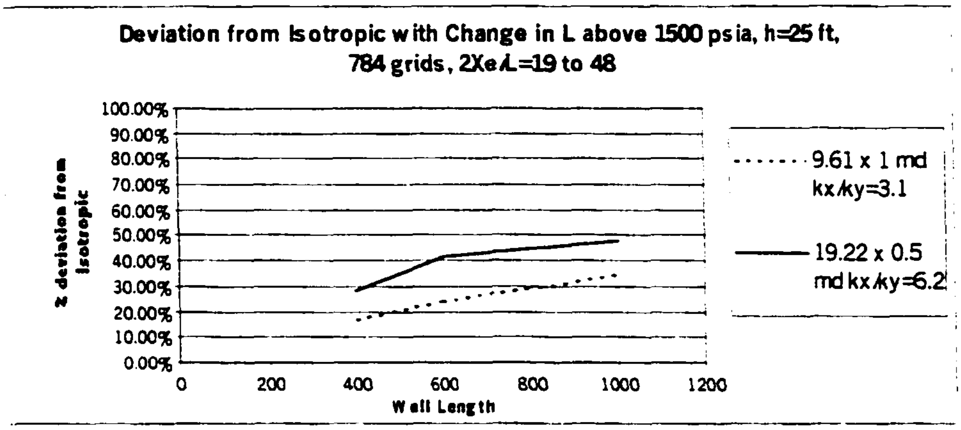

Figure 6.18 Deviation from Isotropic with Change in L above 1500 psia, h=25 ft, 784 grids, 2Xe/L=19 to 48, Large Model

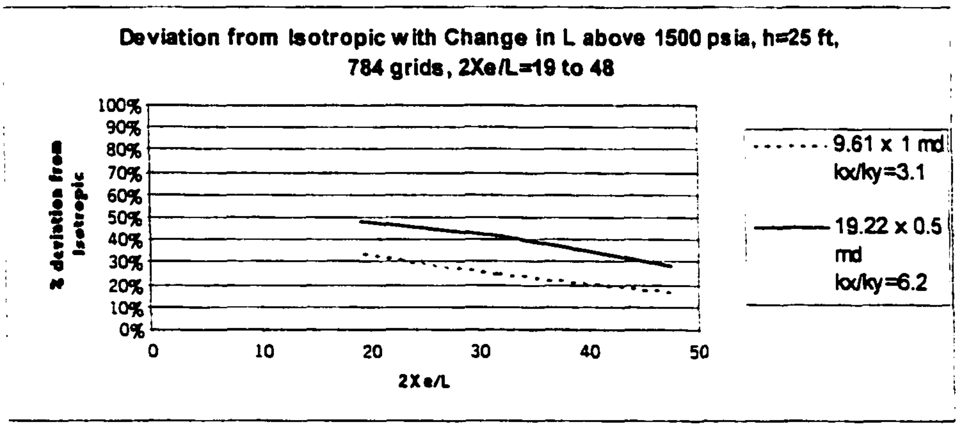

Figure 6.19 Deviation from Isotropic with Change in L above 1500 psia, h=25 ft, 784 grids, 2Xe/L=19 to 48, Large Model

Again an increase in the reservoir thickness also diminishes the deviation from isotropic horizontal permeability as shown by contrasting figures 6.18 and 6.19 with 6.20-1.

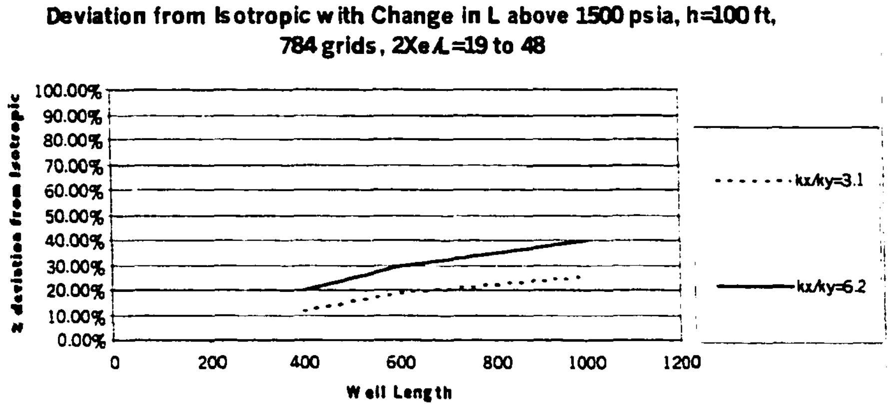

Figure 6.20 Deviation from Isotropic with Change in L above 1500 psia, h=100 ft, 784 grids, 2Xe/L=19 to 48, Large Model

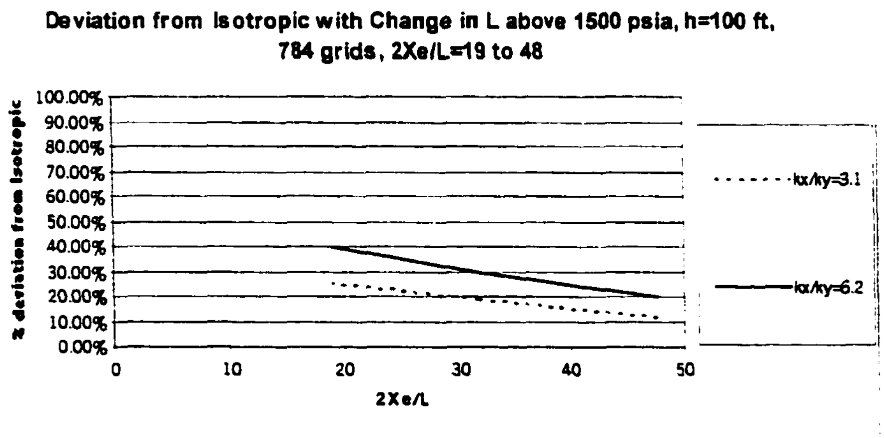

Figure 6.21 Deviation from Isotropic with Change in L above 1500 psia, h=100 ft, 784 grids, 2Xe/L=19 to 48, Large Model

These trends can also be portrayed in more familiar horizontal well terminology as shown in figures 6.22 through 6.25. Though not plotted here, this same general trend toward increasing deviation from isotropic is seen as k_x/k_y increases and L_d increases for any given thickness. Note however the decrease in deviation from isotropic as the thickness increases. The trends are not as clear at lower reservoir pressures however.

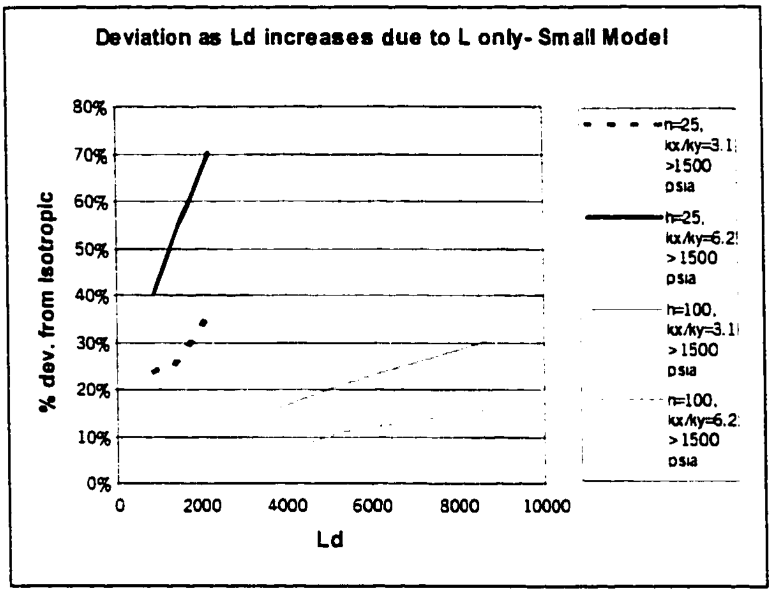

Figure 6.22 Deviation Trend as L_d Varies with Different Thickness (h) - Small Model-

If one tries to make a comparison of changes in deviation as a result of changes in L_d (essentially showing change in L/2h) for any constant ratio of L/2Xe within model types, some confusing results are seen. For instance if one plots the deviation from isotropic of identical well length to horizontal reservoir width ratios, against L_d (essentially L/2h- i.e.combinations of L from 400-1000 and h from 25 to 100) it is apparent that certain trends are evident that are confusing. Figures 6.23 through 6.26 show the comparisons.

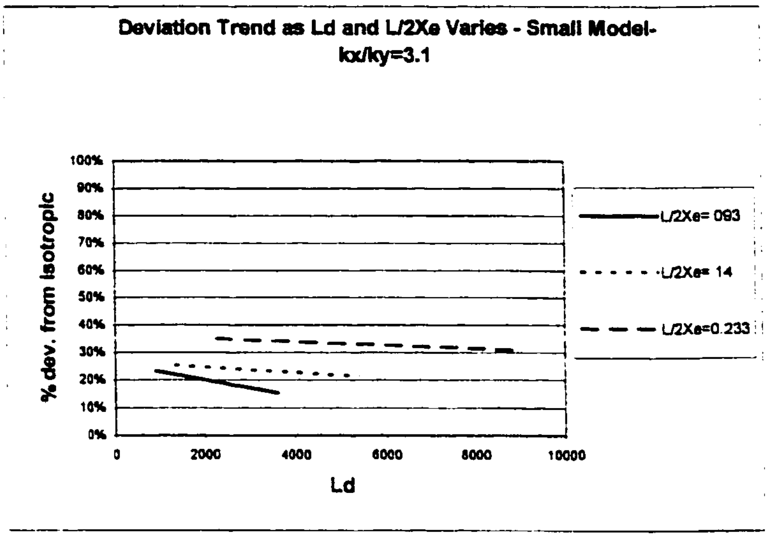

Figure 6.23 Deviation Trend as L_d and L/2Xe Varies - Small Model-k_x/k_y=3.1

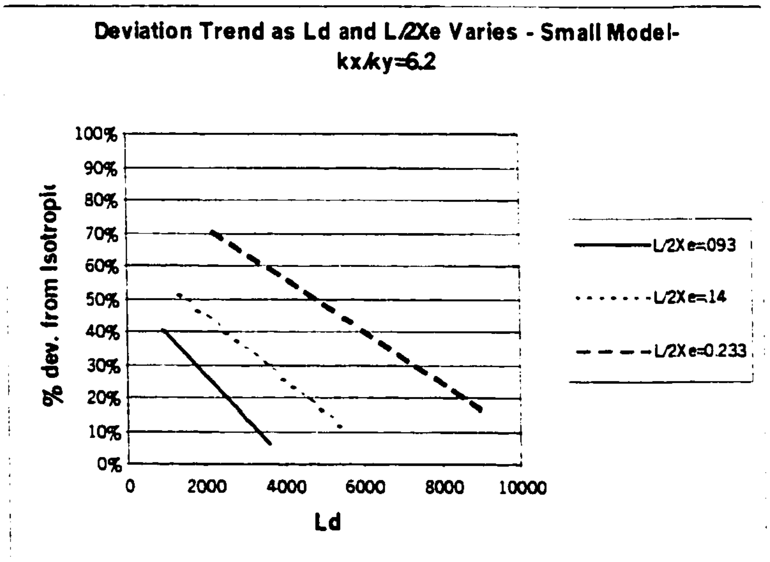

Figure 6.24 Deviation Trend as L_d and L/2Xe Varies - Small Model-k_x/k_y=6.2

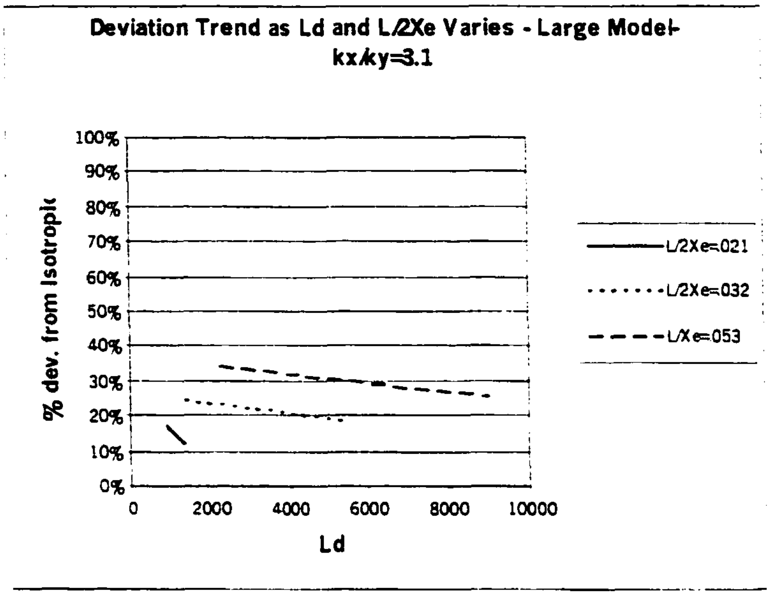

Figure 6.25 Deviation Trend as L_d and L/2Xe Varies - Large Model-k_x/k_y=3.1

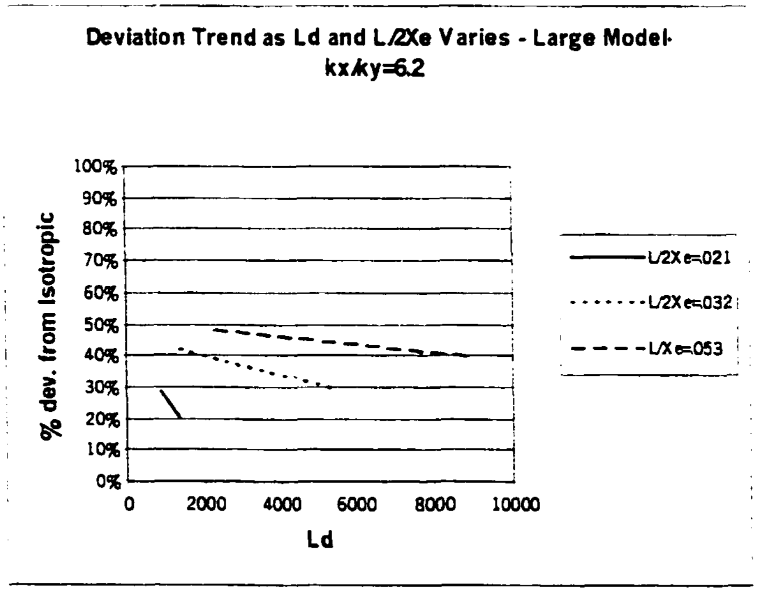

Figure 6.26 Deviation Trend as L_d and L/2Xe Varies - Large Model-k_x/k_y=6.2

6.6.4 Discussion of Experiment Results

Though the expected trend of generally increasing deviation from isotropic, as the ratio of L/2Xe increases (ie the well length increases with respect to the horizontal dimensions) , the unexpected trend is that within each L/2Xe group the deviation decreases with increasing L_d (L/2h). This is confusing but must be a function of the change in h.

The more important things to note in these experiments are:

1. The deviation from the isotropic case increases as the well length increases for any given reservoir thickness and dimension.
2. The deviation becomes more severe with increasing contrast in k_x and k_y.
3. The deviation becomes more severe with decreasing reservoir thickness given a constant well length and horizontal dimension reservoir dimension.
4. The deviation becomes more severe with increasing reservoir pressure.
5. The grid number and size has a relatively minor effect.
6. The flow rate versus pressure deviation from the isotropic horizontal permeability case increases as the ratio of well length to reservoir dimension increases (i.e. the well more fully penetrates the horizontal dimension).
7. The deviation becomes more severe as the contrast in k_x and k_y increases.
8. The deviation becomes more apparent as reservoir pressure increases above the bubble point.

More extensive experiments could be conducted. However until such time as it is determined whether or not these deviations are due to an artifact of the simulator or to a fundamental misconception about effective horizontal permeability, it is sufficient to note that care must be used in interpreting horizontal well simulations in horizontally anisotropic media. Anisotropic permeability is the most common reservoir condition. Traditional theory and analytical equations do not predict that flow rates should vary with changes in horizontal permeability as long as the geometric average of k_x and k_y is constant. Experiments show that as the reservoir becomes large compared to the well length that the deviation becomes less. However the reservoir must become far greater in size relative to the well length than is normally found in practice. With a horizontal well 1000 feet long and a reservoir 19 times that length, the deviation from isotropic case was still significant and the deviation increased as the contrast in k_x and k_y became more pronounced. A comparison of these experiments with other horizontal well simulators would be needed to further study this phenomenon. If the results are the same then more time could be justified in finding empirical correction factors to use with analytical equations.

CHAPTER SEVEN

Horizontal Well Decline Curve Analysis And Studies in Permeability Anisotropy

7.1 Extension of Decline Analysis to Horizontal Wells

If a fractured vertical well increases production rates and increases cumulative production over a certain time period then a horizontal well should have a similar result. In fact if a horizontal well is sufficiently long, (i.e. $L_D > 10$) then the performance of a horizontal well approaches that of a fully penetrating infinite-conductivity fracture and the shape factors will approach those given for fractured wells.

Dimensionless well length L_D is defined as:

$$L_D = \frac{L}{2h}\sqrt{\frac{k_v}{k_h}} \tag{7.1}$$

Where L is the horizontal well length and h is the reservoir thickness in feet. And the previously derived general dimensionless decline analysis should be immediately applicable to a horizontal well by defining the horizontal well in terms of an apparent well bore radius as long as the dimensionless well length is relatively small in comparison to the reservoir dimensions.

7.2 Dimensionless Decline Analysis Using the Horizontal Effective Wellbore Radius Concept and Application

Since it was shown in section 6.2 that an equivalent wellbore radius well could represent the horizontal well it should be possible to extend the generalized decline curve analysis to horizontal wells. Recall that the equivalent well bore radius was expressed as:

$$r_w^{'} = \frac{0.5 r_{eh} L}{a\left[1+\sqrt{1-\left[\frac{L}{2a}\right]^2}\right]\left[\frac{\beta h}{2r_w}\right]^{\frac{\beta h}{L}}} \qquad 7.2$$

And the single-phase flow rate was defined in terms of this wellbore radius as:

$$q = \frac{0.007078\ k_h h(\overline{P_R} - P_{wf})}{\mu_o B_o\left(\ln\frac{r_e}{r_w^{'}} - 0.75\right)} \qquad 7.3$$

Therefore it is only necessary to follow the derivations of the dimensionless decline curve for vertical wells and the extension to horizontal wells is immediate with incorporation of the equivalent wellbore radius. Then as with the radial case, the dimensionless decline rate and time are given by the following expressions (derived in chapters 4 and 5) by just replacing the well bore radius by the effective well bore radius to a horizontal well:

$$q_{Dd} = q_D\left[\ln\frac{r_e}{r_w^{'}} - \frac{1}{2}\right] \quad 7.4$$

or the more general version for other drainage shapes derived in this research:

$$q_{Dd} = \frac{q(t)}{q_{i\max}} = q_D\left[1.151\left[\log\frac{4A}{1.781C_A r_w^{'2}}\right]\right] \quad 7.5$$

And the decline dimensionless time is:

$$t_{Dd} = \frac{t_D}{\frac{1}{2}\left[\left(\frac{r_e}{r_w^{'}}\right)^2 - 1\right]\left[\ln\left(\frac{r_e}{r_w^{'}}\right) - \frac{1}{2}\right]} \quad 7.6$$

or again for more general drainage shapes derived in my previous work:

$$t_{Dd} = \frac{0.00634kt}{\phi\mu c_t r_w^2}\frac{r_w^2}{A}\left[\frac{5.44678}{\log\frac{4A}{1.781C_A r_{w'}^2}}\right] = t_D\frac{r_w^2}{A}\left[\frac{5.44678}{\log\frac{4A}{1.781C_A r_{w'}^2}}\right] \quad 7.7$$

Where the r_w has been replaced by the equivalent well bore radius r_w'. This method will give results that compare well with more laborious equations involving charts and shape factors described in the literature and Joshi's book[23]. However as previously demonstrated (figures 6.3-6.5) the use of the modified $r_w^{'}$ method will yield results as good as the more tedious horizontal shape factors in conjunction with skin factors.

7.3 Re-labeling of Decline Curves for Use in Decline Analysis

The horizontal decline curves then are identical to the previously generated vertical case but relabeled in terms of as $A/r_w^{'}$ or $r_e/r_w^{'}$ instead of r_e/r_w. The curves in terms of A are more appropriate to the linear reservoir convention used with horizontal wells as well as more adaptable to the general shape factors that were previously introduced. The only difference with a horizontal well then is that the apparent well bore radius will be greater than that of the equivalent vertical well. That means the ratio r_e/r_{wa} (r_{eD}) will decrease on the dimensionless decline type curves. k_h and r_{wa} should be calculated exactly as they are for the vertical well except the r_{wa} calculated is a pseudo radius equivalent given by the above expression. Then using the following techniques as with the vertical well we can determine the effect of the horizontal over the vertical well. Therefore the transmissibility can be expressed as:

$$kh = \frac{141.3\mu B}{P_i - P_{wf}} 1.151 \log \frac{4A}{1.181 C_A r_w^{'2}} \left(\frac{q(t)}{q_{Dd}} \right)_{match} \qquad 7.8$$

Since we know $A/r_{w'}^{2}$ from the type curve match, the match point of $q(t)/q_{Dd}$, and the shape factor from the proper curve match we can compute kh for the particular reservoir conditions as we did previously for the vertical well case.

The apparent well bore radius, drainage area and initial reserves can then be computed from the dimensionless decline parameter t_{Dd} and the match points. We know $A/r_{w'}^2$ and t/t_{Dd} from the type curve match point therefore we can compute the apparent well bore radius r_{wa}:

$$r_{wa}^2 = \frac{0.00634k}{\phi\mu c_t \frac{A}{r_w^2}\left(\frac{\log\frac{4A}{1.781C_A r'^2_w}}{5.44678}\right)}\left(\frac{t}{t_{Dd}}\right)_{match} \tag{7.9}$$

Now since we have computed r_{wa} we can calculate the drainage area since from knowing $A/r_{w'}^2$ and computing $r_{wa'}^2$ we can solve for the drainage area A by:

$$A = r_{wa}^2\left(\frac{A}{r_{wa}^2}\right)_{match} \tag{7.10}$$

7.4 Calculation of Reserves from Horizontal Well Decline Curves

Remaining reserves are then computed from the difference between initial reserves and cumulative reserves. This allows for the computation of the original reserves in place from the relationship:

$$N = \frac{A\phi c_t h P_i}{5.615B} \tag{7.11}$$

7.5 Comparison of Vertical and Horizontal Decline Curves

Theoretically then the horizontal and vertical well log-log plots should overlie one another in the pseudosteady state region just as Fetkovich theorized for vertically fractured wells. In other words they would have the same Arps "b" value but exhibit different r_e/r_w ($r_{eD,}$ or the equivalent A/r^2_w) values and thus different q_{Dd} values.

Several horizontal simulation models were conducted to investigate this theory of method equivalency. The simulated vertical vs. horizontal well data of Table 7.1 is graphed in Figure 7.1 and shows this phenomenon.

Horizontal vs. Vertical Comparison of Decline Curves-Simulated Experimental Results.

re	1785	L	1275	ooip	5.48 million	h	100
rw'	39	rw	0.5	Sw	0.25	kv	0.1
a	1842	khor	3.1	x	3315		
beta	5.568	phi	0.05	y	3014		

time	hours	ratev	rateh
31		372	1765
62		320	850
123		294	854
214		266	707
395		239	569
576		219	456
942		187	372
1308		157	332
2304		142	232
3400		128	180
5996		99	93
8592		83	51

Table 7.1 Simulated Vertical and Horizontal Well Data

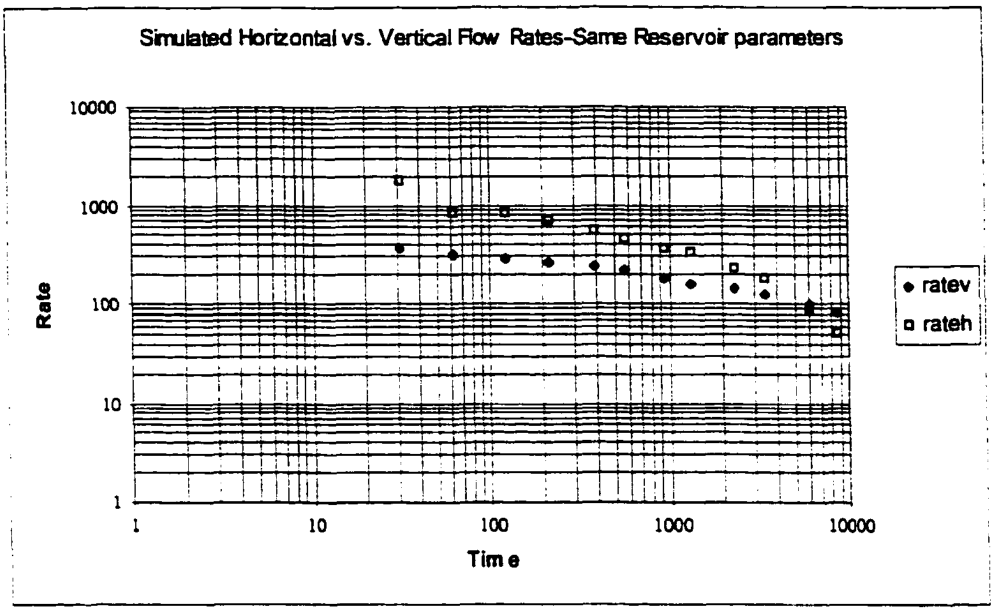

Figure 7.1 Simulated Horizontal vs. Vertical Flow Rates-Same Reservoir Parameters

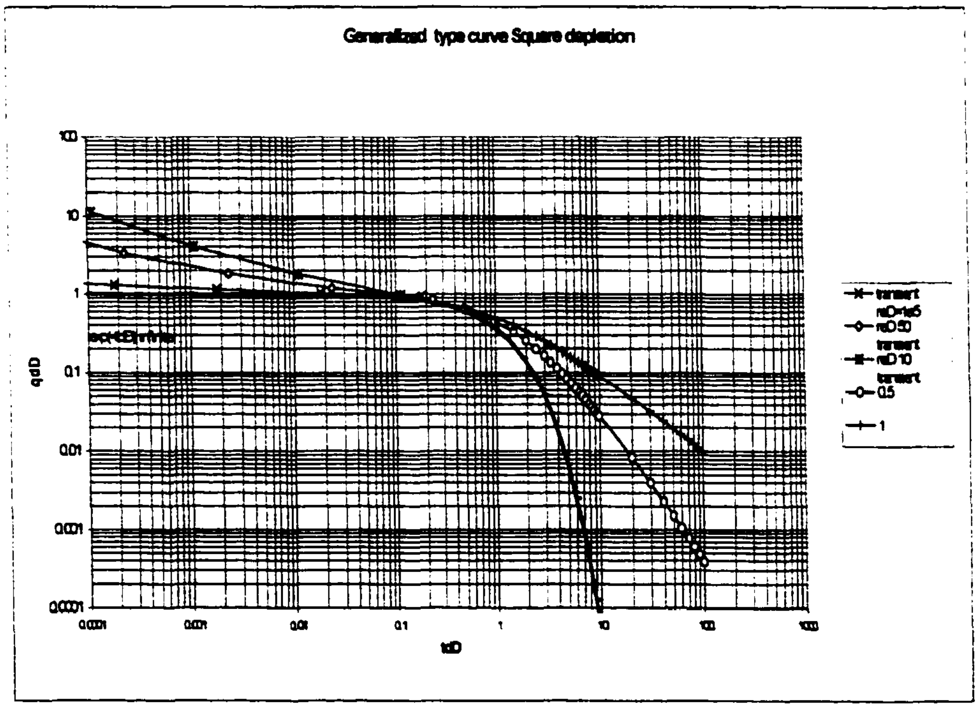

Figure 7.2 Generalized Type Curve Square Depletion

Though the simulation could have been run longer, it still shows the essential effect of a vertical vs. horizontal well on the identical reservoir parameters and size. When Figure 7.2, the dimensionless decline curve, is plotted at the same scale as figure 7.1 a type curve match is made. Using the match points for the vertical well vs. the horizontal well and applying the relationships presented in sections 7.2 through 7.4 yields a match of r_{eD} of 10 for the horizontal well and r_{eD} of 50 for the vertical well. This verifies the prediction of the previous statement that r_{eD} would decrease for the horizontal well because of a larger apparent wellbore radius. Therefore the value of the r_{eD} match can then be used to determine the apparent effective wellbore radius r'_{wa} from the time match points and kh from the rate matches. Once the apparent well bore radius of the horizontal well is determined it can be multiplied by the r_{eD} match point to determine the drainage radius and then used to calculate the reserves as shown in previous chapters.

7.6 Decomposition of k_x and k_y

If the horizontal well is long in comparison to the reservoir dimensions then the drainage shape and well penetration factors become important as was shown in the previous chapter. The horizontal shape expressions can then be incorporated as functions of the following factors:

1. Drainage area shape: $2X_e/2Y_e$ where x and y are the half-length of the reservoir in the x and y directions respectively.

2. Well Penetration ratio: $L/2x_e$

3. Dimensionless well length defined before as: $L_D = \frac{L}{2h}\sqrt{\frac{k_v}{k_h}}$

Methods to predict the performance of horizontal wells in anisotropic, naturally fractured reservoirs require knowledge of or assumptions regarding k_x and k_y since rectangular drainage shapes are usually assumed. And k_x and k_y will determine, to a large extent, the dimensions of the drainage shape. The basic drainage shape is defined as $2X_e/2Y_e$. Unfortunately the horizontal permeability components k_x and k_y (k_h=sqrt($k_x k_y$)) are rarely known. Interference test data, which can provide k_x and k_y information, is also rarely available. However it may be possible to estimate these directional permeabilities if drainage shapes can be inferred from an analysis of actual production decline curve characteristics among offset wells.

7.6.1 General Directional Permeability Background Discussion

Several methods have been introduced to determine productivity and predict future horizontal well performance in anisotropic naturally fractured reservoirs. These methods require assumptions as to directional permeability, k_x, k_y, k_z which are almost never known. It seems that we should be able to perform the inverse and determine reservoir drainage area and shape, and thus infer directional permeabilities, if sufficient production history is known. Predicting the total drainage area around the producing well should be obtainable. However a prediction of how this drainage area is distributed may be difficult to determine. Distribution depends on the value of k_x and k_y. The larger the value of k_y/k_x the longer the drainage distance along the high permeability y direction. A literature review indicates no other attempts to obtain this information with horizontal wells in anisotropic media.

Indeed a determination of reservoir shape and k_x, k_y, k_z could then be used to input to established predictive equations to predict future production more accurately. Also most models seem to ignore relative permeability. The permeability in these equations in fact should be replaced with relative permeability but this is often not done.

Recall that Arps[1,2] and Fetkovich[3] developed decline curve equations, based on pseudosteady state theory as early as 1945, which are still used today. As previously discussed, these relations take the form of:

$$q = \frac{q_i}{\left(1 + b D_i t\right)^{1/b}} \tag{7.12}$$

where:

$$D_i = \frac{0.00634k}{0.5\phi\mu\, c_t r_w^2\left(\frac{r_e^2}{r_w^2} - 1\right)\left(\ln\frac{r_e}{r_w} - 0.5\right)} \tag{7.13}$$

For a horizontal well, the effective well bore radius r_w' can be expressed as:

$$r_w = \frac{0.5\, r_{eh} \frac{L}{a}}{\left(1+\sqrt{1-\left(\frac{0.5L}{a}\right)^2}\right)\left(0.5\,\beta\,\frac{h}{r_w}\right)^{\frac{\beta h}{L}}} \qquad \textbf{7.14}$$

and

$$a = 0.5L\left(0.5+\sqrt{0.25+\left(\frac{2\,r_{eh}}{L}\right)^4}\right)^{0.5} \qquad \textbf{7.15}$$

$$\beta = \left(\frac{k_h}{k_v}\right)^{0.5} \qquad \textbf{7.16}$$

$$k_h = \sqrt{k_x\, k_y} \qquad \textbf{7.17}$$

where r_{eh} is the equivalent drainage area of the horizontal well. If vertical wells are available in the area, traditional test methods and production data can give an estimate of the total drainage area. For instance if the drainage area of a vertical well is 40 acres then the equivalent vertical radius, r_{ev} is 745 feet by using the relationship[6]:

$$AreaofCircle = \pi r_{ev} = acres * 43560 \qquad \textbf{7.18}$$

$$r_{ev} = \sqrt{\frac{A * 43560}{\pi}} \qquad \textbf{7.19}$$

Joshi presents a method for finding the equivalent horizontal well drainage area based on a rectangle bounded on the long sides by semi-circles[23]. Now applying that r_{ev} to the diagram below, the following relationships can be derived:

$$A = \frac{\pi r_{ev}^{2} + 2Lr_{ev}}{43560} \qquad 7.20$$

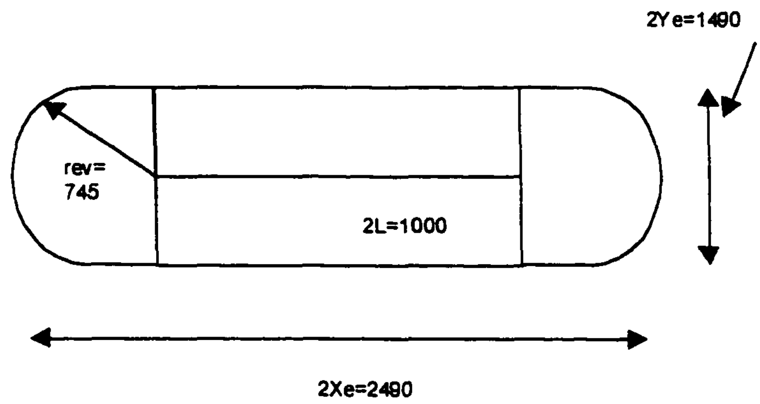

Figure 7.3 Equivalent Horizontal Wellbore Radius

In the above example the equivalent horizontal wellbore radius, r_{eh}, would be 1014 feet for a lateral well of 1000 feet and r_{ev} of 745 feet.

7.6.2 Decomposing k_x and k_y

With this equivalent radius information, r_{eh}, it is possible to insert into equation 7.14 to solve for $r_w^{'}$. If the reservoir thickness is 100 feet this would yield $r_w^{'} = 406/(100\beta)^{0.2\beta}$.

Now r_w' can be obtained by the decline curve methods introduced in Section 7.3 to solve for $\beta=(k_y/k_x)^{0.5}$. Once k_h is found in this manner one can concentrate on decomposing k_h into k_x and k_y if rectangular or elliptical drainage shape is assumed which is reasonable in horizontal wells in naturally fractured reservoirs as well as many drainage shapes in vertical well situations.

It can be shown that the drainage shape is dictated by the contrast in k_x and k_y so that:[23]

$$\frac{2Y_e}{2X_e}=\sqrt{\frac{k_y}{k_x}} \tag{7.21}$$

Therefore it seems that it should be possible to decompose k_x and k_y if there are competing wells with sufficient drainage history to identify the time to competition for drainage area. The hypothesis is that there should be an observable break in the production decline or cumulative versus time plots when wells begin competing for drainage. In other words there should be some type of interference imprint or deviation from the drainage area predicted from early time rate and cumulative data (see figure 7.36 for example). Or alternatively if several wells experience interference at roughly the same time, the distance between the two wells should give the ratio of $2Y_e/2X_e$ by approximately:

$$\frac{t_{yint}}{t_{xint}}\frac{2Y_e}{2X_e}=\sqrt{\frac{k_y}{k_x}} \tag{7.22}$$

$$2X_e * 2Y_e = A * 43560 \qquad 7.23$$

where t is the interference time in the various directions. Vector analysis could be applied to resolve the potential angular problems.

If the time or distance ratio is known then the relative relationship between k_x and k_y should be obtainable. For instance if the time/distance ratios are 3 then k_y=9k_x. Extensive simulation experiments and pressure versus time visualization analysis were conducted to study this hypothesis. The complete graphical output and tabular experimental output is very voluminous but is available from the author.

7.6.3 Studies in Anisotropic Media – k_x k_y Experimental Results

Numerous experiments were conducted to study the effects of horizontal anisotropy on well performance with the objective of finding ways to decompose k_x and k_y using production data that would normally be available to the practicing engineer. Normal data available would be limited to fluid rates, cumulative production volumes and time. Monthly production data are all that can be expected after the first few months of production. Although not published, daily rates are often kept by the operator for early time periods and can be obtained by contacting operators. Thus this analysis will be restricted to that data that can be normally obtained. Unfortunately pressure data are rarely available. Pressure will be used in this analysis but only as a visualization technique to illustrate the various rate decline points of the rate decline curves.

7.6.3.1 Visualization and Identification of Important Points - Rate Decline Curves

A 14,000 ft. by 14,000 ft. 3-well system was tested with orientation as in figure 7.4. The wells are equal distance from each other (3000 feet) and oriented along separate permeability paths, which would be realistic in some field spacing units initially.

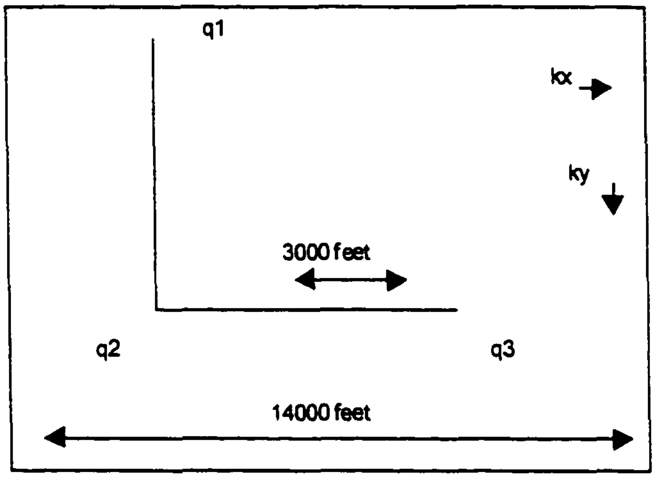

Figure 7.4 Model Geometry

The following graphs depict the rate-time, cumulative-time and pressure distribution versus time. The case of k_x=19.22, k_y=0.5 (geometric mean 3.1 md) is contrasted with the isotropic case of 3.1 md. Figures 7.5 and 7.7 show the rate-time plot for the anisotropic and isotropic cases respectively. Figures 7.6 and 7.8 are the cumulative versus time plot for the anisotropic and isotropic cases respectively. The times to the various slope changes are noted on Figure 7.5 and 7.7 and visual pressure distribution diagrams are plotted for each of these times in figures 7.10 to 7.17 for the anisotropic case and 7.18 through 7.26 for the isotropic case. Figure 7.9 shows the various portions of the rate time curve for which slopes are calculated for each well in the model.

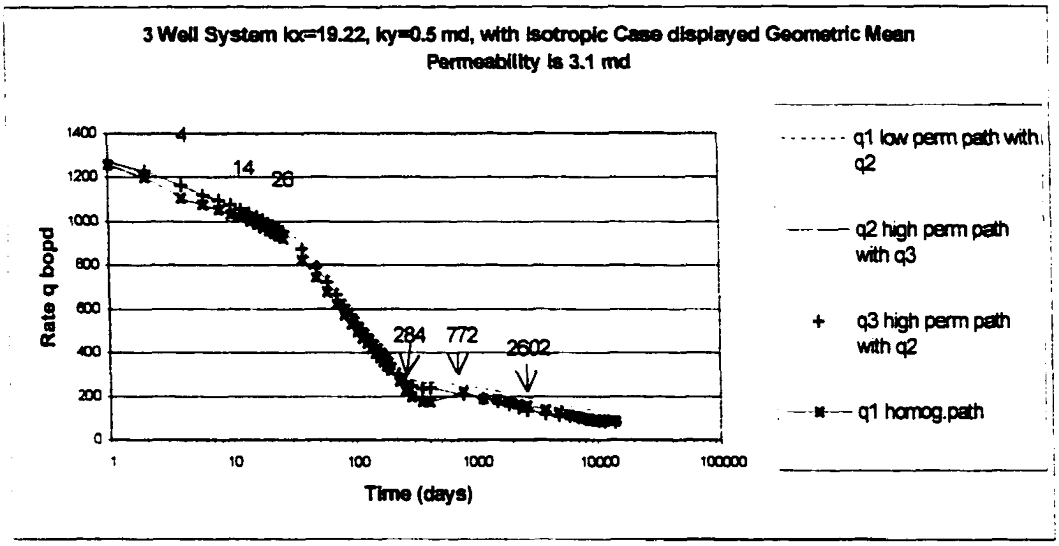

Figure 7.5 3 Well System kx=19.22, ky=0.5 md, with Isotropic Case Displayed Geometric Mean Permeability is 3.1 md

Figure 7.6 shows the effect of the rates illustrated in figure 7.5. Notice the dramatic departure in cumulative production where the well (q1) that is oriented along the low permeability path with respect to q2 retains its higher rates and therefore its higher cumulative production compared to well q3 along the high permeability path. This shows the clear mark of drainage competition more quickly along the high permeability path. Compare this to figure 7.8 which shows the cumulative departure between wells at a much later time with the isotropic case.

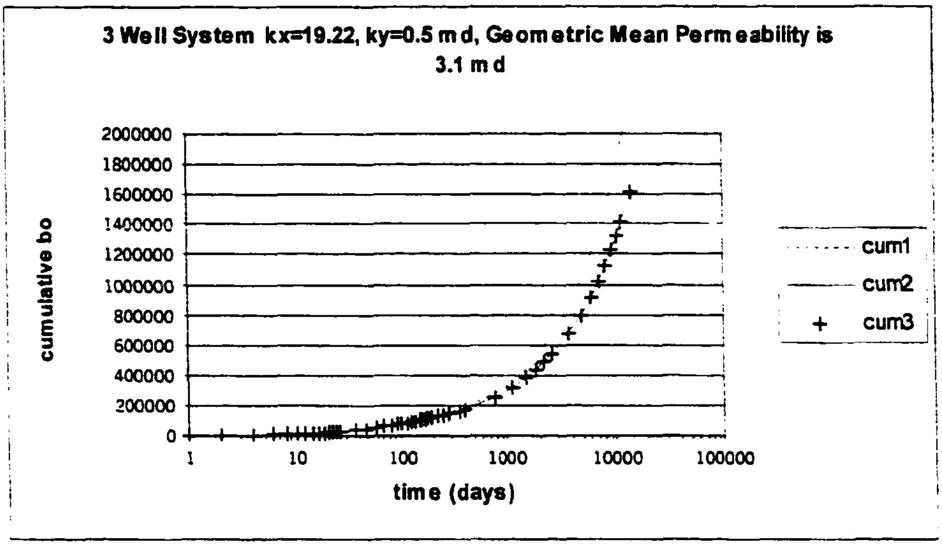

Figure 7.6 3 Well System kx=19.22, ky=0.5 md, Geometric Mean Permeability is 3.1 md

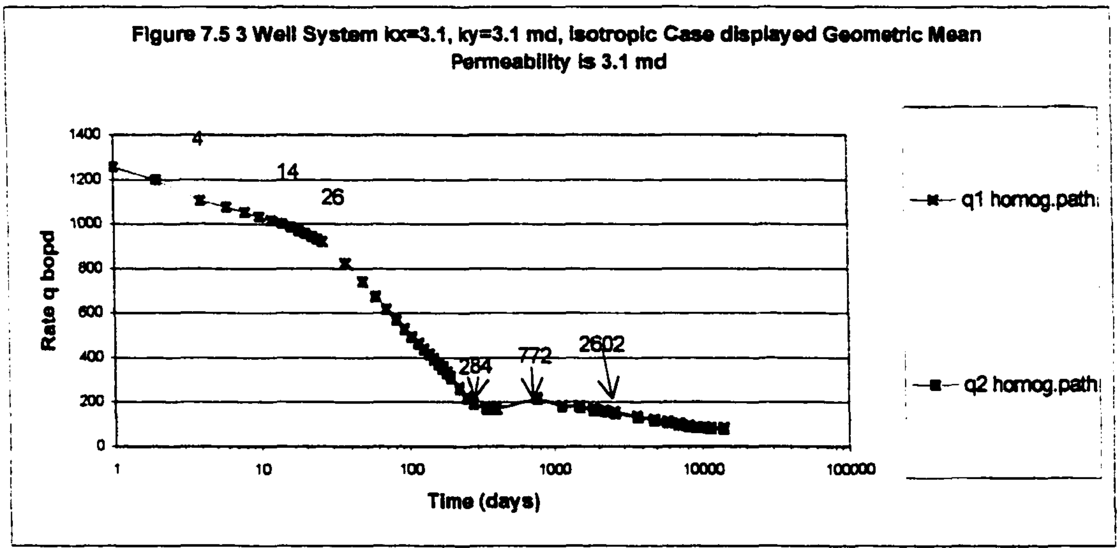

Figure 7.7 3 Well System kx=3.1, ky=3.1 md, Isotropic Case Displayed Geometric Mean Permeability is 3.1 md

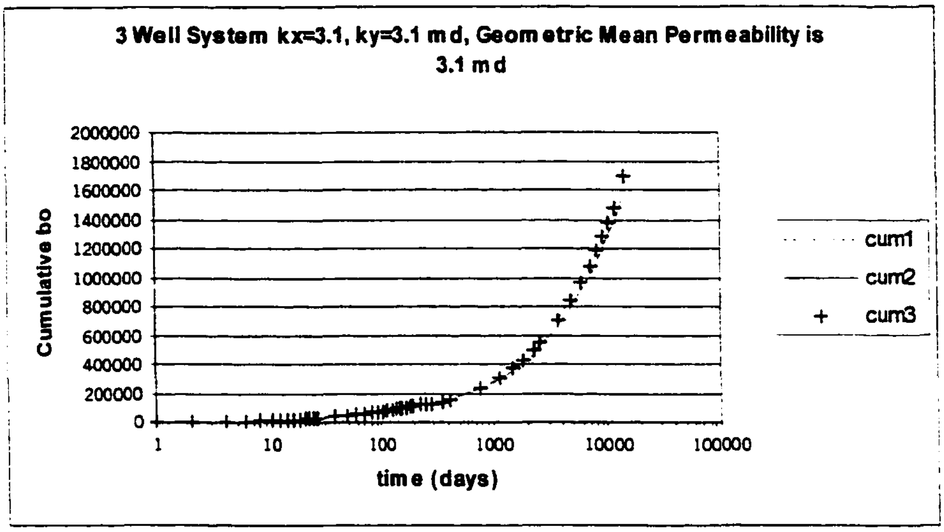

Figure 7.8 3 Well System kx=3.1, ky=3.1 md, Geometric Mean Permeability is 3.1 md

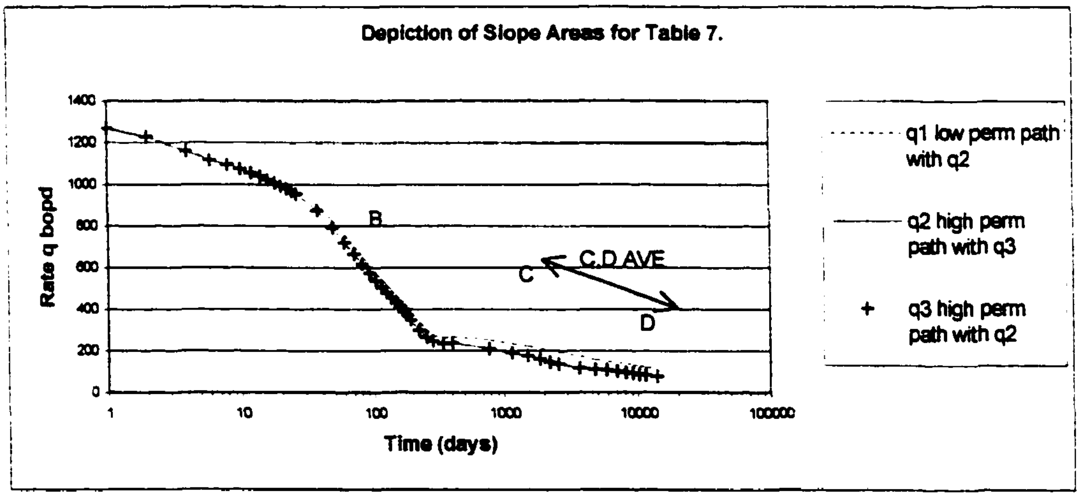

Figure 7.9 Depiction of Slope Areas for Table 7.

Table 7.2 shows the various slopes and departure times of cumulative production between the various competing paths of the two cases as well as the slopes for an intermediate case of k_x =9.61 and k_y = 1.0 md. Figures 7.10 through 7.25 show the pressure distribution profiles that help in understanding what is happening in the model at the various time steps. Figures 7.36 and 7.27 illustrate the effect on the productivity index.

Slopes of Semilog rate versus time plots

SQRT(KX/KY)		q1	q2,q3	q1	q2,q3	q1	q2,q3	q1	q2,q3
CONTRAST	Region	B1	B2	C1	C2	D1	D2	CD1AVE	CD2AVE
6.2	19.22,0.5	710	706	138	106	80	96	103	108
3.1	9.61.1	697	693	100	89	72	69	95	93
1	3.1,3.1	714	707	118	118	22	22	93	103

Times at which q1 deviates from q2,q3 rates for different permeability ratios (geometric mean equal 3.1 md)

SQRT(KX/KY)		Noticable on		Noticable on q1/q3	
CONTRAST	Region	Cumulative vs. Time		Ratio	
		time	ratio	time	ratio
6.2	19.22,0.5	284	5.30	8	4.6
3.1	9.61.1	406	3.70	14	2.6
1	3.1,3.1	1504		37	

Table 7.2 Slopes of Various Portions of the Decline Curve

The data suggest that the cumulative time versus departure time comparison can give a rough approximation of the ratio of permeability in the x and y directions.

Figures 7.10 to 7.13 - Anisotropic Pressure Distribution Profiles for Figure 7.5

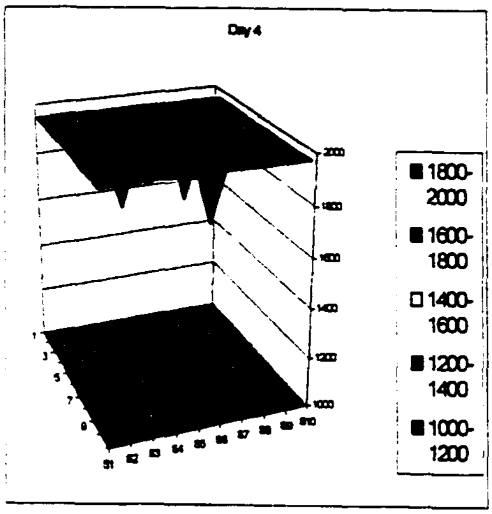

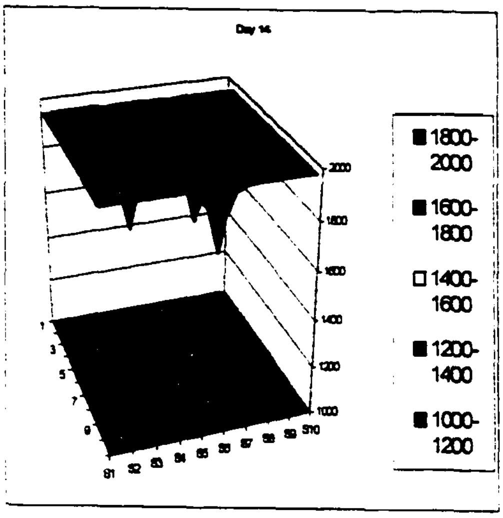

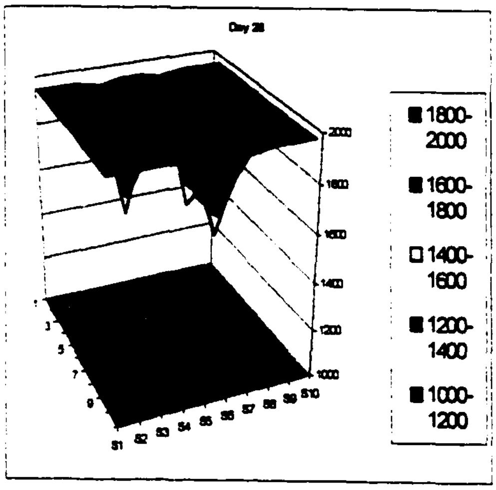

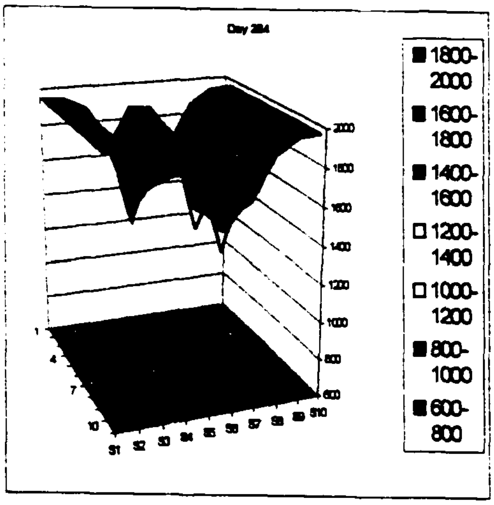

Figures 7.14 to 7.17 - Anisotropic Pressure Distribution Profiles for Figure 7.5

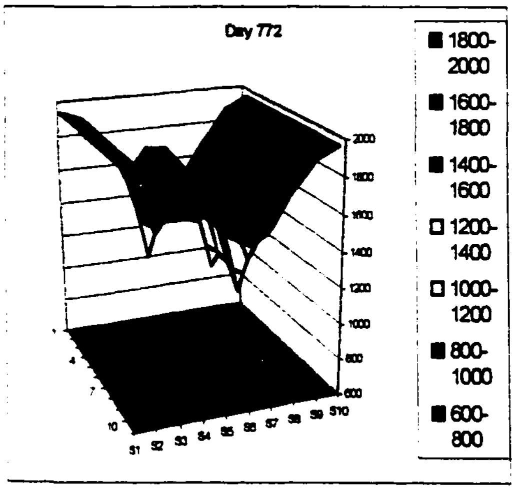

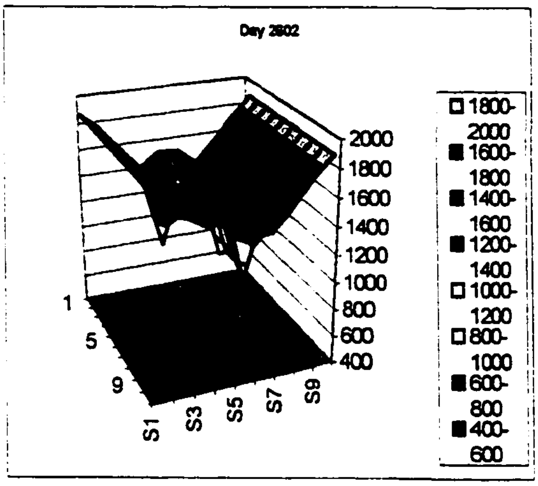

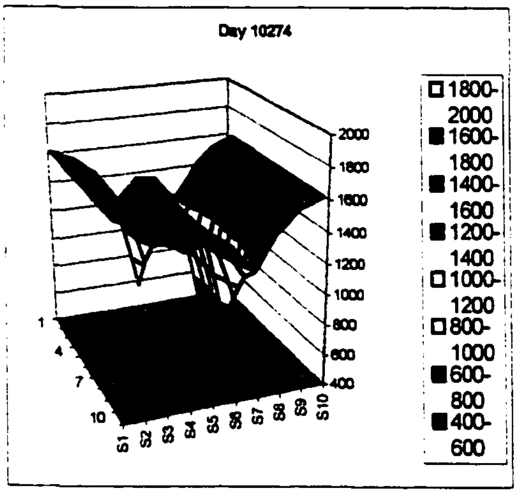

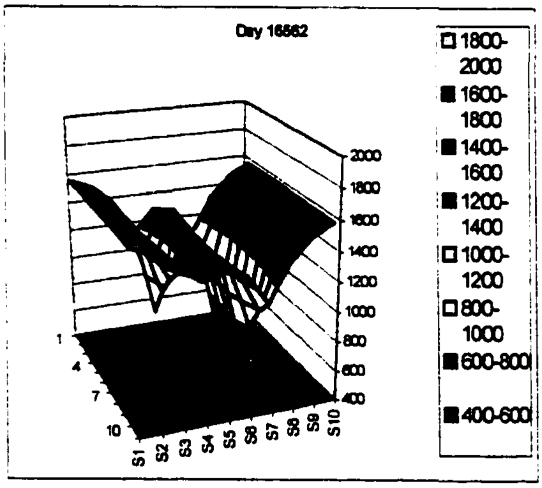

Figures 7.18 to 7.21 Isotropic Case Pressure Distribution Profiles

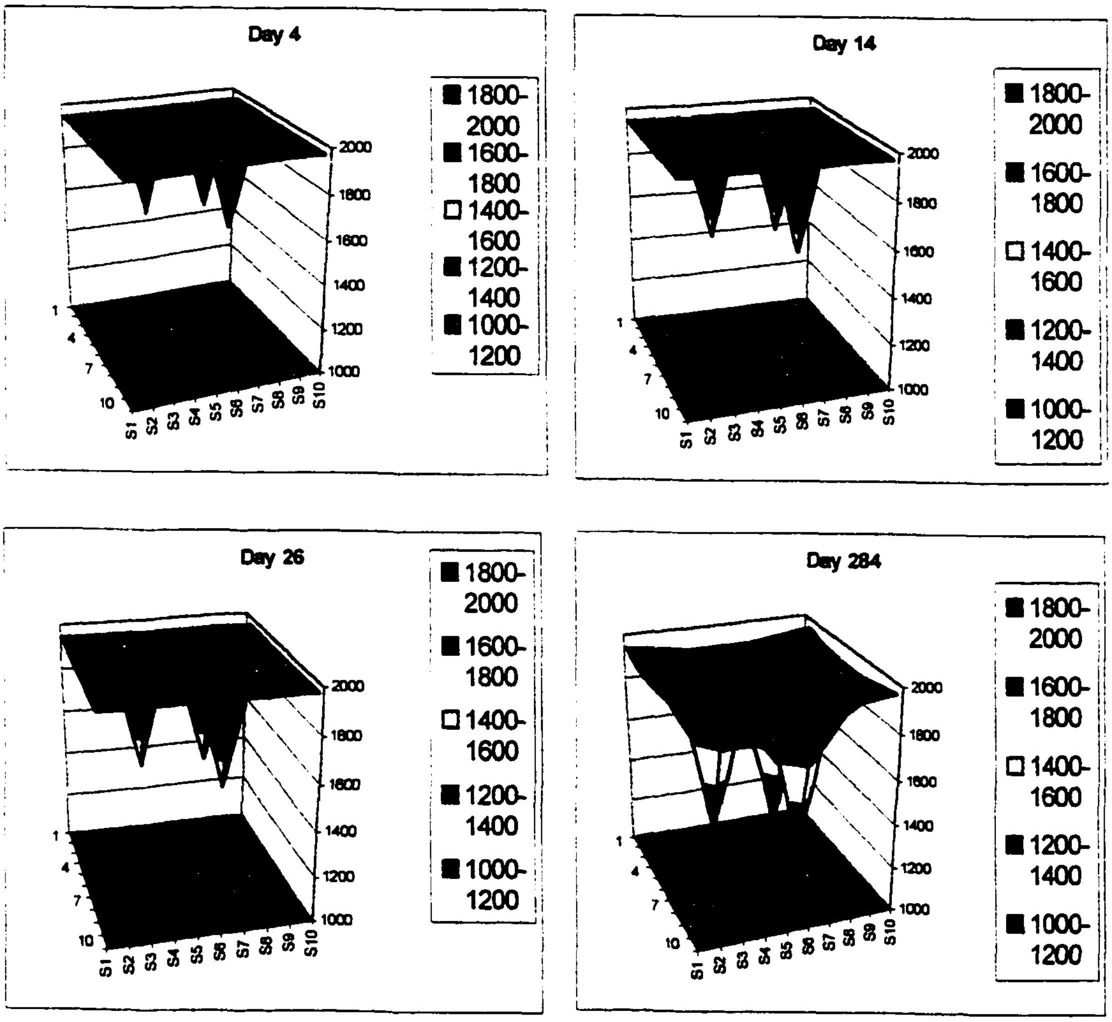

Figures 7.22 to 7.25 Isotropic Case Pressure Distribution Profiles

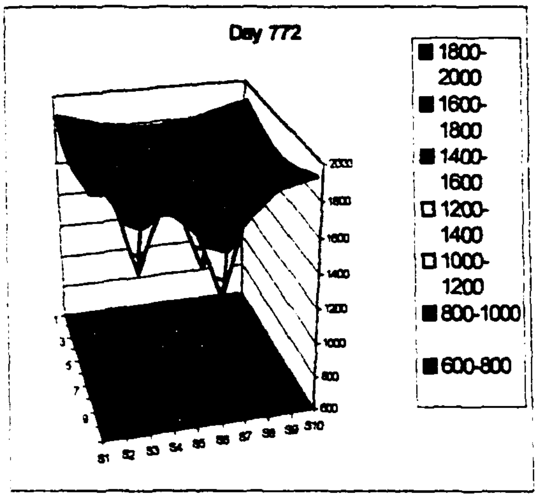

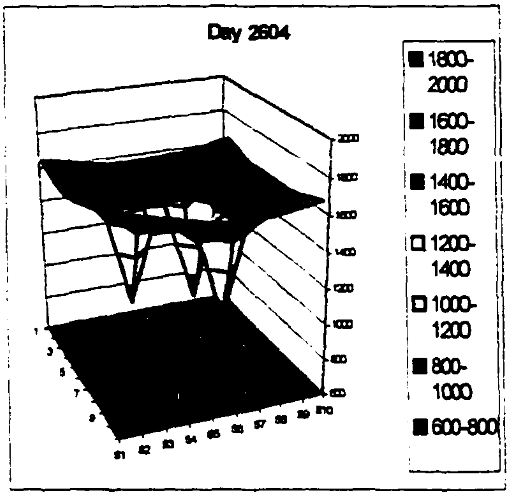

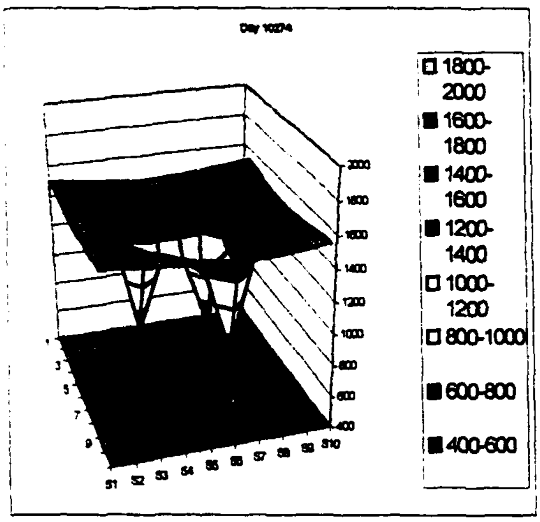

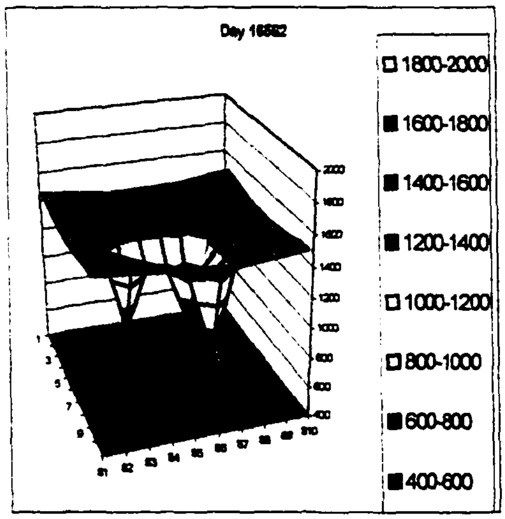

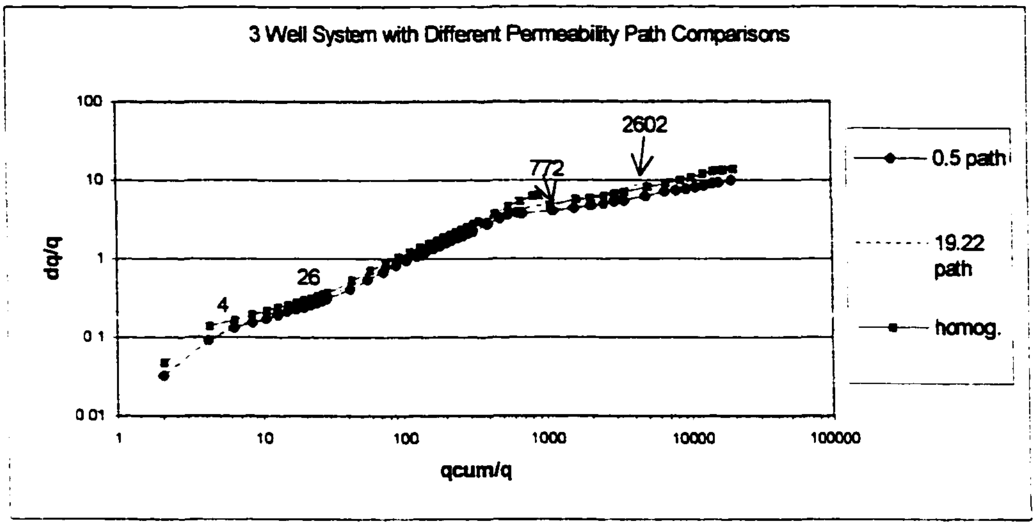

Figure 7.26 3 Well System with Different Permeability Path Comparisons

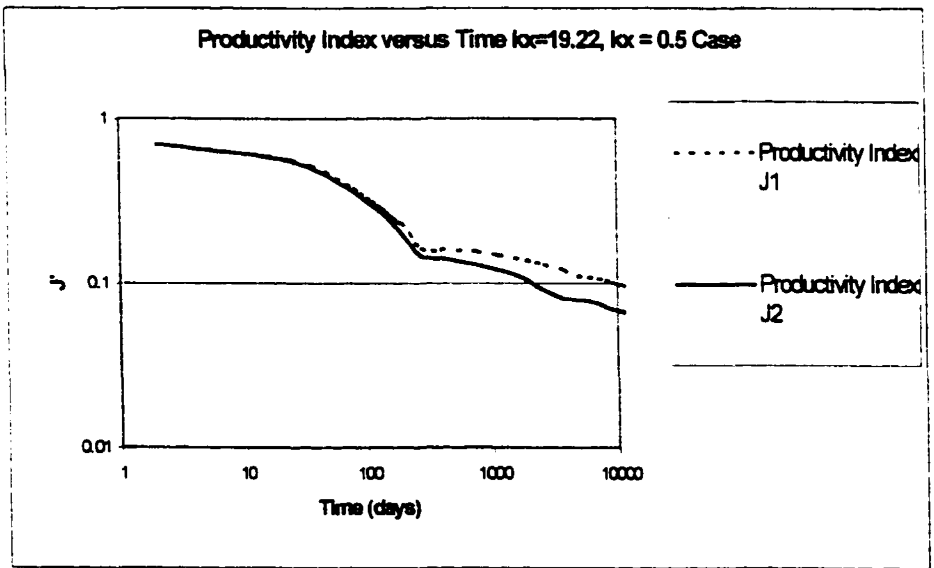

Figure 7.27 Productivity Index $J^{'}=q/(p_{ave}-p_{wf})$ versus Time k_x=19.22, k_x = 0.5 Case

7.6.3.2 Anisotropic Experiments in Two Well System

The same type of analysis can be conducted for the case of a two well system in which the two wells are parallel to the x and y directional permeability. In other words the experiment involves wells q1 and q2 alone and then q2 and q3 alone from the previous model. Then the same type of analysis is shown below for the various anisotropic cases.

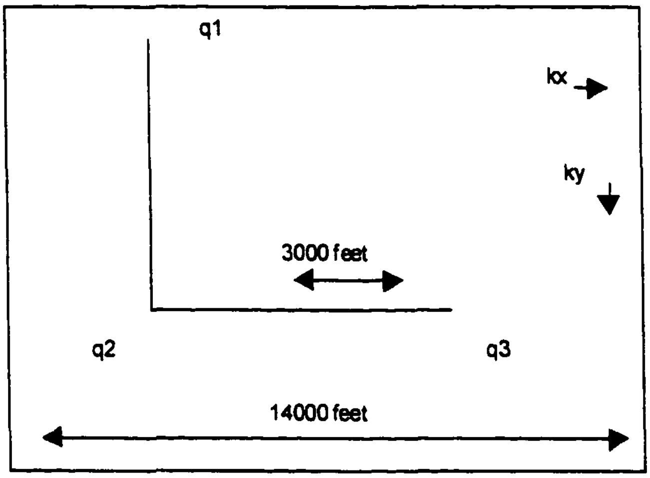

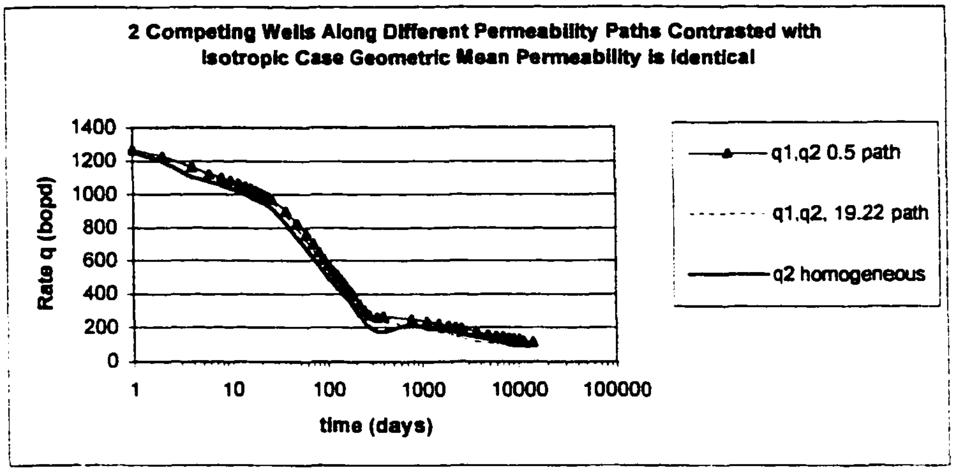

Figure 7.28 2 Competing Wells Along Different Permeability Paths Contrasted with Isotropic Case Geometric Mean Permeability is Identical

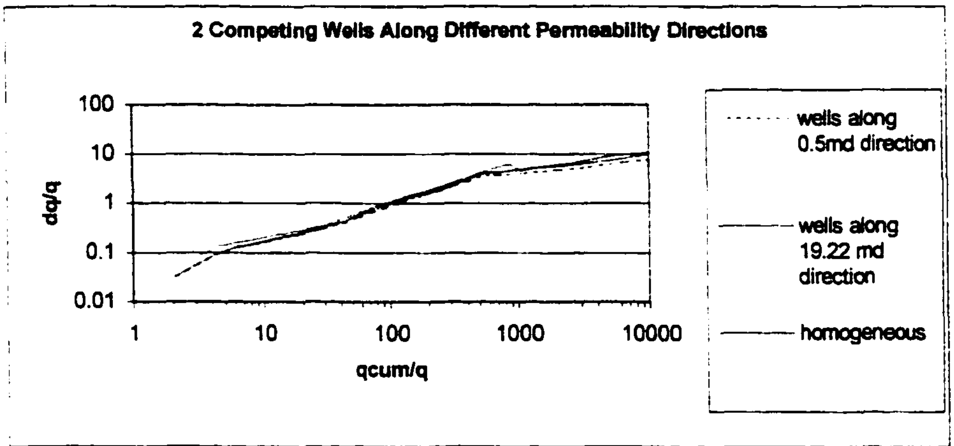

Figure 7.29 2 Competing Wells Along Different Permeability Directions

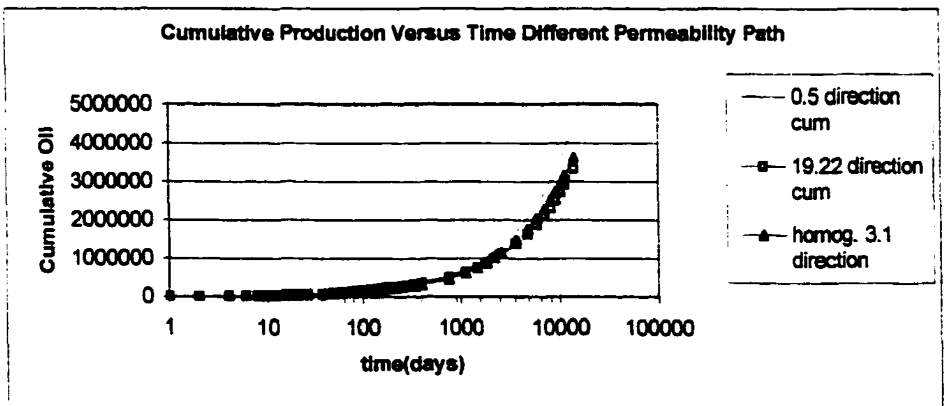

Figure 7.30 Cumulative Production Versus Time Different Permeability Path

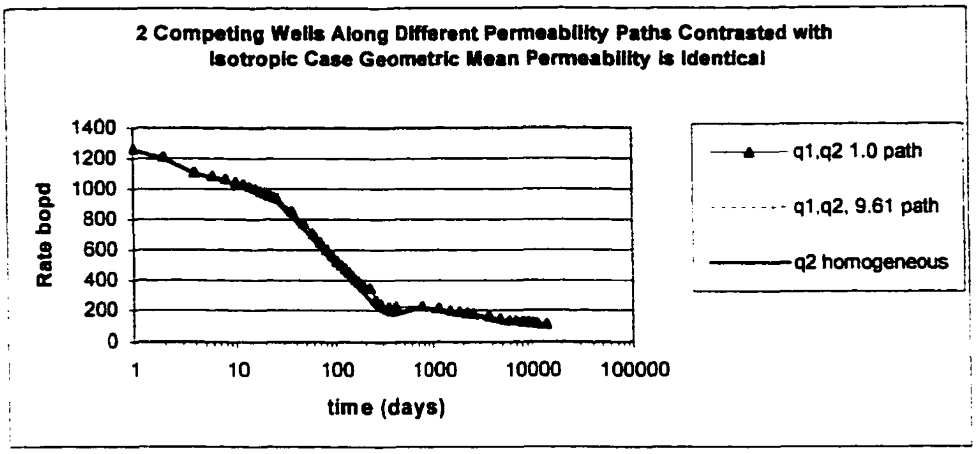

Figure 7.31 2 Competing Wells Along Different Permeability Paths Contrasted with Isotropic Case Geometric Mean Permeability is Identical

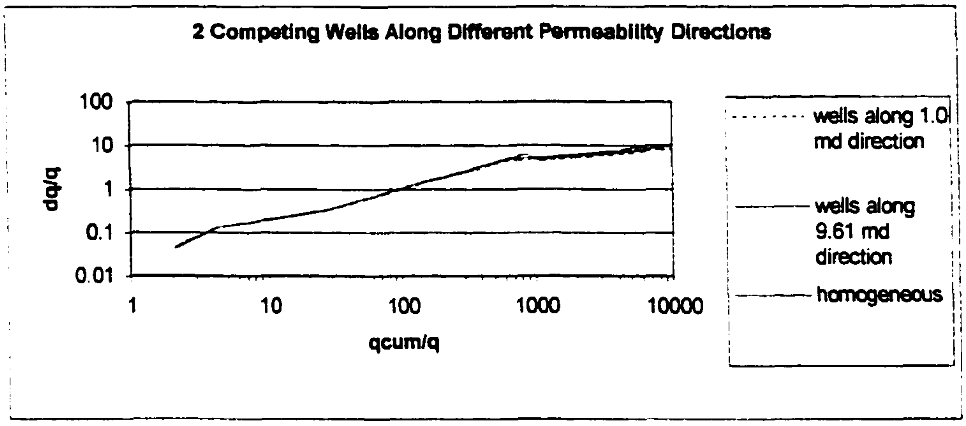

Figure 7.32 2 Competing Wells Along Different Permeability Directions

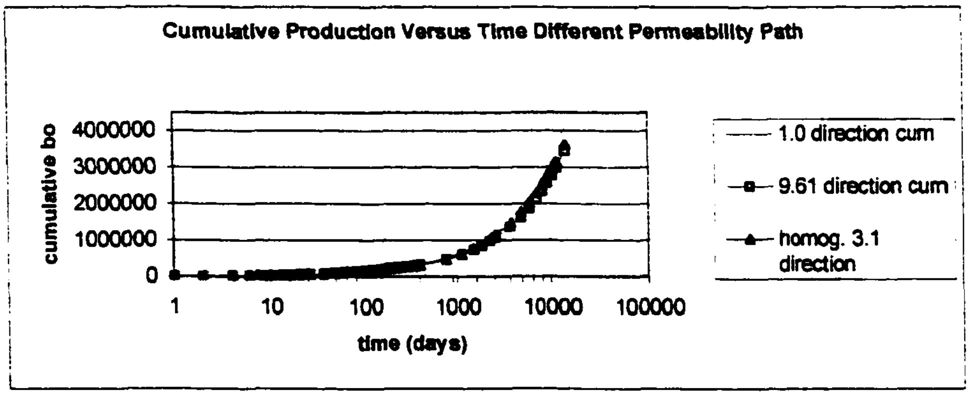

Figure 7.33 Cumulative Production Versus Time Different Permeability Path

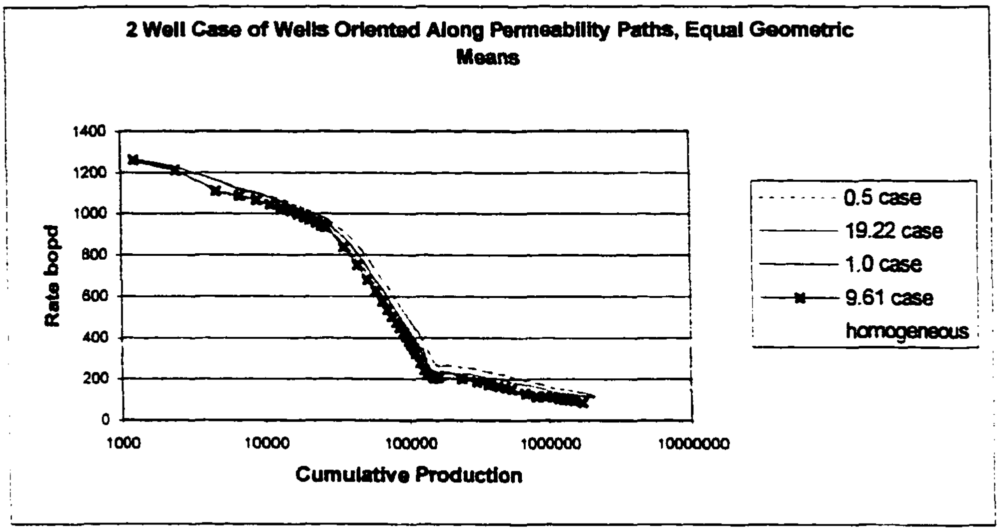

Figure 7.34 2 Well Case of Wells Oriented Along Permeability Paths, Equal Geometric Means

Table 7.3 shows the times at which the various wells along certain permeability paths depart from the isotropic case. Note that the ratio of the times (distance between wells is identical) seems to follow the ratio of the square root of the permeability ratios in the x and y directions.

Permeability Constrast (geometric mean both 3.1 md)	0.5,19.22	1,9.61
Sqrt (kx/ky)	6.2	3.1
Departure Times from Isotropic	406	345
Departure Times from Each Other	2602	1138
Time Ratio	6.4	3.3

Table 7.3 Relation of Permeability Ratio to Cumulative Departure Times

The method thus seems to give a rough approximation to directional permeability.

7.6.4 Determination of the Principle X and Y Permeability Components

If three values of permeability can be determined and the angle between those three values is known then the permeability in the principle x and y directions can be determined by application of rock mechanics techniques. (homework in Rock Mechanics, 1995) For instance in the following diagram:

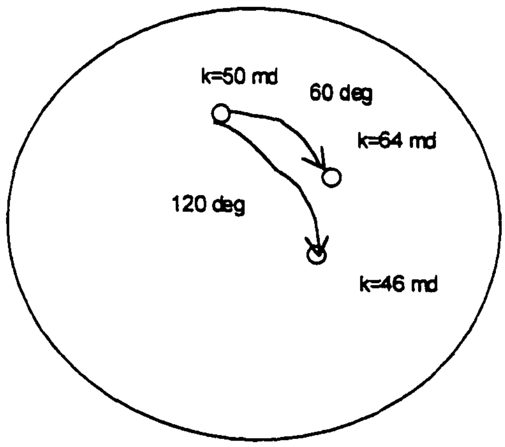

If three points (strain or permeability) and the angles between the observation points are known a Mohr circle approach can be used to calculate the principle values. Alternatively rock mechanics homework indicated that a matrix solution could be used also. These methods used strain values but extension to permeability values should work also.

$$\begin{matrix} k_A \\ k_B \\ k_V \end{matrix} = \begin{pmatrix} \cos^2\alpha_A & \sin^2\alpha_A & \dfrac{\sin 2\alpha_A}{2} \\ \cos^2\alpha_B & \sin^2\alpha_B & \dfrac{\sin 2\alpha_B}{2} \\ \cos^2\alpha_C & \sin^2\alpha_C & \dfrac{\sin 2\alpha_C}{2} \end{pmatrix} \begin{pmatrix} k_x \\ k_y \\ k_{xy} \end{pmatrix} \qquad 7.24$$

$$\begin{matrix} kx \\ ky \\ kxy \end{matrix} = \begin{pmatrix} \cos^2\alpha_A & \sin^2\alpha_A & \dfrac{\sin 2\alpha_A}{2} \\ \cos^2\alpha_B & \sin^2\alpha_B & \dfrac{\sin 2\alpha_B}{2} \\ \cos^2\alpha_C & \sin^2\alpha_C & \dfrac{\sin 2\alpha_C}{2} \end{pmatrix}^{-1} \begin{pmatrix} k_A \\ k_B \\ k_C \end{pmatrix} \qquad 7.25$$

This yields k_x=46 and k_y=61 and k_{xy}=16. This in turn can be used to compute k_1 and k_2 as 64 and 42 md. Alternatively the Mohr circle can be used to arrive at the same results.

7.7 Application to Decline Analysis Methods for Horizontal Wells in Fractured Reservoirs

When a well is first put on production, the pressure transient travels away from the well towards the well drainage boundaries. Once the pressure transient has reached all the drainage boundaries then the average reservoir pressure starts dropping with time. This flow period before the well sees the drainage boundary is known as the transient state.

Depletion state is the post-transient flow period and is also known as the pseudosteady state flow period.

For mathematical treatment, either constant flowing well bore pressure or constant production rates are normally assumed. A constant production rate implies that flowing bottom hole and wellhead pressures are declining with time. This is typical of fields where the production level is limited by such things as production allowable or critical rates due to gas/water coning problems. A constant bottomhole flowing pressure is the more typical situation. Actually this is in reality a constant flowing wellhead pressure which is maintained constant against the backpressure of a production facilities. This constant wellhead pressure implies a decline in production rates.

Type curves for horizontal well flow in a closed rectangle have been constructed in the past. As discussed before these do not model the fractured reservoir well but serve as a starting point for analysis. The methods essentially involve solving the dimensionless pressure solution P_d using the exact mathematical solution of the Laplace transform of the constant production rate equation[33,39,40]. The objective is to calculate dimensionless pressure, P_D and dimensionless rate q_D for different values of dimensionless time t_D. This is done by taking any dimensionless time t_D, calculating the dimensionless pressure, converting to dimensionless rate ($q_D = 1/P_D$) then converting to real rates.

If k_h can be determined, then the following procedure can be used to generate well performance predictions for horizontal wells with the aid of published type curves.

1. Calculate t_D from the various user specified time steps using the following equation:

$$t_D = \frac{0.001055kt}{\phi\mu\, c_t\, L^2} \qquad 7.26$$

2. Determine L_D:

$$L_D = \frac{L}{2h}\left(\frac{K_v}{K_h}\right)^{0.5} \qquad 7.27$$

3. Calculate the term $L/2X_e = L/r_{eh}$, approximated by $= L/A^{0.5}$

4. Calculate $r_{wD} = r_w/h$

5. Use the proper type curve (Figure 7.35) corresponding to the well specifications L_D and $L/2X_e$ (from step 2 and 3) (similar to the one shown in Figure 7.33 from ref 32 and 34) to determine q_D corresponding to the t_D calculated in step one.

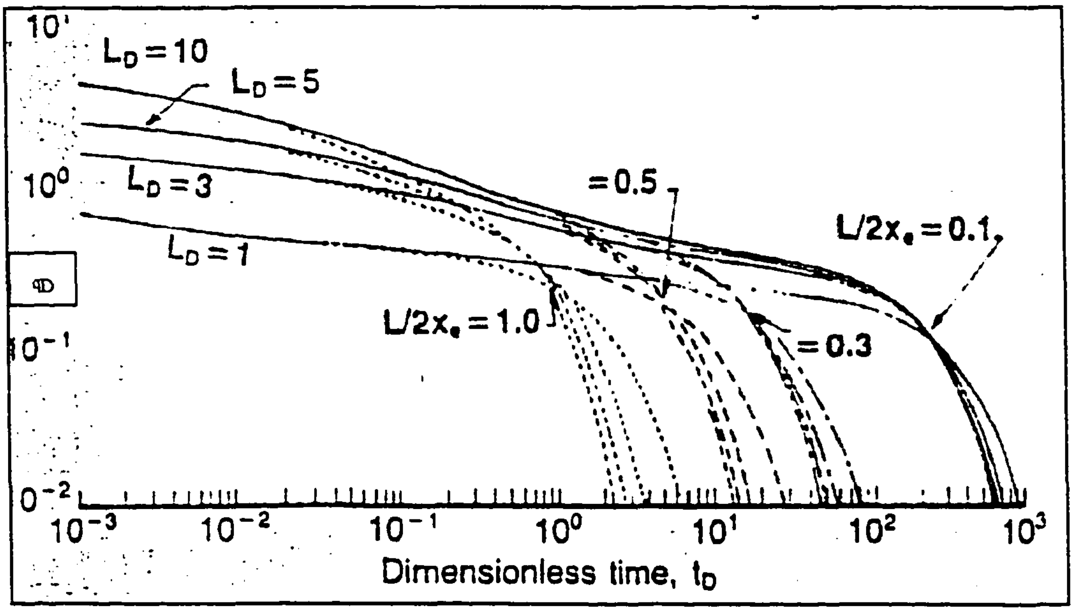

Figure 7.35 Dimensionless Pressure versus Time for Horizontal Wells From Refs 32,34

6. Calculate q from the q_D value determined in step 5 from the following equation:

$$q_D = \frac{141.3\,\mu Bq}{kh(p_i - p_{wf})} \tag{7.28}$$

7. Repeat the calculation for various times (days) and plot as cumulative oil production versus time. This procedure can be repeated for any desired drainage area A and well parameters. For a particular well that is 1500 feet long, 35 feet thick, permeability of 0.7, figure 7.4 shows the predicted production at any particular time for various drainage size assumptions.

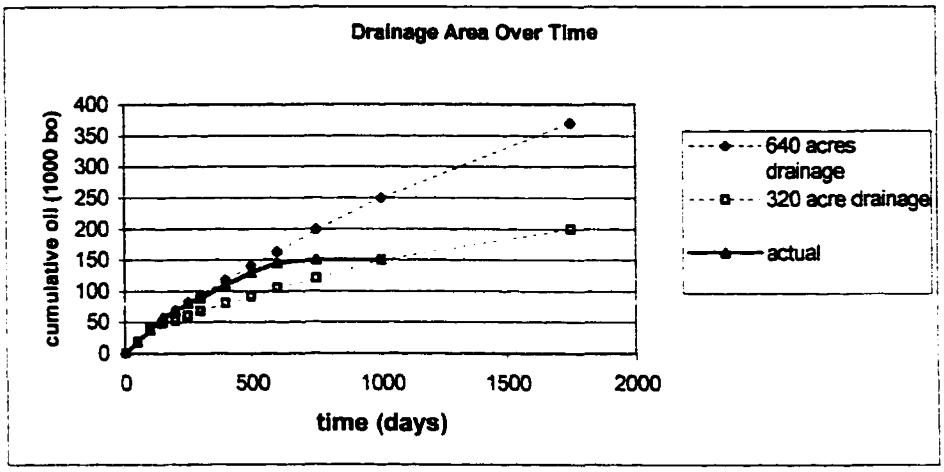

Figure 7.36 Predicted Performance Based on Actual Drainage Area Over Time versus Actual

Thus for a particular set of horizontal well lengths and reservoir parameters the performance can be predicted at any particular drainage size. Notice the deviation of the actual well production from the early time data. This is a result of the well beginning to sense the drainage area from competing wells. These times to drainage competition can be plotted to outline a drainage shape and the permeability contrast can be inferred.

7.8 Extension to Determine Drainage Area – Homogeneous and Fractured Reservoirs

The above method can be modified to predict the drainage area of a well and reservoir parameters in naturally fractured reservoirs by using the fractured type curve since the behavior of horizontal wells approaches that of the infinite conductivity fractured vertical well with long well lengths in thin reservoirs. Thus a set of performance type curves for various reservoir sizes can be constructed just as above in figure 7.36.

Then actual production data from the well can then be compared to the predicted curves for various reservoir sizes to determine the best fit. These can also be used to help identify interference in drainage areas that were referred to in a previous section. The method of construction for fractured wells is as follows:

Repeat steps one through four as above. Instead of step 5. use the fully penetrating vertical fracture type curve. Repeat step six above then repeat for various times and plot as cumulative oil versus time for various drainage areas A again. Then plot the actual production profile on the same graph (Figure 7.36 dashed line) and see which drainage area fits best and note at which time if any the curve deviates from the best fit drainage area. Any flattening as shown in the diagram indicates a reduction in original drainage area. This can be attributable to the time at which drainage areas begin overlapping because of well competition. That information can be used as described in Section 7.6 and 7.7 to decompose k_x and k_y. It is especially useful if several wells are available to gauge changes versus direction and distance.

7.9 Chapter Summary

The determination of directional permeability in an anisotropic reservoir is a difficult but important problem. Knowledge of this directional permeability can lead to better production prediction and design of proper well spacing. Without interference testing there is currently no direct way to estimate the directional permeability k_x and k_y. Decline curve analysis of wells that compete for drainage area provides a method of roughly estimating drainage shape and therefore directional permeability.

CHAPTER EIGHT

Extensions of Decline Curve Analysis To More Complicated Reservoirs -Permeability Heterogeneity And Fractures

8.1 Introduction

The decline curve analysis of this research has so far dealt with vertical and horizontal wells in homogeneous-isotropic and anisotropic reservoirs of constant directional permeability. More common situations involve highly heterogeneous formations where permeability variations are erratic and sometimes compartmentalized. Other common situations involve fractures of various types. This chapter will explore rate decline behavior in heterogeneous and fractured reservoirs through simulation experiments in controlled models. The analysis seeks to characterize various fracture types through characteristics exhibited in certain plotting techniques as well as type curve matching utilizing type curves developed by Poston and Chen for fractured reservoirs.[43,44,45]

8.1.1 Heterogeneous Formation Considerations

Heterogeneous formations can give rise to serious problems in the decline curve analysis and ultimate recovery projections. Heterogeneity can stem from either reservoir layering or rapid changes in spatial permeability within the reservoir[38]. Material balance is also predicated on the single tank model. Reservoir heterogeneity can also give rise to pressure gradients within the reservoir resulting in non-linearity of the pressure vs.

cumulative production plots. This leads to misinterpretation of future production and ultimate recoveries in low permeability and heterogeneous formations.

Scatter and curvature (which is also rate dependent) in the pressure decline vs. cumulative production plots can sometimes be attributed to pressure gradients in tight or heterogeneous reservoirs. It was already noted that late time deviations from early time decline curve predictions occur in reservoirs exhibiting drainage overlap. Scatter and curvature may contain valuable information that can be used to understand the heterogeneity, better predict reserves and forecast future development potential.

Experiments will be conducted with a number of models containing various types of heterogeneity in solution gas oil reservoirs. Experiments that model various fracture types and blocks of varying permeability are especially stressed in this chapter. The decline curves associated with production from those models will be analyzed in detail. Many plotting schemes are introduced in this chapter tin an effort to help identify particular reservoir characteristics. For instance rather than plotting simply rate vs. time, the rate decline can be compared with actual rate as a function of rate-cumulative-time functions. Some of the normalization techniques of the previous chapter will also be applied in an effort to present the data in a form more suitable for well test analysis. However pressure is purposely ignored in the analysis since the purpose is to utilize only the rate decline data that is commonly available to the practicing engineer.

8.2 Geological Model of a Fractured System

Decline curves used to predict future production from fractured flow regimes should model those geological-physical regimes. In other words the model should depict the geological system if possible. Poston and Chen[43,44,45] developed a naturally fractured reservoir model composed of a major and a least one additional minor fracture system and a matrix system of smaller blocks. Type curves were developed to represent a combination of flow through a major fracture system with infinite conductivity, linear flow through a set of lesser subsidiary micro-fractures and flow from the matrix block system. Flow from this system would also be predominately linear rather than radial. Flow from the macro fracture would not affect the shape of the curve since it is treated as infinite acting.

The authors noted that one would expect a horizontal well to intersect a greater number of fractures and thus have a different characteristic decline curve. However their analysis of Austin Chalk wells indicated that this was not the case. Rather, the family of curves that they developed matched for both horizontal and vertical wells except for the early data which is due (according to them) to the transient period being masked in the horizontal wells. This was confirmed by the simulation experiments.

Their model consists of the following attributes:

1) Major fracture with infinite conductivity
2) At least one minor fracture system with linear flow and

3) Rock matrix composed of small blocks

4) Linear rather than radial flow model

To summarize, the objective of their model is to:

1) Couple a single fracture type model to a dual porosity type model.

2) The model should consider the spatially dependent fracture orientation, connectivity, distribution and intensity of fractures.

3) Differentiate between the bounded PSS and transient flow and to predict future producing characteristics.

4) Distinguish macro from micro fractures.

The model would encompass the following assumptions:

1) The wellbore encountered macro fracture is a vertical plane of zero thickness with height equal to the formation thickness and of finite length in the lateral direction.

2) The fracture parallel to the drainage boundary. Uniform flux, infinite conductivity, or uniform flux can be used.

3) Micro fractures are more or less connected and continuous.

4) Production is from the wellbore fractures only. Micro-fractures feed the macro- fractures. Matrix acts as supporting sources to feed the fractures with fluid.

5) Constant pressure production condition.

Chen and Poston developed the following type curves representing the expected producing characteristics for a reservoir of this type[41,42,43]. (Figure 8.1)

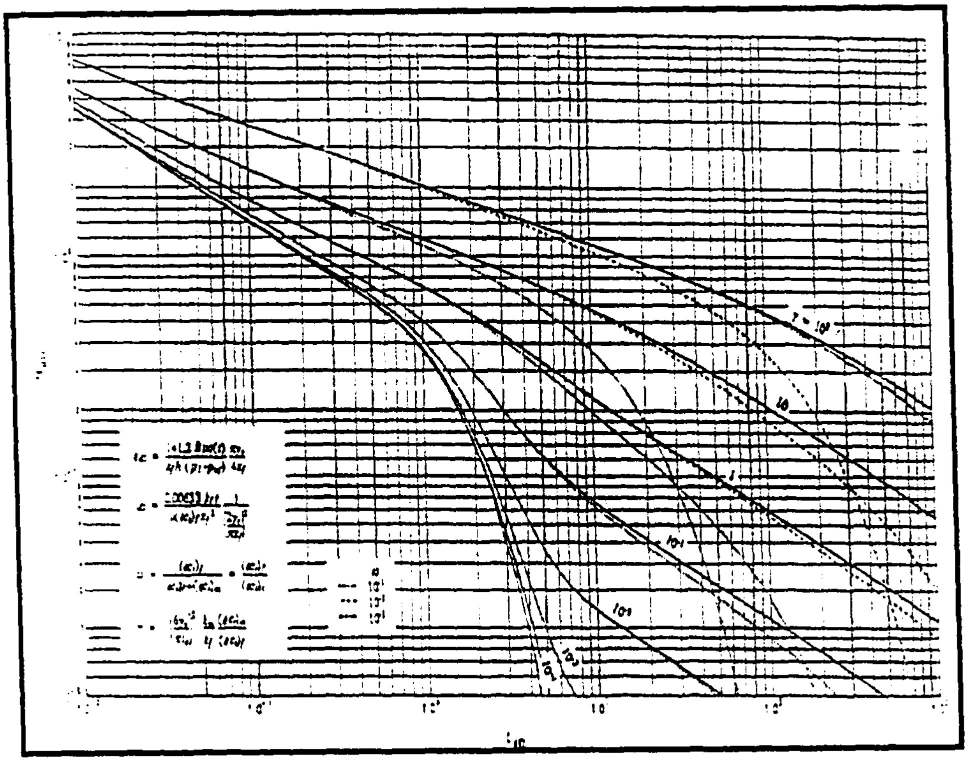

Figure 8.1 Poston-Chen Type Curve for Fractured Reservoir[41]

Three flow regimes would be recognized from these type curves but the flow from the macro-fracture would be treated as infinite acting and thus does not affect the curve shape:

Regime One: Unsteady state flow from the micro-fractures.

Regime Two: Transition of the flow system from mainly the micro-fractures to mainly the matrix.

Regime Three: Pseudo-steady state boundary dominated matrix flow.

Type curves should not only permit differentiation of the pseudosteady sate and transient region but also aid in the estimation of future producing characteristics.

Figure 8.2 (reconstruction method explained later) shows the various theorized parts of the curve for the case of storage capacity of 0.1 and various degrees of fracture intensity as defined by Poston and Chen.

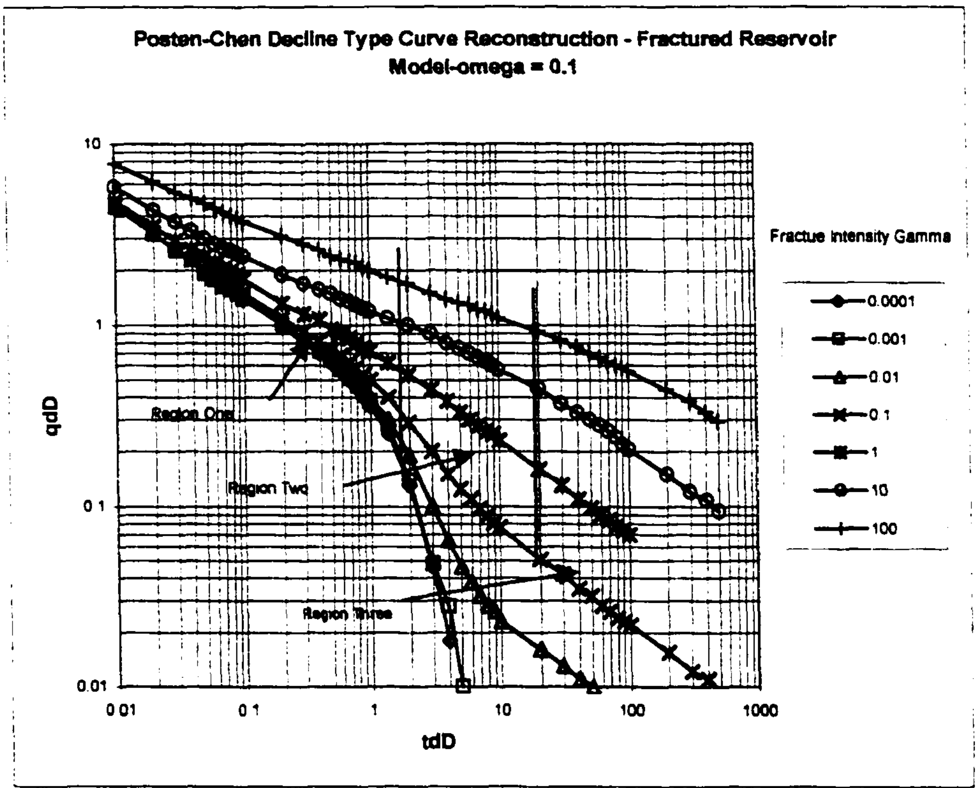

Figure 8.2 Poston-Chen Decline Type Curve Reconstruction - Fractured Reservoir Model-ω (storage capacity) = 0.1

Four fracture system types have been proposed and will be investigated.[49]

<u>Type One</u>: Fractures provide the significant reservoir storage capacity and permeability, which is thought to be characterized by high flow rate and short reservoir life. $k_f >>> k_m$ and $\phi_f >>>> \phi_m$

<u>Type Two</u>: The matrix has good permeability and provides a good feed to the fracture system. High flow rates and longer reservoir life should result.

Type Three: The matrix permeability is low but contains most of the oil. The fractures contain high permeability.

Type Four: The fractures are filled with minerals and partition the formation into blocks.

These various types of fractures will be studied in this chapter.

8.3 Mathematical Introduction and Overview of the Poston-Chen Fracture Model[41,42,43]

A Laplace and Green's function approach is used to provide analytical solutions for the model problem. The details as well as the formulation and construction of the type curves are summarized in the next section. The decline curve dimensionless rate and dimensionless time corresponding to the rectangular coordinates are defined respectively as:

$$q_{dD} = \beta_2 q_D \qquad 8.1$$

and

$$t_{dD} = t_D / (\beta_1 \beta_2) \qquad 8.2$$

where the normalizing factors are:

$$\beta_1 = (16/\pi^3)/(y_e/x_f) \qquad 8.3$$

$$\beta_2 = (\pi/4)/(y_e/x_f) \qquad 8.4$$

The dimensionless rate for the model is given as:

$$q_D(t_D) = \frac{141.2B\mu q(t)}{k_f h(p_i - p_{wf})} \quad 8.5$$

or rearranging and substituting for the normalizing factors and rectangular coordinates:

$$q_{dD} = \left(\frac{\pi}{4}\frac{y_e}{x_f}\right)\frac{141.2B\mu q(t)}{k_f h(p_i - p_{wf})} \quad 8.6$$

Note the similarity with the Fetkovich decline dimensionless decline:

$$q_{Dd} = \left[\ln\left(\frac{r_e}{r_{wa}}\right) - 0.5\right]\frac{141.2\mu Bq(t)}{kh(p_i - p_{wf})} \quad 8.7$$

or using my more general form:

$$q_{Dd} = \frac{141.3\mu Bq(t)}{kh(P_i - P_{wf}}\left[1.151\log\frac{4A}{1.781C_A r_w^2}\right] \quad 8.8$$

Where p_{wf} is the constant bottom hole pressure and q(t) is the time dependent production rate at the wellbore. The dimensionless time is given as:

$$t_D = \frac{0.00633k_f t}{\mu(\phi c_t)_f x_f^2} \quad 8.9$$

or rearranging and substituting for the normalizing factors and rectangular coordinates

$$t_{dD} = \frac{0.00633\, k_f t}{\mu(\phi c_t)_f x_f^2 \left(\frac{2 y_e}{\pi x_f}\right)^2} \qquad \textbf{8.10}$$

These relationships, similar to the form of Fetkovich's radial systems and my general system equations, appear to be rectangular and linear. Note the similarities to the dimensionless decline time Fetkovich type equivalents reproduced below.

$$t_{Dd} = \frac{0.00634kt}{\phi\mu c_t r_w^2} \left[\frac{1}{\frac{1}{2}\left[\left(\frac{r_e}{r_w}\right)^2 - 1\right]\left[\ln\left(\frac{r_e}{r_w}\right) - \frac{1}{2}\right]} \right] \qquad \textbf{8.11}$$

or using my more general form:

$$t_{Dd} = \frac{0.00634kt}{\phi\mu c_t r_w^2} \frac{r_w^2}{A} \left[\frac{5.44678}{\log \frac{4A}{1.781 C_A r_w^2}} \right] = t_D \frac{r_w^2}{A} \left[\frac{5.44678}{\log \frac{4A}{1.781 C_A r_w^2}} \right] \qquad \textbf{8.12}$$

and putting in a similar arrangement to that of the Fetkovich radial form:

$$t_{Dd} = \frac{t_D}{\frac{A}{r_w^2} \frac{\log \frac{4A}{1.781 C_A r_w^2}}{5.44678}} = \frac{t_D}{\frac{0.183594A}{r_w^2} \log \frac{4A}{1.781 C_A r_w^2}} = \frac{t_D}{0.183594(c_1' c_2')} \qquad \textbf{8.13}$$

8.4 Construction and Development of the Decline Curves

Poston and Chen developed type curves based on the fractured reservoir model[41] The solution to the dimensionless rate and rime are based on an iterative calculation of the Laplace transform of the constant production rate equations. Conversion to dimensionless decline parameters follows in a manner similar to that of Fetkovich. An extension to horizontal wells in the transient regime is investigated utilizing the equivalent wellbore radius concept.

8.4.1 Model Assumptions

There are two basic groups of assumptions regarding the geometry and rock properties of the model as follows:

1. A horizontal, uniform thickness, naturally fractured reservoir completely filled with a fluid of small and constant compressibility and constant viscosity, bounded by an upper and lower impermeable strata is considered. The drainage area is assumed rectangular with closed outer boundaries. The wellbore fracture is represented by a vertical place of zero thickness in the y direction with a height equal to the formation thickness and of finite length in the lateral x directions and symmetrical with respect to the wellbore and parallel to the drainage boundary.

2. The micro-fractures are more or less connected and are considered as a continuous network. Uniform spheres are used to approximate the geometry of the matrix blocks. The permeability of the fractures is much larger than that of the matrix blocks. In other words the micro fracture network is visualized as a large-scale version of a conventional intergranular porous medium. Such a continuum model implies that both the size and permeability of the intervening matrix blocks are small enough to avoid disturbance of the macroscopic flow. Fluid flow toward the well and wellbore fracture in the reservoir is considered entirely through the natural fracture network. The fluid in the matrix blocks acts a source to the natural fracture network. Communication between the matrix blocks is not allowed. The mathematical formulation is developed in SPE paper 23527[42]. The wellbore-intercepted fracture is assumed to extend over the entire vertical extent of the formation but is bed contained. Both infinite conductivity and uniform-flux conditions are considered.

8.4.2 Limiting Equations Used in Construction

By solving the governing equation by the Laplace domain instantaneous source and Green's function with product solution approach and defining dimensionless parameters as defined in the previous section, the authors develop the dimensionless rate equation of a fully penetrating fracture intersecting the wellbore as:

$$\bar{q}_D(s)=\frac{2}{\pi y_{eD}}\frac{1}{s}\left[y_{eD}\sqrt{sf(s)}th\left(y_{eD}\sqrt{sf(s)}\right)\right] \tag{8.14}$$

where the decline curve dimensionless rate and time are given as before as:

$$q_{dD}=\beta_2 q_D=q_D\frac{\pi y_e}{4x_f} \tag{8.15}$$

and the dimensionless time is:

$$t_{dD}=\frac{t_{fD}}{\beta_1\beta_2}=\frac{4x_f^2 t_{fD}}{y_e^2} \tag{8.16}$$

Seven limiting forms can be derived from which the decline curves are constructed in a similar way to that of Fetkovich type curves. These limiting forms can be shown to be dependent on two parameters ω and γ as previously defined. These parameters are the storage expansion ratio and the inter-porosity flow or fracture intensity parameters. These two parameters characterize the behavior of the dual porosity system. The seven limiting forms with the constraints are expressed below:

<u>Infinite Region</u>:

$$q_D(t_{fD})=\frac{2}{\pi^{2/3}}\frac{1}{\sqrt{t_{fD}}};\left[t_{fD}<\frac{1}{(3\lambda\omega}\right] \tag{8.17}$$

This limiting form corresponds to the approximations of $(3\lambda\omega^{'}/s)<<<1$ and hence $f(s)=1$.

$$q_D(t_{fD}) = \frac{2}{\pi^{2/3}}\frac{1}{\sqrt{t_{fD}}}+\frac{\sqrt{3\lambda\omega^{'}}}{\pi};\left[\frac{1}{3\lambda\omega^{'}}<t_{fD}<\frac{0.3\omega^{'}}{\lambda}\right] \quad 8.18$$

$$q_D(t_{fD})=\frac{2(\lambda\omega^{'})^{1/4}}{\pi\Gamma(3/4)}\frac{1}{t_{fD}^{1/4}};\left[t_{fD}>\frac{0.3\omega^{'}}{\lambda}\right] \quad 8.19$$

where Γ is the Gumma function and $\Gamma(3/4)$ is 1.225420.

The finite acting limiting forms are:

$$q_D(t_{fD})=\frac{1}{\beta_2}\sum_{n=1}^{\infty}\exp\left[-(2n-1)^2\frac{t_{fD}}{\beta_1\beta_2}\right] \quad 8.20$$

$$q_D(t_{fD})=\frac{1}{\beta_2}\sum_{n=1}^{\infty}\exp\left[-(2n-1)^2\frac{\omega t_{fD}}{\beta_1\beta_2}\right] \quad 8.21$$

$$q_D(t_{fD})=\frac{1}{\beta_2}\sum_{n=1}^{\infty}\frac{1}{a}\exp\left[\frac{-(2n-1)^2}{a}\frac{\omega t_{fD}}{\beta_1\beta_2}\right] \quad 8.22$$

and

$$q_D(t_{fD})=\frac{1}{\beta_2}\sum_{n=1}^{\infty}\frac{\gamma}{\gamma-(2n-1)^2}erfc\left[b\sqrt{\frac{t_{fD}}{\beta_1\beta_2}}\right]\exp\left[b^2\frac{t_{fD}}{\beta_1\beta_2}\right] \quad \mathbf{8.23}$$

where:

$$a=1+(2n-1)^2\frac{3}{5}\frac{(1-\omega)^3}{\omega}\frac{1}{\gamma} \quad \mathbf{8.24}$$

$$b=\frac{(2n-1)^2\sqrt{\gamma}}{\gamma-(2n-1)^2} \quad \mathbf{8.25}$$

$$\gamma=3\lambda\omega^{'}\beta_1\beta_2=3\lambda[(1-\omega)/\omega]\beta_1\beta_2 \quad \mathbf{8.26}$$

$$\beta_1=\frac{16y_{eD}}{\pi^3} \quad \mathbf{8.27}$$

$$\beta_2=\frac{\pi y_{eD}}{4} \quad \mathbf{8.28}$$

If the erfc function is approximated as erfc $(z)\approx\exp(-z)^2/\sqrt{\pi}z$ for large values of the argument then the last limiting equation can be approximated by:

$$q_D(t_{fD})=\frac{1}{\beta_2}\sum_{n=1}^{\infty}\frac{\sqrt{\gamma/\pi}}{(2n-1)^2}\frac{1}{\sqrt{t_{fD}/(\beta_1\beta_2)}} \quad \mathbf{8.29}$$

The limiting equations can then be plotted for various ranges of reservoir size and limiting parameters just as with the Fetkovich construction where the q_{Dd} was constructed for increasing reservoir size r_{eD}. The fracture dimensionless curves are constructed for increasing y_e/x_f.

$$q_{dD} = \beta_2 q_D = q_D \frac{\pi y_e}{4x_f} \tag{8.30}$$

and the dimensionless time is:

$$t_{dD} = \frac{t_{fD}}{\beta_1 \beta_2} = \frac{4x_f^2 t_{fD}}{y_e^2} \tag{8.31}$$

The lines will converge and overlap. The values of the limiting areas can then be extracted and re-plotted to form the Type curve shown in figure 8.3 which closely replicates the Poston and Chen curves in Figure 8.1.

The Poston-Chen curve for a storage compressibility of 0.1 with superimposed Fetkovich type curve is shown in figure 8.3. Note the convergence of the two type curves in the depletion period for low values of fracture intensity. The transient period is also markedly different in the fractured regime.

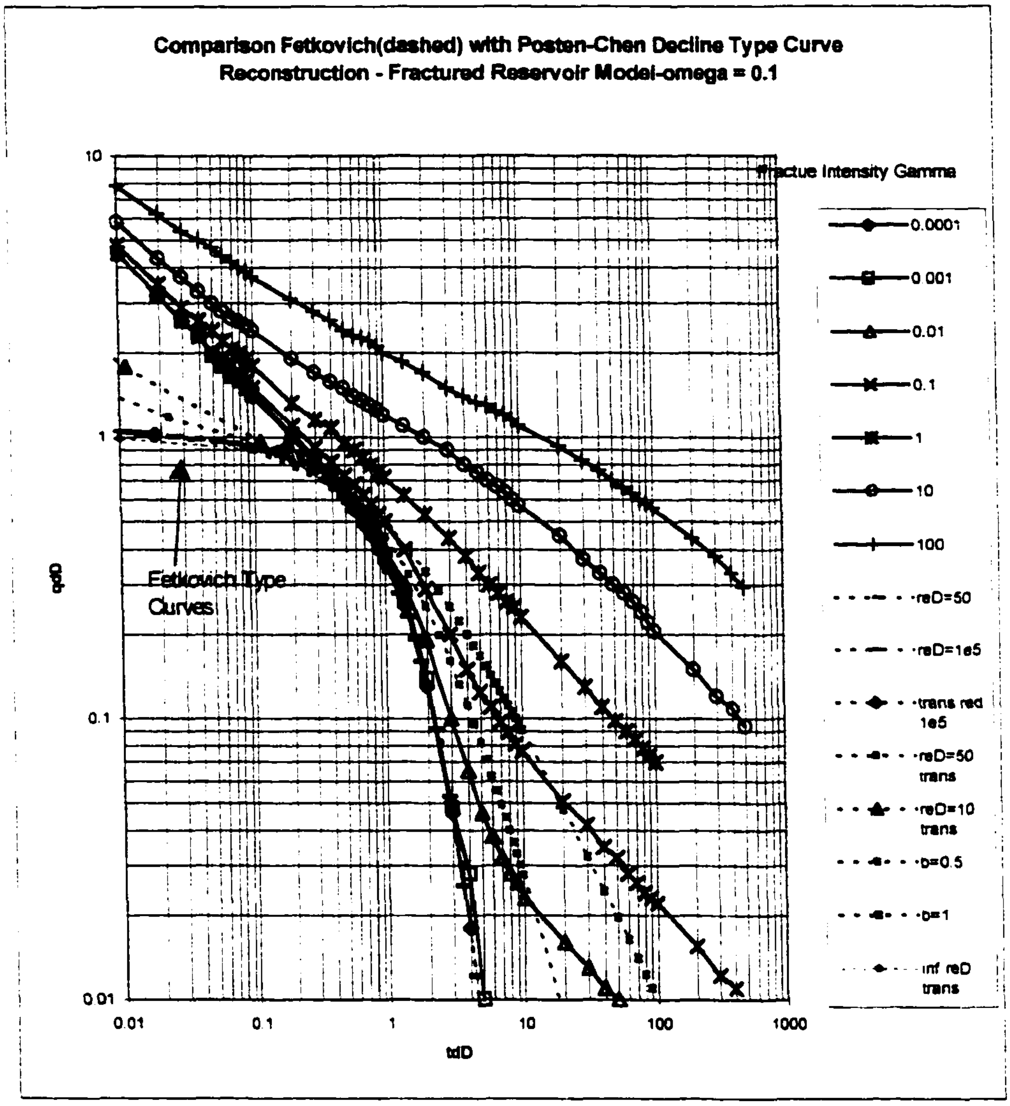

Figure 8.3 Comparison Fetkovich (dashed lines) with Poston-Chen Decline Type Curve Reconstruction - Fractured Reservoir Model-Storage Compressibility $\omega = 0.1$

An examination of the curves indicates that the Poston and Chen curves treat the initial period, as infinite acting which is not always typical of a horizontal well in fractured media. As the simulation experiments indicate even with fracture permeability of as much as 4000 md the initial flow does not always follow the early time Poston-Chen curves but does match the late time portions very well. The examples in their published papers from Austin Chalk reservoirs also did not match the early time behavior but similar to the simulation experiments showed a much "flatter" early time slopes. However the combined Fetkovich type superimposed on the Poston Chen curves in Figure 8.3 do provide the extremes to compare. The actual early time path of a fractured well will be somewhere in between the two cases. Since the curves are primarily being used to classify fracture types this is not a serious limitation but does present some difficulties in curve matching.

If the dimensionless well length is known then an alternative early time behavior can be approximated using the Poston Chen's Fetkovich equivalent dimensionless constants and applying the horizontal dimensionless rate and time values

$$q_{dD} = \left(\frac{\pi}{4}\frac{y_e}{x_f}\right)\frac{141.2B\mu q(t)}{k_f h(p_i - p_{wf})} = \left(\frac{\pi}{4}\frac{y_e}{x_f}\right)q_D \qquad 8.32$$

$$t_{dD} = \frac{0.00633\,k_f t}{\mu(\phi c_t)_f x_f^2 \left(\dfrac{2y_e}{\pi x_f}\right)^2} = \frac{t_D}{\left(\dfrac{2y_e}{\pi x_f}\right)^2} \qquad 8.33$$

similar to values from figure 7.33 of the previous chapter.

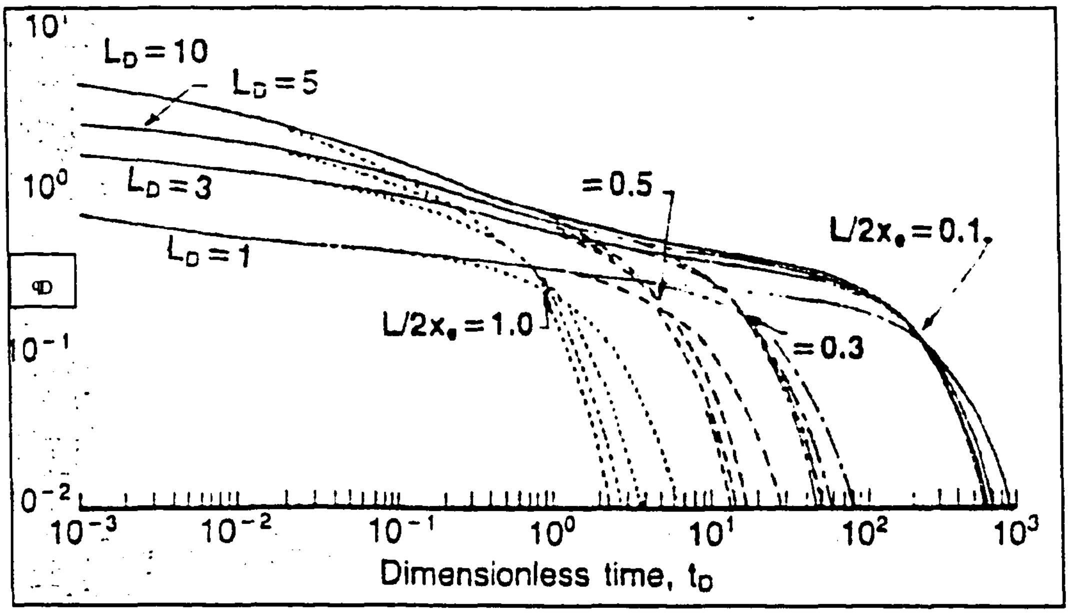

Reproduced Figure 7.33[32,34]

The Poston-Chen early time infinite conductivity assumptions are more similar to using the fully penetrating infinite conductivity fracture such as shown in figure 8.4.[33]

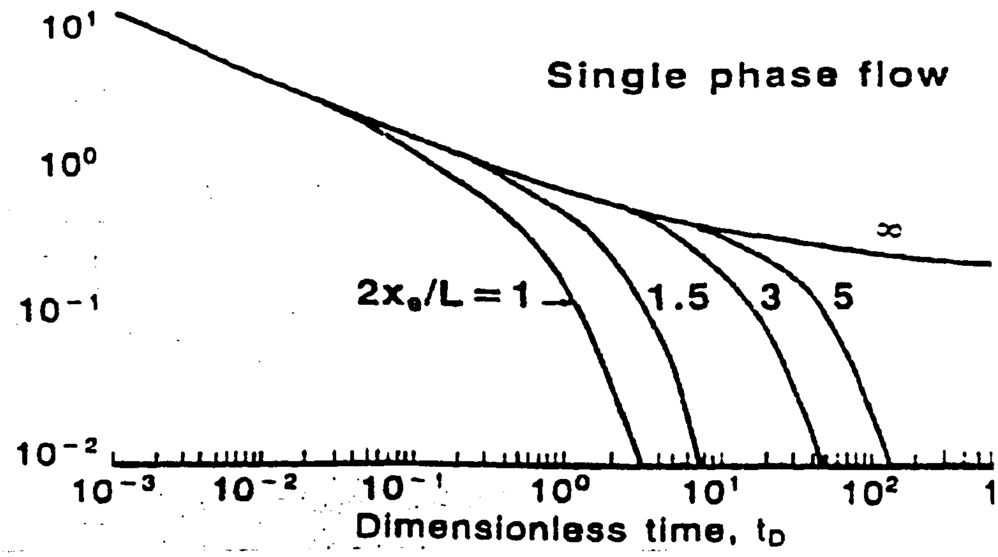

Figure 8.4 Fracture Dimensionless Rate versus Dimensionless Time Horizontal Wells[33]

Thus a more reasonable early time curve falls in between the Fetkovich type curve and the Poston-Chen early time. This preserves the Poston Chen late time behavior but changes the early time behavior to that actually seen in some of the field and in the simulation experiments.

8.4.3 New Dual Porosity Dimensionless Parameters

For the standard homogeneous type curve models of Arps and Fetkovich there is just one correlation parameter r_e/r_w or $\sqrt{A}/r_w$ for the more general case in the transient portion and one parameter "b" for the pseudosteady state decline solution. Dimensionless parameters characterizing a dual porosity behavior are traditionally defined as the 1) storage expansion ratio ω and 2) the inter-porosity flow parameter λ. The storage capacity expansion factor is defined as:

$$\omega = \frac{(\phi\, c_t)_f}{(\phi\, c_t)_f + (\phi\, c_t)_m} = \frac{(\phi\, c_t)_f}{(\phi\, c_t)_t} \qquad 8.34$$

which is known as the ratio of storage expansion of the fracture system to the total system. For many fractured systems (Type 3 fractures) the fracture porosity is low and the storage expansion ratio is just the ratio of ϕ_f/ϕ_m. The presence of fluid influx from the matrix blocks will thus override the compressibility effect and produce a production "tail".

A useful variation of this storage expansion factor is:

$$\omega^* = (1-\omega)/\omega = (\phi_{ct})_m / (\phi_{ct})_f \qquad 8.35$$

Thus ω is based on expressions for inter-porosity flow and storage compressibility. The term defines the difference between the fracture and matrix flow. which can theoretically be used to characterize the type of fracture system.

For a formation such as the Austin Chalk which has low fracture porosity ϕ_f but good fracture permeability k_f (type 3) and often also has good matrix support, values of ω averages about 10^{-3}. The Austin Chalk has fracture porosity of about 0.005. So ω is approximately $(\phi)_f / (\phi)_m$ or 0.005/0.16 . The presence of fluid influx from the matrix blocks will override the compressibility effect and produce a production tail in such cases.

The second limiting parameter λ can be re-characterized and defined as γ. The γ term is proportional to the fracture intensity, FI, and is thus a direct indicator of fracture intensity if the matrix and fracture compressibility are the same and ω is of the order 10^{-3}. The smaller the value of γ the smaller the production rate, life of the well and thus less tail on the decline curve. A large value of γ can imply a high fracture intensity and good fracture connectivity and tends to be characteristic of small values of storage expansion ratio. Thus according to Posten and Chen, the extended production tailing is a result of primarily matrix fluid contribution and not compressibility effects.

γ is related to the inter-porosity parameter λ and ω^* by:

$$\gamma = 3\lambda\omega^*\beta_1\beta_2 = 3\lambda\ \beta_1\beta_2(\ 1-\omega)/\omega \qquad \textbf{8.36}$$

$$\gamma = (FI)^2 x_f^2 \frac{k_m(\phi\, c_t)_m}{k_f(\phi\, c_t)_f}\beta_1\beta_2 = \left(\frac{6}{\pi}\frac{y_e}{l_c}\right)^2 \frac{k_m}{k_f}\frac{(\phi\, c_t)_m}{(\phi\, c_t)_f} \qquad \textbf{8.37}$$

Poston and Chen state that in the Austin Chalk, γ can often be a direct indicator of fracture intensity if the ratio of $k_m\phi_m c_{tm}/k_f\phi_f c_{tf}$ is approximately one. Whether this is a common occurrence is unknown however it will be tested in the simulation experiments.

Figures 8.4 and 8.5 show Poston and Chen's general storage compressibility ω and fracture intensity relationships.

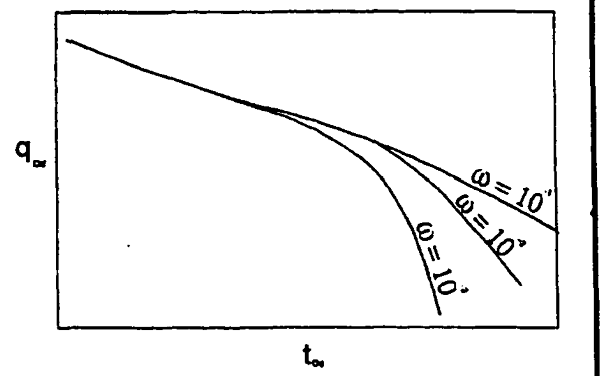

Fig. 8 - Idealized Change in Fracture Storage-Compressibility Term, ω.

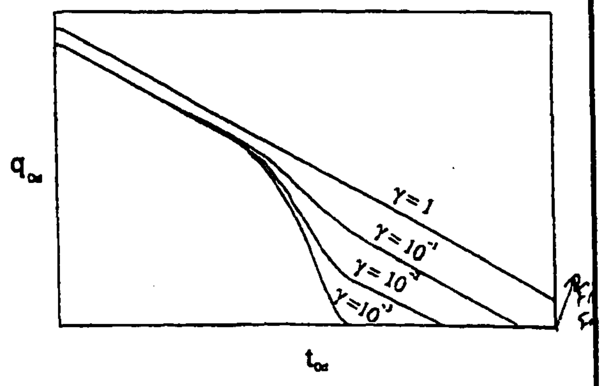

Fig. 9 - Idealized Change in Fracture Intensity Term, γ.

Figures 8.6 and 8.7 Dimensionless Type Curves for Variations in Storage Compressibility and Fracture Intensity [41,42,43]

8.5 Application

The Austin Chalk of south Texas and the Viola of Oklahoma provide two good contrasting fractured carbonate examples. The Austin Chalk exhibits high initial production from the fracture system followed by a steep drop off in production as the fracture systems are depleted. The Austin Chalk does, in many cases, continue to provide some support to production from the matrix after the steep initial drop. However, the Viola rate drop-off is very abrupt and provides little post drop off production support from the outlying matrix system. Once the fracture system is depleted the wells are usually abruptly uneconomic. Presumably the matrix permeability is too limited to provide pressure support.

The unique feature of the dual fracture - matrix type curves lies in the abrupt decline followed by the extended production tail of the decline curve for certain storage compressibility conditions. The author's indicate that the tail is a consequence of the matrix contribution in this formulation. The simulation experiments indicate that the tail may also be a result of the solution gas effect. Naturally fractured reservoirs with small matrix permeability would display a pronounced fall off later in the life of the well.

Recall that the Poston Chen models use the following relationships:

$$q_{dD} = \left(\frac{\pi}{4}\frac{y_e}{x_f}\right)\frac{141.2B\mu q(t)}{k_f h(p_i - p_{wf})} \tag{8.38}$$

$$t_D = \frac{0.00633\, k_f\, t}{\mu(\phi\, c_t)_f\, x_f^2} \quad \textbf{8.39}$$

with correlation parameters:

$$\omega = \frac{(\phi\, c_t)_f}{(\phi\, c_t)_f + (\phi\, c_t)_m} = \frac{(\phi\, c_t)_f}{(\phi\, c_t)_t} \quad \textbf{8.40}$$

$$\gamma = (FI)^2 x_f^2 \frac{k_m(\phi\, c_t)_m}{k_f(\phi\, c_t)_f}\, \beta_1 \beta_2 = \left(\frac{6}{\pi}\frac{y_e}{l_c}\right)^2 \frac{k_m(\phi\, c_t)_m}{k_f(\phi\, c_t)_f} \quad \textbf{8.41}$$

Poston and Chen used these type curves and drew certain conclusions based on matching of data for Austin Chalk production data. Since actual reservoirs are heterogeneous and anisotropic in unknown ways, simulation experimentation offers a method to test and properly validate the type curve model. Only then can they be used to help characterize fracture types. Comparisons of short and long term production decline curves are useful.

8.6 Experiments with Fractured Media

In an effort to both test the Poston Chen Type curves, to try to classify the various fracture types by decline curve characteristics and to possibly modify the Poston Chen curves to a more realistic early time behavior, simulation models were constructed for each fracture type. The type curves were then applied to each experimental output and comparisons are made between various graphical output of the various fracture types. Recall that the fractures were classified by types into the following four categories.[49]

Type One: Fractures provide the majority of the movable reservoir storage capacity and permeability, which is characterized by high flow rate and short reservoir life. $k_f >>> k_m$ and $\phi_f >>>> \phi_m$

Type Two: The matrix has good permeability and provides a good feed to the fracture system. High flow rates and longer reservoir life result.

Type Three: The matrix permeability is low but contains most of the oil. The fractures contain high permeability.

Type Four: The fractures are filled with minerals and partition the formation into blocks.

Unfortunately it was difficult to model an extreme case type 1 fracture where there was almost no storage capacity in the matrix while keeping other parameters fairly constant. However it was possible to model a system that contained a large part of the storage capacity in the fracture (18%) relative to the type two and three fractures cases where fracture storage was only 1%. A reasonable qualitative comparison could thus be obtained. This is not considered a serious limitation since even in very tight formations such as the Viola of Oklahoma there is significant though immovable oil in the matrix.

8.7 Model Descriptions

To properly compare and classify the various fracture types it was necessary to construct models that contained, as much as feasible, identical characteristics such as reservoir dimensions, total pore volume, total fluid volumes, initial fluid saturation, grid spacing, grid number and PVT parameters. In other words the experiments were designed to test fracture type classifications in a scenario that compared only the relative changes in matrix and fracture storage capacity and permeability by keeping the sum total reservoir rock and fluid volumes and initial saturation identical. Therefore models were constructed as follows:

All models contained 784 grid blocks (near the capacity of the boastvhs simulator) in a nearly square reservoir. The total system oil in place was a constant 3.37 million stock tank barrels and initial gas in solution was 1.5 bscf in all cases. Relative matrix-fracture pore volume was adjusted to maintain a constant total system pore volume within each model but was distributed between the fracture and matrix to fit the model type as well as possible according to the following generalized summary table 8.1. The initial reservoir pressure is 2000 psia and bubble point is 1600 psia. The horizontal reservoir length to horizontal well length ratio X_e/L was a constant 8.5 for all cases.

Constant OOIP is 3.37 Million Stock Tank Barrels

Model	Order of initial q Highest =1	Matrix k. md	Fracture k. md	$ooip_f/ooip_t$	Storage Factor ω^{**}	k_f/k_m $1/\lambda^*$	k_m/k_f λ^*	k_{pv}	Fracture Intensity
Type 1	6	0.1	1000	4%	.036	10000	.0001	44.6	.00036
Type 1h	5	0.1	4000	4%	.036	40000	.000025	178.1	.00036
Type 1n	4	0.1	1000	18%	.146	10000	.0001	177.6	.0015
Type 1hn	3	0.1	4000	18%	.146	40000	.000025	710.4	.0015
Type 2	2	10.1	1000	1%	.007	100	.01	18.62	.00038
Type 2h	1	10.1	4000	1%	.007	400	.0025	44.43	.00038
Type 3	8	0.1	1000	1%	.007	10000	.0001	8.7	.00038
Type 3h	7	0.1	4000	1%	.007	40000	.000025	34.52	.00038
Type 4		10.1	4000 with compartments	1%	.007	400	0025	34.43	.00038

Table 8.1 Simulation Model Parameters

It was shown in the master's thesis that as the fracture intensity increases, the performance derived oil relative permeability approaches a straight line between zero and irreducible liquid saturation.[12] Low fracture intensity wells have k_{ro} similar to laboratory determined matrix curves. Wells with higher fracture intensity generally exhibit more favorable k_{ro} at high gas saturation and approach straight lines. As the degree of fracturing increases, k_g/k_o becomes more unfavorable toward oil recovery. In this case however the relative permeability curves were kept constant in the experiments to avoid introducing an unknown parameter. The effect of the relative permeability in the matrix versus the fracture could be investigated later.

The author has used traditional fractured reservoir parameters in Table 8.1 as well as defined several variables that are variations of the traditional fracture parameters. Traditional parameters include as storage coefficient, ω, fracture transfer rate, λ, fracture intensity term $\upsilon = \frac{\phi_t - \phi_m}{1 - \phi_m}$, and Poston Chen correlation, parameter γ.[44,47,48] The fracture intensity term requires a calculation of the total system porosity using the pore volume weighted porosity of the fracture and matrix. Modified parameters are also used since it is difficult to estimate the compressibility. A simple storage factor $\omega'' = \frac{V_f \phi_f}{V_f \phi_f + V_m \phi_m}$ is used for discussion purposes to show the relationship of fracture porosity to total system porosity. This is essentially the same as the traditional ω without the compressibility terms (see equation 8.40). The oil filled fracture pore volume to total system pore volume ($ooip_f/ooip_t$) can also approximate the storage coefficient. This term allows a more direct conceptual comparison of the various experimental outputs. Likewise the traditional $\lambda=cr^2_w k_m/k_f$, which is an indication of fluid transfer rate from matrix to fractures is simplified in the discussions to $\lambda^{'}=k_m/k_f$ for conceptual clarity since only one well dimension is used. This term is then further modified to incorporate pore volume weighted permeability for the system. This should provide another possible useful parameter to classify the system in the presence of a horizontal well that intersects both matrix and fractures.

For instance k_{pv}, for comparison purposes, will be defined as the pore volume weighted bulk permeability:

$$k_{pvt} = \frac{\Sigma k_f V_{pvf} + \Sigma k_m V_{pvm}}{V_{pvt}} \qquad 8.42$$

V_{pvf} = Pore volume of fracture
V_{pvm}= Pore volume of matrix
V_{pt} = Total model pore volume

All of these various traditional and modified parameter values are shown in table 8.1 so that a comparison can be made as the individual model outputs are compared and contrasted. It will be useful to refer to Table 8.1 during the discussion of the graphical output.

8.8 Simulation Output

The reservoir simulation output is too voluminous to include in this report but the following sections summarize some of the main points of the various experiments. More complete tabular simulation output and calculations are included in the appendix G. More complete experimental and graphical output is available from the author.

The experimental output collected consisted of tabular pressure, oil, gas, water rate and cumulative data as well as phase saturation data for each time step. That output was input to spreadsheets and used in various calculations that were graphed. As mentioned before, pressure data was collected to help in the analysis of the rate data but is not used in the characterization since this type of data will not be available for most reservoir situations. Even valuable early time daily rate data are hard to obtain. One can only reasonably expect to have monthly rate and cumulative production data after the first year of production and occasionally some sporadic bottomhole shut-in pressure data. Since most domestic onshore wells produce at maximum rate limited only by separator backpressure, flowing wellhead pressures are of little value and can give misleading results. Poston and Chen used those values in their analysis but the general applicability and availability of such data is questionable. This analysis is restricted to data that can be obtained by the practicing from traditional public data sources. Graphical output for each fracture experiment as well as tabular results (included in Appendix G) consisted of the information listed in Table 8.3. Only selected output that was deemed most relevant is included in this report.

Graph Type	Cartesian	Semi-Log	Log-Log
Oil Rate versus Time: q vs. t	X	X	X
Oil and Gas Rate versus Cumulative: q vs. q_{cum},	X	X	X
Cumulative Oil and Gas vs. Time: q_{cum} vs. t	X	X	X
Oil Rate q vs. $(t_p+\Delta t)/\Delta t$ Note: not well testing definition (see report body)			X
Pressure Average vs. $(t_p+\Delta t)/\Delta t$ Note: not well testing definition		X	X
Oil Rate Change Δq vs. $(t_p+\Delta t)/\Delta t$ Note: not well testing definition (see report body)			X
Average Reservoir Pressure versus Cumulative Oil: P vs. q_{cum}	X		X
Oil Rate Change/Oil Rate versus Cumulative Oil/Rate: $(\Delta q/q)$ vs q_{cum}/q	X	X	X
Pressure Change/Rate vs Cumulative Oil/Rate: $(\Delta p/q)$ vs q_{cum}/q		X	X
Pressure Change vs time: Δp vs. t		X	X
Oil Rate Change vs time: Δq vs. t		X	X
Oil Rate Change vs Pressure Change: Δq vs. Δp		X	X
Pressure Change vs Cumulative: Δp vs. q_{cum}		X	X
Pressure Change vs square root of time: Δp vs. sqrt t		X	X
Oil Rate Derivative versus Cumulative Oil: q' vs. q_{cum} (also smoothed)		X	X
Oil Rate Derivative versus Time: q' vs. t (also smoothed)		X	X
Pressure $_{(ave)}$ Oil Rate Derivative versus Time: P' vs. t (also smoothed)		X	X
Oil Rate Derivative * Time vs Cumulative Oil: q' *t vs. q_{cum}		X	X
Oil Rate Change/Oil Rate Derivative versus Time: $(\Delta q/q)'$ vs t		X	X

Table 8.2 Graph Output Generated

Surface diagrams of the pressure and saturation conditions for each grid block at selected time steps were also utilized in the analysis. The primary graphs that proved diagnostic in classifying the fracture types were the rate-time, cumulative-time, rate derivative-time, rate-$(t_p+\Delta t)/\Delta t$, Δq-time and the $(\Delta q/q)$ vs. (q_{cum}/q) plots. Note that t_p

is not the traditional well test parameter but rather defined as $t_p = [(q_{cum} / q) + \Delta t] / \Delta t$. The physical significance, if any, of this parameter is unknown but it seemed to have some value in classifying the reservoirs.

The $(\Delta q/q)$ vs. (q_{cum} / q) plots were generated to approach the problem from a normalization and material balance standpoint that seems to have some semi-quantitative usefulness. This type of plot presents the data in a manner similar to well test analysis. A plot of log $(\Delta p/q)$ or $(\Delta q/q)$ vs. log (q_{cum} / q) (or the inverse) should transfer the data to data suitable for well test analysis. If pressure was available then linear flow would be characterized by 1/2 slope and pseudosteady state exponential decline would exhibit unit slope. Plateaus in the plot could be characteristic of possible hierarchical fracture systems and dual porosity character should be visible. Qualitative extension to rate data may be possible.

Decline curves were developed under the assumption of constant flowing bottom hole pressure but most wells declining to production capability, exhibit decreasing tubing head pressure which reflects a declining flowing bottom hole pressure. Therefore a normalization technique should be useful. Normalizing the flow rates by dividing the production rates by the change in tubing head pressure ($FTHP_{initial}$ - $FTHP_{current}$) was used by Poston and Chen to approximate the constant flowing bottomhole pressure assumptions. Though this is an ideal situation, using that data to approximate actual bottomhole flowing pressures is dangerous since practically speaking most US wells decline to pipeline or separator pressure very quickly and produce against a constant backpressure.

Since this type of data are not often available, this work modified the method to use rate divided by changes in rate ($q/\Delta q$), (or the inverse) which seem to approximate the general shape of the $q/\Delta p$ curves. Although this ($q/\Delta q$) cannot be used in a strictly quantitative sense it does give relative characteristics of the various fracture types. The normalization should also magnify the changes in storage compressibility and fracture intensity terms.

If the material balance equation is arranged in the form of a straight line for PSS flow then a Cartesian plot of $\Delta p/q$ vs. q_{cum}/q should yield a straight line of slope m that defines the matrix pore volume where the slope (m) = 5.615* (B_o/V_pc_t) where V_p is the pore volume. The rate of change of $\Delta q/q$ vs. cumulative q/q is plotted as an approximation to such pressure data. As such the actual pore volume can not be computed exactly but the relative slope can be used for qualitative interpretation.

As with the derivative of pressure ($\Delta p/dt$), the derivative of rate with respect to time ($\Delta q/dt$) should give an indication of the storage compressibility since pressure and rate are related quantities. The deeper the trough on the pressure derivative plots the lower the storage factor (i.e. lower fracture storage). This parameter can also be seen on the semi-log pressure-time plot as a double straight line offset. The larger the offset the lower the storage factor and the more time delayed is the offset to the lower value of λ. Although pressure is not used here it was hoped that the ($\Delta q/q$) vs. log (q_{cum} /q) plot would transfers the rate data to a pseudo-pressure plot which will exhibit the same phenomenon. These topics will be discussed in more detail as each graph is discussed.

8.9 Analysis of Experimental Results

To summarize, the analysis consists of an examination of the following types of data:

1. Simulation experiments to approximate rate decline performance of four different fracture types.
2. Type curve matching of the rate-time experimental output to the Poston-Chen-Fetkovich curves.
3. Comparison to conclusions and results obtained by Poston and Chen from actual field data from Austin Chalk reservoirs.
4. Graphical analysis of various calculation data from simulation output.
5. Visualization of pressure and saturation profiles using surface diagrams from simulation tabular output.

Figures 8.9 through 8.16 show the basic rate versus time data for the various fracture experiments on log-log plots. This is the first data to examine for general comparison between the experiments.

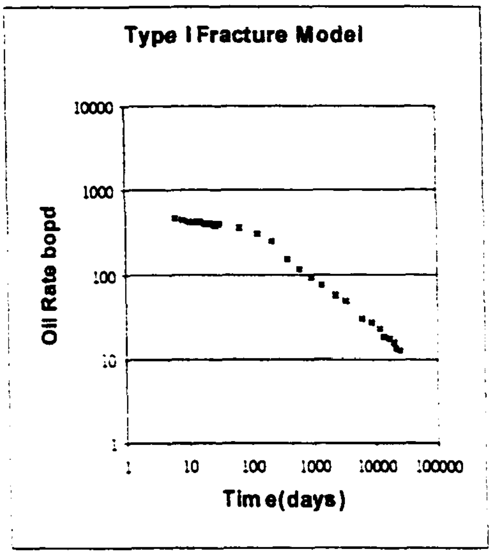

Figure 8.8 - Rate Time Plots Type 1

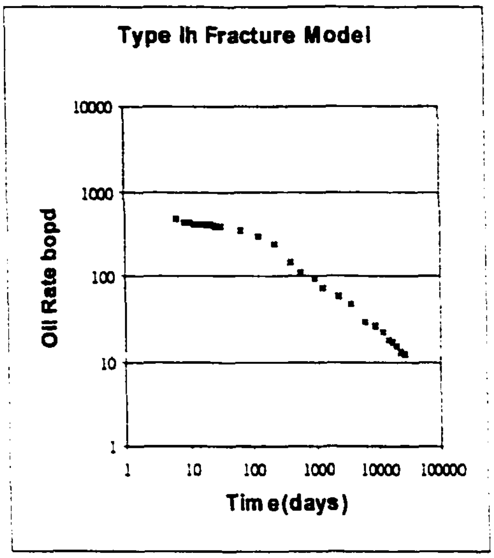

Figure 8.9 - Rate Time Plots Type 1h

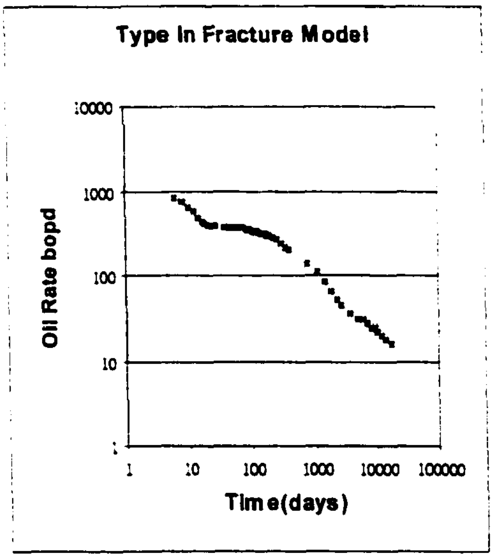

Figure 8.10 - Rate Time Plots Type 1n

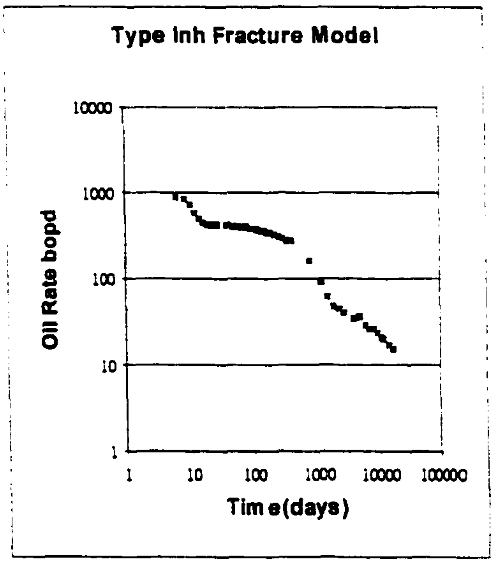

Figure 8.11 - Rate Time Plots Type 1nh

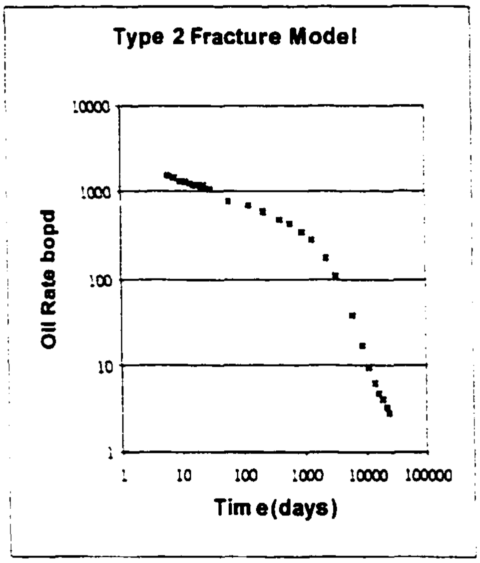

Figure 8.12 - Rate Time Plots Type 2

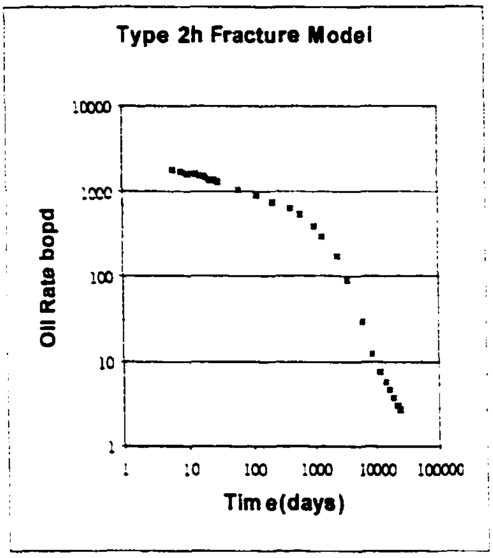

Figure 8.13 - Rate Time Plots Type 2h

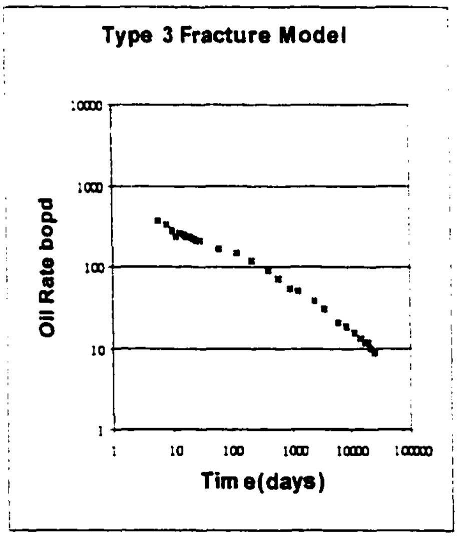

Figure 8.14 - Rate Time Plots Type 3

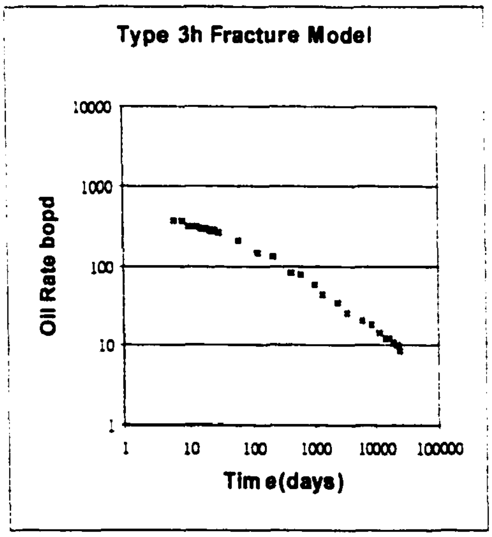

Figure 8.15 - Rate Time Plots Type 3h

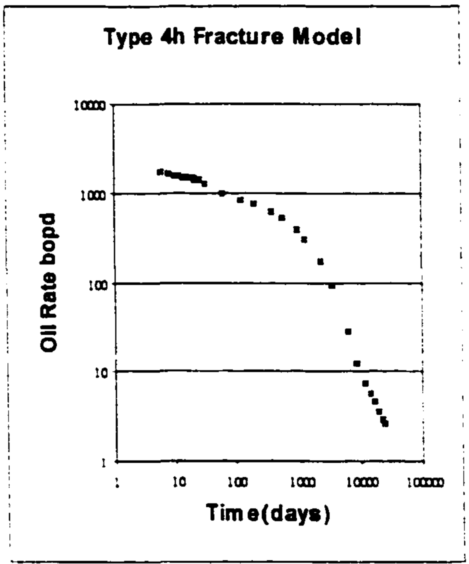

Figure 8.16 Rate Time Plots Type 4h

This rate-time output indicates that though there are distinct differences between model types there is very little difference in curve shape within each type of model when only fracture permeability is increased from 1000 to 4000 md (i.e. type 1 versus type 1h). However there are significant differences between fracture types. Type 1 fractures predictably show modest initial production rates followed by steep decline. Figures 8.17 and 8.18 show the composite curve for all model types superimposed on both semi-log and log-log scales.

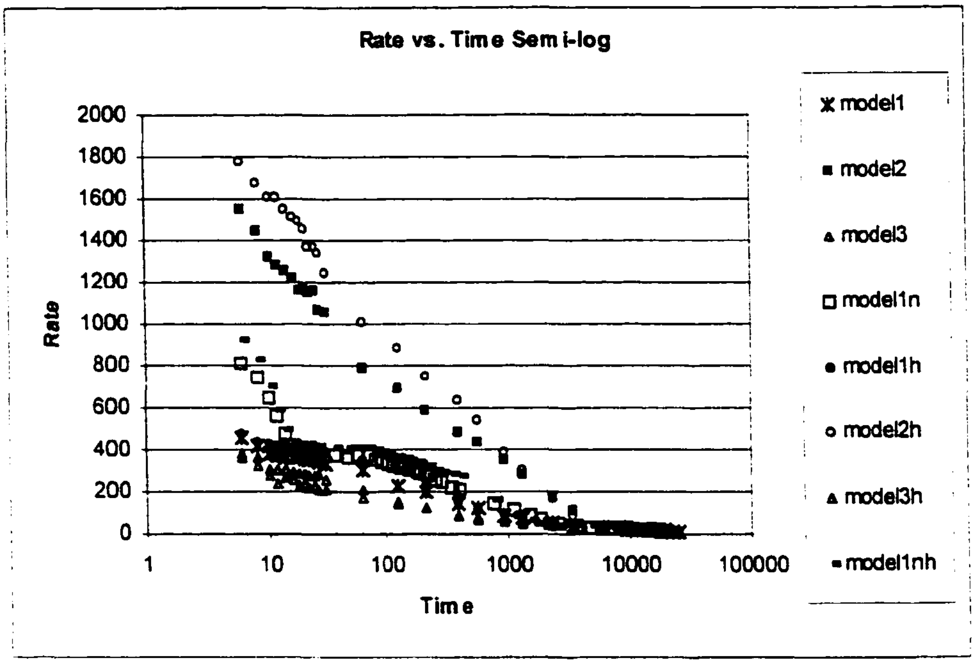

Figure 8.17 Composite Rate-Time Relationship Semi-Log Scale

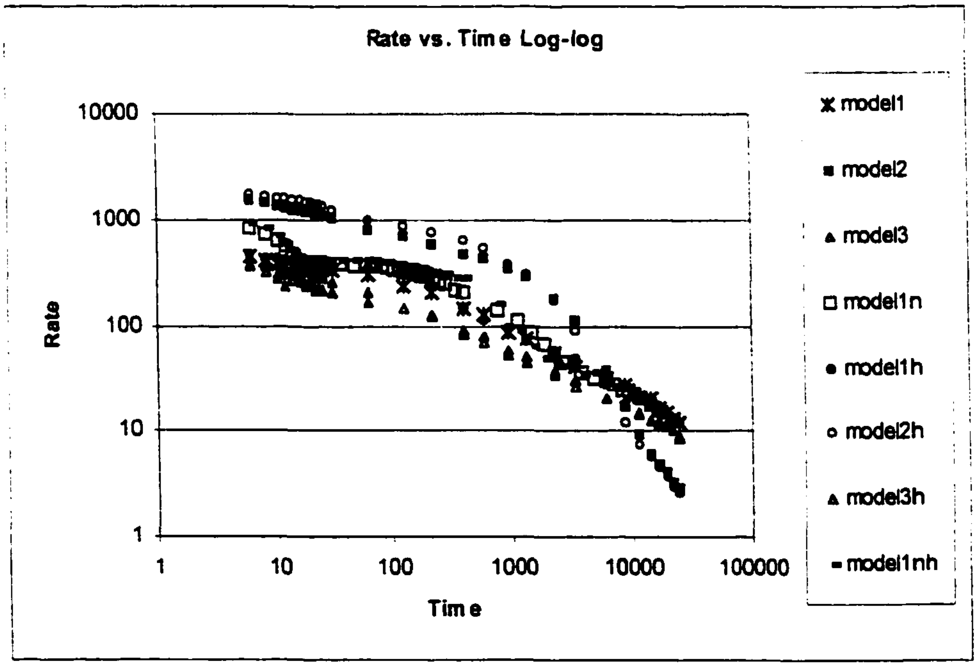

Figure 8.18 Composite Rate-Time Relationship Log-Log Scale

8.9.1 Matching of Experimental Rate-Time Data to Poston-Chen Type Curves

Figure 8.18 shows the expected trends based on the Poston-Chen type curves where the pseudo-fracture intensity term, γ, is increasing as the curves flatten out for any given storage compressibility coefficient, ω. Likewise as the transfer rate $\lambda' = k_m/k_f$ decreases (ω held constant), the curves flatten at late times. Also for a given fracture intensity the flattening of the curves indicates larger fracture storage capacity. Other broad features to note include the high initial rate exhibited by the type 2-fracture case where both the matrix and the fractures exhibit good permeability and the fracture storage capacity is low relative to the matrix. Also note that when the fracture storage increases to almost 20% of total pore volume the flow rate approaches that of the type two case but decreases very rapidly while the type two continues on a less steep decline rate presumably due to the matrix contribution.

The Poston-Chen and superimposed Fetkovich type curves were overlaid on the rate time output at the appropriate scales for comparison. For instance the following diagrams show the type curves plotted at the same scale as the rate time output. When overlain the storage compressibility and fracture intensity terms can be matched and used for interpretation. Recall that Poston and Chen claimed that the parameter γ was a direct indicator of fracture intensity if ω is on the order of 10^{-3}. This claim will be checked in the analysis.

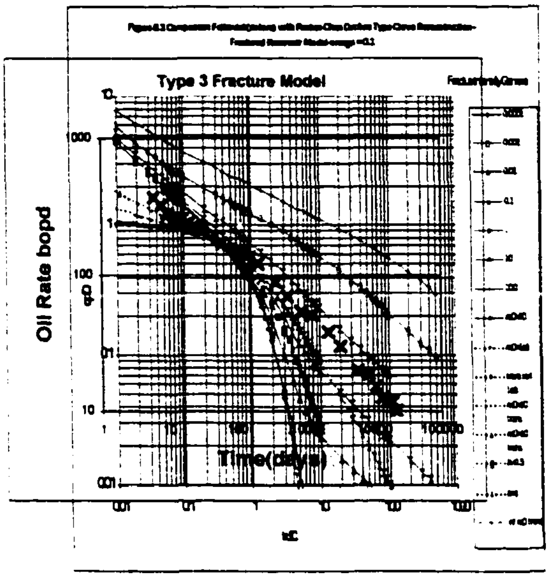

Figure 8.19 Type Curve Matching Example

This type curve matching process can be applied to each simulation model output. The following table illustrates the best matches of the rate-time data using the combined Fetkovich-Poston Chen type curve matches of the various models that were depicted in Table 8.1. Though the overall expected trends were present, the type curves did not prove useful in quantitative analysis.

Model Type	1	1h	1n	1nh	2	2h	3	3h	4
ω			ω Values Merge at Low γ Values	ω Values Merge at Low γ Values	ω Values Merge at Low γ Values	ω Values Merge at Low γ Values	ω	ω	ω Values Merge at Low γ Values
Very Early Time	Fetkovich	Fetkovich			?	?	?	?	
Early Time					0.001	0.001	?	?	0.001
Middle-Late Time	0.01	0.01	0.01	0.01	0.001	0.001	0.01	0.01	.001
Very Late Time	0.01	0.01	0.01	0.01	?	?	0.01	0.01	.001
γ									
Very Early Time	Fetkovich	Fetkovich	0.001	0.001	R_{eD}=10	R_{eD}=10	10	10	R_{eD}=10
Early Time	10	10	0.001	0.001	10	10	10	10	10
Middle-Late Time	1	1	0.1	0.1	10	10	10	10	10
Very Late Time	1	1	0.1	0.1	0.001	0.001	10	10	0.001

Table 8.3 Type Curve Match Summary Information

Recall in figure 8.1 that the storage compressibility term converged at short times and large values of γ so that these values are not distinguishable on the Poston-Chen curves. Also as the storage compressibility term approaches values of 10^{-3}, the curves are only dependent on the γ term and can theoretically be used as a direct indicator of fracture intensity. At intermediate to late time the values of γ did seem to be an inverse indicator of fracture intensity. Poston and Chen also noted that storage compressibility remained fairly constant over time for any particular model but that fracture intensity seemed to increase after shut-in periods. They related this to the system "sensing" more fractures further into the reservoir system with time. In general the type curve match to the experimental data of this study seemed to change over time to less fracture intensity at very late time values. Since only one type of fracture system was present in each model this change must indicate that over time the relative total compressibility of the matrix and fracture is changing over time in different ways with different fracture types. This could be the only explanation (assuming the type curves are valid) since the fracture intensity term was defined as $\gamma = (FI)^2 x_f^2 \frac{k_m}{k_f} \frac{(\phi c_t)_m}{(\phi c_t)_f}$ and all other parameters are invariant in the experiments. The implication is that the total compressibility in the fractures is increasing relative to the matrix over time for the cases of low matrix permeability and low fracture storage capacity. This should be reflected also by changing values of $\omega = \frac{(\phi c_t)_m}{(\phi c_t)_f + (\phi c_t)_m}$ however the observed values are in the range that merges into the main stem so that it is difficult to distinguish. These results are very confusing in light of the known experimental model parameters and cast some doubt on the use of the Poston-Chen curves for use as fracture storage compressibility and fracture intensity indicators.

In general it did not appear that the experimental results correlated precisely with these Poston and Chen curves except in a very general sense. However one could say that there was a general shift toward lower γ values as the fracture storage increased relative to the matrix and as the fracture intensity increased. There was also a decrease in the ω term as the matrix permeability increased which must be related to the compressibility of the system since permeability is not directly related by the definition.

8.9.2 Comparison of Rate-Time and Cumulative-Time Data

Figure 8.20 depicts the log-log rate-time behavior comparison of fracture systems with relatively high matrix storage capacity relative to the fracture storage capacity but with varying matrix permeability so that principally λ is contrasted.

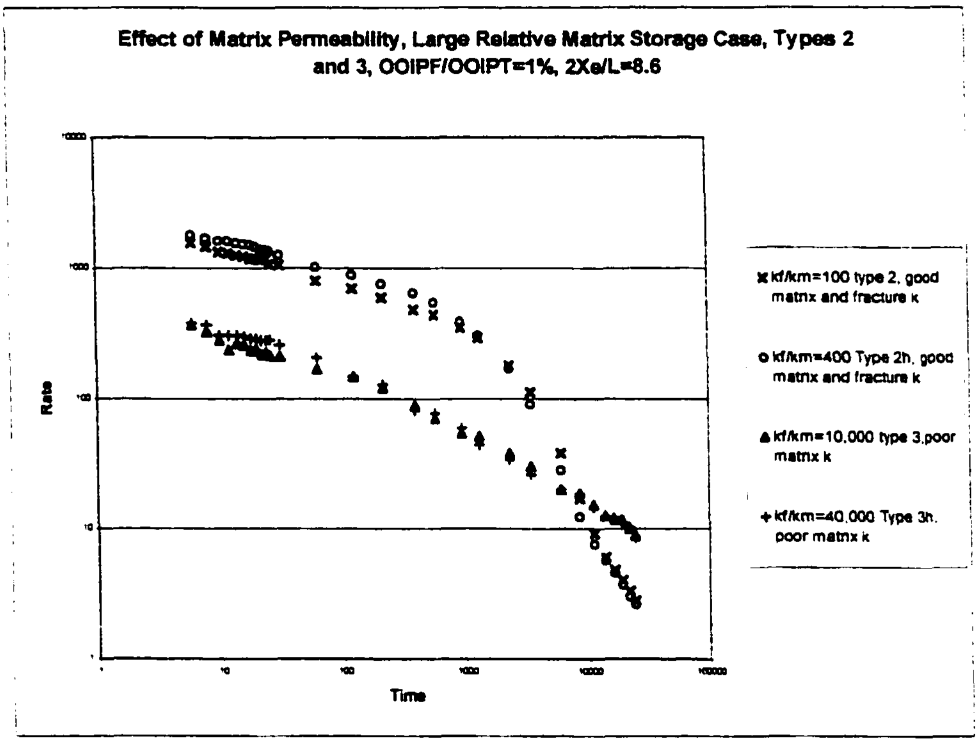

Figure 8.20 Comparison of the Effect of Matrix Permeability in Cases of Large Matrix Storage Capacity – Types 2 and 3

The comparison shows the marked contrast of high initial rates for the cases where the matrix and fractures have high permeability compared to cases where only the fracture has high permeability. The decline paths cross at late times. Note that the effect of increasing the fracture permeability from 1000 to 4000 md, (decreasing λ) increases flow rate within each group as expected by theory but notice that it is a relatively minor effect compared to increasing the matrix permeability.

Figures 8.21 and 8.22 show the magnified early and late time portions of the decline curves to better illustrate this phenomenon.

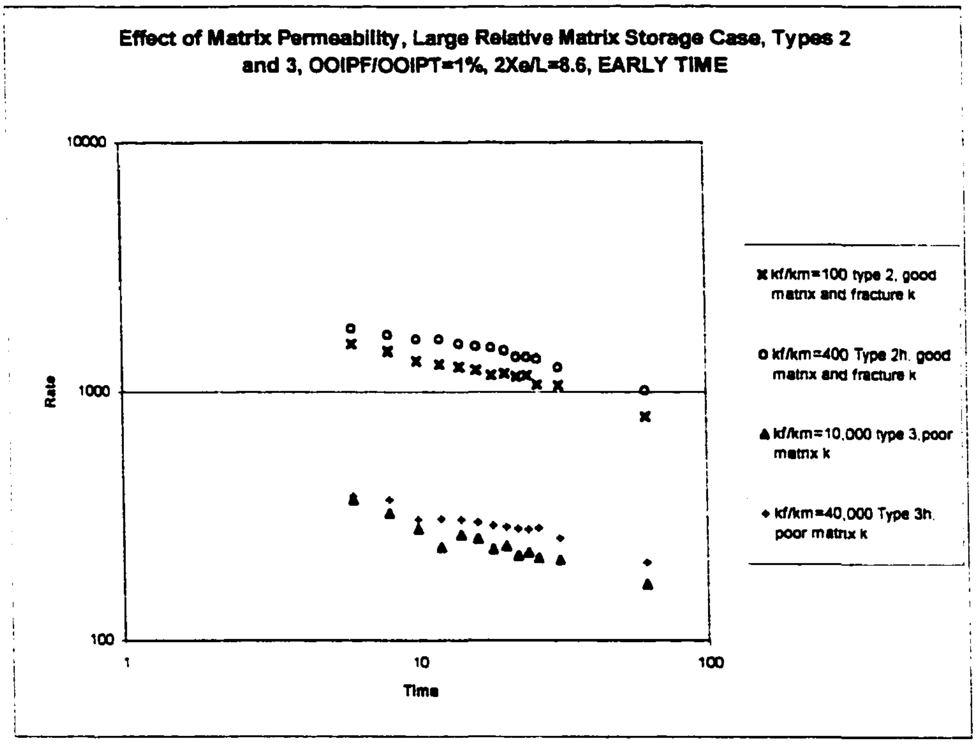

Figure 8.21 Early Time Comparison of the Effect of Matrix Permeability in Cases of Large Matrix Storage Capacity – Types 2 and 3

Notice in Figure 8.22 that the effect diminishes at late times and at very late times the curves even cross.

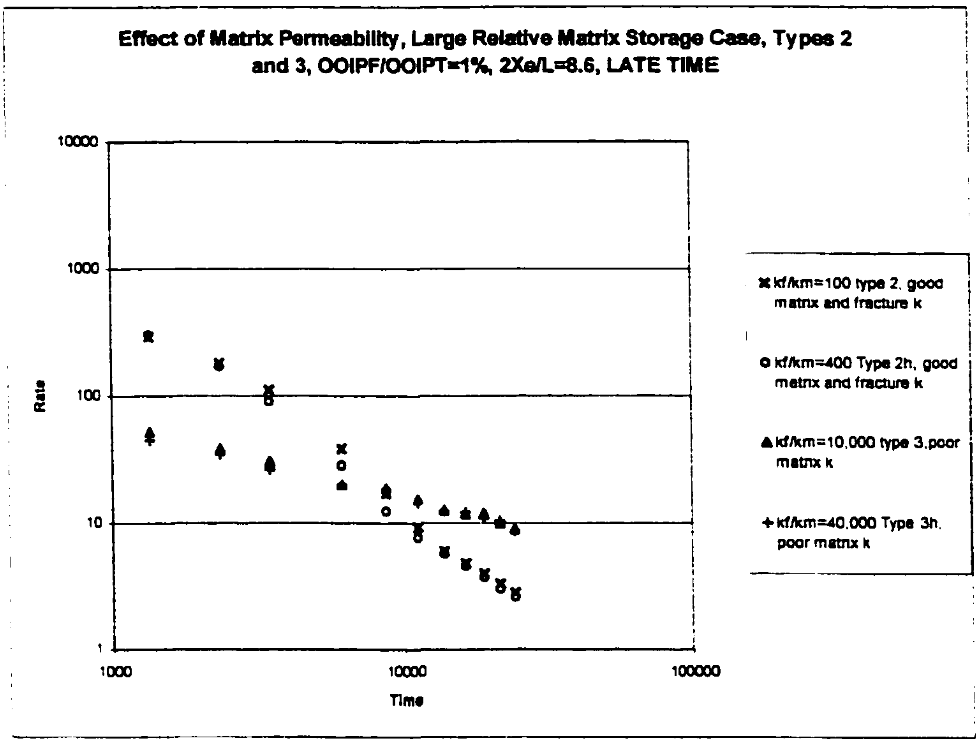

Figure 8.22 Late Time Comparison of the Effect of Matrix Permeability in Cases of Large Matrix Storage Capacity – Types 2 and 3

These effects can also be illustrated through the cumulative production versus time plots. Note in Figure 8.23 that the slope of the high matrix permeability case is very large compared to the low matrix permeability case. However they slowly converge at late times, presumably as the matrix and fractures have been depleted in the high permeability cases. Again the shift to higher cumulative production as a result of higher initial flow rates with increasing matrix permeability is shown.

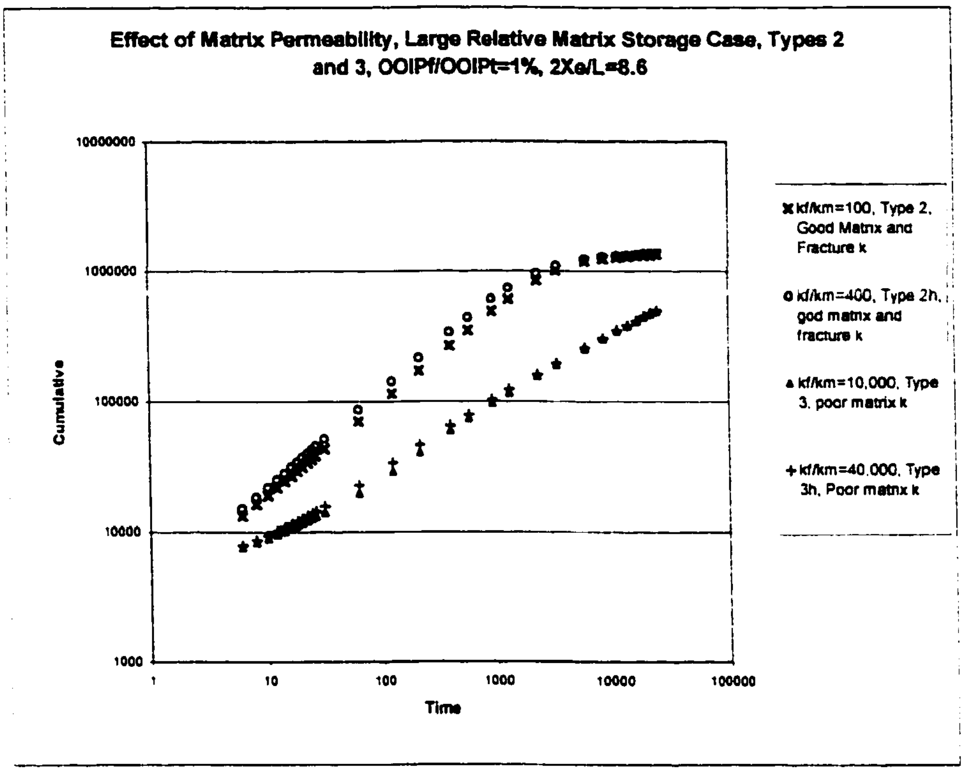

Figure 8.23 Comparison of the Cumulative Production Effects of Matrix Permeability in Cases of Large Matrix Storage Capacity – Types 2 and 3

Figure 8.24 illustrates the effect of increases in the relative storage capacity of the fracture relative to the matrix system in cases where the matrix permeability is poor. As the storage capacity of the fracture increases from 1% to 18% of the total system storage capacity (total system ooip remaining constant) the initial flow rates increase substantially and shift the curves upward to the right. The rate-time behavior converges at late times as the fracture is depleted. As before the effect of the fracture permeability is less important than as associated matrix support even at early times.

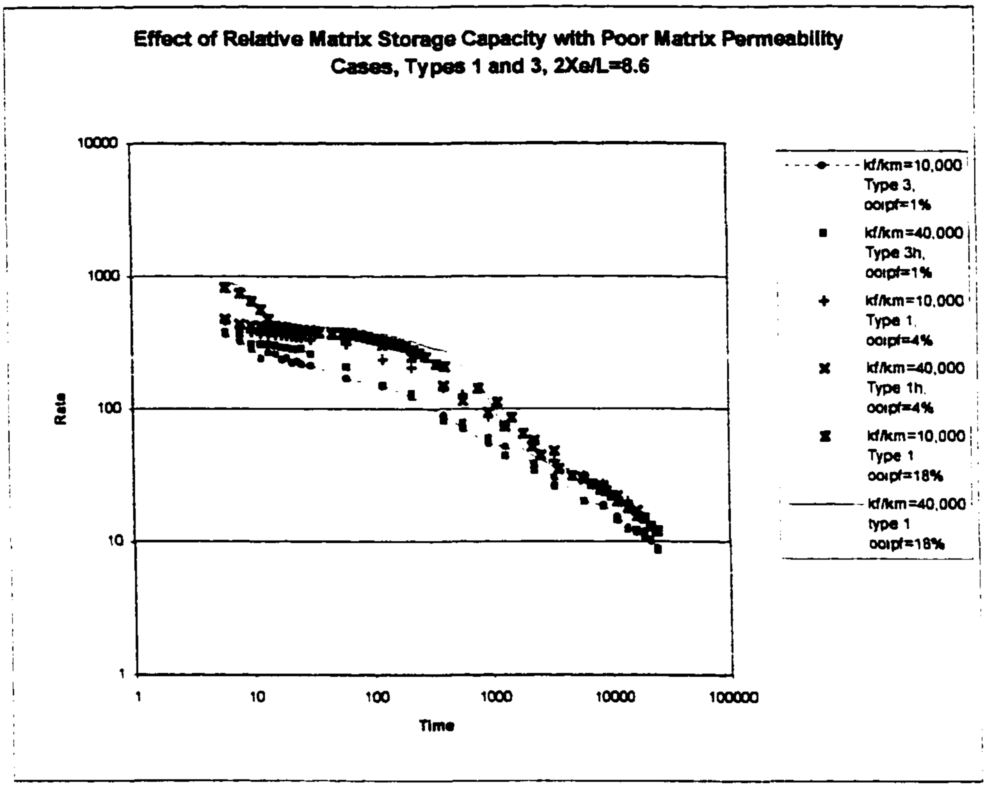

Figure 8.24 Effect of Increasing Fracture Storage Capacity on Systems with Low Matrix Permeability

Notice how the effect of additional fracture storage results in a plateau in the rate decline followed by a rapid decline to the rate exhibited by the model containing less fracture storage.

Again a similar effect can be seen on the cumulative versus time plot shown in Figure 8.25. The curves are shifted upward and to the left as a result of the more rapid cumulative production build-up resulting from the higher flow rates.

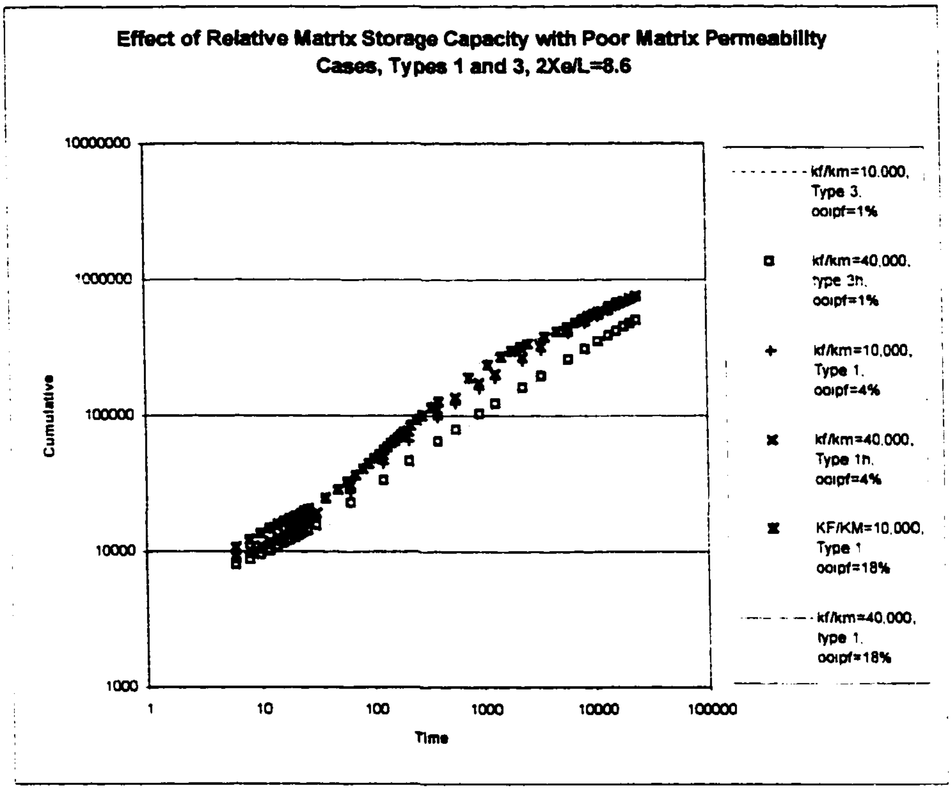

Figure 8.25 Effect of Increasing Fracture Storage Capacity from 1% to 18% of System Total

Table 8.4 illustrates the predominant characteristics of the rate-time and cumulative time data for the various fracture types.

Type	Characteristics
1	• Modest initial rate but initial rate increasing and approaching Type 2 as ω' approaches 0.15. • Rapid initial decline followed by relatively long transition period. • Semi-log and log-log plots show four linear slope changes with steep early decline, a long zero slope transition, a long linear portion and a very late time low slope linear portion. The middle zero slope transition diminish as ω' drops to 0.04. • The cumulative-time plot exhibits an increasingly "S" shape with ω' increasing and late time flattening but not as flat as type 2.
2	• High initial flow rates. • Very little early time character. Initial linear decline is short with very indistinct transition on log-log. Very modest early-middle slope change on semi-log plot only. • Low and prolonged subsequent decline rate compared to type1 with a rapid rate decline at late time beginning later than type 1 but slope is greater and eventually crosses type 1 decline. • The cumulative-time plot is linear on log-log with very late time slope change to near zero slopes.
3	• Low initial rates. • Similar early characteristics to type 2 but lower initial rates and longer period of middle linear behavior with slope similar to type 2 but at lower rates. • Very late time slope increase after the curve crosses the type 2 plot. • The cumulative-time plot shows and early time linear slope changing to a steeper prolonged linear shape on log-log until very late slope change. Curve converges to type 2 at late time
4	• No distinguishing characteristics from type 2.

Table 8.4 Predominant Characteristics of Rate-Time and Rate-Cumulative Data Behavior

8.9.3 Comparison of the $\Delta p/q$ vs. q_{cum}/q Data between Fracture Types

As mentioned before, the $\Delta p/q$ vs. q_{cum}/q plot is very useful in reservoir analysis of fracture type, calculation of pore volume and estimation of storage compressibility. However as noted, pressure data are almost never available to a practicing engineer. Therefore $\Delta q/q$ has been plotted as an approximation to $\Delta p/q$. A comparison of $\Delta q/q$ vs. q_{cum}/q with $\Delta p/q$ vs. q_{cum}/q plots below (figures 8.25-8.28) show that the plots are very similar in shape. The interesting thing to note is that if one uses rates instead of pressure, such as $\Delta q/q$ vs. q_{cum}/q, then the same general patterns are seen in the plots. The later unit slope on the pressure plots corresponds to an exponential decline on the production curve. Although the unit pressure slopes are not exhibited on the rate declines, the semi-unit linear characteristics are the same and can be used to classify the matrix-fracture system.

With this type of plot using pressure, one would typically expect a ½ slope in the early time region characteristic of linear flow. Also the unit slope pseudosteady region is magnified. The late time would be characterized by exponential decline because the boundary effects are felt by the system. This would result in a unit slope on such plots. Figure 8.25 shows this early ½ slope followed by a transition period and subsequent unit slope. Figure 8.26 shows the same type of plot using $\Delta q/q$, as an approximation for $\Delta p/q$ since the flowing pressure data are rarely available. Note that although the slopes are not ½ and unity, the curves do show the same basic shape and can be used to indicate the time at which pseudosteady state is obtained.

Note in figure 8.27 that the early time ½ slope is not apparent on the graph. This is probably because of the small amount of oil in the fractures and the system senses the fracture depletion relatively quickly. There is also relatively little matrix permeability support. The unit slope is present but without an apparent transition zone. Conversely, the $\Delta q/q$ plot shown in figure 8.28 does show an early break in slope at approximately 62 days. Surface diagrams of the pressure field indicate that this corresponds to the time that the system first senses the exterior boundaries of the model. This phenomenon is not exhibited as well on the $\Delta p/q$ plot. But it does show the possible value of the $\Delta q/q$ type of diagram, which will be used to compare and contrast the various models.

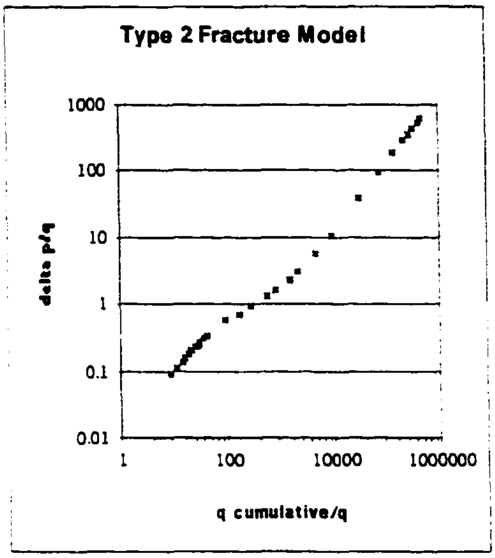

Figure 8.25 Model Types 2 (semi-log)
$\Delta p/q$ versus q_{cum}/q

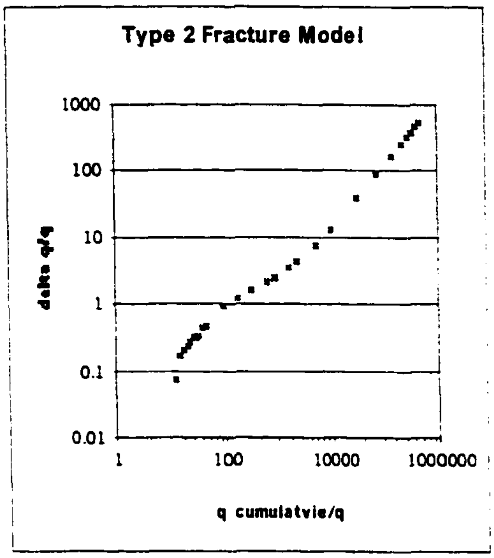

Figure 8.26 Model Types 2 (log-log)
$\Delta q/q$ versus q_{cum}/q

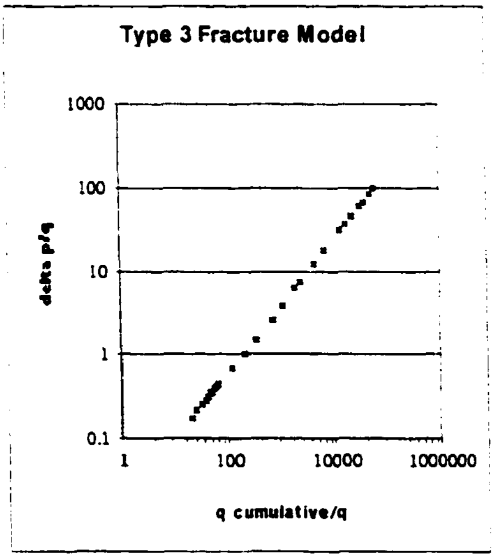

Figure 8.27 Model Type 3 (semi-log)
$\Delta p/q$ versus q_{cum}/q

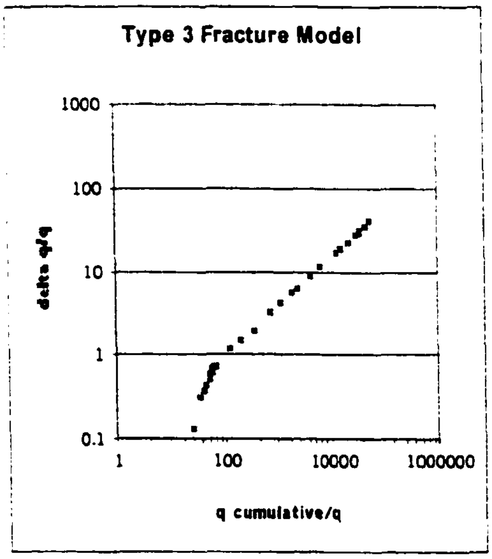

Figure 8.28 Model Type 3 (log-log)
$\Delta q/q$ versus q_{cum}/q

The following section discusses an examination of the graphs of $\Delta q/q$ vs. q_{cum}/q plots for the various models. Figures 8.29 and 8.30 show the effect of changing the relative fracture to matrix storage volume, ω, but keeping the ratio of matrix to fracture permeability, λ constant. Note in both figures 8.29 and 8.30 that as the fracture storage capacity increases, there is a pronounced change in the shape and in fact a double offset character is exhibited even though the matrix permeability is very low. Also note that as the fracture storage is increased, that the time between the slope change is delayed. This shows that the time delay may indicate the relative contrast in fracture to matrix storage or an indicator of ω^*. Also of note is that as λ increases, given a constant relative fracture to matrix storage ratio, there are an increase in the "width" of the transition zone. In other words there is more of a time delay from the onset of the first slope change to the second. Figure 8.31 and 8.32 show the log-log and semi-log expanded views to better show these phenomenon. These diagrams illustrate an important discovery that the ratio of the $\Delta q/q$ for the beginning or the transition zone yields an indicator of the relative storage capacity of the fracture system. In other words on figure 8.31, the ratio of $\Delta q_A/q_A$ to $\Delta q_B/q_B$ is 4.38 (1.1698/0.2672), which corresponds to the ratio of the relative fracture storage capacities of the two models. Thus if one has a reference well, all other field well decline curves can be used as an indicator of relative fracture storage capacity.

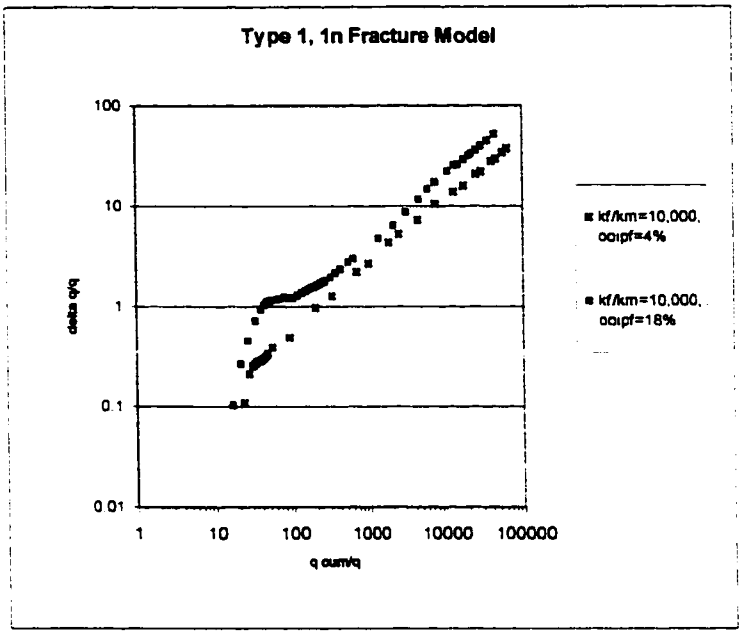

Figure 8.29 Type 1 Fracture Increasing Matrix Pore Volume Relative to Fracture λ'=1 ee^{-4}

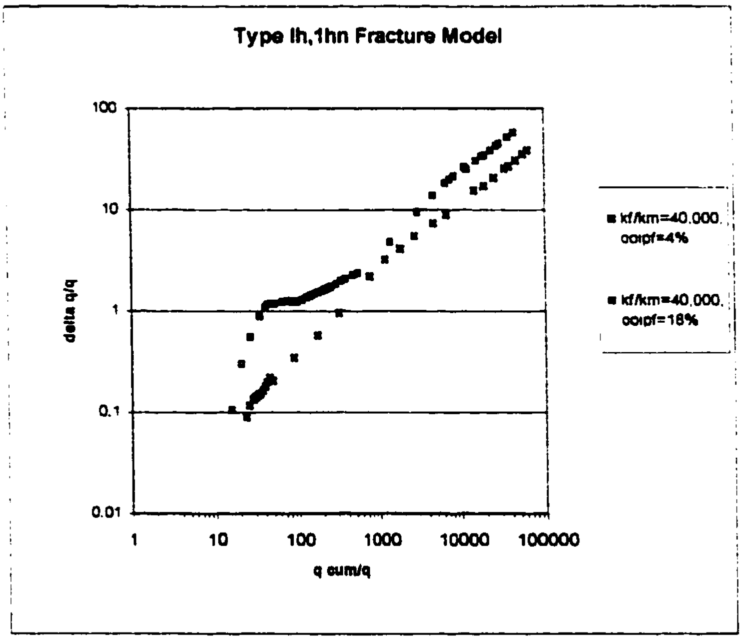

Figure 8.30 Type 1 Fracture Increasing Matrix Pore Volume Relative to Fracture λ'=2.5 ee^{-6}

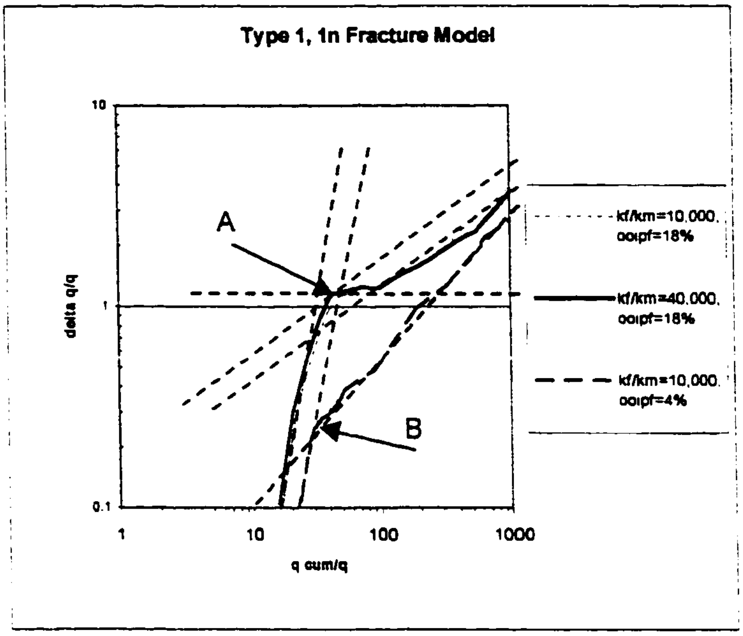

Figure 8.31 Expanded Type 1,1n,1nh Fracture Model-Effect of Increasing Matrix Pore Volume Relative to Fracture and Change in k_f/k_m Log-Log

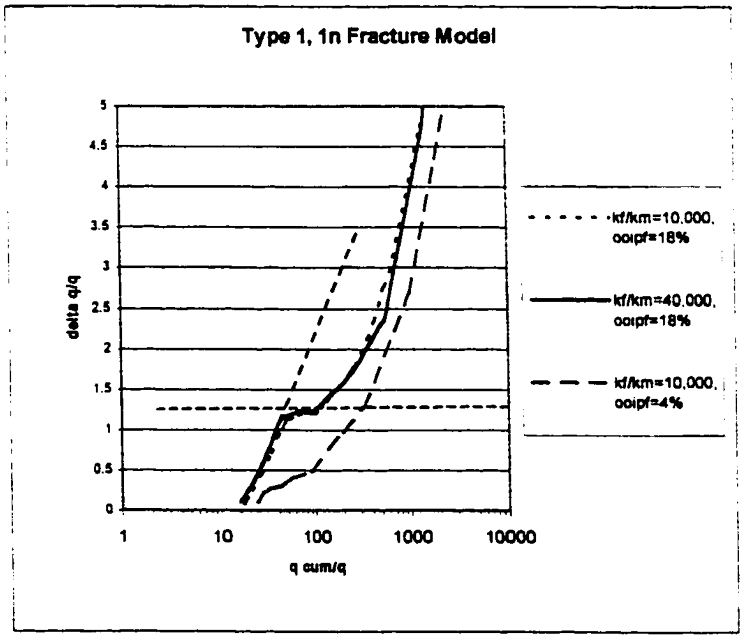

Figure 8.32 Expanded Type 1,1n,1nh Fracture Model-Effect of Increasing Matrix Pore Volume Relative to Fracture and Change in k_f/k_m Semi-Log

Figure 8.33 shows the effect of increasing the fracture storage volume in cases of poor matrix permeability. Except for early time data, which is often not recorded, the slopes again show near unit slopes.

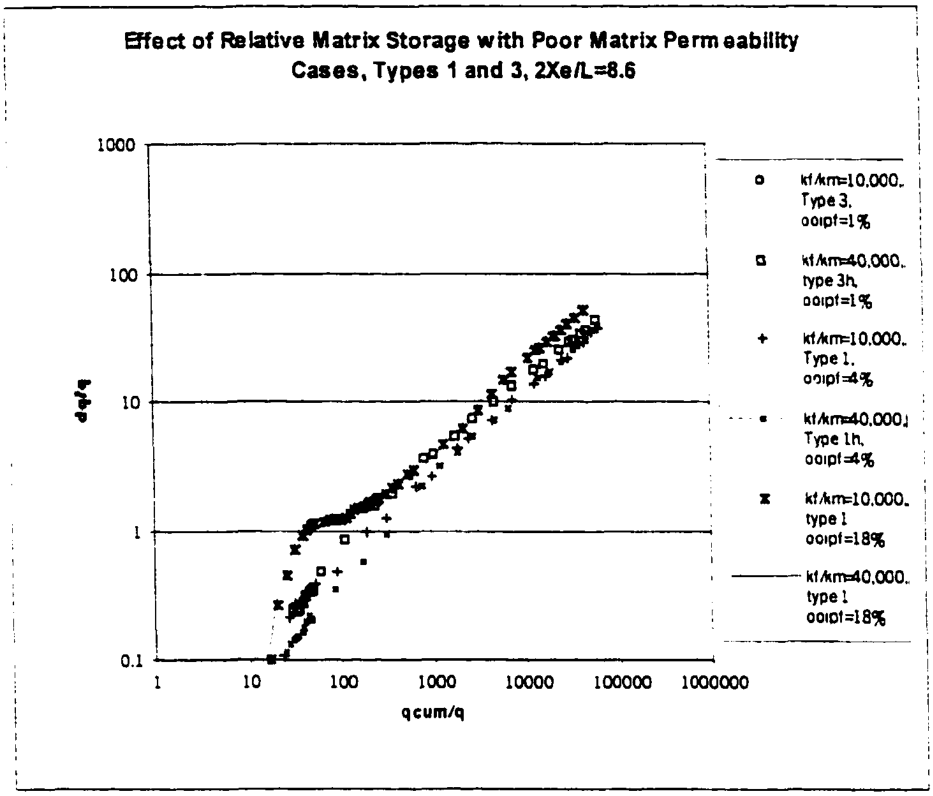

Figure 8.33 Effect of Increasing Fracture Storage Capacity in Case of Poor Matrix Permeability Log-Log

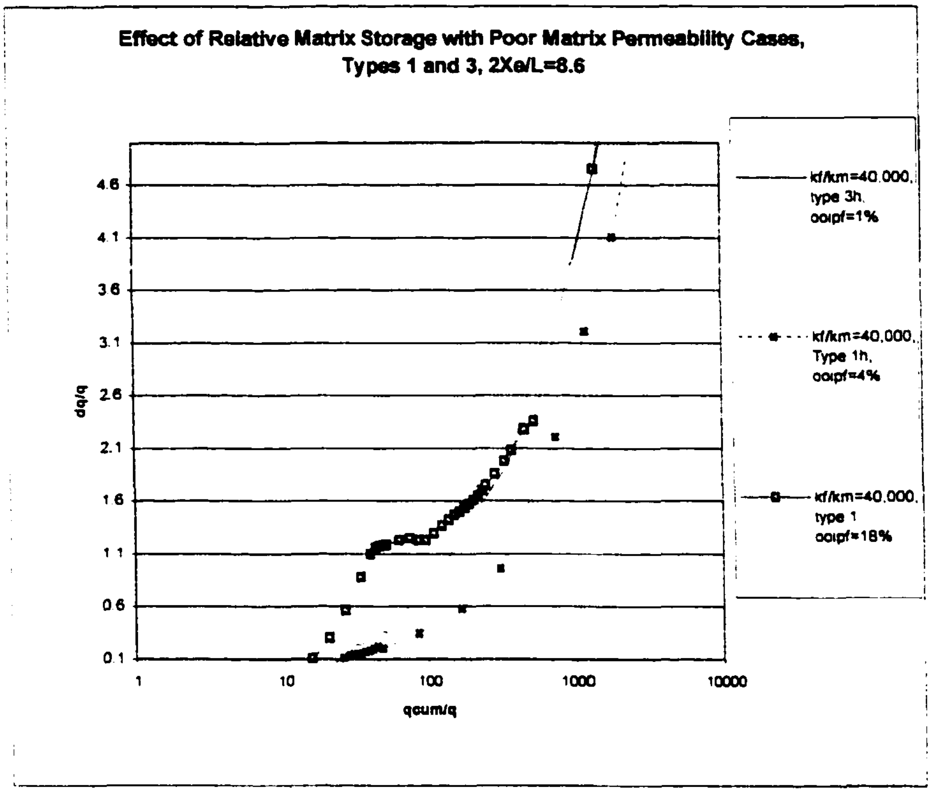

Figure 8.34 Effect of Increasing Fracture Storage Capacity in Case of Poor Matrix Permeability Expanded Semi-Log

Figure 8.35 shows the effect of changes in matrix permeability in cases of large matrix storage capacity relative to fracture storage capacity. Note the typical dual porosity offset in the slope for the Type 2 fracture.

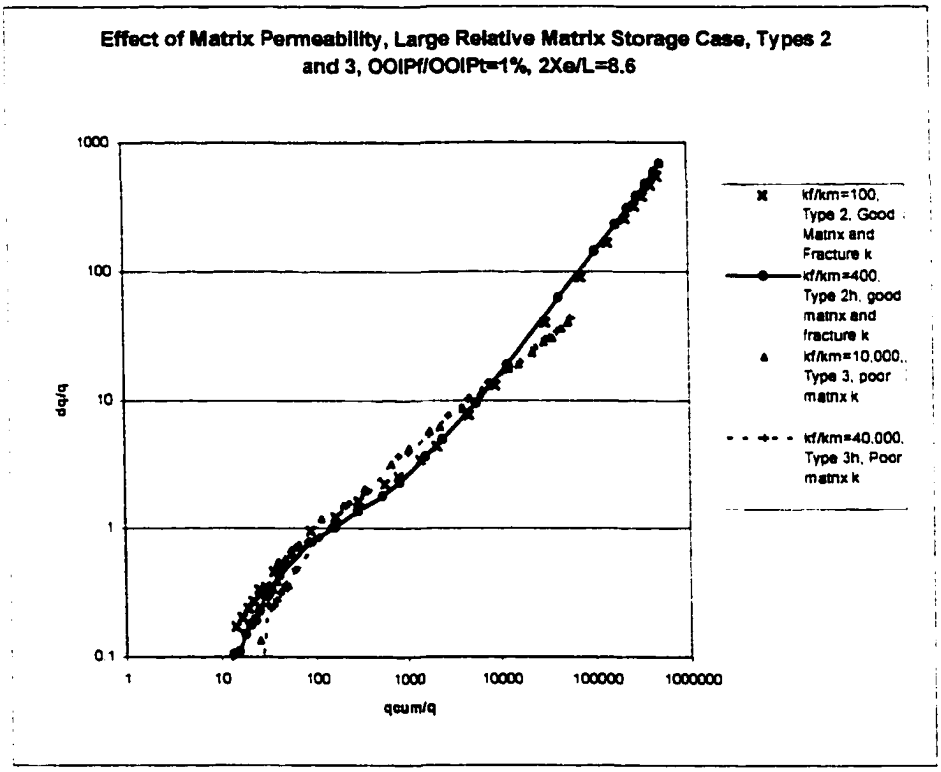

Figure 8.35 Effect of Increasing Matrix/Fracture Permeability-Large Matrix Storage Capacity

The slope of the Cartesian plot can also give a qualitative indication of pore volume. Actual values of pore volume can be obtained if pressures instead of rate data are available. However using the same techniques on $\Delta q/q$ versus q_{cum}/q data can give a relative value of pore volume between the fracture types from the relationship: slope (m)=5.615* ($B/V_p c_t$). In other words the matrix pore volume will be inversely proportional to the slope of the Cartesian straight-line portions at late time. The steeper the slope the less the V_{pm}.

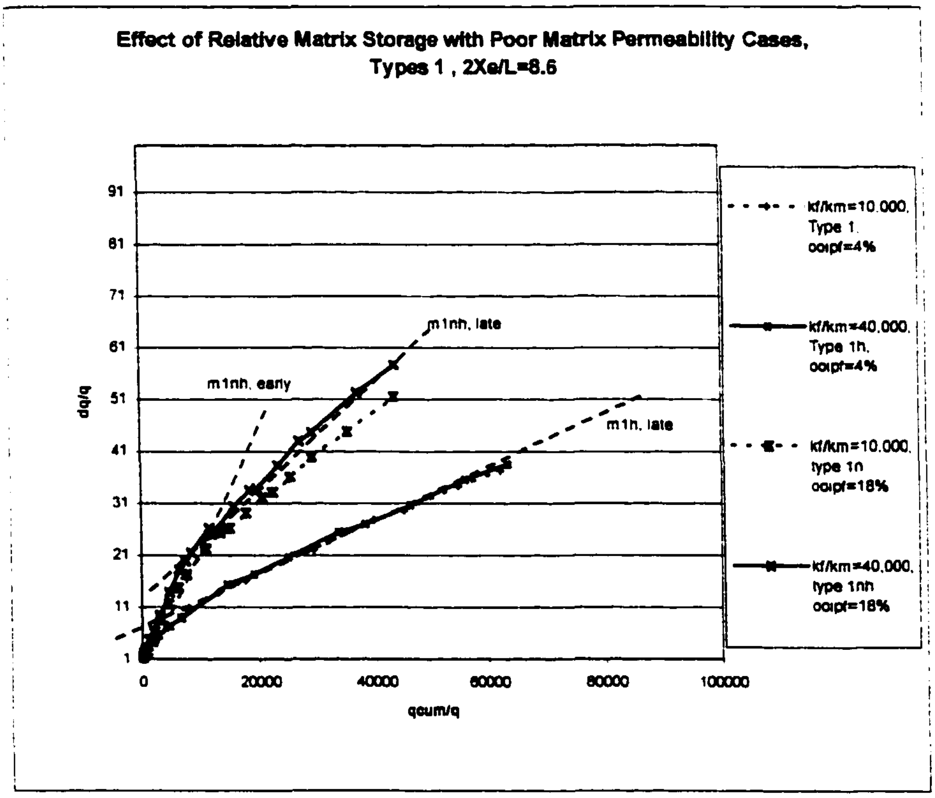

Figure 8.36 Cartesian Plot of $\Delta q/q$ versus q_{cum}/q Showing Effect of Matrix Pore Volume on Slope

The graphs generally confirm that the late time slope increases with increasing fracture and decreasing matrix pore volume since the lower slope indicates more matrix pore volume. However there is also an unexpected secondary effect related to λ since the slope steepens slightly with increasing fracture permeability (λ decreasing). This phenomenon is most apparent as the fracture volume increases to 18% of the total. Although the phenomenon is also seen on the Type 1 and 3 it is much less noticeable.

Figure 8.35 shows the Cartesian case of the Type 2 models. . Notice that the late time portion is again linear and the early time linear portion is not visible, as the duration is very short.

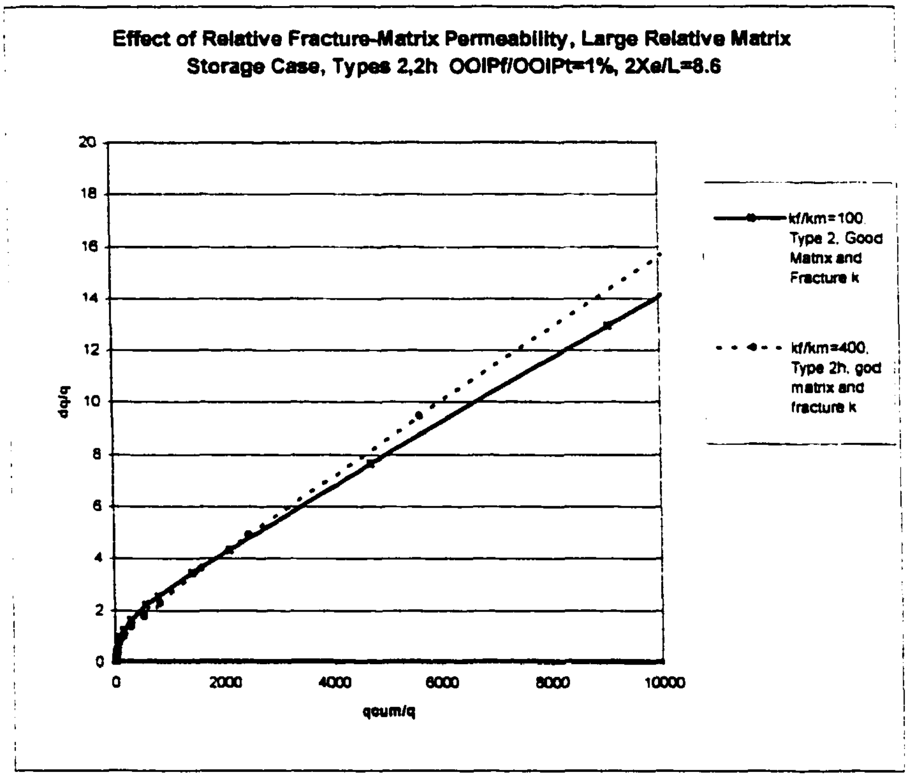

Figure 8.37 Expanded Cartesian Plot of $\Delta q/q$ versus q_{cum}/q, type 2 - Effect of Fracture-Matrix Permeability in Large Relative Matrix Pore Volume Case

Table 8.5 summarizes the predominant characteristics from $\Delta q/q$ versus q_{cum}/q graphs that have been discussed.

Type	Cartesian	Semi-Log	Log-Log
1	• 2-linear slopes, intersecting at increasing $\Delta q/q$ as ω' increases. • Intersection shifts to lower q_{cum}/q and slope increases as λ' decreases. • Late time linear slope increases as matrix pore volume increases.	• Early semi-linear slope with zero slope transition to later concave upward shape. • Zero slope transition disappears at low ω'. • The early linear period remains as as ω' shrinks until it disappears as the model approaches type 3. • Duration of the zero slope transition decreases slightly with increasing λ' for a given ω'	• Early semi-linear slope (approx. ½ slope) with zero slope transition to later semi-linear shape. • Zero slope transition disappears at low ω'. • The early linear period remains as as ω' shrinks until it disappears as the model approaches type 3. • Duration of the zero slope transition decreases slightly with increasing λ' for a given ω'
2	• Early very short duration linear followed by prolonged linear slope that shifts to higher slope with decreasing λ'	• Concave upward in entirety with shift to higher dq/q with decreasing λ'	• Double offset "dual-porosity" unit slope shape is present with early and late time slopes almost parallel. • Transition zone offsets the two linear portions but is not zero slope.
3	• 2-linear slopes, intersecting at increasing dq/q as ω' increases. • Intersection shifts to lower q_{cum}/q and slope increases as λ' decreases.	• Early, very short duration semi-linear slope but <u>no</u> zero slope transition. • Concave upward shape begins immediately after early linear.	• Early, very short duration semi-linear slope with change to prolonged linear middle-late time and shift to higher $\Delta q/q$ with decreasing λ'

Table 8.5 Predominant Characteristics from $\Delta q/q$ versus q_{cum}/q Graphs

8.9.4 Comparison of Derivative Data between Fracture Types

The derivative of rate with respect to time is examined next. The rate derivative is often so noisy that it is useless in quantitative analysis. The derivatives of simulated rate data are no exception. However, qualitative comparisons between the various data can be made. Also an additional smoothing technique is introduced that seems to be useful. This technique involves not only using a smoothed derivative as introduced in Chapter 5 but utilizes the cumulative data instead of the rate data. Using cumulative data is itself a method of smoothing. And since cumulative production is the integral of rate data, taking the second derivative of the cumulative data appears to result in a better smoothed derivative of rate versus time. Figures 8.38 and 8.39 illustrate this concept. Notice the significant improvements in the derivative with the use of the second derivative of cumulative over the erratic nature of the simple smoothed rate derivative. This type of derivative will be used in the following analysis whenever it appears to offer a smoother pattern in the early time region. However the pure rate derivatives were always plotted for comparison in the analysis. The rate derivative analysis is followed by a comparison to the derivative of $\Delta q/q$ with respect to time. The derivative of $\Delta q/q$ with respect to time appears to offer some aid in better direct comparison with pressure derivative analysis.

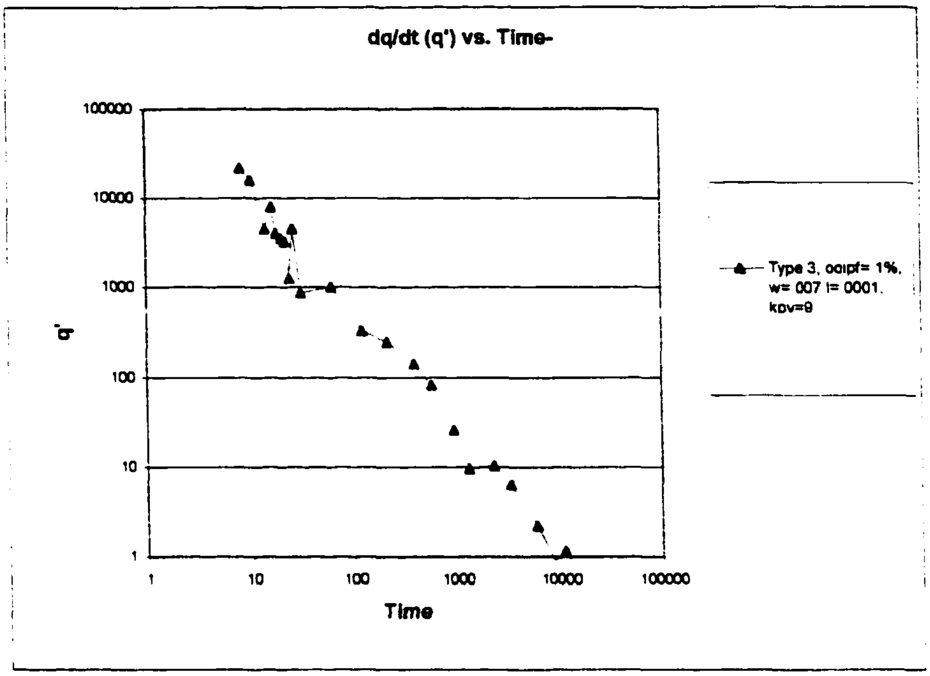

Figure 8.38 First Derivative of Rate with respect to Time

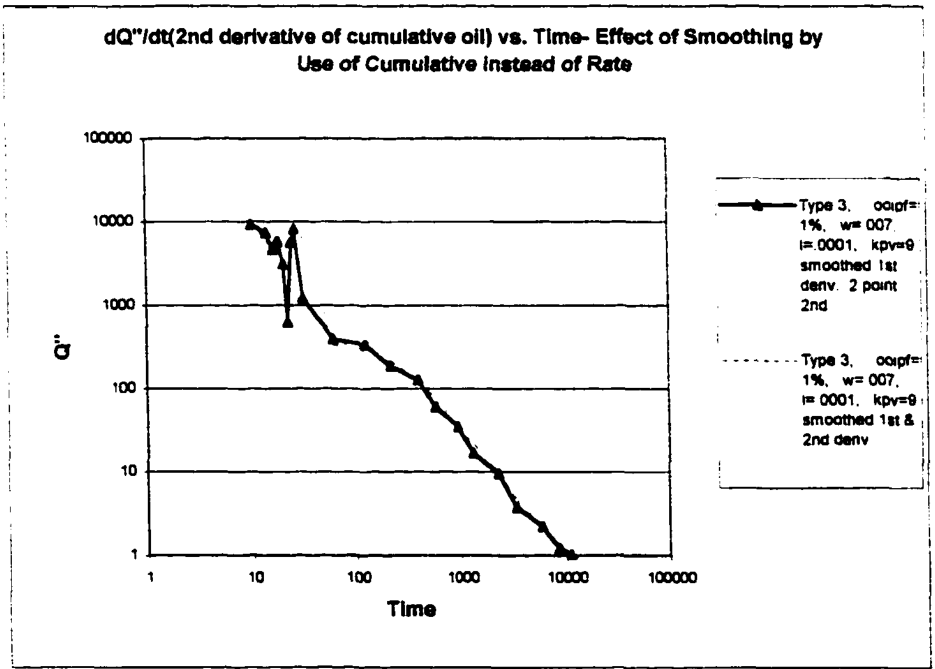

Figure 8.39 Second Derivative of Cumulative with respect to Time

Figure 8.40 shows the rate derivative comparison of the Type 2 and Type 3 fracture models illustrating the effect of changes in the matrix permeability but constant low fracture to storage capacity ratio. Figure 8.41 shows the derivative plotted on a scale modified by time ($Q^{''}$*t) to level the plot for analysis purposes Note that the depth of the minimum is slightly greater with the type2. Typically one expects the depth of the minimum to be the same when storage coefficient is identical so that compressibility factors must also be present. Also note that as $\lambda^{'} = k_m/k_f$ decreases (from Type 2 to Type 3), the minimum shifts to the right toward more time delay. The minimum delay is opposite on the $(\Delta q/q)'$ plot which is more consistent with pressure data. However the time delay is so small and happens at such an early time that it may not be useful in classifying the reservoir types.

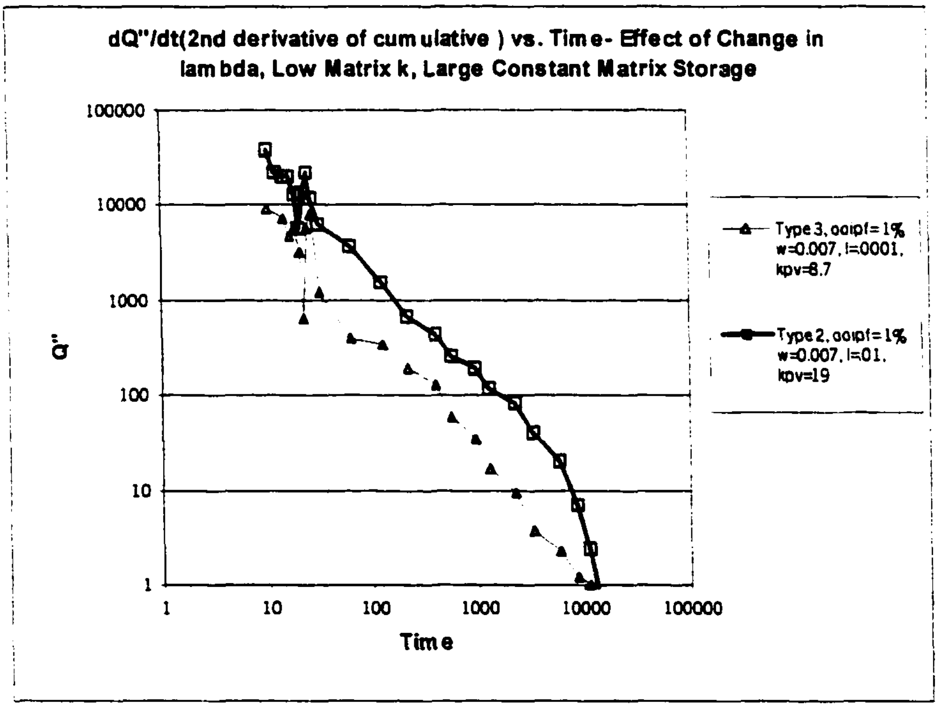

Figure 8.40 $Q^{''}$ versus Time-Effect of Change in k_f/k_m, Large Constant Matrix Storage

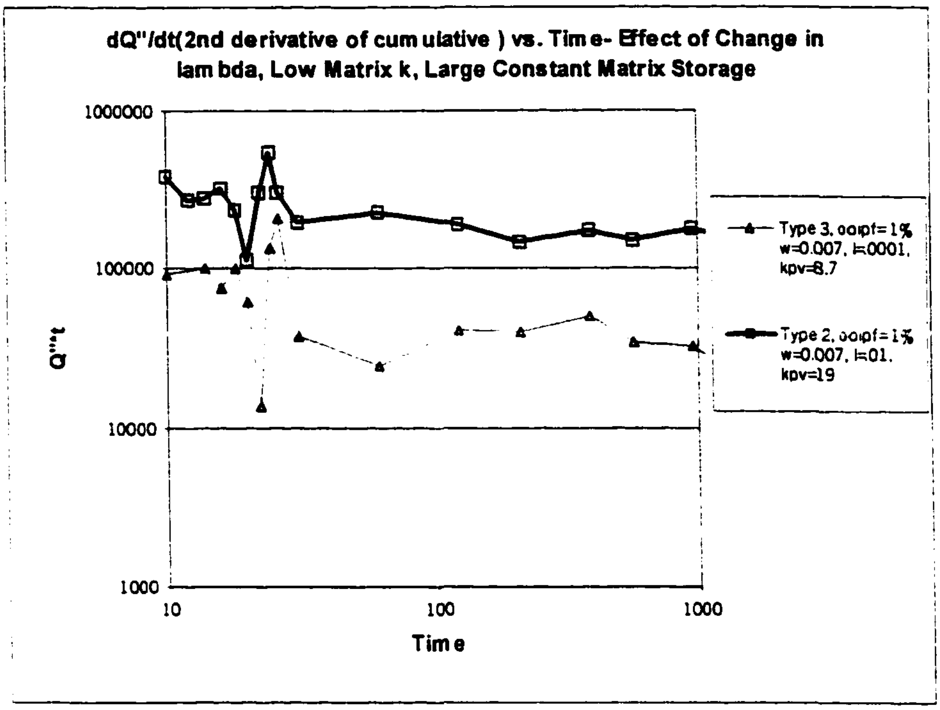

Figure 8.41 $Q^{''}$*t versus Time-Effect of Change in k_f/k_m , Large Constant Matrix Storage

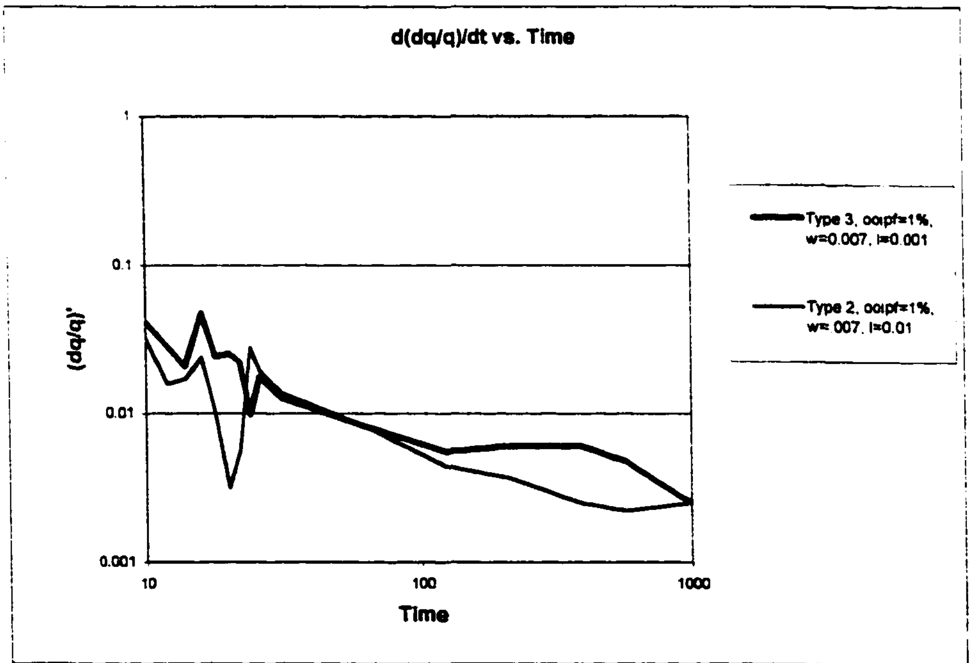

Figure 8.42 $(\Delta q/q)^{'}$ versus Time-Effect of Change in k_f/k_m , Large Constant Matrix Storage

Figures 8.43. 8.44 and 8.45 show the effect of changing the relative storage capacity $\omega^{\cdot}$ while the relative matrix to fracture permeability ratio remains constant. As expected the increase in $\omega^{\cdot}$ (increasing fracture storage) shifts the minimum to a higher time delay, however the depth of the minimum also increases with increasing $\omega^{\cdot}$ which is the opposite of that seen in pressure derivative data. Also note that the derivative minimum is time delayed and deeper and wider than either the Type 2 or Type 3.

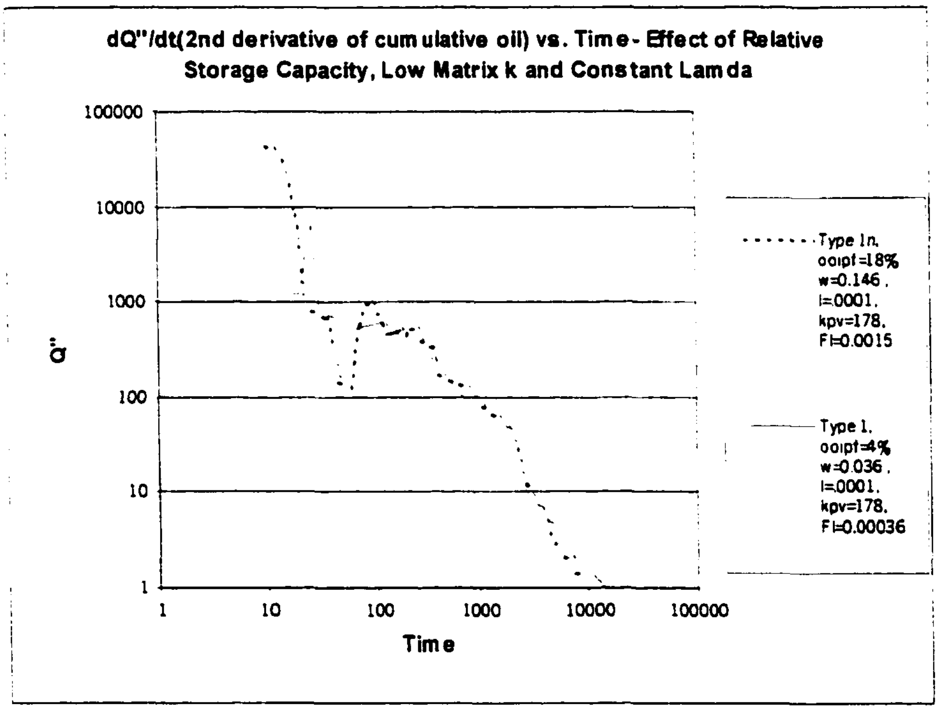

Figure 8.43 Q'' versus time- Effect of Changing the Relative Matrix to Fracture Storage

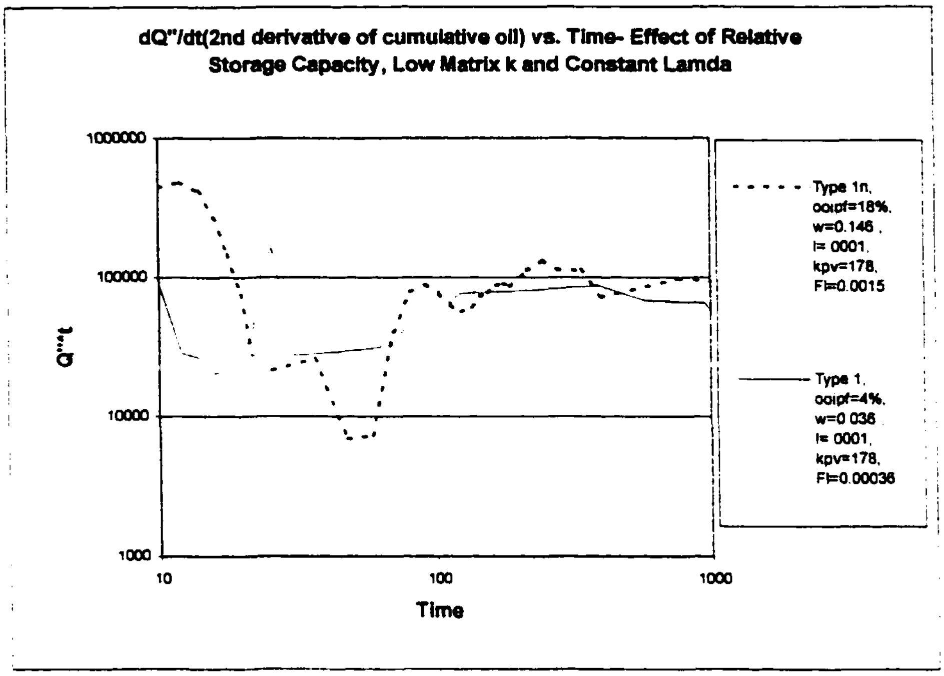

Figure 8.44 Q''*t versus time- Effect of Changing the Relative Matrix to Fracture Storage

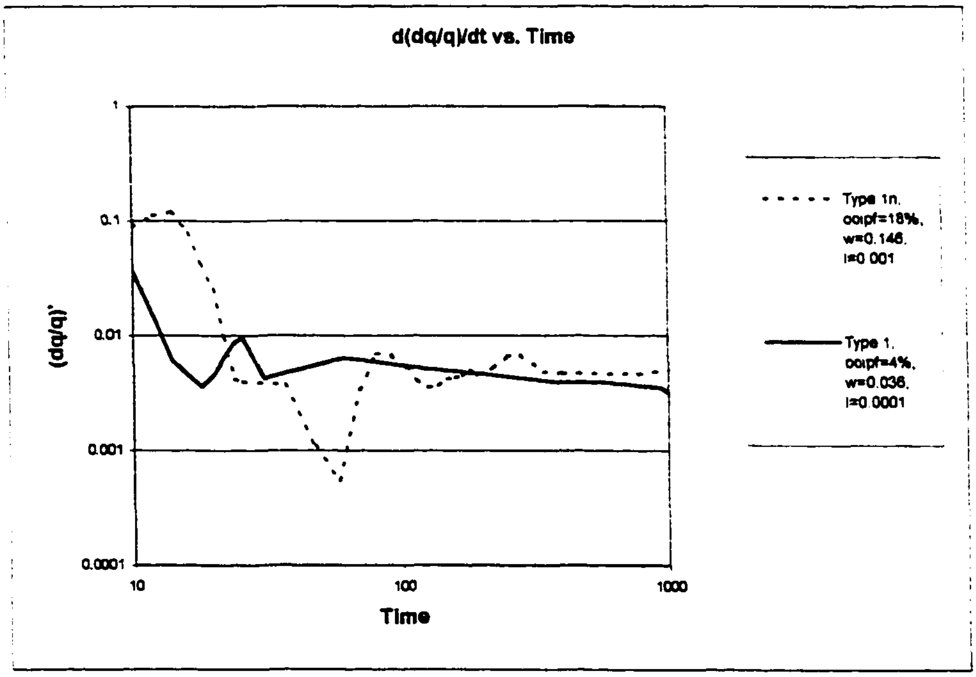

Figure 8.45 $(\Delta q/q)'$ versus time- Effect of Changing the Relative Matrix to Fracture Storage

Figure 8.46 shows the effect of the Type 4 case where the fracture has developed compartments or permeability barriers within the fracture. No effect was detected on the rate time plots of the previous sections. However there does appear to be an effect on the derivative curve. Note that the derivative contains many early spikes rather than one single spike. This may be useful in distinguishing this fracture type. The only difference in the two curves is the effect of placing several low permeability barriers in the fracture.

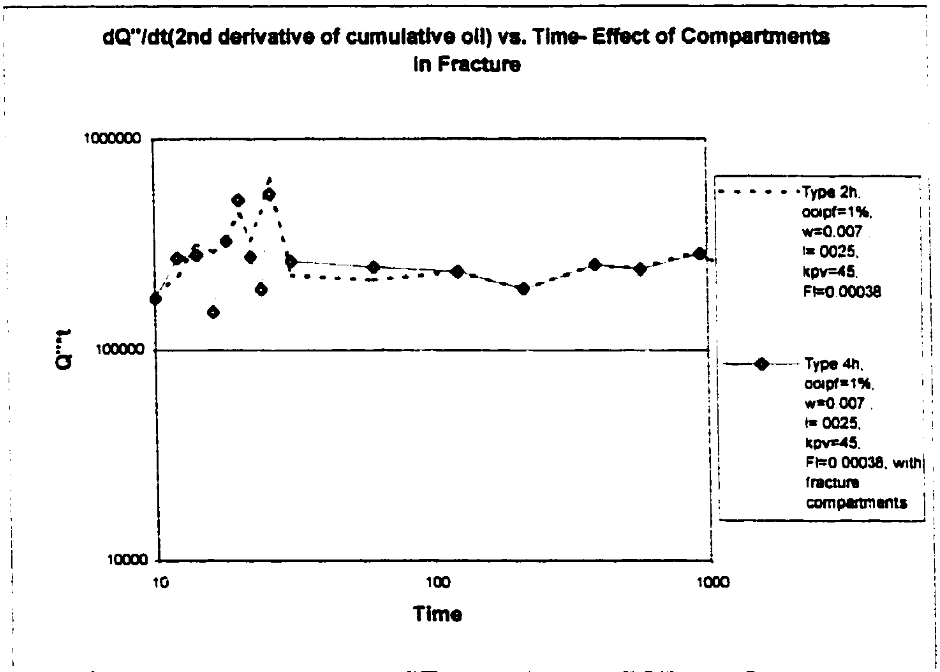

Figure 8.46 Effect of Permeability Compartments Inside Fracture-Q''*t Plot

In summary, the derivatives appear to have limited usefulness in quantitatively characterizing the fractures because of the early time data necessary to use the techniques and the erratic nature of the typical rate derivatives and even the cumulative production derivatives. As figure 8.47 indicates there are few distinguishing characteristics between the various fracture types except at very early times. However the depth and time delay to the minimums can be used in a qualitative sense to help characterize the fractures.

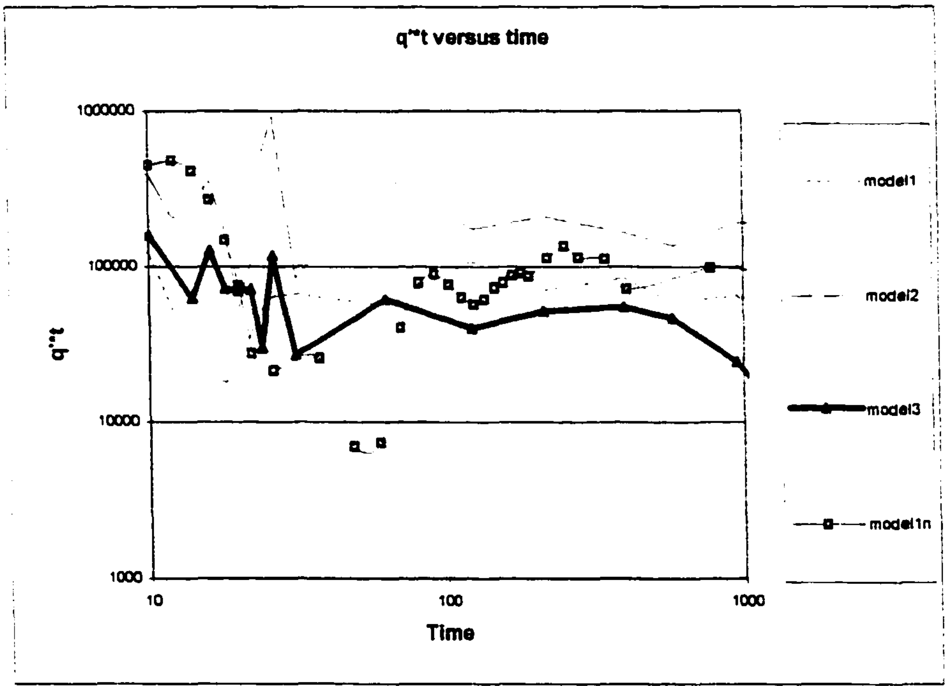

Figure 8.47 Comparison of Various Model Rate Derivatives – q'*t

If the engineer is fortunate enough to have flow pressures then those can be used to apply more typical pressure derivative analysis for quantitative analysis of the reservoir.

Well test analysis employs techniques where Δp and p'^*t are plotted so that the Δp vs. time, derivative early time unit slope, width, depth, and characteristic line intersections can yield values of fracture length, fracture permeability, well bore storage, as well as λ and ω.[49] Very early time data are also needed in that analysis. Since neither pressure nor early time data are normally available, a plot of similar nature encompassing Δq and the rate derivative might at least yield some qualitative characteristics of the respective fracture types. Figure 8.48 is the plot of Δq and q'^*t versus time for the models exhibiting the $1/\lambda' = 10{,}000$ permeability ratio case. Figure 8.49 is the plot of the normalized $\Delta q/q$ and q'^*t versus time.

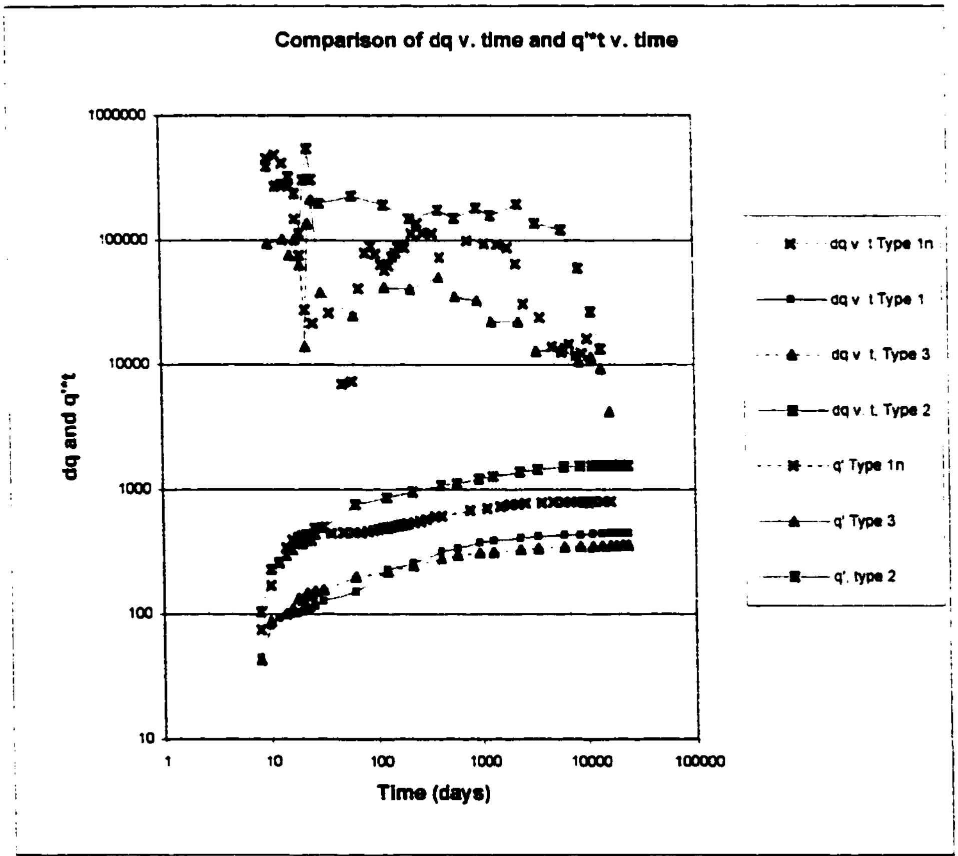

Figure 8.48 Plot of Δq and q'^*t vs time-Models Exhibiting 10,000 md Fracture Permeability

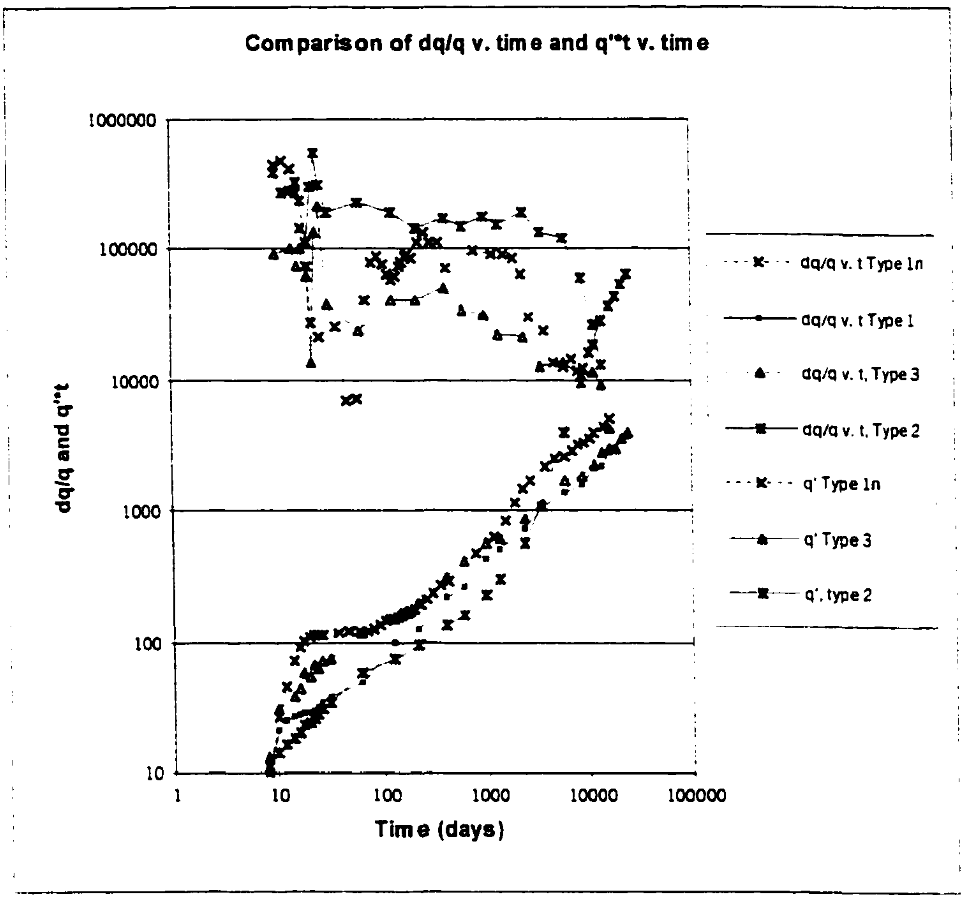

Figure 8.49 Plot of (Δq/q)*1000 and q'*t vs time-Models Exhibiting 10,000 md Fracture Permeability

An interesting feature of figure 8.49 is the way the Type 1n and Type 3 models converge at the end of the zero slope transition zone. The area between the two curves probably yields some measure of the fracture storage capacity since that is the only differing parameter. The derivative helps better locate the slope changes. Table 8.6 summarizes some of the distinguishing characteristics of the derivative plots.

Type	Characteristics
1	• Minimum is time delayed, longer duration and deeper than Types 2 and 3.
2	• Early short duration rate derivative minimum. • Shallow depth to minimum compared to Type1. • Onset of minimum is very early
3	• Early short duration rate derivative minimum. • Shallow depth to minimum compared to Type1 but similar to Type 2. • Onset of minimum is earliest and slightly before Type 2.
4	• Numerous early derivative spikes. Otherwise the same as Type 2.

Table 8.6 Predominant Characteristics of the Derivative Plots

8.9.5 Comparison of q vs. $(t_p + \Delta t)/ \Delta t$ Data between Fracture Types

Other distinguishing plots include the rate, q, and rate-change Δq versus $(t_p+\Delta t)/ \Delta t$ plots. This t_p is <u>not</u> the same as that used in constant rate well testing but is rather an averaging type of function where t_p is the cumulative oil produced up to a certain time step divided by the current instantaneous producing rate. This quantity is then added to the cumulative producing time and divided by cumulative time. The physical significance, if any, of this plot is not known but it does seem to distinguish the various fracture types. The following graphs (figures 8.50-8.51) show the comparison.

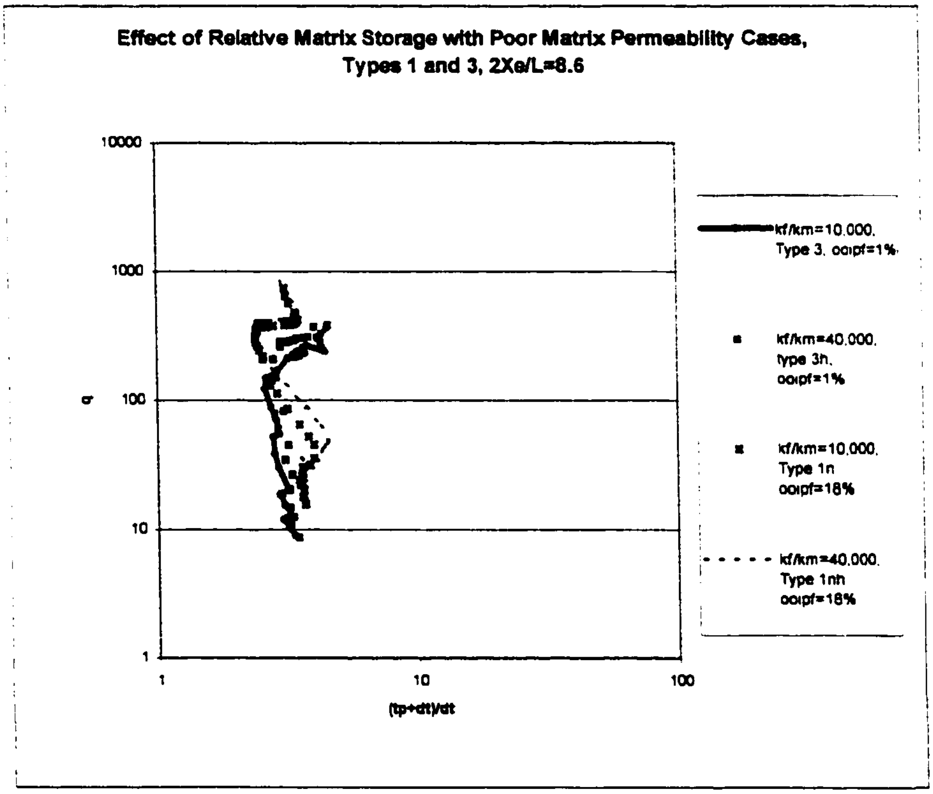

Figure 8.50 Effect of Increase in Relative Matrix Storage Volume-Poor Matrix Permeability

Again the complete tabular output is in listed in appendix G. Table 8.7 describes the distinguishing characteristics for each type.

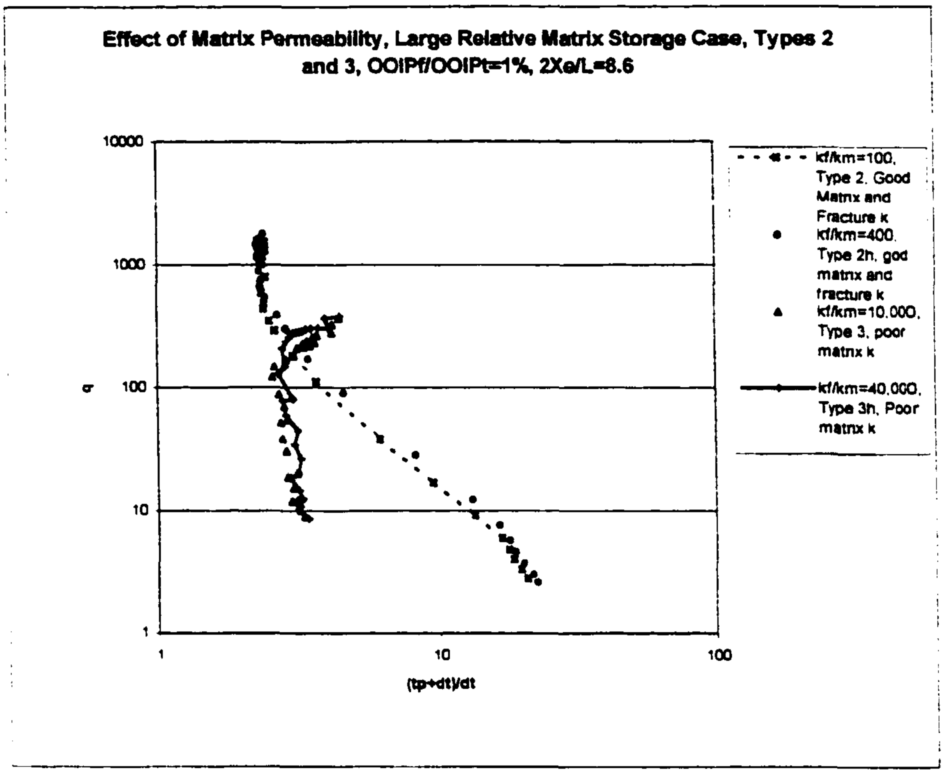

Figure 8.51 Effect of Change in Matrix Permeability in Case of Large Matrix Storage Capacity-q vs. $(t_p + \Delta t)/\Delta t$

The pressure and saturation surface diagrams in combination with the graphical and tabular data help illustrate what is happening throughout the reservoir model as a function of time and space at the inflection points. For instance, the tabular data help to identify the actual producing times for the $(t_p + \Delta t)/\Delta t$ minimums and reference to the pressure or saturation surface diagram helps interpret the physical significance of such points. This is also helpful in interpreting slope changes in the rate-time type plots. Compete surface diagrams of the pressure profiles are available from the author.

Model Type	Time Corresponding to $(t_p+\Delta t/\Delta t)$ Minimum	Description
Type 1	Sharp Day 147	Tight (less than one q cycle) double minimum, double maximum curvature exhibiting a "snake" like appearance
Type 2	Day 576	Near linear elongated (3 q cycles) "big-dipper" pattern.
Type 3	Day 1308	Tight (less than one q log cycle) single minimum curvature "toboggan" pattern.
Type 4	Day 576	Same as Type 2

Table 8.7 Comparisons of (tp+dt)/dt Plots

This type of plot shows one of the most distinguishing signatures of the various fracture types as can be seen on figures 8.50 and 8.51. Similarly the Δq versus $(t_p+\Delta t)/\Delta t$ plots (figure 8.52) show some distinctive patterns that can be used in characterization.

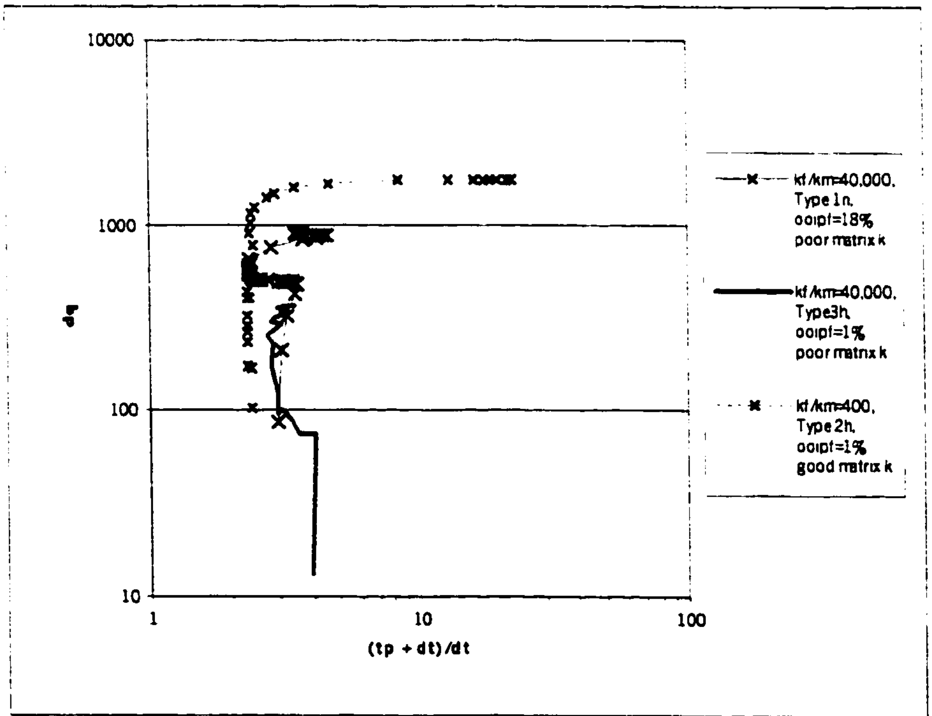

Figure 8.52 Δq versus $(t_p+\Delta t)/\Delta t$

8.10 Discussion of the Surface Diagram Interpretation

The average grid block and saturation surface diagrams are helpful in identifying to various changes in the graphs that have been discussed. A few things that are illustrated by the surface diagrams that might not be obvious from general graphing techniques presented (figures 8.53 and 8.54). First of all the reservoir is sensing the pressure drop and saturation change throughout the fracture by day 18. Also the average reservoir pressure and saturation by grid block shows a pattern that is more elongated with type 1 and 3 than for type 2 and 4 where the matrix permeability support is better. All external boundaries are beginning to sense the pressure drop by day 125 for types 1 and 3.

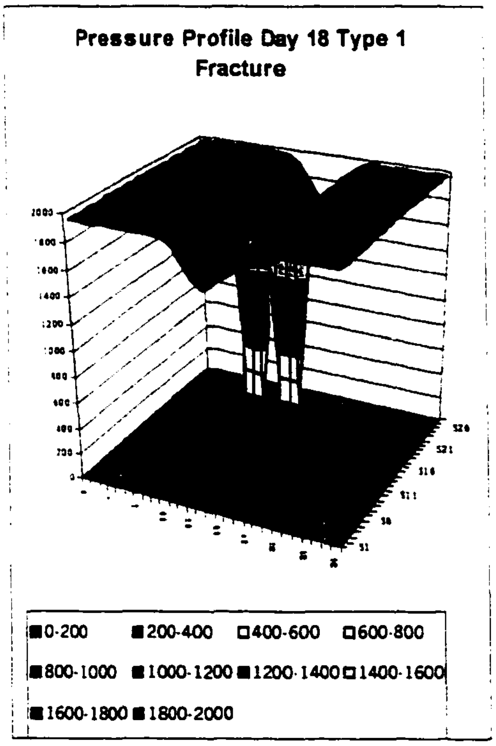

Figure 8.53 Surface Diagram of Average Pressure across Model Day 18

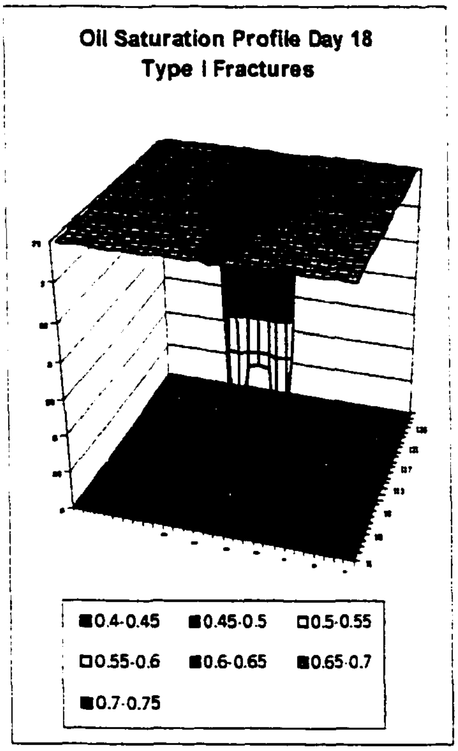

Figure 8.54 Surface Diagram of Oil Saturation across Model Day 18

8.11 Summary of Primary Diagnostic Indicators

The characteristic patterns of the various fracture types have been discussed in detail and summaries were presented in Tables 8.3- 8.7. Although many more types of graphs were generated, as indicated in Table 8.2, the more diagnostic plots included rate-time, cumulative-time, $\Delta q/q$ vs. q_{cum}/q, q vs. $(t_p + \Delta t)/\Delta t$ plots, and various derivatives such as rate-time, cumulative-time, $\Delta q/q$ –time, and Δq-time plots. Table 8.8 summarizes some of the more distinctive points from the previous tables as well as some additional information from plots listed in Table 8.2 that were not discussed or presented. For a "quick-look" classification, the $(t_p + \Delta t)/\Delta t$ plot gives a good indicator of general fracture type. More extensive experiments should be conducted to verify the general usefulness of this type of graph. Further experimentation with changes in well length down should also be pursued. Although initially it appeared that the Poston-Chen type curves could provide a framework for further rate decline analysis, after considerable work in duplicating and applying the curves it appeared that they were useful in only a limited qualitative sense. They do however allow better curve fitting of the late time "tail" section, which is characteristic of some dual porosity systems.

Type	Characteristics
1	• Modest initial rate but rate increasing and approaching type 2 as ω' increases. • Rapid initial decline followed by relatively long transition period. • Semi-log and log-log plots show four linear slope changes with steep early decline, a long zero slope transition, a long linear portion and a very late time low slope linear portion. The middle zero slope transition diminish as ω' drops. • Cumulative versus time log-log plot shows "s" curvature with ω' increasing and late time flattening but not as flat as type 2. • Early semi-linear log-log slope with zero slope transition to later semi-linear shapes again. • The early log-log linear period remains as as ω' shrinks until it disappears as the model approaches type 3. • Double porosity offset parallel unit slope behavior is <u>not present</u> on log-log dp/q vs. q_{cum}/q plot but unit slope late time is observed. If tangent drawn from beginning of transition, a double parallel slope can be created. • Cartesian 2-linear slopes, intersecting at increasing $\Delta q/q$ as ω' increases. • Approximate early half slope is observed on log-log plot. • Well-defined early time rate-time and rate-cumulative derivative minimum with "deep" minimum, time delayed and longer duration than type 2 and 3. • Poston-Chen fracture intensity γ term is low during middle-late time compared to type 2,3. • Poston-Chen storage compressibility term ω is fairly constant and higher than type 2 over time. • $(t_p+\Delta t/\Delta t)$ shows tight (less than on q cycle) double minimum, double maximum curvature exhibiting a "snake" like appearance. • Δq versus time log-log plot shows increased late time flattening from type 1 to type 3. • $\Delta q/q$ versus time, log-log plot early time deviation from linear seems to be an indicator of fracture storage volume.
2	• High initial rate • Very little early time character. Initial linear decline is short with very indistinct transition on log-log. Very modest early-middle slope change on semi-log plot only. • Low and prolonged subsequent decline rate compared to type1 with a rapid rate decline at late time beginning later than type 1 but slope is greater and eventually crosses type 1 decline. • The cumulative-time plot is linear on log-log with very late time slope change to near zero slopes. • Double porosity offset parallel unit slope behavior is <u>present</u> on log-log $\Delta q/q$ vs. q_{cum}/q plot but transition is not zero slope. • Cartesian early very short duration linear followed by prolonged linear slope. • Less well defined early time rate-time and rate-cumulative derivative with shallower minimum than type 1. • Near linear elongated (3 q cycles) "big-dipper" pattern on $(t_p+\Delta t/\Delta t)$. • Poston-Chen fracture intensity term γ is high and appears to be more constant than type 1except a very late time. • Poston-Chen storage compressibility term ω is generally lower than the type 1 or 3. • The very early time type curve match is more "fetkovich" type than Poston-Chen fracture type. • Δq versus time log-log plot shows increased late time flattening from type 1 to type 3.
3	• Low initial rates. • Similar early characteristics to type 2 but lower initial rates and longer period of middle linear behavior with slope similar to type 2 but at lower rates. • Very late time slope increase after the curve crosses the type 2 plot. • The cumulative-time plot shows and early time linear slope changing to a steeper prolonged linear shape on log-log until very late slope change. Curve converges to type 2 at late time. • Log-log early, very short duration semi-linear slope with change to prolonged linear middle-late time and shift to higher $\Delta q/q$ with decreasing λ'. • Double porosity offset parallel unit slope behavior is <u>not present</u> on log-log $\Delta p/q$ vs. q_{cum}/q plot and unit slope late time is not observed but slope is close to unity. • Cartesian 2-linear slopes, intersecting at increasing $\Delta q/q$ as ω' increases. • Poorly defined early time rate-time and rate-cumulative derivative minimum with erratic late time slope • Tight (less than one q log cycle) single minimum curvature "toboggan " pattern. • Poston-Chen fracture intensity term is high compared to type 1 and more consistent than type 2. • Δq versus time log-log plot shows increased late time flattening from type 1 to type 3.
4h	Same as Type 2 except derivative exhibits very "spiky" early nature

Table 8.8 Summary of Fracture Type Characteristics

Chapter 9

Summary and Conclusions

9.1 Summary

This research has resulted in several new contributions to the area of performance and decline curve analysis of both vertical and horizontal wells in anisotropic and fractured porous media. The important discoveries and future research ideas have been summarized by topic in the following sections.

Generalized Dimensionless Decline Curves

This area of research extends the previously developed dimensionless decline type curve concepts and techniques to more general cases of varying reservoir shapes and well locations. Fetkovich[3] had previously derived dimensionless decline curves for single-phase radial systems with centrally located wells. He then combined these relationships with the empirical hyperbolic pseudo-steady state relationships of Arps, to formulate a combined dimensionless decline curve as previously shown in Chapter 5. This research derives the dimensionless decline rate and time relationships for the cases of more general reservoir geometry and well location. These relationships are then used to construct new type curves for various reservoir shapes and well locations for single-phase cases. The data are then tabulated and combined with the Arps depletion stems to form a more generalized dimensionless decline curve system. This is the only publication that contains the complete set of tabulated dimensionless rate and time data for both infinite and bounded reservoir cases as well as the dimensionless decline rate and time data for the Fetkovich and new generalized type curves. The more generalized equations for calculation of transmissibility, permeability, reservoir area or radius and reserve estimation are also derived and presented for the first time in this research.

Chapter 5 figures show the effect of the more generalized dimensionless decline form as a shift in the single-phase pseudosteady state decline stem toward the origin for cases of increasing shape irregularity and wells closer to the boundaries. This effect manifests itself by an increasing deviation from the Fetkovich radial-well centered solution as the shape factor decreases. Without the use of such a system the user would choose the wrong depletion stem resulting in errors in the computation of reserves and permeability.

Solution Gas Reservoir Parameter Estimation

This research also introduces some novel approaches for estimating, from field production data, the simulation reservoir properties such as oil-water and gas-oil relative permeability, PVT properties, and capillary pressure in the absence of laboratory measurements. Appendix B and C contain the techniques and references for estimating all the reservoir properties needed for input to reservoir simulations. Of particular note are the techniques introduced to estimate flow rates in cases of two phase flow where a $k_{ro}/\mu_o B_o$ correlation as a function of grid block averaged pressure and saturation is used to modify the single phase flow equation in cases above and below the bubble point in solution gas reservoirs. Experimental results show that these methods yield good approximations to simulated results. Also of note are the techniques for estimating relative permeability in cases of solution gas reservoirs.

Flow Rate Correction Factors in Cases of Horizontal Permeability Anisotropy

Extensive simulation experimentation confirms that corrections must be applied to traditional horizontal well inflow performance relationships in cases of horizontal permeability anisotropy. This research demonstrates that unless the reservoir is extremely large in comparison to the length of the horizontal well, deviation from permeability isotropy in the principal x and y directions will yield results that deviate from those predicted by commonly accepted geometric mean averaging. All analytical flow equations incorporate the geometric mean horizontal permeability concept and thus predict that if the geometric mean is constant, the flow rate will remain constant. As demonstrated in Chapter 6. extensive experiments demonstrate however that as the contrast in x and y permeability increases, while maintaining a constant geometric mean horizontal permeability, the simulated horizontal flow rates deviate increasingly from one another. With vertical wells however, the simulated flow rate remains constant no matter what the contrast in x and y permeability as long as the geometric mean permeability is invariant.

Graphical relationships are presented showing the effect of permeability anisotropy on flow rate as a function of dimensionless well length, grid block size and well to boundary ratios. The experiments also indicate that the deviance from isotropic cases increases above the bubble point pressure. This is an important observation that should lead the engineer to exercise caution when interpreting rate data.

Decomposition of x and y Directional Permeability

Chapter 7 introduces new techniques to estimate directional permeability contrasts from the decline characteristics of both horizontal and vertical wells that compete for drainage area. The techniques are validated with simulation data and an example from actual field data is introduced. The research shows both experimentally and mathematically that departures of cumulative production data trends from the early time trends of competing wells will indicate relative contrasts in directional permeability that is approximately related to the ratio of the square root of k_y/k_x. Dual and multi-well experiments illustrate this phenomenon. The concept is also expanded to horizontal wells and vertically fractured reservoirs using a method that makes use of the horizontal well decline type curves applied to cumulative-time production data.

Horizontal Well Decline Curve Analysis and Effective Wellbore Radius

This research also showed that the traditional pseudosteady state horizontal well equations that utilize skin factors to account for well length, dimensionless well length and reservoir to well length can instead be expressed in terms of an effective wellbore radius. This concept not only allows the flow rate to be expressed in terms of one term that incorporates a number of skin factors but it is easier to use since the user does not need to use charts and graphs to determine skin factors. Therefore the generalized decline curves introduced in chapter 5 or Fetkovich radial type curves can be used directly with horizontal wells since the skin factors have been incorporated into the effective well bore radius. Theoretically then the horizontal and vertical well log-log plots should overlie one another in the pseudosteady state region just as Fetkovich theorized for vertically fractured wells. In other words they would have the same Arps "b" value but exhibit different r_e/r_w (r_{eD}, or the equivalent A/r^2_w) values and thus different q_{Dd} - t_{Dd} match values. An example was introduced for isotropic conditions where the effect of the horizontal well was to shift the match to a lower r_{eD} match value in the transient area thus resulting in the calculation of larger radius of drainage, r_e. It was found that this method did not work as well when the horizontal well length became very large in comparison to the reservoir size and the permeability field was anisotropic.

Fractured Reservoir Classifications

The simulated production rate decline characteristics of fractured reservoirs that are intersected by horizontal wells were studied through the use of simulation experiments. Tables and charts were produced that help classify each of four different fracture types through characteristic rate-cumulative-time decline patterns. Pressure data is purposely ignored in an effort to utilize only data that would typically be available to the practicing engineer. Although many types of graphs were generated, as indicated in Table 8.2, the more diagnostic plots included rate-time, cumulative-time, $\Delta q/q$ vs. q_{cum}/q, q vs. $(t_p + \Delta t)/ \Delta t$ plots, and various derivatives such as rate-time, cumulative-time, $\Delta q/q$ – time, and Δq-time plots. These diagrams illustrate an important discovery that the ratio of the $\Delta q/q$ for the beginning of the transition zone yields an indicator of the relative storage capacity of the fracture system. Thus if one has a reference well, all other field well decline curves can be used as an indicator of relative fracture storage capacity. For a "quick-look" classification, the $(t_p + \Delta t)/ \Delta t$ plot gives a good indicator of general fracture type. Poston and Chen's fractured reservoir type curves were plotted on the same graph as the Fetkovich type curves in an effort to classify fracture types. Though the Posten and Chen type curves proved less useful than anticipated, the difference in the Fetkovich and Posten and Chen curves did provide some useful information.

9.2 Conclusions

1. The generalized decline curves confirm that the Fetkovich dimensionless decline type curves change significantly as the reservoir geometry and well location become more irregular.
2. The more generalized equations for calculation of transmissibility, permeability, reservoir area or radius and reserve estimation are also derived and presented for

the first time in this research which will result in more accurate parameter estimation in cases of non radial geometry.

3. All the required simulation PVT and relative permeability data can be calculated from production field data by the methods of Appendix B and C.
4. A two-phase flow approximation utilizing grid block averaged pressure and saturation has been developed to use with calibrating and validating simulation output in cases of solution gas reservoirs.
5. Graphical relationships showing the effect of permeability anisotropy on flow rate as a function of dimensionless well length, grid block size and well to boundary ratios are presented that will help better predict the horizontal flow rate in bounded and horizontally anisotropic reservoirs.
6. It is shown that the generalized dimensionless decline curves can be used with horizontal wells by introducing the equivalent horizontal well radius as long as the horizontal well length is not too long compared to the reservoir dimensions.
7. The research shows both experimentally and mathematically that departures of cumulative production data trends from the early time trends of competing wells will indicate relative contrasts in directional permeability that is approximately related to the ratio of the square root of k_y/k_x.
8. Fracture types can be classified and sometimes quantified by the use of certain plotting techniques and deviation from Fetkovich dimensionless type curve behavior.

9.3 Recommendations for Future Research

Although many new concepts have been introduced, there are still several areas that merit further investigation. First, the generalized decline formulation has not been incorporated into the Arps empirical hyperbolic stems since there is no simple mathematical formulation for the cases in which additional reservoir energy, besides the rock and fluid compressibility, is present. Presumably however a downward shift to the origin similar to that of the mathematically derived single-phase solution would occur. This could be explored in future research by the use of simulation experimentation and examination of the depletion stems in the case of various solution gas and water drive conditions for non-radial and non well centered situations. The departure of the dimensionless decline curves from the exponential single-phase solution should give relative permeability information and should be explored further. Secondly, future research should be conducted with other simulators to test the observation that as the contrast in x and y permeability increases, while maintaining a constant geometric mean horizontal permeability, the simulated horizontal flow rates deviate increasingly from one another. This has been observed in an extensive set of experiments but should be further investigated with other simulators. Thirdly, further research is needed in using the departure in the Arps depletion stems from the single-phase solution as a tool of estimating relative permeability and drive energy. Fourthly more research is needed in applying the Posten Chen-Fetkovich type curves for characterization of reservoirs. There is also a need for more research in extracting more quantitative information from the $\Delta q/q$ vs. q_{cum}/q, q vs. $(t_p + \Delta t)/\Delta t$ plots.

NOMENCLATURE

A	Well drainage area in acres
A'	0.75 for circular drainage areas
	0.738 for rectangular areas
B_o	Oil formation volume factor
b	Decline exponent(dimensionless) b=0 for exponential, 0<b<1 for hyperbolic
B_o	Formation volume factor
c'	Shape factor conversion constant = 1.386
c_t	Total compressibility
c_f	Fracture compressibility
c_m	Matrix compressibility
D_i	Decline coefficient in days^{-1}
D_q	Near well turbulence factor
GOR	Gas to oil ratio
h	Reservoir thickness
IPR	Inflow performance relationship
k	Permeability, md
k_v	Vertical permeability
k_h	Horizontal permeability
k_{ro}	Relative Permeability to Oil
k_x	Permeability perpendicular to fractures(along well bore)
k_y	Permeability along fractures(perpendicular to wellbore)
L	Length of horizontal well
L_D	Dimensionless well length
p_D	Dimensionless pressure
p_i	Initial reservoir pressure
p_{wf}	Well flowing pressure
PSS	Pseudosteady state
q	Oil production rate STB/day
q_D	Dimensionless oil production rate
q_{dD}	Decline Dimensionless oil rate
q_i	Production rate at start of depletion STB/day
r_e	Well drainage radius in feet
r_{eh}	Horizontal well drainage radius
r_w	Well radius in feet
$r_{w'}$	Effective well radius
S	Saturation
s_m	Mechanical skin factor, dimensionless
s_f	$-\ln[L/(4r_w)]$= negative skin factor of an infinite conductivity fully penetrating fracture of length L.
$S_{CA,h}$	Shape related skin factor
t	Time in hours
t_D	Dimensionless time
t_{da}	Dimensionless time based on drainage area

V_p Pore Volume
x_e, y_e Half the drainage distance in the x and y direction
x_w, y_w, z_w Distance of horizontal well center from drainage area boundaries in feet
μ Viscosity
Δ Change
λ Fluid transfer coefficient
ρ_w Water density
ρ_o Oil density
ϕ Porosity
ϕ_m Matrix Porosity
ϕ_f Fracture Porosity
ϕ_e Effective porosity
γ Poston-Chen Fracture Intensity
ω Storage Compressibility
ω' Ratio of Matrix to Fracture Storage

REFERENCES

1. Arps, J. J.: "Analysis of Decline Curves", *Petroleum Technology* (September 1944), May 1944 TP 1758.

2. Arps, J.J. : "Analysis of Decline Curves," *Petroleum Transactions*, AIME, Vol. 160, 1945, 228-47.

3. Fetkovich, M..J.: "Decline Curve Analysis Using Type Curves," *JPT*, (June 1980), 1065-77.

4. Golan, M., Whitson, C.: *Well Performance*, 2nd edition, Prentice Hall, Englewood Cliffs, NJ, (1991). (121)

5. Chang, M.M. et al, "User's Guide and Documentation Manual For Boastvhs for the PC", U.S. Department of Energy, (January 1992).

6. Craft, B.C., Hawkins, M., Terry, R.E.: *Applied Petroleum Reservoir Engineering*, 2nd Edition, Prentice Hall, Englewood Cliffs, NJ (1991).

7. Evinger, H.H., Muskat, M.: "Calculation of Theoretical Productivity Factor" *JPT* (September 1941), SPE TP 1352.

8. Vogel, J.V.: "Inflow Performance Relationships for Solution Gas Drive Wells", *JPT*, (June 1968) 83-92.

9. Tracy, G.W.: "Simplified Form of the Material Balance Equation," *Trans. AIME* (1955), 204.243

10. Tarner, J.: "How Different Size Gas Caps and Pressure Maintenance Affect Amount of Recoverable Oil," *Oil Weekly* (June 12, 1944), 32.

11. Tsarevich, K.A.: "Calculation of the Flow Rates for the Center Well in a Circular Reservoir under Elastic Conditions," *Problems in Reservoir Hydrodynamics*, Part 1, Leningrad (1966) 9-34.

12. Cline, S.B.: "Reservoir Simulation as a Tool For Modifying Geological and Well Log Interpretations – A Fractured Pennsylvanian Sandstone Field Study", MS Thesis, University of Oklahoma, (1993).

13. Willhite, G. P: *Waterflooding*, SPE, Richardson, TX (1986)

14. Calhoun, J.C.: *Fundamentals of Reservoir Engineering*, University of Oklahoma Press, (1953)

15. Mattax, C.C., Dalton, D.L.: *Reservoir Simulation*, Monograph Series, SPE, Richardson, TX (1990) 13, 81.

16. Bass, D.M.: "Properties of Reservoir Rocks" *Petroleum Engineering Handbook*, SPE Richardson, TX (1992), 26-33.

17. Van Everdingen, A.F., Hurst, W.: "The Application of the Laplace Transformation to Flow Problems In Reservoirs", Petroleum Transactions, AIME, (December, 1949), TP 2732.

18. Van Everdingen, A.F.: "The Skin Effect and Its Influence on the Productive Capacity of a Well", Petroleum Transactions, AIME, Vol 198, (1953) TP 3581.

19. Stehfest, H.: "Algorithm 386: Numerical Inversion of Laplace Transforms," Communications of the ACM, 1970, 13, No. 1, 47-49.

20. Lee, J.: *Well Testing*, SPE Textbook Series, Dallas, TX (1982).

21. Matthews, C..S., Russell, D.G.: *Pressure Buildup and Flow Tests in Wells*, Monogrph Series, SPE Dallas TX (1967), 1.

22. Earlougher, R.C.: *Advances in Well Test Analysis*, SPE Mongraph Series, SPE, Dallas TX (1977).

23. Joshi, S.D.: *Horizontal Well Technology*, PennWell Publishing Co., Tulsa (1991) 34, 62-65, 292.

24. Tiab, D.: "Direct Type Curve Synthesis of Pressure Transient Tests", SPE 18992, SPE Rocky Mountain Symposium, Denver, CO (March 6-8, 1989).

25. Tiab, D., Puthigai, S.K.: "Pressure Derivative Type Curves for Vertically Fractured Wells", *SPE Formation Evaluation*, (March 1988), 156-158.

26. Tiab, D.: "Analysis of Pressure and Pressure Derivative without Type Curve Matching-Vertically Fractured Wells in Closed Systems, SPE 26138, SPE meeting Anchorage Alaska, (May 1993).

27. Mutalik, P.N., Godbole, S.P. and Joshi, S.D.: "Effect of Drainage Area Shapes on Horizontal Well Productivity", SPE paper, 18301, SPE Annual Conference Houston TX, (October 1988).

28. Kuchuk, F.J., Goode, P.A., et al: "Pressure Transient Analysis and Inflow Performance for Horizontal Wells", SPE paper 18300 Houston, TX (October 1988).

29. Babu, D.K., Odeh, A.S.: "Productivity of a Horizontal Well", SPE paper 18298, Houston, (October 1988) 373-382.

30. Joshi, S.D.: "Augmentation of Well Productivity With Slant and Horizontal Wells". *JPT*, (June 1988).

31. Slichter, C.S.: "Theoretical Investigation of the Motion of Ground Water," 19th annual report, U.S. Geological Survey (1897-1898) 301-84.

32. Joshi, S.D. "A Review of Horizontal Well and Drainhole Technology", Paper SPE 16868 SPE Annual Conference, Dallas 1987.

33. Joshi, S.D., Mutalik, P.N.: "Decline Curve Analysis Predicts Oil Recovery from Horizontal Wells". *Oil and Gas Journal.* (Sept. 7th, 1992).

34. Lock, C.D. and Sawyer, W.K. "Constant Pressure Injection in a Fractured Reservoir. Paper SPE 5594, SPE Annual Meeting Dallas, (Sept 28 1975).

35. Gringarten, A.: "Interpretation of Tests in Fissured and Multilayered Reservoirs With Double Porosity Behavior: Theory and Practice" , SPE 10044, *JPT* April, 1984 549-564.

36. Camacho, R.G., Raghavan, R.: "Some Theoretical Results Useful in Analyzing Well Performance Under Solution Gas Drive". *SPE Formation Evaluation*, (June 1991), 190-191.

37. Camacho, R: "Constant Pressure Production in Solution Gas Drive Reservoirs: Transient Flow". *SPE Formation Evaluation*, (June 1991), 199-208.

38. Fetkovich, M.J.: "The Isochronal Testing of Oil Wells", SPE 4529, SPE Preprint, 1973.

39. Ozkan, E., Raghavan, R.: "Horizontal Well Pressure Analysis", *SPE Formation Evaluation*, (December 1989), 567-575.

40. Russell, D.G.:"Transient Pressure Behavior in Vertically Fractured Reservoirs", *JPT*, Petroleum Transactions, October 1964, 1159-1170.

41. Mukherjee, H, Economides, M.:"A Parametric Comparison of Horizontal and Vertical Well Performance", SPE Formation Evaluation, (June 1991), 209-215.

42. Wiggins, M.: "Generalized Inflow Performance Relationships for Three Phase Flow", SPE Reservoir Engineering, (August 1994), 181-182.

43. Poston, S.W., Chen, H.Y.: "Fitting Type Curves to Austin Chalk Wells", SPE paper 21653, presented SPE meeting, Oklahoma City (April 7-9, 1991) 227-235.

44. Chen, H.Y., Raghavan, R.: "An Application of the Product Solution Principle for Instantaneous Source and Green's Functions", *SPE Formation Evaluation*, (June 1991).

45. Poston, S.W., Chen, H.Y, Raghavan, R: " Mathematical Development of Austin Chalk Type Curves" SPE 23527, SPE preprint 1991.

46. Cline, S.B., Tiab, D.: "Quantification of the Relative Importance of Fracture and Matrix Flow Units to Reservoir Storage Capacity and Transmissibility", SPE 27716. Permian Basin Oil and Gas Recovery Conference, (March 1994) 775-790.

47. Da Prat, G., Cinco,, L, Ramey, H.J.: :Decline Curve Analysis Using Type Curves for Two-Porosity Systems", SPE 9292, SPE Annual Meeting, Dallas TX (September 1980).

48. Agarwal, R.G., Gardner, D.C., et al: "Analyzing Well Production Data Using Combined-Type-Curve and Decline Curve Analysis Concepts", *SPE Reservoir Evaluation and Engineering*, (October 1999), 478-486.

49. Engler, T.W.: "Interpretation of Pressure Tests in Naturally Fractured Reservoirs by the Direct Synthesis Technique", PhD Dissertation, University of Oklahoma, (1995)

Appendix A

Derivation of the Saturated Analytic Approximation Equations and Relationship to IPR Relationships

As summarized in Chapter 3, for undersaturated conditions, the combined variation of viscosity and formation volume factor decreases approximately linearly with pressure as:

$$q = \frac{0.007078 k_h h}{\left(\ln \frac{r_e}{r_w} - 0.738\right)} \int \frac{dp}{\mu_o B_o} \qquad \text{...A1}$$

The integral is evaluated from P_{wf} to P_e (the pressure at the external boundary). Since $1/\mu_o B_o$ is a straight line, the area is a trapezoid, so the integral can be represented by:

$$\int \frac{dp}{\mu_o B_o} = \frac{P_e - P_{wf}}{(\mu_o B_o)_{\bar{P}_R}} \qquad \text{A2}$$

Where,

$$\frac{1}{(\mu_o B_o)_{\bar{P}_R}}$$

is the value at an average pressure $P_R = (P_e + P_{wf})/2$. The resulting inflow equation, at average reservoir pressure for pseudosteady state conditions becomes:

$$q = \frac{0.007078\, k_h h(\overline{P_R} - P_{wf})}{(\mu_o B_o)_{\bar{P}R}\left(\ln\frac{r_e}{r_w} - 0.738\right)} \qquad \text{...A3}$$

Golan[4](166) and Muskat et al [7] note that below the bubble point, (i.e. saturated reservoir conditions) equation 3 would become (neglecting skin and turbulence effects):

$$q = \frac{0.007078 h\, k_h}{\left(\ln\frac{r_e}{r_w} - 0.738\right)} \int \frac{k_{ro}}{\mu_o B_o} dp \qquad \text{...A4}$$

The integral is evaluated from P_{wf} to $P_{Rave.}$

Evinger and Muskat[7](1942) and later Vogel[8] et al (1976) noted that the pressure function could be accurately represented versus pressure by a straight line ranging from $k_{ro}/\mu_o B_o$ at reservoir pressure (up to the bubble point) to the origin. (Fig A-1) However, if this is the case, there is no need to evaluate the integral this way. If the straight-line assumption is valid, the problem reduces to expressing the area under the trapezoid situation as shown below.

$$f(p) = \int \frac{K_{ro}}{\mu_o B_o}$$

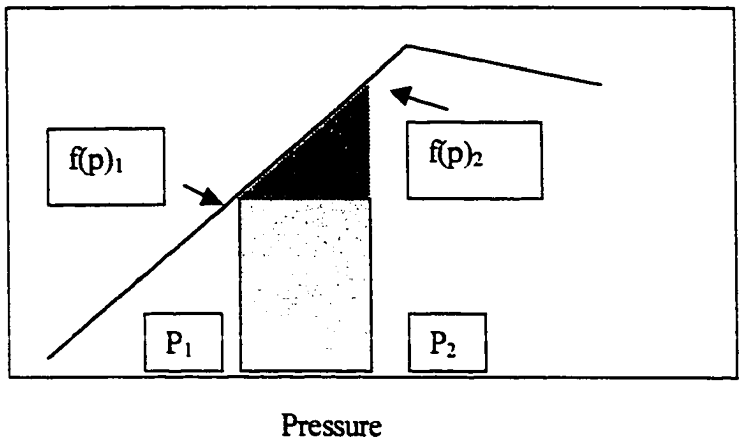

Figure A-1 Mobility Function versus Pressure

The area can be expressed as the sum of a triangle and rectangle:

$A = (\Delta P)f(p_1) + 0.5(\Delta P)(f(p_2)-f(p_1))$

$A = (\Delta P)f(p_1) + 0.5\,(\Delta P)f(p_2) - 0.5(\Delta P)f(p_1)$

$A = 0.5(\Delta P)\,(f(p_1) + f(p_2))$

$A = \Delta P\,(f(p_1) + f(p_2))/2$

Or substituting for the pressure functions:

$$Area = \Delta P\left(\frac{k_{ro}}{\mu_o B_o}\right)_{ave}$$

The value of ($k_{ro}/\mu_o B_o$) at any pressure can be obtained by calculating the slope of the line below the bubble point and multiplying by the pressure at the desired point.

Oil flow under saturated conditions can then be described above and below the bubble point if we substitute $(k_{ro}/\mu_o B_o)_{ave}$ evaluated at average reservoir pressure P_R-P_{wf} or simply P_R if flowing bottom hole pressure is low.

$$q = \frac{0.007078 h k_h}{\left(\ln \frac{r_e}{r_w} - 0.738\right)} \left[(\overline{P_R} - P_{wf}) \left[\frac{k_{ro}}{(\mu_o B_o)} \right] \right]_{PaveS_o} \quad \text{...A5}$$

or more generally:

$$q_o = J(P_R - P_{wf})$$

Where J incorporates all of the terms in the above equation except the pressure differential so that:

$$J = \frac{0.007078 h k_h}{\left(\ln \frac{r_e}{r_w} - 0.738\right)} \left[\frac{k_{ro}}{(\mu_o B_o)_{ave}} \right] \quad \text{A6}$$

Therefore since we know the mobility as a function of pressure and saturation that is input to simulators we can use the same function to analytically check against simulation output. Actually it seems to me that K_{ro} should be computed at the average oil saturation at any given average pressure situation rather than at the average pressure as noted in Muskat'. Muskat never mentions this in his paper but perhaps the integral of K_{ro} should not be from P_{wf} to P_e but from S_{oi} to S_{oe} since K_{ro} is only indirectly related to pressure through the saturation function.

Now the above expression can be represented by the equivalent IPR depletion expression in terms of a backpressure constant C as follows:

Equation 4 can be written as:

$$q_o = C' \int_{P_{wf}}^{P_R} \frac{k_{ro}}{\mu_o B_o} dp \qquad \textbf{A7}$$

Or as previously shown:

$$q_o = C' \text{ Area Under Curve}$$

Where C' is given as:

$$C' = \frac{0.007078 h k_h}{\left(\ln \frac{r_e}{r_w} - 0.738\right)} \qquad \textbf{A8}$$

Letting $(k_{ro}/\mu_o B_o)$ be denoted by M_{PR} and M_{Pwf} for the respective pressures, the area under the curve is represented by the relationship:

$$Area = \frac{1}{2}\left[\left(M_{PR} + \frac{M_{PR}}{P_R} P_{wf}\right)\left(P_R - P_{wf}\right)\right] \qquad \textbf{A8}$$

$$Area = \frac{1}{2}\left[\left(\frac{M_{PR}}{P_R} P_R + \frac{M_{PR} P_{wf} P_R}{P_R^2}\right)\left(P_R - P_{wf}\right)\right] \qquad \textbf{A9}$$

$$Area = \frac{M_{PR}}{2P_R}\left(P_R + P_{wf}\right)\left(P_R - P_{wf}\right) \qquad \textbf{A10}$$

Substituting this expression into the rate equation yields:

$$q_o = \frac{C^* M_{PR}}{2P_R}\left(P_R^2 - P_{wf}^2\right) \qquad \textbf{A11}$$

Where C^{*} was previously defined. Combining the first terms and calling them C results in the equivalent to the pressure squared IPR relation:

$$q_o = C\left(P_R^2 - P_{wf}^2\right) \qquad \textbf{A12}$$

Where C is defined below the bubble point as:

$$C = \frac{kh}{141.2\mu_o B_o}\frac{1}{2P_R}M_{PR} = \frac{kh}{141.2\mu_o B_o}\frac{1}{2P_R}\int_{P_{wf}}^{P_R}\frac{k_{ro}}{\mu_o B_o}dp \qquad \textbf{A12}$$

The addition of a turbulence term Dq_o .the denominator of C and substitution into equation X. solving for q yields a back pressure equation with exponent n.

$$q_o = C\left(P_R^2 - P_{wf}^2\right)^n \qquad \textbf{A13}$$

Where C is the backpressure constant approximated by:

$$C = \left[\frac{kh}{141.2}\frac{1}{2P_R}\left(\frac{k_{ro}}{\mu_o B_o}\right)\right]^n \qquad \textbf{A14}$$

For pseudosteady state, excluding damage and turbulence factors, the backpressure constant C varies only because of depletion and the resulting change in average $(k_{ro}/\mu_o B_o)_{ave}$. And as shown previously, these properties are evaluated at the average reservoir pressure. Plotting the well test data as q_o vs. ΔP^2 on log–log graphs determines the coefficient and the exponent of the backpressure equation.

This relationship can be useful in understanding the decline curves and relating Arps empirical decline curves with the exponential decline shown by Fetkovich. For instance the variation in the decline from the Fetkovich exponential decline is expressed by a "b" factor. The primary deviation is a result of the variation of $k_{ro}/\mu_o B_o$ with declining reservoir pressure under pseudosteady state conditions.

It is shown in chapter 4 that the rate is expressed by Arps[1] as:

$$q = \frac{q_i}{(1 + bD_i t)^{\frac{1}{b}}} \qquad \textbf{A15}$$

or defined in dimensionless decline parameters:

$$q_{dD} = \frac{q_t}{q_i} = [1 + bDt_{dD}]^{\frac{1}{b}} \qquad \textbf{A16}$$

The decline D is assumed as unity in the literature. Exponential decline where b=0 is the equivalent of the Fetkovich[38,42] derivation is expressed in Arp's symbology as:

$$q_{dD} = e^{-t_{dD}} \qquad \textbf{A17}$$

Now applying the definition of t_{dD}:

$$q_{dD} = \left[1 + b \frac{0.0063kt}{\frac{1}{2}\phi \mu c r_w^2 \left(\left(\frac{r_e}{r_w} \right)^2 - 1 \right) \left(\ln \frac{r_e}{r_w} - \frac{1}{2} \right)} \right]^{\frac{1}{b}} \qquad \textbf{A18}$$

Appendix C will illustrate methods of using these IPR relationships in conjunction with the type curve matching to extract relative permeability data from the rate-time production data.

APPENDIX B

Program For Estimating Reservoir PVT Data

The following program, OILPROP, was written in Pascal 3.0. All the user must know is the following information: Reservoir temperature in degrees F, oil gravity [deg API], gas gravity [air=1.0], initial reservoir pressure [psia], and **either** the bubble point pressure [psia] or the initial solution gas-oil ratio (RSOI[scf/stb]). The program will then determine the complete suite of PVT oil and gas properties: solution gas to oil ratio (RSO[scf/stb]), oil formation volume factor (Bo[bbl/stb]), and oil phase viscosity for oil (m_o[cp]). If the pressure is below the bubble point then the program will also compute the following gas properties: the gas deviation factor Z, the gas formation volume factor (Bg[bbl/scf]) and the gas phase viscosity (m_g[cp]). The user may specify the beginning and ending pressures to evaluate and any number of equally spaced pressures in between.

This program utilizes equations for oil and gas properties that can be found in Craft, Hawkins and Terry [6].

The program first prompts the user for the input data. The program then proceeds according to the following pseudo-code flow chart:

```
WHILE PRESSURE >= MINIMUM PRESSURE SPECIFIED DO
          BEGIN
     IF BUBBLE POINT PRESSURE IS GIVEN THEN
          CALCULATE RSO
     ELSE
               USE RSOI TO CALCULATE BUBBLE POINT PRESSURE
          CALCULATE RSO
               IF PRESSURE > BUBBLE POINT PRESSURE THEN
                         BEGIN
                              RSO=RSOB
                              CALC. OIL VIS. ABOVE BUBBLE
                         END
                    IF PRESSURE<=BUBBLE POINT THEN
                         BEGIN
                              CALC. PSEUDO CRITICAL PROPS
                              CALC. THE Z FACTOR
                              CALC. GAS FORM. VOLUME FACTOR
                              CALC. THE GAS VISCOSITY
                              CALC. THE OIL VISCOSITY
                         END
                    CALCULATE THE OIL FORMATION VOLUME
                    FACTOR
                    PRINT RESULTS
          REPEAT PROCESS UNTIL ALL PRESSURE POINTS ARE
       EVALUATED
     END
```

RSO is calculated by the following equation, 1.26, from Craft Hawkins and Terry [6].

$$R_{so} = \gamma_g \left(\frac{P}{18(10)^{YG}} \right)^{1.204} (scf / stb) \qquad \textbf{B1}$$

γ_g = gas gravity
$YG = 0.0091\,T - 0.0125\,\rho_{0API}$
ρ_0 = API oil gravity
T = degrees Fahrenheit
P = Pressure psia

Applicable Range

$130 < P_{bubble}$ (psia) < 7000
$100 < T°\,F < 258$
$20 <$ GOR (scf/stb) < 1425
$16.5 < \rho_0$ °API < 63.8
$0.59 < \gamma_g < 0.95$
$1.024 <$ Bo (bbl/stb) < 2.05

When RSOI is known but the bubble point pressure is unknown then the above equation is solved for the bubble point pressure.

The following equations are used to determine the oil viscosity below and above the bubble point pressure respectively.

1) $P <= P_b$

$$A \mu_{od}^{B} (cp) \qquad \textbf{B2}$$

$$A = 10.75 (R_{so} + 100)^{-0.515} \qquad \textbf{B3}$$

$$B = 5.44 (R_{so} + 150)^{-0.338} \qquad \textbf{B4}$$

$$\log\left(\log(\mu_{od} + 1)\right) = 1.8653 - 0.02508\, \rho_{oAPI} - 0.5644 \log(T) \qquad \textbf{B5}$$

Applicable Range

$59 < T\,°F < 176$
$-58 < T_{pour}°\,F < 59$
$5.0 < \rho_0\,API < 58$

2) $P > P_b$

$$\mu_o = \mu_{ob} \left(\frac{P}{P_b} \right)^{m} (cp) \qquad \textbf{B6}$$

$$m=2.6P^{(1.187)}\exp(-11.513-8.98(10^{-6})P) \quad \textbf{B7}$$

$\mu_{ob} = \mu_o$ at P_{bubble}

Applicable Range

$126 < P$ psig < 9500
$0.117 < \mu_o < 148$
$9.3 <$ GOR scf/stb < 2199
$15.3 < \rho_0$ API < 59.5
$0.511 < \gamma_g < 1.351$

The Z factor is calculated using the Abou Kassem equation, (equation 1.10 Craft and Hawkins [6]). My program uses the Newton-Raphson method to find the root of that equation which provides the Z value. This is an iterative process that also requires the derivative of the equation. The user can specify the iteration stopping criteria and the maximum number of iterations. The explanation of the terms in the below listed Abou Kassem equation can be found in the program listing.

$$Z = 1 + C_1(T_{pr})\,\rho_r + C_2(T_{pr})\,\rho_r^2 - C_3(T_{pr})\,\rho_r^5 + C_4(\rho_r, T_{pr}) \quad \textbf{B8}$$

Applicable range

$0.2 < P_{pr} < 30$

$1.0 < T_{pr} < 3.0$ and $P_{pr} < 1.0$ with $0.7 < T_{pr} < 1.0$

poor results if $T_{pr} = 1.0$ and $P_{pr} > 1.0$

Once Z is calculated, the gas formation volume factor is found from the following equation:

$$B_g = 0.00504\left(\frac{ZT}{P}\right)(bbls\,/\,scf) \qquad \textbf{B9}$$

Z=gas deviation factor

T=°Rankine

P=pressure psia

The gas viscosity is determined from the following relation:

$$\mu_g = (10^{-4})K\exp(X\,\rho^{Y}) \qquad \textbf{B10}$$

$$\rho = 1.4935(10)^{-3}\frac{PMW}{ZT} \qquad \textbf{B11}$$

$$K = \frac{9.4 + 0.02MW(T)^{1.5}}{209 + 19MW + T} \qquad \textbf{B12}$$

$$X = 3.5 + \frac{986}{T} + 0.01MW \qquad \textbf{B13}$$

Y=2.4-0.2X

P=Pressure

T=Temperature °R

MW=molecular weight

Applicable Range

$100 < P \text{ psia} < 5000$
$100 < T° F < 340$
$0.9 < CO_2 \%$ by mole < 3.2

Z must already be corrected for contaminants

The oil formation volume factor is determined from the following equations:

1)**P<Pb**

$$B_o = 0.972 + 0.000147(F)^{1.175} \qquad \textbf{B14}$$

$$F = R_{so}\left(\frac{\mu_g}{\mu_o}\right)^{0.5} + 1.25T \qquad \textbf{B15}$$

$$\gamma_o = \frac{141.5}{131.5 + \rho_{oAPI}} \qquad \textbf{B16}$$

2)P>Pb

$$B_o = B_{ob} \exp\left(C_o (P_b - P) \right) \qquad \textbf{B17}$$

B_{ob}= B_o at P_{bubble}

$$C_o = \frac{5 R_{sob} + 17.2T - 1180 \gamma_g + 12.61 \rho_{oAPI} - 1433}{P(10^5)} \qquad \textbf{B18}$$

Applicable Range

$126 < P$ psig < 9500
$1.006 < Bo$ bbl/stb < 2.226
$9.3 < GOR$ scf/stb < 2199
$15.3 < \rho_{OAPI} < 59.5$
$0.511 < \gamma_g < 1.351$

The program was tested using the data provided in problem 1.20 in Craft, Hawkins and Terry [6].

That input data was as follows:

Bubble Point Pressure = 2800

Gas Gravity = 0.8

Oil Gravity = 30 API

Temperature = 165° F

The test was run assuming and initial reservoir pressure of 3200 psia and the minimum pressure of interest was 800 psia. The results are included in this report. The program was also tested by substituting the initial solution gas to oil ratio for the bubble point pressure. Excellent agreement was obtained.

The program is simple to use and offers a quick method to accurately calculate reservoir oil and gas properties at a wide variety of application ranges of pressure and temperature. These results may aid the user in understanding and evaluating various reservoir characteristics.

THE INPUT DATA IS LISTED BELOW

THE FIRST Z ESTIMATE IS:	1.0000
THE % STOPPING CRITERIA IS:	0.0100
THE MAX. # ITERATIONS FOR Z IS:	50
THE RESERVOIR PRESSURE (psia)IS	3200.00
THE RESERVOIR TEMPERATURE IS (DEG F)	165.00
THE GAS GRAVITY IS	0.8000
THE API OIL GRAVITY IS	30.0000
THE BUBBLE POINT PRESSURE(psia) IS	2800.00

IF ZEROS APPEAR IN THE FOLLOWING TABLE IT MEANS
***THAT THE PARAMETERS DO NOT APPLY AT THOSE ***
***PRESSURES AND TEMPERATURES ***

PRESSURE psia	Z	GAS VISCOCITY cp	BG bbl/scf	BO bbl/stb	RSO scf/stb	OIL VIS cp
3200.00	0.0000	0.0000	0.0000	1.3597	649.8896	0.8413
3080.00	0.0000	0.0000	0.0000	1.3614	649.8896	0.8315
2960.00	0.0000	0.0000	0.0000	1.3633	649.8896	0.8221
2840.00	0.0000	0.0000	0.0000	1.3653	649.8896	0.8131
2720.00	0.8083	0.0212	0.0009	1.3541	627.5990	0.8294
2600.00	0.8050	0.0206	0.0010	1.3365	594.4142	0.8602
2480.00	0.8028	0.0199	0.0010	1.3192	561.5405	0.8935
2360.00	0.8016	0.0193	0.0011	1.3022	528.9899	0.9297
2240.00	0.8016	0.0187	0.0011	1.2855	496.7752	0.9692
2120.00	0.8027	0.0181	0.0012	1.2691	464.9108	1.0123
2000.00	0.8052	0.0176	0.0013	1.2530	433.4125	1.0597
1880.00	0.8090	0.0170	0.0014	1.2372	402.2975	1.1120
1760.00	0.8141	0.0165	0.0015	1.2218	371.5853	1.1700
1640.00	0.8206	0.0160	0.0016	1.2068	341.2976	1.2345
1520.00	0.8284	0.0155	0.0017	1.1921	311.4591	1.3068
1400.00	0.8374	0.0151	0.0019	1.1777	282.0976	1.3884
1280.00	0.8475	0.0147	0.0021	1.1638	253.2457	1.4809
1160.00	0.8587	0.0143	0.0023	1.1503	224.9410	1.5866
1040.00	0.8709	0.0139	0.0026	1.1372	197.2284	1.7085
920.00	0.8839	0.0136	0.0030	1.1245	170.1617	1.8502
800.00	0.8976	0.0133	0.0035	1.1124	143.8075	2.0165

Table B-1 Sample PVT Program Output

```
PROGRAM OILPROP(INPUT,OUTPUT);

{$I c:\pas\scott\INFO.TXT}

VAR
CH,CHO:CHAR;
DEVICE:TEXT;
TRES,GASGRAV,PRESS,PBUB,PMIN,PMAX,ROOT,
PPR,TPR,PPC,TPC,STOPER,C1,C2,C3,C4,
BGI,RHO,MG,OILGRAV,BOB,BO,RSO,RSOI,RSOB,APIGRAV,
Z,N,OILVISC,MEWLIVE,MEWABOVE,MEWOBUB:REAL;
ITERMAX:INTEGER;
(*ROOT is the first root estimate, STOPER is the iteration stopping
criteria expressed as % error, ITERMAX is the max # of iterations*)
(*------------------------------------------------------*)
{$I c:\pas\scott\WHICHONE.PAS}

(*-----------------------------------------------------*)

 PROCEDURE READATA;
 (*This procedure prompts the user for the input data*)
 BEGIN
   WRITELN('INPUT RESERVOIR TEMP IN DEGREES F:');
   READLN(TRES);
   WRITELN('INPUT GAS GRAVITY:');
   READLN(GASGRAV);
   WRITELN('RESERVOIR PRESSURE:');
   READLN(PRESS);
   WRITELN('You may enter either Bubble Point pressure or solution gas ratio');
   WRITELN('If you wish to enter bubble point pressure then type Y');
   WRITELN('If not type N but you will then have to enter RSOI in the next step');
  READLN(CHO);
  IF (CHO='y') OR (CHO= 'Y') THEN
  BEGIN
     WRITELN('BUBBLE POINT PRESSURE=');
     READLN(PBUB);
  END
    ELSE
  BEGIN
     WRITELN('RSOI=');
     READLN(RSOI);
  END;


     WRITELN('INPUT OILGRAVITY IN API UNITS');
```

```
    READLN(APIGRAV);
    WRITELN('MAX PRESSURE TO EVALUATE');
    READLN(PMAX);
    WRITELN('MIN PRESSURE TO EVALUATE');
    READLN(PMIN);
    WRITELN('NUMBER OF POINTS TO EVALUATE ');
    READLN(N);
END;
(*-----------------------------------------------*)
PROCEDURE READATAZ;
(*this procedure reads in the Z factor estimate,stopper and max iterations*)
BEGIN
    WRITELN('SPECIFY THE INITIAL Z VALUE GUESS:');
    READLN(ROOT);
    WRITELN('SPECIFY THE % STOPPING CRITERIA FOR NEWTON
RAPHSON:');
    READLN(STOPER);
    WRITELN('SPECIFY THE MAXIMUM NUMBER OF ITERATIONS:');
    READLN(ITERMAX);
END;(*of readata*)

(*-----------------------------------------------*)

PROCEDURE WRITEDATA:
(*this procedure writes the input data to the printer or screen*)
BEGIN
    WRITELN(DEVICE,'THE INPUT DATA IS LISTED BELOW');
    WRITELN(DEVICE);
    WRITELN(DEVICE,'THE FIRST Z ESTIMATE IS:          ',ROOT:10:4);
    WRITELN(DEVICE,'THE % STOPPING CRITERIA IS:       ',STOPER:10:4);
    WRITELN(DEVICE,'THE MAX. # ITERATIONS FOR Z IS:   ',ITERMAX:10);
    WRITELN(DEVICE,'THE RESERVOIR PRESSURE (psia)IS   ',PRESS:10:2);
    WRITELN(DEVICE,'THE RESERVOIR TEMPERATURE IS (DEG F)',TRES:10:2);
    WRITELN(DEVICE,'THE GAS GRAVITY IS                ',GASGRAV:10:4);
    WRITELN(DEVICE,'THE API OIL GRAVITY IS            ',APIGRAV:10:4);
    IF (CHO='Y') OR (CHO='y') THEN
    WRITELN(DEVICE,'THE BUBBLE POINT PRESSURE(psia) IS ',PBUB:10:2)
    ELSE
    WRITELN(DEVICE,'SOLUTION GAS RATIO (SCF/STB)RSOI IS ',RSOI:10:4);
    WRITELN(DEVICE);
    WRITELN(DEVICE,'***IF ZEROS APPEAR IN THE FOLLOWING TABLE IT
MEANS***');

    WRITELN(DEVICE,'***THAT THE PARAMETERS DO NOT APPLY AT THOSE
***');
```

```
  WRITELN(DEVICE,'***PRESSURES AND TEMPERATURES                    ***');
  WRITELN(DEVICE);
END;(*of writedata*)

(*-----------------------------------------------*)
FUNCTION DR(TRY:REAL):REAL;
(*This function evaluates Rho sub r in the Abou- Kassem equation*)
BEGIN
  DR:=0.27*PPR/(TRY*TPR);
END;
(*-----------------------------------------------*)

PROCEDURE PSEUDOCRITICAL;
(*This procedure calculates the pseudocritical values for use in
 the calculation of the Z factor*)
BEGIN
  PPC:=756.8-131.0*GASGRAV-3.6*GASGRAV*GASGRAV;
  TPC:=169.2+349.5*GASGRAV-74*GASGRAV*GASGRAV;
  PPR:=PRESS/PPC;
  TPR:=(460+TRES)/TPC;
END;
(*-----------------------------------------------*)
PROCEDURE CONSTANTS;
(* The procedure calculates some of the terms that are used in the
Abou-Kassem equation evaluated in function funcvalue*)
BEGIN
  C1:=0.3265-1.07/TPR-(0.5339/(EXP(3*LN(TPR))))+
  (0.01569/(EXP(4*LN(TPR))))-
  (0.05165/(EXP(5*LN(TPR))));
  C2:=0.5475-0.7361/TPR+(0.1844/(TPR*TPR));
  C3:=0.1056*(-0.7361/TPR+0.1844/(TPR*TPR));
END;
(*-----------------------------------------------*)
FUNCTION FUNCVALUE(TRY:REAL):REAL;
(*this function is specified by the user. We will find the root
of this function later in the newtrap procedure. TRY is the root
estimate input from the newtrap procedure*)
BEGIN


FUNCVALUE:=TRY-(1+C1*DR(TRY)+C2*DR(TRY)*DR(TRY)-
C3*EXP(5*LN(DR(TRY)))+
  (0.6134*(1+0.721*DR(TRY)*DR(TRY))*((DR(TRY)*DR(TRY))/
  (EXP(3*LN(TPR))))*EXP(-0.721*DR(TRY)*DR(TRY))));
END;(*of function*)
```

```
(*-------------------------------------------------*)

FUNCTION DERIV(TD:REAL):REAL;
(*this is the derivative of the above function. The derivative is
used in the calculation of the root. td is the root estimate
input from procedure newtrap*)
BEGIN
   DERIV:=1+(C1*DR(TD))/TD+(2*C2*DR(TD)*DR(TD))/TD-
   (5*C3*EXP(5*LN(DR(TD))))/TD+
   ((2*0.6234*DR(TD)*DR(TD))/
   (TD*EXP(3*LN(TPR))))*
   (1+0.721*DR(TD)*DR(TD)-EXP(2*LN((0.721*DR(TD)*DR(TD)))))*
   EXP(-0.721*DR(TD)*DR(TD));

END;(*of function*)

(*-------------------------------------------------*)
PROCEDURE GASFVF;
(*This procedure claculates the gas formation volume factor in BBl/SCF*)
BEGIN
  BGI:=(0.00504*Z*(TRES+460))/PRESS;
END;
(*-------------------------------------------------------*)

PROCEDURE MEWGAS:
(*This procedure calculates the gas viscocity in centipoise*)
var
MW,RHO,K,X,Y:REAL;
BEGIN
  MW:=28.97*GASGRAV;
  RHO:=1.4935*0.001*((PRESS*28.97*GASGRAV)/(Z*(460+TRES)));
  K:=(EXP(1.5*(LN((460+TRES))))*(9.4+0.02*MW))/(209+19*MW+(460+TRES));
  X:=3.5+(986/(460+TRES))+0.01*MW;
  Y:=2.4-0.2*X;
  MG:=0.0001*K*EXP(X*EXP(Y*LN(RHO)));
END;
(*-----------------------------------------------------*)
PROCEDURE OILFVF:
(*This procedure calculates the oil formation volume factor Bo in BBL/STB*)
VAR
  CO,F:REAL;
BEGIN
   OILGRAV:=141.5/(131.5+APIGRAV);
   F:=RSO*EXP(0.5*LN(GASGRAV/OILGRAV))+1.25*TRES;
   BO:=0.972+0.000147*EXP(1.175*LN(F));
```

```
  IF PRESS > PBUB THEN
  BEGIN
    CO:=(5*RSOB+17.2*TRES-1180*GASGRAV+12.61*OILGRAV-1433)/(PRESS*
    EXP(5*LN(10)));
    BO:=BO*EXP(CO*(PBUB-PRESS));
  END;
END;
(*-----------------------------------------------------*)
PROCEDURE RSOBELOWBUB;
(*This procedure calculates the residual gas saturation at the
bubble point and below the bubble point*)
VAR
  YG:REAL;
BEGIN
   YG:=0.00091*TRES-0.0125*APIGRAV;
   RSO:=GASGRAV*EXP(1.204*LN((PRESS/(18*EXP(YG*LN(10))))));
   RSOB:=GASGRAV*EXP(1.204*LN((PBUB/(18*EXP(YG*LN(10))))));
END;
(*-----------------------------------------------------*)

PROCEDURE PRESSBUB;
(*This procedure calculates the bubble point pressure if only the
initial residual gas saturation is known*)
VAR
  YG:REAL;
BEGIN
   YG:=0.00091*TRES-0.0125*APIGRAV;
   PBUB:=18*EXP(YG*LN(10))*EXP((1/1.204)*LN(RSOI/GASGRAV));
END;

(*-----------------------------------------------------*)
PROCEDURE NEWTRAP(VAR XORIG,STOPIT:REAL;MAXIT:INTEGER);
(*this procedure calculates the root of a given function using
the Newton-Rhapson method. The procedure requires the input of
XORIG=original root estimate, STOPIT=stopping criteria, and
MAXIT= the max # of iterations.*)
   VAR
     ERAPROX,ROOTESTA:REAL;
     ITER:INTEGER;
BEGIN
   ITER:=0;
   ERAPROX:=1.1*STOPER;
     WHILE (ERAPROX>STOPER) AND (ITER<MAXIT) DO
       BEGIN
         ROOTESTA:=XORIG-(FUNCVALUE(XORIG)/DERIV(XORIG));
```

```
        (*newtrapson equation where funcvalue is the function
        and deriv is the derivative of the function*)
        ITER:=ITER+1;
        IF ROOTESTA <> 0.0 THEN (*tests to avoid zero division*)
           ERAPROX:= ABS((ROOTESTA-XORIG)/ROOTESTA)*100;
           (*calculates the approx error from preceding estimate*)
        XORIG:=ROOTESTA;
       END;
    Z:=ROOTESTA;
END;(*end of newtrap procedure*)

(*------------------------------------------------*)

PROCEDURE COMPARE(VAR ROOTESTA:REAL);
(*this procedure compares the function value with the calculated root
to zero. If it is close to zero the method has probably worked*)
BEGIN
 WRITELN(DEVICE);
 WRITELN(DEVICE,'IF THE FUNCTION VALUE IS CLOSE TO ZERO THE
METHOD WORKS');
 WRITELN(DEVICE,'THE FUNCTION VALUE WITH CALC. ROOT IS
',FUNCVALUE(ROOTESTA));
END;(*of compare*)

(*----------------------------------------------------*)

PROCEDURE OILVIS;
(*This procedure calculates the oil viscocity both below the bubble
point (mewlive) and above the bubble point(mewabove)*)
VAR
  CONST1,CONST2,CONST3,MEWOD,A,B,ABUB,BBUB,MFACT:REAL;
BEGIN
   CONST1:=1.8635-0.025086*APIGRAV-0.5644*(LN(TRES)/LN(10));
   CONST2:=EXP(CONST1*LN(10));
   CONST3:=EXP(CONST2*LN(10));
   MEWOD:=CONST3-1.0;
   A:=10.715*EXP(-0.515*LN(RSO+100));
   B:=5.44*EXP(-0.338*LN(RSO+150));
   MEWLIVE:=A*EXP(B*LN(MEWOD));
   ABUB:=10.715*EXP(-0.515*LN(RSOB+100));
   BBUB:=5.44*EXP(-0.338*LN(RSOB+150));
   MEWOBUB:=ABUB*EXP(BBUB*LN(MEWOD));
   MFACT:=2.6*EXP(1.187*LN(PRESS))*EXP(-11.513-(8.98*0.00001*PRESS));
   MEWABOVE:=MEWOBUB*EXP(MFACT*LN(PRESS/PBUB));
END;
```

```
(*------------------------------------------------------*)

PROCEDURE TITLES;
(*This procedure prints the output titles*)
BEGIN
WRITELN(DEVICE,'PRESSURE','    Z   ',' GAS VISCOCITY','  BG  ',
'  BO  ','  RSO',' OIL VIS ');
WRITELN(DEVICE,' psia','         ','    cp     ',' bbl/scf',
' bbl/stb',' scf/stb','    cp   ');
END;

(*------------------------------------------------------*)

PROCEDURE PRINTRESULTS;
(*This procedure prints the results to a printer or screen*)
BEGIN
WRITELN(DEVICE,PRESS:9:2,Z:9:4,MG:12:4,BGI:9:4,BO:9:4,RSO:9:4,OILVISC:9:4
);
END;
(*----------------------------------------------------------*)
BEGIN(*of main control program*)
CHO:=' ';
WHICHONE(DEVICE);
READATA;
READATAZ;
WRITEDATA;
TITLES;
WHILE PRESS  >= PMIN DO
  BEGIN
    IF (CHO= 'y') OR (CHO= 'Y') THEN
    RSOBELOWBUB
    ELSE
    PRESSBUB;
    RSOBELOWBUB;
      IF PRESS > PBUB THEN
        BEGIN
          RSO:=RSOB;
          OILVIS;
          OILVISC:=MEWABOVE;
          Z:=0;MG:=0;BGI:=0;
        END;
      IF PRESS <= PBUB THEN
        BEGIN
         PSEUDOCRITICAL;
```

```
        CONSTANTS;
        NEWTRAP(ROOT,STOPER,ITERMAX);
        GASFVF;
        MEWGAS;
        OILVIS;
        OILVISC:=MEWLIVE;
       END;
   OILFVF;
   PRINTRESULTS;
   PRESS := PRESS-(PMAX-PMIN)/N;
  END;
END. (*of main*)


PROCEDURE Whichone (VAR device: TEXT);
 (*This "INCLUDED" procedure enables the user to assign the output to
  either the console or printer. *)

VAR ch: CHAR;
   i: INTEGER;

BEGIN (* of whichone procedure *)
 CH:= ' ';
 CLRSCR;
 WHILE (ch <> 'p') and (ch <> 'P') AND
     (ch <> 'c') and (ch <> 'C') DO
   BEGIN  (* while *)
    FOR i := 1 to 10 DO
     WRITELN;
    WRITE ('SELECT PRINTER OR CONSOLE (P/C) ==> ');
    READLN (ch);
    IF (ch = 'p') or (ch = 'P')
     THEN ASSIGN (device, 'LST:')
     ELSE
      BEGIN   (* if *)
       WRITELN;
       WRITELN ('INVALID RESPONSE. PLEASE RETRY.');
       WRITELN;
      END; (* if *)
    END;  (* while *)
     CLRSCR;
     REWRITE (device)
    END;  (* of whichone procedure *)
```

Appendix C

Guide To Estimating and Deriving the Reservoir Properties Needed In Reservoir Simulation and Two-Phase Analytical Calculations from Field Production Data

Numerical simulations and two-phase analytical calculations such as presented in this dissertation require knowledge of certain fluid and rock properties. Normally these properties are not easily obtained or not available to the non-operating interests and thus must be estimated from production data. This section presents several original and some widely used methods to estimate all the properties required for input to simulation experiments. Methods for estimating absolute permeability methods are not included but a comprehensive discussion is given in my MS thesis, 1993. [12] A flow diagram of the process of estimating parameters is also given in that thesis.

Estimating PVT Data

PVT data can be generated from a simply a knowledge of the dead oil viscosity from a produced oil sample and produced gas-oil ratio (GOR) information obtained from production data. The details are described in the PVT section of this and my computer algorithms for calculation are shown in appendix B.

Relative Permeability Data

Two methods, depending on the type of data available to the engineer are presented for calculating relative permeability data are. One method can be used when there is a core analysis available. Core analysis is used but then modified to fit field production information. The other method assumes no knowledge of core information but only field evidence of produced fluids ratios. An example is provided in which the matrix relative permeability to oil and gas is determined based on observed residual oil saturations as noted on core analysis and connate water saturations calculated from logs. The relative permeability to oil endpoint can be taken as the lowest residual oil saturation from the core or analogy to other field data. The water endpoint can be used as the lowest water saturation calculated from log analysis in a field or analogous formation.

Capillary Pressure

Based on log calculated water saturation at various well locations and structure maps from a field, a capillary pressure relation can be developed to correspond to the transition zone found in the field or an analogous field. A discussion of the method and an example of capillary pressure curve estimation are shown in the capillary pressure section of this report. This capillary pressure curve was slightly modified to obtain a water saturation distribution that more closely resembled that calculated from well logs.

C.2 RESERVOIR PROPERTIES

C.2.1 Discussion of the PVT Data

Pressure, volume and temperature data can be generated from dead oil viscosity, gas gravity, initial produced GOR's, and initial reservoir pressure and temperature. No other data are often available or necessary to generate the PVT relations.

In this example, a service company laboratory measured a dead oil viscosity of 2.53 cp at the formation temperature of 116 degrees F. This oil viscosity corresponds to an API gravity of 38.1-degree oil. Gas gravity of 0.775 was estimated in this example based on the composition of the gas, which was primarily methane. Gas gravity can easily be estimated based on the composition, which will normally consist of predominantly methane, ethane and propane. The reader is referred to the Petroleum Engineering handbook for calculations using mole fractions.

Relative gas and oil production statistics can be obtained from operators or from the various state and private databases. This information should then be tabulated on a spreadsheet to identify producing gas to oil ratio (GOR) trends among wells within a field. GORs are then projected back to first production using linear or non-linear regression or trend analysis. This example (Table A-1) illustrates that the initial GOR was quite variable for the first reported production from different wells. As the data indicate, no gas production was recorded for the field during the first six months of production. No pipeline was available during this time and gas was just vented to the atmosphere. Therefore the first GORs recorded in the field are likely higher than the initial solution GOR value. Therefore backward GOR projections were used to estimate an initial field GOR of 450 SCF/STB. This corresponds to a bubble point pressure of 1600 psia. Initial reservoir pressure was estimated as 1900 psia based on a normal pressure versus depth profile and comparison to initial pressures in fields of similar depth.

This example illustrates a logical and practical approach to estimating the information needed to input to the PVT program considering the typical set of data available to the engineer. Normally the initial GOR must be estimated from produced GORs some time after initial production, the initial reservoir pressure must be estimated from knowledge of the pressure versus depth profile for an area, and the gas gravity must be approximated from knowledge of the gas composition. Once these estimates are computed the engineer can use the algorithm of Appendix B to compute the PVT properties needed for simulation experiments.

GOR ANALYSIS FOR PVT PROPERTIES

CUMMULATIVE OIL PRODUCTION AND GOR DATA

Shaded region indicates backward projection of data using regression techniques

Production tabulation of the first wells in the field

Pipeline installed in December 1983 gas flared until that time

	Aigner		Warren Wells		Warren		Warren		Chenoweth	
PROD	A 1-25		W-1,1A,1B,1C		W-4		W-3A,3B,3C		C-1	
DATE	CUM OIL	GOR	CUM OIL	GOR	CUM OIL	GOR	CUM OIL	GOR	CUM OIL	GOR
Jun-83			358	457.5						
Jul-83			716	468.2						
Aug-83			1413	489						
Sep-83			2489	521.1						
Oct-83			3389	547.9						
Nov-83			4642	585.3						
Dec-83	6263	341.4	6995	655.5	2973		874			
Jan-84	15585	445.8	9159	720	5224		6678			
Feb-84	17854	471.2	9981	744.6	5896		8760		2004	160.5
Mar-84	21403	492	16298	933	7681	2521	13174	3690	4194	349.3
Apr-84	25536	590	20796	852	8678	1605	20027	2817	5814	489
May-84	30131	615	27662	1272	10843	2065	29690	2634	8157	691
Jun-84	34393	637	31806	1835	12591	3694	37380	2711	10540	817
Jul-84	39085	690	36020	2026	14335	3645	46610	2163	12788	760
Aug-84	43280	774	39087	2863	15601	4669	60177	2674	14863	1182
Sep-84	48148	754	41434	2851	16858	4423	70147	3342	16571	1105
Oct-84	53199	989	43621	3236	17920	5186	78598	3629	18218	1630
Nov-84	59625	1219	45264	4013	18797	5827	85118	4025	19738	1543
Dec-84	64048	1301	46516	4513	18797		91235	3899	20862	2395
Jan-85										

Table C-1 GOR Analysis for PVT Estimation

Based on the estimated initial solution GOR, oil gravity, gas gravity and formation temperature, PVT properties were calculated using computer program OILPROP that uses the relations from Craft and Hawkins.[6] (see attached OILPROP program listing in Appendix

B) Table 2 shows the output from this program for the example. These relations are graphed on Figure 1. Data computed by this method serve as reasonable estimates of the formation PVT properties to use in reservoir simulation.

PVT DATA

PRESSURE psia	Z	GAS VISCOSITY cp	Bg bbl/scf	Bo bbl/stb	RSO mcf/stb	OIL VISCOSITY cp
2000	0.0000	0.0000	0.0000	1.2216	0.4430	0.8005
1868	0.0000	0.0000	0.0000	1.2228	0.4430	0.7886
1735	0.0000	0.0000	0.0000	1.2242	0.4430	0.7775
1602	0.0000	0.0000	0.0000	1.2258	0.4430	0.7673
1470	0.7814	0.0151	0.0015	1.2227	0.4337	0.7691
1338	0.7955	0.0145	0.0017	1.1994	0.3871	0.8200
1205	0.8115	0.0140	0.0020	1.1769	0.3415	0.8789
1073	0.8291	0.0135	0.0022	1.1552	0.2969	0.9480
941	0.8480	0.0130	0.0026	1.1345	0.2534	1.0299
809	0.8680	0.0127	0.0031	1.1147	0.2111	1.1286
676	0.8887	0.0123	0.0038	1.0959	0.1703	1.2495
544	0.9100	0.0120	0.0049	1.0783	0.1310	1.4004
412	0.9316	0.0117	0.0066	1.0619	0.0937	1.5928
279	0.9535	0.0115	0.0099	1.047	0.0587	1.8428
147	0.9755	0.0114	0.0193	1.0339	0.0271	2.1686
14.7	0.9976	0.0112	0.1970	1.0236	0.0017	2.5529

Table C-2 Program OILPROP Output

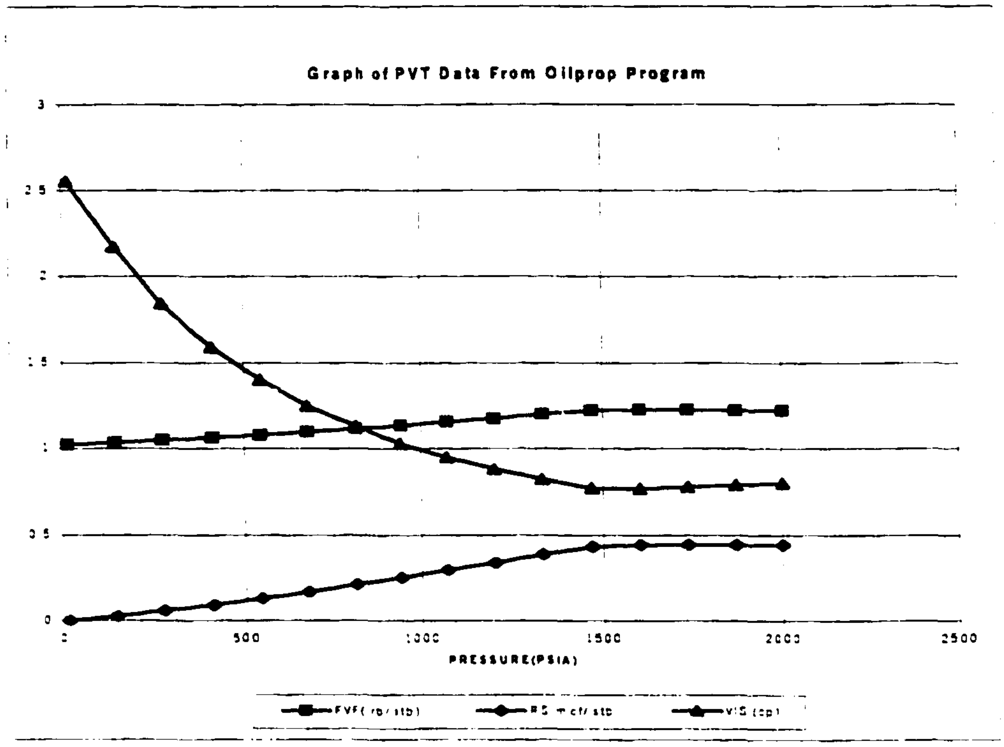

Figure C-1 Graph of PVT Data From Oilprop Program

C.2.2 Oil-Water Relative Permeability Data

Relative permeability data can be generated empirically by using relationships that follow the general form as follows: A first estimate utilizes the following equations for water wet reservoirs from Willhite[1]

$$K_{ro} = (1\text{-}SwD)^{x} \qquad \text{C1}$$

$$K_{rw} = C\ SwD^{3y} \qquad \text{C2}$$

$$SwD = \frac{S_w - S_{iw}}{1 - S_{or} - S_{iw}} \qquad \textbf{C3}$$

S_{iw} = irreducible water saturation
S_{or} = residual oil saturation
K_{ro} = oil relative permeability
K_{rw} = water relative permeability

where C is generally in the range of 0.78, x between 2 and 3 and y between 3 and 4.

The first task is then to derive estimates for the residual oil saturation S_{or} and irreducible water saturation in the particular geologic formation in question. In the example shown here, S_{or} was based on the core analysis (Table 3A). S_{or} was assumed to be the geometric mean of $1-S_w$ in the core. This is reasonable since presumably the core has been flushed by filtrate water during drilling thus reducing the zone to S_{or}. S_{iw} was taken as the lowest water saturation found in the field from log analysis.

The next step is to modify the exponents in the equation by trial and error until the curves that are generated explain the field phenomenon that is observed. The first try using the exponents of x=2.56 and y=3.72 with C=0.78 did not explain the example field production.(see Table 5C and Figure 2C). Field experience suggested that water was not produced until reaching 48-50% water saturation levels. The Willhite[13] relationships indicated that water flow would equal oil flow at 41% water saturation. This was not reasonable based on field experience. This points out the danger of using relations without verifying them with actual field experience and shows the way to use field production data and well log calculations to calibrate generalized relationships.

EXAMPLE CORE ANALYSIS

SAMPLE	DEPTH	POROSITY	PERM TO AIR(md)		WATER	GRAIN	predict
		%	HORIZ	VERT	SAT	DENSITY	
1	4655	2.40	0.11	0.01	81.50	2.76	0.224558
2	4656	7.10	0.16	0.11	72.80	2.65	3.480689
3	4657	10.10	0.16	0.57	67.00	2.65	8.481165
4	4658	10.80	8.30	14.00	52.80	2.65	10.04609
5	4659	9.30	10.00	10.00	41.80	2.66	6.884807
6	4660	10.30	14.00	14.00	48.10	2.67	8.911997
7	4661	12.20	9.90	4.70	57.80	2.66	13.66994
8	4662	11.70	13.00	4.10	46.60	2.66	12.29819
9	4663	13.30	51.00	39.00	45.90	2.66	17.00233
10	4664	7.30	9.20	6.20	44.90	2.70	3.73381
11	4665	4.00	0.27	0.34	57.10	2.73	0.816471
12	4666	5.60	7.20	0.02	62.50	2.65	1.910762
13	4667	5.60	0.10	1.78	76.60	3.06	1.910762

Table C-3 Example Core Analysis

RELATIVE PERMEABILITY ESTIMATES FROM WILLHITE GENERAL fORM

SWIRR= 0.2
SOR= 0.39

SW	SWD	KO	KW
0.200	0.000	0.910	0.000
0.210	0.024	0.875	0.000
0.260	0.146	0.706	0.000
0.300	0.244	0.582	0.000
0.350	0.366	0.439	0.001
0.400	0.488	0.312	0.006
0.450	0.610	0.202	0.026
0.500	0.732	0.111	0.085
0.550	0.854	0.042	0.232
0.583	0.934	0.012	0.417
0.584	0.937	0.011	0.425

Table C-4 Relative Permeability Estimates from Willhite General Form

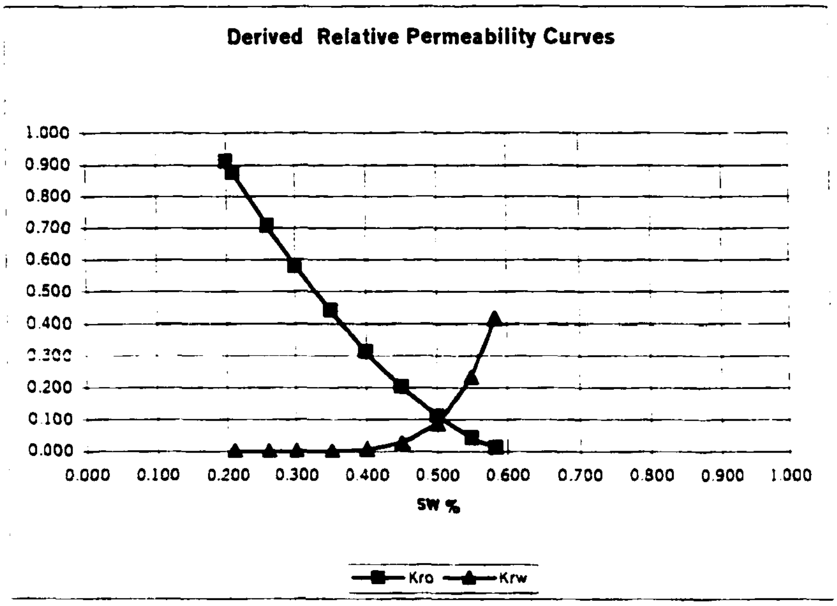

Figure C-2 Derived Relative Permeability Curves

Based on the water saturation calculations from log analysis and a comparison of those values with production data (Table C-5) it was apparent that the relative permeability data needed to be adjusted from that predicted by the initial equations. Based on the core analysis, the residual oil saturation of 39% (61% SW) was again chosen as one endpoint. The other endpoint was chosen as 80% oil saturation based on the highest log calculated oil saturation in the field. However, details of the curves were adjusted between endpoints by changing the constants and exponents in the equations to reflect the production actually found in the field. For instance, production and log analysis indicated that water was almost immobile up to 48% water saturation and then rose rapidly with increasing water saturation. Changing the constants and exponents on the generalized relative permeability relations resulted in the relative permeability curve shown in Figure 3A. This curve explained observed production in the field with the few exceptions and honored the petrophysical data.

RATIO OF PRODUCED FLUID FLOWS

WELL NAME	AVE. PERM(md)	AVE. Sw(%)	OIL BOPD	INITIAL WATER BWPD	GAS MCFD	RATIO OF FLUIDS OIL/WTR	OIL/GAS
Aigner 1-25	21.07	22.98	832		950		0.88
Warren 3C-24	18.71	25.14	210		300		0.70
Warren 3A-24	20.79	26.13	216		700		0.31
Aigner 4-25	11.99	26.78	144		210		0.69
Habben 1-30	11.02	31.00	330				
Warren 6-30	10.99	33.70	181	0	500		0.36
Warren 1B-25	11.35	40.48	231	25	493	9.24	0.47
Warren 4C-24	15.40	41.10	223		200		1.12
COP 1-23	9.80	42.00	19	8		2.38	
Habben 2-30	7.62	42.44	141	53		2.66	
Warren 4A-24	7.74	43.50	130		100		1.30
Bridal 1-26	9.90	43.90	20	20	35	1.00	0.57
Warren 4-24	10.90	46.70	205		175		1.17
Spudds 2-24	3.56	46.70					
Aigner 5-25	8.80	47.90	300	5	120	60.00	2.50
Spudds 1-24	6.33	48.00					
Luster 2-30	5.65	48.62	12	35		0.34	
Grace 1-A-25	9.10	49.21	241		100		2.41
Aigner 3-25	11.67	49.30	180	15	90	12.00	2.00
Habben 4-30	4.28	49.50	94	40	98	2.35	0.96
Chenoweth 1-23	13.24	49.88	130	30	100	4.33	1.30
Heppler 1-23	7.99	50.11	36	2		18.00	
Habben 3-30	6.67	51.20					
Warren1-25	4.95	51.60	47	20	175	2.35	0.27
Warren 1C-24	13.61	53.10	300	0	200		1.50
Forney 1-23	5.41	54.52	20	20	30	1.00	0.67
Warren 6A-30	4.06	58.14	130		100		1.30
Ruth 1-23	10.38	58.17					
Ruth 2-23	20.79	59.00	0				
Spudds 3-24	7.90	62.91					
Warren 5A-25	0.00	66.30					
Reba 1-26	10.46	66.87	40		50		0.80
Luster 1-30	4.66	71.00	6	20	20	0.30	0.30
Warren 1A-25	5.32	71.70	150	0	200		0.75
Warren 2-26	5.50	71.80	42	30	190	1.40	0.22
Chenoweth 2-23	5.92	75.70	135	20	110	6.75	1.23
Endres 1-26	6.92	77.00	42	2		21.00	
Chenoweth 3-23	3.90	85.41	33	10	80	3.30	0.41
Warren 2A-26	5.25	87.13	60	10	42	6.00	1.43

Table C-5 Ratio Of Produced Fluid Flows

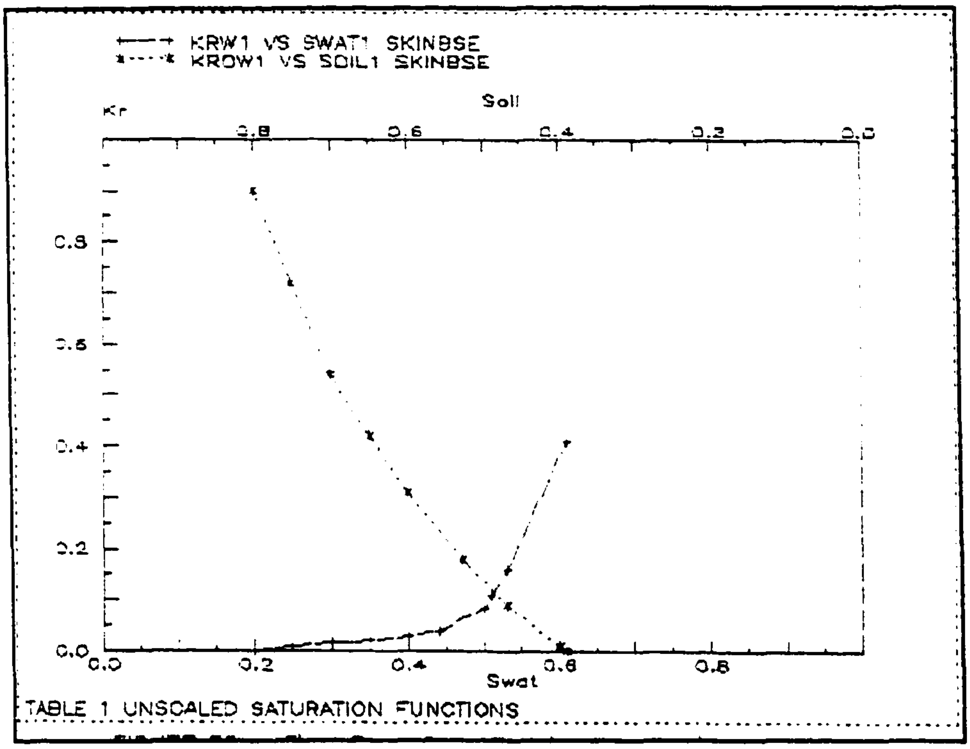

Figure C-3 Final Relative Permeability Curve

Often a fracture system is also present which requires a separate relative permeability curve. In this example because oil was produced from some wells at up to 75% water saturation even though the core data indicated that oil flow should cease at 61% water saturation. This results from the fracture system. In the fractures, both oil and water flow at higher relative saturation than in the matrix. To account for this, a separate linear relative permeability curve was used for the fractures that allowed oil to flow at higher water saturation than in the matrix. Conversely, water flowed at higher oil saturation. This is a reasonable explanation for the oil flow in wells with high water saturation.

C 2.2.3 Using Producing Gas Oil Ratio to Determine Relative Permeability to Oil-Gas Curves

The producing gas-oil ratio is known to be a function of reservoir pressure and reservoir saturation. If one assumes that the pressure gradient is the same through both the gas and the oil phase, a radial flow system with incremental thickness dr, reservoir pressure P and pressure gradient dp/dr in psi/ft, a total of q_o reservoir barrels per day flowing past the radius r and q_g barrels of reservoir gas per day flowing past the radius r then applying Darcy's law the following expressions can be written for the velocity of oil and gas (ν) respectively[14]:

$$v_o = \frac{q_o}{2\pi rh} = \frac{-7.07 k_o dp}{2\pi \mu_o dr} \qquad \text{C4}$$

$$v_g = \frac{q_g}{2\pi rh} = \frac{-7.07 k_g dp}{2\pi \mu_g dr} \qquad \text{C5}$$

The stock tank oil produced per day Q_o is of course q_o/B where B is the formation volume factor. The standard cubic feet of gas produced per day Q_g will be equal to the rate of movement of the reservoir gas converted to surface conditions plus the gas which is evolved from the oil produced, or:

$$Q_g = \frac{q_g}{v} + rQ_o \qquad \text{C6}$$

where r is the gas in solution at the current pressure expressed as SCF/STB.

The producing gas-oil ratio is by definition however, the quotient Q_g/Q_o so by dividing the above equation through by $Q_o=q_o/B$ and substituting into the oil and gas velocity relationships yields the following useful relationship:

$$R = \frac{q_g B}{q_o v} + r = \frac{k_g \mu_o B}{k_o \mu_g v} + r \qquad \textbf{C7}$$

The quantities in this equation are only valid at the pressure and temperature existing at radius r.[14] Since these quantities are really not measurable and only an average pressure is measurable by shutting in the well other assumptions are necessary. If the value of Δ P across the system approaches zero as a limit then one value of P, the average pressure would suffice to define the system. Therefore the assumption means that the production is occurring at zero pressure differential. This is often a reasonable approximation in practice.

In summary the assumptions are that 1) the pressure draw-down is zero, 2) the gas and oil are uniformly distributed 3) the gas and oil are flowing according to equilibrium relative permeability, and 4) the pressure gradients in the gas are the same as those in the oil phase.

The above-derived equation can be re-written as:

$$\frac{k_g}{k_o} = (R - r)\frac{\mu_g v}{\mu_o B} \qquad \textbf{C8}$$

From material balance considerations the average oil saturation S_o can be expressed as:

$$S_o = \frac{(N - \Delta N)B}{Pore\,Volume} = \frac{(N - \Delta N)B}{NB_o/(1 - S_w)} = \left(1 - \frac{\Delta N}{N}\right)\frac{B}{B_o}(1 - S_w) \qquad \textbf{C9}$$

These last two expressions involve only the average pressure at any given time, the cumulative production, and the producing gas-oil ratio at a given time. The water saturation is assumed constant. Calculations of k_g/k_o and S_o made at a number of times in the reservoir's history can be plotted to give the expected relationship. This is normally done on semi-log scale[14]. The following example provides an illustration of how the method works. The field data are tabulated in Table C-6. Using the average pressure, produced gas, production and formation volume factor a gas to oil relative permeability curve can be constructed as shown in figure C-4.

Table C-6 Gas-Oil Relative Permeability Data and Construction

N= 1.17E+08

Average Pressure	R	delta N	deltaN/N	B	v	r	muo/mug	So	kg/ko
3448	850	4.76E+05	0.00408584	1.443	0.00084	752	30.4	0.71	0.00187
3303	920	1.74E+06	0.01496137	1.432	0.000875	725	32.1	0.696	0.00321
3153	990	2.82E+06	0.02418884	1.42	0.00091	695	34	0.684	0.00556
2938	1020	4.65E+06	0.03993133	1.403	0.00097	657	36.8	0.664	0.00682
2813	1000	6.03E+06	0.05175966	1.393	0.00101	632	38.4	0.652	0.00694
2678	1180	7.36E+06	0.06317597	1.382	0.001062	608	40.5	0.638	0.01085
2533	1420	8.75E+06	0.07511588	1.371	0.00122	580	42.4	0.625	0.0162
2453	1510	9.87E+06	0.08474678	1.364	0.001162	565	43.6	0.615	0.01848
2318	1660	1.13E+07	0.09664378	1.354	0.00123	540	45.5	0.609	0.0224
2153	1920	1.26E+07	0.1083176	1.34	0.00133	509	48	0.589	0.0292
1978	2220	1.40E+07	0.12015451	1.326	0.001453	476	50.8	0.575	0.0377
1818	2480	1.53E+07	0.13151073	1.313	0.00159	446	53.8	0.563	0.0456
1658	2710	1.66E+07	0.14207725	1.301	0.001758	416	57.4	0.55	0.054
1625	2800	1.69E+07	0.1453133	1.298	0.001795	410	58.2	0.546	0.0567

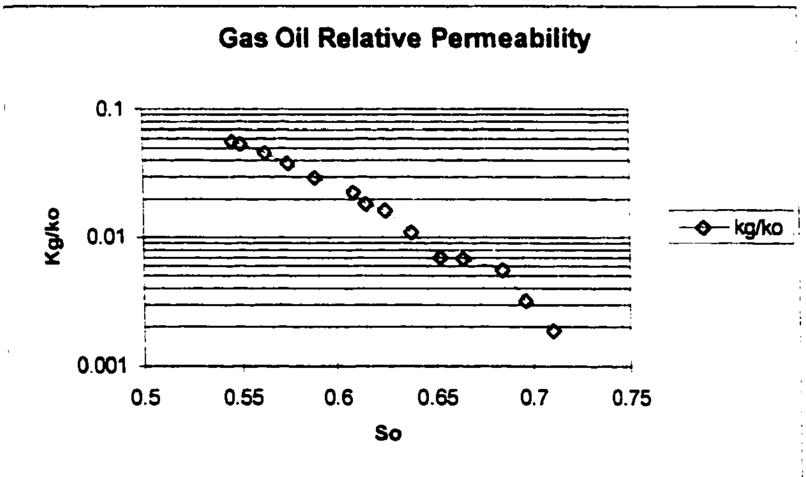

Figure C-4 Gas Oil Relative Permeability

C 2.2.4 Use of Decline Curves in Determining Contributions of Solution Gas Energy and Estimating Mobility Functions

The rate decline path will be exponential where b=0 and the Fetkovich radial solutions and Arps empirical solutions converge when the only reservoir energy is the compressibility of the rock and fluid. (See chapter 5 for my more general solutions) In a solution gas reservoir where water drive is absent the decline path will be more hyperbolic where b values of 0 to 0.5 exist. This deviation from b=0 should give information that can be used in determining

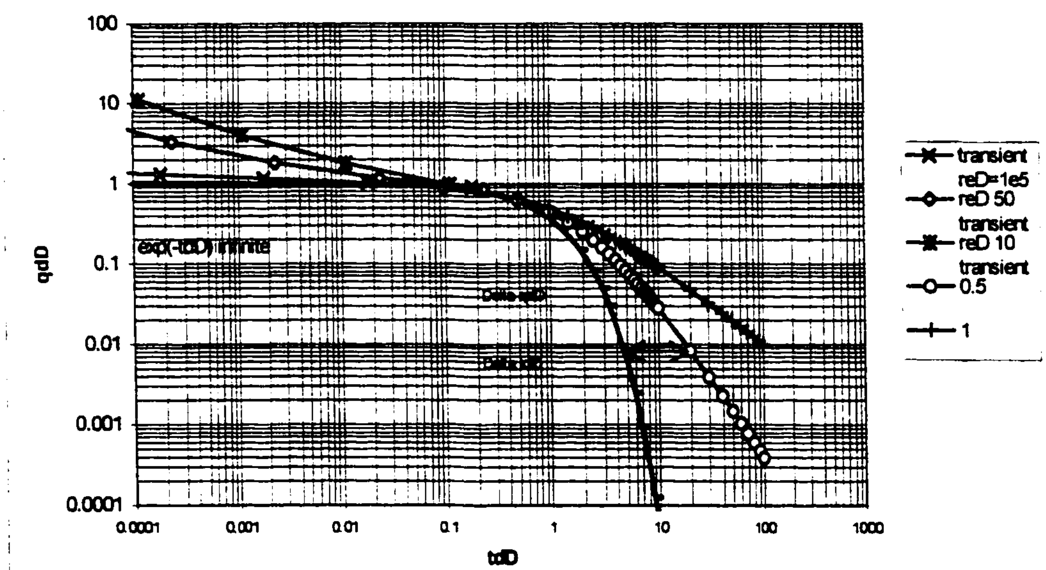

Figure 5.10 Composite Fetkovich Type Curve Transient and Exponential Depletion

the mobility-pressure function that was described in chapter 3 and the appendix A. This concept can be shown in reproduced figure 5.10 where Δq_{Dd} and Δt_{Dd} represent the deviation from the actual path and that predicted exponential path with no energy in the system other than the fluid and rock compressibility. The solution gas provides additional pressure support that more than offsets the increased resistance from the reduction in $k_{ro}/(\mu_o B_o)$ with a reduction in pressure and oil saturation. Also with a purely exponential decline with no additional drive energy, the IPR will be constant with declining pressure. Field experience indicates that the IPR does change with depletion since exponential depletion is rare. Once the decline path is known from the above chart the difference between the decline path and the predicted exponential path should give information about the pressure mobility function and adjustments to IPR over time without the need for well testing techniques.

$$\int \frac{k_{ro}}{\mu_o B_o} dp \cong \frac{(P_R - P_{wf})k_{ro}}{(\mu_o B_o)_{P_{avg}}} \qquad \text{C10}$$

Determination of Relative Permeability from Rate-Time Decline Data

In order to determine the ratio of k_g/k_o, k_{ro}, k_{rg} from rate-time data one needs to know the original oil in place, the current oil saturation and the productivity factor. The analysis (after Fetkovich work)uses the concept that once a well and its offsets have reached pseudo-steady state flow, a no-flow boundary will result at a distance between all wells. The distance to the boundary of no-flow will depend on the flow rate of each offset well. Thus drainage volume of each well should remain constant if all wells are on decline and continue producing wide open against a common backpressure. If one assumes decline below the bubble point is proportional to:

$$\frac{(\overline{P_R} - P_{wf})}{\mu_o B_o} \qquad \textbf{C11}$$

then the Pore Volume V_p can be determined from the expression:

$$V_p = \frac{5.615 \mu_o B_o}{(\mu c_t)_{\overline{P_R}} (\overline{P_R} - P_{wf})} \frac{t}{t_{dD}} \frac{q(t)}{q_{Dd}} \qquad \textbf{C12}$$

and the reserves in place are computed from:

$$N = \frac{V_p (1 - S_{wi})}{B_{oi}} \qquad \textbf{C13}$$

The productivity factor is obtained from:[38]

$$PF = \frac{7.08kh}{\ln \frac{r_e}{r_{w'}} - \frac{1}{2}} = \frac{\mu_o B_o}{\overline{P} - P_{wf}} \frac{q(t)}{q_{Dd}} \qquad \textbf{C14}$$

The relative permeability is then estimated from:

$$k_{ro} = \frac{q_o(\mu_o B_o)}{PF(\overline{P} - P_{wf})} \quad \text{C15}$$

A more rigorous approach uses the m(p) relationship from Fetkovich's isochronal testing of wells paper.[38] Pore volume is thus expressed as:

$$V_p = \frac{5.615\left[\frac{q(t)}{q_{Dd}}\frac{t}{t_{Dd}}\right]}{(\mu_o c_t)_{\overline{P_R}}\left[\frac{\overline{P_R} - P_B}{(\mu_o B_o)_{\overline{P_R P_b}}} + \frac{P_b^2 - P_{wf}^2}{2P_b(\mu_o B_o)_{P_b}}\right]} \quad \text{C16}$$

And N is calculated in the same way using the above equation.

The productivity factor PF is then estimated by:

$$PF = \frac{7.08kh}{\ln\frac{r_e}{r_{w'}}} = \frac{\frac{q(t)}{q_{Dd}}}{\left[\frac{\overline{P_R} - P_B}{(\mu_o B_o)_{\overline{P_R P_b}}} + \frac{P_b^2 - P_{wf}^2}{2P_b(\mu_o B_o)_{P_b}}\right]} \quad \text{C17}$$

The relative permeability to oil is then computed below the bubble point by:

$$k_{ro} = \frac{2\overline{P_R}(\mu_o B_o)_{\overline{P_R}} q_o}{PF(P_R^2 - P_{wf}^2)} \quad \text{C18}$$

For each production period examined the new value of k_{ro} is calculated and the relative permeability relation is computed and plotted as a function of saturation.

C 2.2.5 Use in Adjusting the IPR Curve with Depletion

It is well established that the inflow performance curve changes with decreasing reservoir pressure.

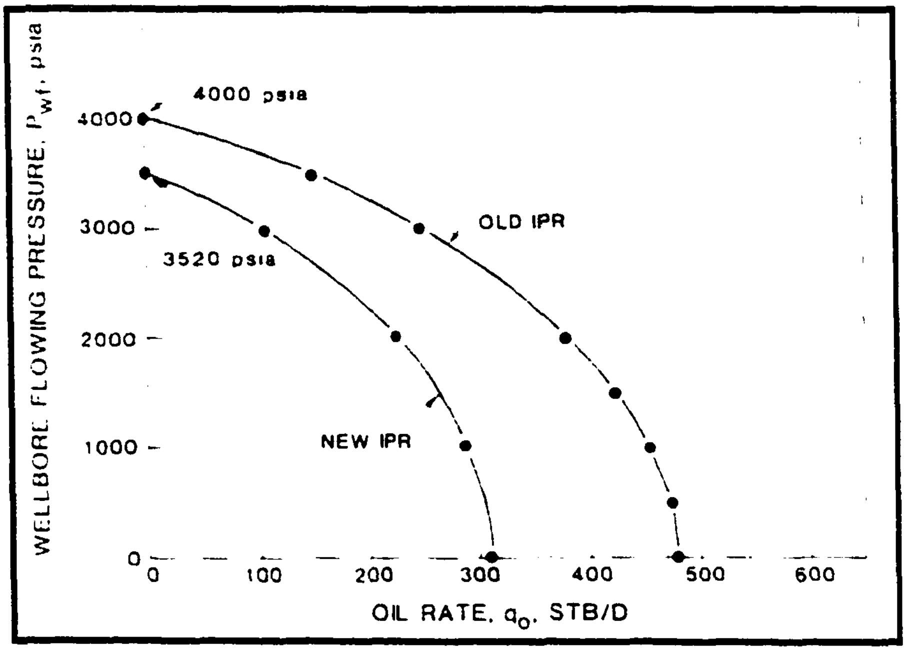

Figure C-5[4] Change in IPR with Depletion

In Appendix A it was shown that the IPR relations can be expressed as:

$$q_o = \frac{kh}{141.2\mu_o B_o} \frac{1}{2P_R} (P_R^2 - P_{wf}^2) k_{PR} \frac{1}{\ln \frac{r_e}{r_w} - \frac{3}{4}} \quad \text{C18}$$

or:

$$q_o = C(P_R^2 - P_{wf}^2) \quad \text{C19}$$

$$q_o = C(P_R^2 - P_{wf}^2) \qquad \textbf{C19}$$

Where:

$$C = \frac{kh}{141.2\mu_o B_o} \frac{1}{2P_R} k_{PR} \frac{1}{\ln \frac{r_e}{r_w} - \frac{3}{4}} \qquad \textbf{C20}$$

As the reservoir pressure drops the resistance to oil flow increases since the ratio of $\frac{k_{ro}}{\mu_o B_o}$ decreases as the average pressure decreases. Therefore the change in IPR with declining pressure should be related to the change in $\frac{k_{ro}}{\mu_o B_o}$ that can be predicted from either the decline path method or the empirical method from field data presented earlier. Thus the IPR relation at any particular reservoir pressure should be expressed as:

$$q_o = C'(P_R^2 - P_{wf}^2) \qquad \textbf{C21}$$

where:

$$q_o = q_{o\,max} \left(\frac{\frac{k_{ro}}{\mu_o B_o} new}{\frac{k_{ro}}{\mu_o B_o} old} \right) \left(\frac{P_R new}{P_R old} \right) \left(1 - \frac{P_{wf}}{P_R} \right)^n \qquad \textbf{C22}$$

And if the IPRs are known then the inverse can be applied to determine the change in mobility function over time using the above relationship. Mattax and Dalton [15] presented a similar form previously developed by Whitson and Golan for above the bubble point conditions in which:

$$J_F = \frac{\left(\dfrac{k_{ro}}{\mu_o B_o}\right)_F}{\left(\dfrac{k_{ro}}{\mu_o B_o}\right)_P} J_P \qquad \textbf{C23}$$

Thus the relationship can be used to determine the productivity at any future date (J_F) if the mobility functions are known. Conversely it should be possible to infer the mobility functions if the performance functions are known. Mattax and Dalton indicate that the relationship can be used with small error below the bubble point also.

C 2.2.5 Capillary Pressure Estimation

Capillary pressure can be thought of as a force per unit area resulting from the interaction of surface forces and the geometry of the medium in which they exist[16]. The effect of the capillary pressure relationship is to distribute the saturation properly over the depth of the reservoir. Although capillary pressure is not used in the analytical equations presented in this research, it is often needed in the numerical simulations. The following presents my method of determining capillary pressure without core experiments. The capillary pressure can be estimated from reservoir data alone by calculating the length of the oil to water transition zone and knowing the oil-water density contrast. The density is determined from an oil and water sample while the height of the oil column and transition zone is determined from production data and well log water saturation calculations. A transition zone of approximately 80 feet occurs in this example reservoir. The structurally highest well in the field occurs at a subsea depth of about

3510 feet. Based on log analysis, the water saturation gradually increases from a low of about 20% at the structurally highest part of the field to nearly 100% over about an 80-foot transition zone. The exact oil-water contact is unknown but is estimated to be 3590 feet subsea.

Capillary pressure is determined from the relationship $P_c = (\rho_w - \rho_o)gh = \frac{2\sigma\cos\theta}{R}$.

Based on oil and water density differences, the 80 foot transition zone of the example and the equations for capillary pressure, a preliminary curve can be developed to distribute the saturations across the transition zone as calculated from log analysis. It is a good idea to draw a map projection of the average water saturations within the field and to overlay this map on the structure map to make sure the two functions roughly agree. Table C-7 shows the results of the calculation. Figure C-6 shows the field average water saturation change with depth. Figure C-7 shows the capillary pressure curve calculated from the length of the transition zone and the oil and water density differences. Slight modifications to this capillary pressure data may be necessary to obtain an initial water saturation distribution that match the water saturation map generated from log analysis.

CAPILLARY PRESSURE DATA

Pc=DELTA DENSITY*g*h= 2*sigma*cos/R
OIL DENSITY = 50.33 #/cubic ft.
WATER DENSITY= 71.76 #/cubic ft.
TRANSITION ZONE= 80 FT.

WATER SAT. %	SUBSEA DEPTH	Pc psi
20	3510	11.91
25	3520	10.42
30	3530	8.93
35	3540	7.44
40	3550	5.95
47	3560	4.46
53	3565	3.72
60	3570	2.98
75	3580	1.49
100	3590	0.00

Table C-7 Capillary Pressure Calculation Data

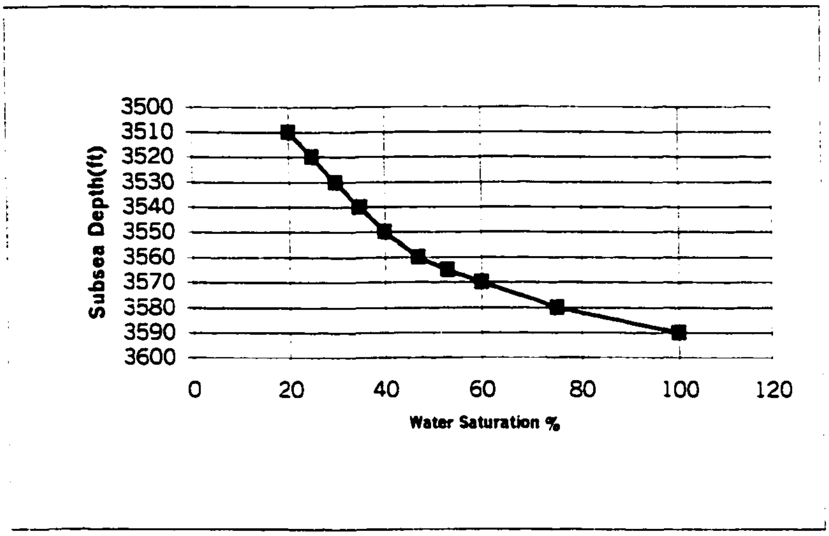

Figure C-6 Saturation v. Depth Profile

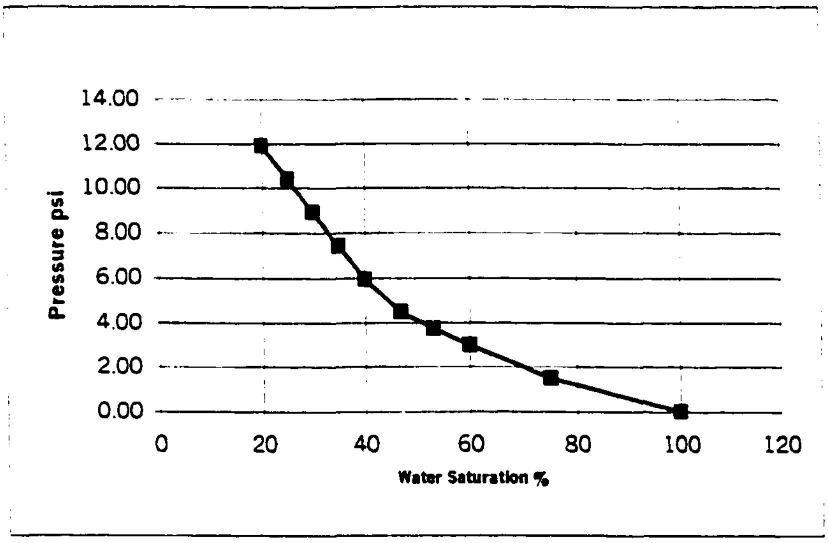

Figure C-7 Capillary Pressure Profile

APPENDIX D

Tabular Generalized Type Curve Solutions

Table D-1 Tabular Data for Fetkovich Decline Type Curves Figures 5.1 – 5.4

Infinite values from program, finite depletion values closed system from table c-5 Lee welltesting book ref 20

Radial Cases

		fetkovich constants		Depletion Portion											
		c1	2.49673			c1	3.41202			c1	4.10517				
		c2	199.5			c2	1249.5			c2	4999.5				
infinite		reD=20	20			reD =50	50			reD=100	100				
tD	qD	tD	tdD	qD	qdD	tD	tdD	qD	qdD	tD	tdD	qD	qdD		
0.01	6.1289	100	0.20084	0.3394	0.84705	600	0.14074	0.2652	0.90487	2000	0.09745	0.2304	0.94583		
0.1	2.2488	130	0.2611	0.3174	0.79215	800	0.18765	0.2915	0.9946	3000	0.14617	0.2179	0.89452		
1	0.98443	160	0.32135	0.2975	0.74248	1000	0.23456	0.2393	0.8165	4000	0.1949	0.207	0.84977		
10	0.53392	200	0.40169	0.2726	0.68084	1300	0.30493	0.222	0.75747	5000	0.24362	0.1967	0.80749		
100	0.34556	240	0.48203	0.2502	0.62443	1600	0.37529	0.206	0.70288	6000	0.29234	0.1869	0.76726		
1000	0.25096	300	0.60253	0.2197	0.54831	2000	0.46912	0.1865	0.63634	8000	0.38979	0.1686	0.69213		
10000	0.19593	400	0.80338	0.177	0.44174	2400	0.56294	0.1682	0.5739	10000	0.48724	0.1536	0.63055		
100000	0.16037	500	1.00422	0.1426	0.35589	3000	0.70368	0.1543	0.52648	13000	0.63341	0.1304	0.53531		
1000000	0.13561	600	1.20506	0.1148	0.28651	4000	0.93824	0.1133	0.38658	16000	0.77958	0.1118	0.45898		
1E+07	0.11742	700	1.40591	0.0925	0.23086	5000	1.17279	0.0833	0.28422	20000	0.97448	0.091	0.37357		
1E+08	0.10351	800	1.60675	0.0745	0.18593	6000	1.40735	0.0682	0.2327	24000	1.16937	0.0741	0.30419		
1E+09	0.09253	1000	2.00844	0.0483	0.12054	8000	1.87647	0.0418	0.14262	30000	1.46172	0.0645	0.26478		
1E+10	0.08365	1300	2.61097	0.0283	0.07063	10000	2.34559	0.0254	0.08667	40000	1.94896	0.0326	0.13383		
1E+11	0.07632	1600	3.21351	0.0132	0.03294	13000	3.04926	0.012	0.04094	50000	2.4362	0.0195	0.08005		
1E+12	0.07017	2000	4.01688	0.0056	0.01398	16000	3.75294	0.0056	0.01911	60000	2.92344	0.0117	0.04803		
		3000	6.02532	0.0006	0.0015	20000	4.69118	0.0021	0.00717	80000	3.89791	0.0042	0.01724		
						24000	5.62941	0.0006	0.00205	100000	4.87239	0.0015	0.00616		
						30000	7.03676	0.0002	0.00068	110000	5.35963	0.0009	0.00369		

c1	4.79832			c1	5.71461			c1	6.40776		
c2	19999.5			c2	125000			c2	500000		
reD=200	200			reD=500	500			reD=1000	1000		
tD	tdD	qD	qdD	tD	tdD	qD	qdD	tD	tdD	qD	qdD
10000	0.10421	0.1943	0.93231	100000	0.13999	0.1566	0.89491	30000	0.00936	0.1773	1.1361
13000	0.13547	0.186	0.89249	130000	0.18199	0.1498	0.85605	40000	0.01248	0.1729	1.1079
16000	0.16673	0.182	0.87329	160000	0.22399	0.1435	0.82005	50000	0.01561	0.1697	1.0874
20000	0.20841	0.1742	0.83587	200000	0.27999	0.1354	0.77376	100000	0.03121	0.1604	1.0278
24000	0.25009	0.1668	0.80036	240000	0.33598	0.1277	0.72976	200000	0.06242	0.1518	0.9727
30000	0.31262	0.1562	0.7495	300000	0.41998	0.117	0.66861	300000	0.09364	0.1464	0.9381
40000	0.41682	0.1401	0.67224	400000	0.55997	0.1012	0.57832	400000	0.12485	0.1416	0.90734
50000	0.52103	0.1236	0.59307	500000	0.69996	0.0875	0.50003	500000	0.15606	0.1371	0.8785
60000	0.62523	0.1126	0.54029	600000	0.83996	0.0756	0.43202	600000	0.18727	0.1327	0.85031
80000	0.83365	0.0905	0.43425	800000	1.11994	0.0565	0.32288	700000	0.21849	0.1285	0.8234
100000	1.04206	0.0728	0.34932	1000000	1.39993	0.0422	0.24116	800000	0.2497	0.1244	0.79712
130000	1.35468	0.0524	0.25143	1300000	1.8199	0.0273	0.15601	900000	0.28091	0.1204	0.77149
160000	1.66729	0.0378	0.18138	1600000	2.23988	0.0176	0.10058	1000000	0.31212	0.1166	0.74714
200000	2.08412	0.0244	0.11706	2000000	2.79985	0.0098	0.056	1400000	0.43697	0.1024	0.65615
240000	2.50094	0.0138	0.06622	2400000	3.35982	0.0055	0.03143	2000000	0.62424	0.0844	0.54081
300000	3.12617	0.0082	0.03935	3000000	4.19978	0.0023	0.01314	2400000	0.74909	0.0741	0.47481
400000	4.16823	0.0028	0.01344	4000000	5.59971	0.0005	0.00286	3000000	0.93637	0.061	0.39087
500000	5.21029	0.0009	0.00432	5000000	6.99963	0.0001	0.00057	4000000	1.24849	0.0442	0.28322
								5000000	1.56061	0.032	0.20505
								7000000	2.18485	0.0167	0.10701
								8400000	2.62183	0.0106	0.06792
								1E+07	3.12122	0.0063	0.04037
								1.4E+07	4.36971	0.0017	0.01089
								2E+07	6.24244	0.0004	0.00256
								3E+07	9.36366	0.0001	0.00064

Table D-1 Tabular Data for Fetkovich Decline Type Curves Figures 5.1 – 5.4 Continued

Infinite values from program, finite depletion values closed system from table c-5 Lee welltesting book ref 20

Radial Cases

fetkovich constants		Depletion Portion					
c1	8.71034			c1	11.0129		
c2	5E+07			c2	5E+09		
reD=10000	10000			reD= 1e5 depletion	100000		
tD	tdD	qD	qdD	tD	tdD	qD	qdD
3E+06	0.00689	0.1263	1.10012	1.4E+08	0.00254	0.1017	1.12001
4E+06	0.00918	0.124	1.08008	2E+08	0.00363	0.1	1.10129
5E+06	0.01148	0.1222	1.0644	2.4E+08	0.00436	0.099	1.09028
6E+06	0.01378	0.121	1.05395	3E+08	0.00545	0.098	1.07927
8E+06	0.01837	0.1188	1.03479	3.5E+08	0.00636	0.0971	1.06936
1E+07	0.02296	0.1174	1.02259	4E+08	0.00726	0.0966	1.06385
1E+07	0.02755	0.1162	1.01214	5E+08	0.00908	0.0956	1.05284
1E+07	0.03215	0.1152	1.00343	6E+08	0.0109	0.0948	1.04403
2E+07	0.03674	0.1143	0.99559	7E+08	0.01271	0.0941	1.03632
2E+07	0.04133	0.1135	0.98862	8E+08	0.01453	0.0935	1.02971
2E+07	0.04592	0.1128	0.98253	8.4E+08	0.01525	0.0933	1.02751
2E+07	0.05511	0.1115	0.9712	9E+08	0.01634	0.093	1.0242
3E+07	0.06888	0.1098	0.9564	1E+09	0.01816	0.0925	1.0187
4E+07	0.09184	0.1071	0.93288	1.4E+09	0.02542	0.0911	1.00328
5E+07	0.11481	0.105	0.91459	2E+09	0.03632	0.0896	0.98676
7E+07	0.16073	0.0998	0.86929	3E+09	0.05448	0.0877	0.96583
8E+07	0.18369	0.0975	0.84926	4E+09	0.07264	0.0861	0.94821
9E+07	0.20665	0.0952	0.82922	5E+09	0.0908	0.0845	0.93059
1E+08	0.22961	0.093	0.81006	6E+09	0.10896	0.0829	0.91297
1E+08	0.27553	0.0887	0.77261	7E+09	0.12712	0.0814	0.89645
1E+08	0.32146	0.0846	0.73689	8E+09	0.14528	0.0799	0.87993
2E+08	0.39034	0.0788	0.68637	9E+09	0.16344	0.0784	0.86341
2E+08	0.45922	0.0734	0.63934	1E+10	0.1816	0.077	0.848
2E+08	0.55107	0.0668	0.58185	1.3E+10	0.23609	0.0728	0.80174
3E+08	0.68884	0.058	0.5052	1.6E+10	0.29057	0.0689	0.75879
4E+08	0.91845	0.0458	0.39893	2E+10	0.36321	0.0639	0.70373
5E+08	1.14806	0.0362	0.31531	2.4E+10	0.43585	0.0594	0.65417
6E+08	1.37767	0.0286	0.24912	3E+10	0.54481	0.0531	0.58479
7E+08	1.60729	0.0226	0.19685	4E+10	0.72642	0.0441	0.48567
8E+08	1.8369	0.0178	0.15504	5E+10	0.90802	0.0366	0.40307
1E+09	2.29612	0.0111	0.09668	6E+10	1.08963	0.0304	0.33479
1E+09	3.21457	0.0043	0.03745	7E+10	1.27123	0.0253	0.27863
2E+09	4.59224	0.0011	0.00958	8E+10	1.45284	0.021	0.23127
3E+09	6.88836	0.0001	0.00087	9E+10	1.63444	0.0174	0.19162
				1E+11	1.81605	0.0145	0.15969
				1.3E+11	2.36086	0.0083	0.09141
				1.6E+11	2.90568	0.0048	0.05286
				2E+11	3.6321	0.0023	0.02533
				2.4E+11	4.35851	0.0011	0.01211
				3E+11	5.44814	0.0004	0.00441
				3.4E+11	6.17456	0.0002	0.0022

Table D-2 Tabular Data for Fetkovich Decline Type Curves Figures 5.1 – 5.4 Transient Portion

infinite reservoir solutions-transient portion from program

c1		1.8026		2.49573		3.41202		4.10517		4.79832		6.40776	
c2		49.5		199.5		1249.5		4999.5		19999.5		500000	
reD		10	reD 10 transient	20		50	reD 50 transient	100		200		1000	
tD	qD	tdD	qdD	tdD	qdD	tdD	qdD	tdD	qdD	tdD	qdD	tdD	qdD
0.01	6.1289	0.0001	11.0479	2E-05	15.2961	2.3E-06	20.9119	4.9E-07	25.1602	1E-07	29.4084	3.1E-09	39.2725
0.1	2.2488	0.0011	4.05365	0.0002	5.6124	2.3E-05	7.67296	4.9E-06	9.23171	1E-06	10.7905	3.1E-08	14.4098
1	0.98443	0.0112	1.77452	0.00201	2.45687	0.00023	3.3589	4.9E-05	4.04125	1E-05	4.72361	3.1E-07	6.30799
10	0.53392	0.1121	0.96244	0.02008	1.33252	0.00235	1.82175	0.00049	2.19183	0.0001	2.56192	3.1E-06	3.42123
100	0.34556	1.1207	0.6229	0.20084	0.86243	0.02346	1.17906	0.00487	1.41858	0.00104	1.65811	3.1E-05	2.21426
1000	0.25096	11.207	0.45238	2.00844	0.62633	0.23456	0.85628	0.04872	1.03023	0.01042	1.20419	0.00031	1.60809
10000	0.19593	112.07	0.35318	20.0844	0.48899	2.34559	0.66852	0.48724	0.80433	0.10421	0.94013	0.00312	1.25547
100000	0.16037	1120.7	0.28908	200.844	0.40024	23.4559	0.54719	4.87239	0.65835	1.04206	0.76951	0.03121	1.02761
1000000	0.13561	11207	0.24445	2008.44	0.33845	234.559	0.4627	48.7239	0.5667	10.4206	0.6507	0.31212	0.86896
1E+07	0.11742	112072	0.21166	20084.4	0.29305	2345.59	0.40064	487.239	0.48203	104.206	0.56342	3.12122	0.7524
1E+08	0.10351	1E+06	0.18659	200844	0.25833	23455.9	0.35318	4872.39	0.42493	1042.06	0.49667	31.2122	0.66327
1E+09	0.09253	1E+07	0.1668	2008441	0.23094	234559	0.31572	48723.9	0.37986	10420.6	0.444	312.122	0.59293
1E+10	0.08365	1E+08	0.15079	2E+07	0.20878	2345588	0.28543	487239	0.34341	104206	0.40139	3121.22	0.53603
1E+11	0.07632	1E+09	0.13758	2E+08	0.19048	2.3E+07	0.26042	4872392	0.31332	1042058	0.36623	31212.2	0.48907
1E+12	0.07017	1E+10	0.12649	2E+09	0.17513	2.3E+08	0.23943	4.9E+07	0.28807	1E+07	0.33671	312122	0.44965

infinite reservoir solutions-transient portion from program

c1	8.71034		11.0129			
c2	5E+07		5E+09			
reD	10000	transient reD=1e5	100000		INFINITE-TRANSIENT	
tD	tdD	qdD	tdD	qdD	tdD	qdD
0.01	2.3E-11	53.385	1.8E-13	67.4971	0.0001	0.9999
0.1	2.3E-10	19.588	1.8E-12	24.7659	0.001	0.999
1	2.3E-09	8.5747	1.8E-11	10.8415	0.01	0.99005
10	2.3E-08	4.6506	1.8E-10	5.88002	0.1	0.90484
100	2.3E-07	3.0099	1.8E-09	3.80563	0.2	0.81873
1000	2.3E-06	2.1859	1.8E-08	2.7638	0.4	0.67032
10000	2.3E-05	1.7066	1.8E-07	2.15776	0.6	0.54881
100000	0.00023	1.3969	1.8E-06	1.76614	1	0.36788
1000000	0.0023	1.1812	1.8E-05	1.49346	1.3	0.27253
1E+07	0.02296	1.0228	0.00018	1.29314	1.9	0.14957
1E+08	0.22961	0.9016	0.00182	1.13995	2.5	0.08208
1E+09	2.29612	0.806	0.01816	1.01906	3	0.04979
1E+10	22.9612	0.7286	0.1816	0.92126	3.5	0.0302
1E+11	229.612	0.6648	1.81605	0.84055	5	0.00674
1E+12	2296.12	0.6112	18.1605	0.77281	6	0.00248
					7	0.00091
					9	0.00012
					10	4.5E-05

Table D-3 Arps Depletion Solutions for Fetkovich Type Curves Figures 5.1 – 5.4

arps depletion solutions from program

b values	0	0.1	0.2	0.3	0.4	0.5	0.6	0.7	0.8	0.9	1
tdD	qdD	qdD	qdD	qdD	qdD	qdD	qdD	qdD	qdD	qdD	qdD
0.1	0.90484	0.9053	0.90573	0.90617	0.9066	0.90703	0.90745	0.90787	0.90828	0.90869	0.90909
0.5	0.60653	0.6139	0.62092	0.62759	0.63394	0.64	0.64579	0.65134	0.65666	0.66176	0.66667
1	0.36788	0.3855	0.40188	0.41705	0.4312	0.44444	0.45688	0.46858	0.47963	0.49009	0.5
1.5	0.22313	0.2472	0.26933	0.28981	0.30882	0.32653	0.34309	0.35862	0.37323	0.38699	0.4
2	0.13534	0.1615	0.18593	0.20874	0.23005	0.25	0.26972	0.28631	0.30289	0.31854	0.33333
2.5	0.08208	0.1074	0.13169	0.15484	0.17678	0.19753	0.21715	0.23571	0.25328	0.26992	0.28571
3	0.04979	0.0725	0.09537	0.11771	0.1393	0.16	0.17978	0.19863	0.2166	0.2337	0.25
3.5	0.0302	0.0497	0.07043	0.09137	0.11207	0.13223	0.15173	0.17049	0.18848	0.20572	0.22222
4	0.01832	0.0348	0.05292	0.07221	0.09174	0.11111	0.13008	0.1485	0.16632	0.18349	0.2
4.5	0.01111	0.0243	0.04039	0.05796	0.07623	0.09467	0.11298	0.13094	0.14844	0.16541	0.18182
5	0.00674	0.0173	0.03125	0.04716	0.06415	0.08163	0.09921	0.11664	0.13375	0.15044	0.16667
5.5	0.00409	0.0125	0.02449	0.03883	0.05459	0.07111	0.08795	0.1048	0.12148	0.13786	0.15385
6	0.00248	0.0091	0.0194	0.03232	0.04691	0.0625	0.0786	0.09487	0.1111	0.12713	0.14286
6.5	0.0015	0.0067	0.01554	0.02716	0.04067	0.05536	0.07074	0.08644	0.10221	0.11788	0.13333
7	0.00091	0.005	0.01256	0.02302	0.03553	0.04938	0.06407	0.07921	0.09453	0.10984	0.125
7.5	0.00055	0.0037	0.01024	0.01967	0.03125	0.04432	0.05835	0.07295	0.08783	0.10277	0.11765
8	0.00034	0.0028	0.00842	0.01692	0.02766	0.04	0.05341	0.06749	0.08193	0.09653	0.11111
8.5	0.0002	0.0021	0.00697	0.01465	0.02462	0.03628	0.0491	0.06269	0.07672	0.09096	0.10526
9	0.00012	0.0016	0.00581	0.01276	0.02203	0.03306	0.04533	0.05844	0.07207	0.08598	0.1
9.5	7.5E-05	0.0013	0.00488	0.01118	0.01981	0.03025	0.042	0.05465	0.0679	0.08149	0.09524
10	4.5E-05	0.001	0.00412	0.00984	0.01789	0.02778	0.03904	0.05127	0.06415	0.07743	0.09091
20	2.1E-09	2E-05	0.00032	0.00152	0.00412	0.00826	0.01391	0.02089	0.02897	0.03795	0.04762
30	9.4E-14	1E-06	5.9E-05	0.00046	0.00164	0.00391	0.00739	0.01209	0.01789	0.02466	0.03226
40	4.2E-18	1E-07	1.7E-05	0.00019	0.00084	0.00227	0.00468	0.00814	0.01264	0.01809	0.02439
50	1.9E-22	2E-08	6.2E-06	9.7E-05	0.00049	0.00148	0.00327	0.00598	0.00964	0.01421	0.01961
60	8.8E-27	4E-09	2.7E-06	5.5E-05	0.00032	0.00104	0.00243	0.00464	0.00771	0.01165	0.01639
70	4E-31	9E-10	1.3E-06	3.4E-05	0.00022	0.00077	0.00189	0.00374	0.00638	0.00984	0.01408
80	1.8E-35	3E-10	7E-07	2.2E-05	0.00016	0.00059	0.00152	0.0031	0.00542	0.0085	0.01235
90	8.2E-40	1E-10	4E-07	1.5E-05	0.00012	0.00047	0.00126	0.00263	0.00469	0.00747	0.01099
100	3.7E-44	4E-11	2.4E-07	1.1E-05	9.3E-05	0.00038	0.00106	0.00227	0.00412	0.00666	0.0099

Table D-4 Equivalent Radial Transient Generalized Solutions Shape Factor 31.62

CA	31.62	Equivalent Radial in Transient Region							
	logterm	1.34421927		1.949557		2.74635034		3.34854065	
	c1c2	76.7565332	76.852962	448.66156	448.02359	3968.51442	3950.9477	19311 7745	19273.9233
	c1	1.54733081		2.244135		3.16132387		3.85450514	
	fetkovich constants								
infinite reservoir solutions	A/rw^2	311.017673		1253.4955		7850.84004		31412.7849	
c1		1.55258509		2.2457323		3.16202301		3.85517019	
c2		49.5		199.5		1249.5		4999.5	
reD		10	reD 10 transient	20		50	reD 50 transient	100	
tD	qD	tdD	qdD	tdD	qdD	tdD	qdD	tdD	qdD
0.01	6.1289	0.00013028	9.4834358	2.229E-05	13.754079	2.5262E-06	19.375438	5.1782E-07	23.6238765
0.1	2.2488	0.00130282	3.4796375	0.0002229	5.0466109	2.5262E-05	7 1091851	5.1782E-06	8 66801116
1	0.98443	0 01302821	1.5232389	0.0022289	2.2091939	0.00025262	3.1121021	5.1782E-05	3.79449049
10	0.53392	0.13028207	0 8261509	0.0222885	1.1981886	0.0025262	1 687894	0.00051782	2.05799738
100	0.34556	1.3028207	0.5346956	0.2228851	0.7754833	0.025262	1 0924271	0.00517819	1 3319628
1000	0.25096	13.028207	0.3883181	2.2288515	0.5631881	0.25262002	0.7933658	0.05178188	0.96732661
10000	0.19593	130.28207	0.3031685	22.288515	0.4396934	2.52620022	0.6193962	0.5178188	0.75521319
100000	0.16037	1302.8207	0.2481454	222.88515	0 3598919	25.2620022	0.5069815	5.17818805	0 61814699
1000000	0.13561	13028.207	0.2098335	2228.8515	0.3043272	252.620022	0.4287071	51 7818805	0.52270944
10000000	0.11742	130282.07	0.1816876	22288.515	0.2635063	2526.20022	0.3712026	517 818805	0 45259599
100000000	0.10351	1302820.7	0.1601642	222885.15	0.2322904	25262.0022	0.3272286	5178.18805	0 39897983
1E+09	0.092533	13028207	0.1431792	2228851.5	0.2076565	252620.022	0.2925268	51781 8805	0 35666892
1E+10	0.083653	130282070	0.1294389	22288515	0 1877286	2526200.22	0.2644542	517818.805	0.32244092
1E+11	0.076324	1302820695	0.1180985	222885150	0.1712814	25262002.2	0.2412849	5178188 05	0.29419125
1E+12	0.070173	1 3028E+10	0.1085808	2.229E+09	0.1574777	252620022	0.2218396	51781880.5	0.27048219

Table D-4 Equivalent Radial Transient Generalized Solutions Shape Factor 31.62 Continued

	CA	31.62	Equivalent Radial in Transient Region							
logterm	3.9506332		5.34858364		7.3485841		9.34858408			
c1c2	91143.538	90964.073	3084951.89	3078874.6	423851478	423017014	5.3921E+10	5.381E+10		
c1	4.5475739		6.15675463		8.4589551		10.7611551			
fetkovich constants										
A/rw^2	125660.56		3141589.51		314159262		3.1416E+10			
c1	4.5483174		6.15775528		8.4603404		10.7629255			
c2	19999.5		499999.5		50000000		5000000000			
reD	200		1000		10000	transient reD=1e5	100000		INFINITE-TRANSIENT	
	tdD	qdD	tdD	qdD	tdD	qdD	tdD	qdD	tdD	qdD
	1.097E-07	27.871626	3.2415E-09	37.734133	2.359E-11	51.84409	1.8546E-13	65.954044	0.0001	0.9999
	1.097E-06	10.226584	3.2415E-08	13.84531	2.359E-10	19.022498	1.8546E-12	24.199686	0.001	0.9990005
	1.097E-05	4.4767682	3.2415E-07	6.060894	2.359E-09	8.3272492	1.8546E-11	10.593604	0.01	0.99004983
	0.0001097	2.4280407	3.2415E-06	3.2872144	2.359E-08	4.5164063	1.8546E-10	5.7455959	0.1	0.90483742
	0.0010972	1.5714596	3.2415E-05	2.1275281	2.359E-07	2.9230765	1.8546E-09	3.7186248	0.2	0.81873075
	0.0109717	1.1412591	0.00032415	1.5450991	2.359E-06	2.1228594	1.8546E-08	2.7006195	0.4	0.67032005
	0.109717	0.8910062	0.00324154	1.2062929	2.359E-05	1.6573631	1.8546E-07	2.1084331	0.6	0.54881164
	1.0971705	0.7292944	0.03241542	0.9873587	0.0002359	1.3565626	1.8546E-06	1.7257664	0.8	0.44932896
	10.971705	0.6166965	0.32415416	0.8349175	0.0023593	1.1471189	1.8546E-05	1.4593202	1	0.36787944
	109.71705	0.5339761	3.24154163	0.7229261	0.0235932	0.9932505	0.00018546	1.2635748	1.3	0.27253179
	1097.1705	0.4707194	32.4154163	0.6372657	0.2359317	0.8755864	0.00185457	1.1138872	1.9	0.14956862
	10971.705	0.4208007	324.154163	0.569703	2.359317	0.7827325	0.01854574	0.995762	2.5	0.082085
	109717.05	0.3804182	3241.54163	0.515031	23.59317	0.707617	0.18545738	0.9002029	3	0.04978707
	1097170.5	0.347089	32415.4163	0.4699081	235.9317	0.6456213	1.85457381	0.8213344	3.5	0.03019738
	10971705	0.3191169	324154.163	0.4320379	2359.317	0.5935903	18.5457381	0.7551425	5	0.00673795
									6	0.00247875
									7	0.00091188
									9	0.00012341
									10	4.54E-05

Table D-5 Depletion Solutions Generalized for Figure 5.9

New adaptation of Fetkovich for Other Shapes-Rectangular xy=2:1 Well Near Boundary-Figure 5.9

infinite values from infq.out, finite values from table c-5 Lee book

Depletion Region Stems Various Reservoir Sizes

CA	10.8374	logterm	2.4145937			logterm	3.2113871		
		c1c2	555.68286	448.02359		c1c2	4628.8057	3950.94775	
		c1	2.7794389			c1	3.6966277		
		fetkovich constants				fetkovich constants			
	Equivalent	A/rw^2	1253.4955			A/rw^2	7850.84		
		c1	2.2457323			c1	3.162023		
		c2	199.5			c2	1249.5		
infinite		reD	20			reD =50 depletion	50		
tD	qD	tD	tdD	qD	qdD	tD	tdD	qD	qdD
0.01	6.1289	100	0.1799588	0.3394	0.9433415	600	0.1296231	0.2852	0.98034566
0.1	2.2488	130	0.2339464	0.3174	0.8821939	800	0.1728308	0.2915	1.07756697
1	0.98443	160	0.287934	0.2975	0.8268831	1000	0.2160384	0.2393	0.88460301
10	0.53392	200	0.3599175	0.2728	0.7582309	1300	0.28085	0.222	0.82065135
100	0.34558	240	0.431901	0.2502	0.6954156	1600	0.3456615	0.206	0.7615053
1000	0.25098	300	0.5398763	0.2197	0.6106427	2000	0.4320769	0.1865	0.68942108
10000	0.19593	400	0.719835	0.177	0.4919607	2400	0.5184923	0.1682	0.62177278
100000	0.16037	500	0.8997938	0.1426	0.396348	3000	0.6481153	0.1543	0.57038965
1000000	0.13561	600	1.0797526	0.1148	0.3190796	4000	0.8641538	0.1133	0.41882792
10000000	0.11742	700	1.2597113	0.0925	0.2570981	5000	1.0801922	0.0833	0.30792909
100000000	0.10351	800	1.4396701	0.0745	0.2070682	6000	1.2962307	0.0682	0.25211001
1E+09	0.092533	1000	1.7995876	0.0483	0.1342469	8000	1.7283076	0.0418	0.15451904
1E+10	0.083653	1300	2.3394639	0.0283	0.0786581	10000	2.1603845	0.0254	0.09389434
1E+11	0.076324	1600	2.8793402	0.0132	0.0366886	13000	2.8084998	0.012	0.04435953
1E+12	0.070173	2000	3.5991752	0.0056	0.0155649	16000	3.4566152	0.0056	0.02070112
		3000	5.3987628	0.0006	0.0016677	20000	4.3207689	0.0021	0.00776292
						24000	5.1849227	0.0006	0.00221798
						30000	6.4811534	0.0002	0.00073933

Table D-5 Depletion Solutions Generalized for Figure 5.9 Continued

logterm	3.81357741			logterm	4.415669975		
c1c2	21993.74438	19273.92334		c1c2	101872.2221	90964.07317	
c1	4.389808956			c1	5.082877709		
fetkovich constants				fetkovich constants			
A/rw^2	31412.78494			A/rw^2	125660.5646		
c1	3.855170186			c1	4.548317367		
c2	4999.5			c2	19999.5		
reD=100	100			reD=200	200		
tD	tdD	qD	qdD	tD	tdD	qD	qdD
2000	0.090934948	0.2304	1.011411984	10000	0.098162186	0.1943	0.987603139
3000	0.136402422	0.2179	0.958539372	13000	0.127610842	0.186	0.945415254
4000	0.181869896	0.207	0.908690454	16000	0.157059497	0.182	0.925083743
5000	0.22733737	0.1967	0.863475422	20000	0.196324372	0.1742	0.885437297
6000	0.272804844	0.1869	0.820455294	24000	0.235589246	0.1668	0.847824002
8000	0.363739792	0.1686	0.74012179	30000	0.294486558	0.1562	0.793945498
10000	0.45467474	0.1536	0.674274656	40000	0.392648743	0.1401	0.712111167
13000	0.591077161	0.1304	0.572431088	50000	0.490810929	0.1236	0.628243685
16000	0.727479583	0.1118	0.490780641	60000	0.588973115	0.1126	0.57233203
20000	0.909349479	0.091	0.399472615	80000	0.785297487	0.0905	0.460000433
24000	1.091219375	0.0741	0.325284844	100000	0.981621858	0.0728	0.370033497
30000	1.364024219	0.0645	0.283142678	130000	1.276108416	0.0524	0.266342792
40000	1.818698958	0.0326	0.143107772	160000	1.570594974	0.0378	0.192132777
50000	2.273373698	0.0195	0.085601275	200000	1.963243717	0.0244	0.124022216
60000	2.728048437	0.0117	0.051360765	240000	2.35589246	0.0138	0.070143712
80000	3.637397916	0.0042	0.018437198	300000	2.944865575	0.0082	0.041679597
100000	4.546747396	0.0015	0.006584713	400000	3.926487434	0.0026	0.014232058
110000	5.001422135	0.0009	0.003950828	500000	4.908109292	0.0009	0.00457459

Table D-5 Depletion Solutions Generalized for Figure 5.9 Continued

logterm	5.211569113			logterm	5.813620407		
c1c2	751477.4937	683073.28		c1c2	3353175.435	3078874.561	
c1	5.999025695			c1	6.692058451		
fetkovich constants				fetkovich constants			
A/rw^2	785395.0218			A/rw^2	3141589.512		
c1	5.464608098			c1	6.157755279		
c2	124999.5			c2	499999.5		
reD=500	500			reD=1000	1000		

tD	tdD	qD	qdD	tD	tdD	qD	qdD
100000	0.133071184	0.1566	0.939447424	30000	0.008946743	0.1773	1.186501963
130000	0.172992539	0.1498	0.898654049	40000	0.011928991	0.1729	1.157056908
160000	0.212913895	0.1435	0.860860187	50000	0.014911239	0.1697	1.135642319
200000	0.266142368	0.1354	0.812268079	100000	0.029822478	0.1604	1.073406175
240000	0.319370842	0.1277	0.766075581	200000	0.059644956	0.1518	1.015854473
300000	0.399213553	0.117	0.701886006	300000	0.089467433	0.1464	0.979717357
400000	0.532284737	0.1012	0.6071014	400000	0.119289911	0.1416	0.947595477
500000	0.665355921	0.0875	0.524914748	500000	0.149112389	0.1371	0.917481214
600000	0.798427105	0.0756	0.453526343	600000	0.178934867	0.1327	0.888036156
800000	1.064569474	0.0565	0.338944952	700000	0.208757345	0.1285	0.859929511
1000000	1.330711842	0.0422	0.253158884	800000	0.238579822	0.1244	0.832492071
1300000	1.729925395	0.0273	0.163773401	900000	0.2684023	0.1204	0.805723837
1600000	2.129138947	0.0176	0.105582852	1000000	0.298224778	0.1166	0.780294015
2000000	2.661423684	0.0098	0.058790452	1400000	0.417514689	0.1024	0.685266785
2400000	3.193708421	0.0055	0.032994641	2000000	0.596449556	0.0844	0.564809733
3000000	3.992135527	0.0023	0.013797759	2400000	0.715739467	0.0741	0.495881531
4000000	5.322847369	0.0005	0.002999513	3000000	0.894674334	0.061	0.408215565
5000000	6.653558211	0.0001	0.000599903	4000000	1.192899112	0.0442	0.295788984
				5000000	1.49112389	0.032	0.21414587
				7000000	2.087573446	0.0167	0.111757376
				8400000	2.505088136	0.0106	0.07093582
				10000000	2.982247781	0.0063	0.042159968
				14000000	4.175146893	0.0017	0.011376499
				20000000	5.964495561	0.0004	0.002676823
				30000000	8.946743342	0.0001	0.000669206

Table D-5 Depletion Solutions Generalized for Figure 5.9 Continued

logterm	7.813620837			logterm	9.813620841		
c1c2	450673858.2	423017014.4		c1c2	56802982197	53814627319	
c1	8.994258946			c1	11.29845895		
fetkovich constants				fetkovich constants			
A/rw^2	314159262.2			A/rw^2	31415926533		
c1	8.460340372			c1	10.76292546		
c2	49999999.5			c2	5000000000		
reD=10000	10000			reD= 1e5 depletion	100000		
tD	tdD	qD	qdD	tD	tdD	qD	qdD
3000000	0.006656699	0.1263	1.135974905	140000000	0.002473368	0.1017	1.148849875
4000000	0.008875598	0.124	1.115288109	200000000	0.003533383	0.1	1.129645895
5000000	0.011094498	0.1222	1.099098443	240000000	0.004240059	0.099	1.118349436
6000000	0.013313397	0.121	1.088305332	300000000	0.005300074	0.098	1.107052977
8000000	0.017751196	0.1188	1.068517963	350000000	0.00618342	0.0971	1.096886164
10000000	0.022188995	0.1174	1.055926	400000000	0.007066765	0.0966	1.091237935
12000000	0.026626794	0.1162	1.045132889	500000000	0.008833457	0.0956	1.079941476
14000000	0.031064593	0.1152	1.036138631	600000000	0.010600148	0.0948	1.070904309
16000000	0.035502392	0.1143	1.028043797	700000000	0.01236684	0.0941	1.062996787
18000000	0.039940191	0.1135	1.02084839	800000000	0.014133531	0.0935	1.056218912
20000000	0.04437799	0.1128	1.014552409	840000000	0.014840207	0.0933	1.05395962
24000000	0.053253588	0.1115	1.002859872	900000000	0.015900222	0.093	1.050570682
30000000	0.066566985	0.1098	0.987569632	1000000000	0.017666914	0.0925	1.044922453
40000000	0.08875598	0.1071	0.963285133	1400000000	0.024733679	0.0911	1.02910741
50000000	0.110944975	0.106	0.944397189	2000000000	0.035333827	0.0896	1.012162722
70000000	0.155322965	0.0998	0.897627043	3000000000	0.053000741	0.0877	0.99069945
80000000	0.17751196	0.0975	0.876940247	4000000000	0.070667655	0.0861	0.972625116
90000000	0.199700955	0.0952	0.856253452	5000000000	0.088334568	0.0845	0.954550781
100000000	0.22188995	0.093	0.836466062	6000000000	0.106001482	0.0829	0.936476447
120000000	0.26626794	0.0887	0.797790768	7000000000	0.123668396	0.0814	0.919531759
140000000	0.31064593	0.0846	0.760914307	8000000000	0.141335309	0.0799	0.90258707
170000000	0.377212916	0.0788	0.708747605	9000000000	0.159002223	0.0784	0.885642382
200000000	0.443779901	0.0734	0.660178607	10000000000	0.176669137	0.077	0.869827339
240000000	0.532535881	0.0668	0.600816498	13000000000	0.229669878	0.0728	0.822382212
300000000	0.665669851	0.058	0.521667019	16000000000	0.282670619	0.0689	0.778326022
400000000	0.887559801	0.0458	0.41193706	20000000000	0.353338273	0.0639	0.721843727
500000000	1.109449752	0.0362	0.325592174	24000000000	0.424005928	0.0594	0.671009662
600000000	1.331339702	0.0286	0.257235806	30000000000	0.53000741	0.0531	0.59984197
700000000	1.553229652	0.0226	0.203270252	40000000000	0.706676547	0.0441	0.49817384
800000000	1.775119602	0.0178	0.160097809	50000000000	0.883345684	0.0366	0.413450398
1000000000	2.218899503	0.0111	0.099836274	60000000000	1.06001482	0.0304	0.343412352
1400000000	3.106459304	0.0043	0.038675313	70000000000	1.236683957	0.0253	0.285800411
2000000000	4.437799006	0.0011	0.009893685	80000000000	1.413353094	0.021	0.237225638
3000000000	6.656698509	0.0001	0.000899426	90000000000	1.59002223	0.0174	0.196558386
				1E+11	1.766691367	0.0145	0.163798655
				1.3E+11	2.296698777	0.0083	0.093760609

Table D-6 Depletion Solutions Generalized for Figure 5.7 Continued

New adaptation of Fetkovich for rectangular shape x:y=2:1 Well at Center Figure 5.7

infinite values from infq.out, finite values from table c-5 Lee book

Depletion Region Stems Various Reservoir Sizes

CA	21.8369	logterm	2.1103279			logterm	2.9071212		
		c1c2	485.66059	448.02359		c1c2	4190.2452	3950.94775	
		c1	2.4291984			c1	3.3463872		
		fetkovich constants				fetkovich constants			
	Equivalent	A/rw^2	1253.4955			A/rw^2	7850.84		
		c1	2.2457323			c1	3.162023		
		c2	199.5			c2	1249.5		
infinite		reD	20			reD =50 depletion	50		
tD	qD	tD	tdD	qD	qdD	tD	tdD	qD	qdD
0.01	6.1269	100	0.2059051	0.3394	0.8244699	600	0.1431897	0.2652	0.88746189
0.1	2.2458	130	0.2676766	0.3174	0.7710276	800	0.1909196	0.2915	0.97547188
1	0.98443	160	0.3294482	0.2975	0.7226865	1000	0.2386495	0.2393	0.80079046
10	0.53392	200	0.4118102	0.2726	0.6626853	1300	0.3102444	0.222	0.74289797
100	0.34556	240	0.4941723	0.2502	0.6077854	1600	0.3818392	0.206	0.68935677
1000	0.25096	300	0.6177153	0.2197	0.5336949	2000	0.477299	0.1865	0.62410122
10000	0.19593	400	0.8236205	0.177	0.4299681	2400	0.5727588	0.1682	0.56286233
100000	0.16037	500	1.0295256	0.1426	0.3464037	3000	0.7159486	0.1543	0.51634755
1000000	0.13561	600	1.2354307	0.1148	0.278872	4000	0.9545981	0.1133	0.37914567
10000000	0.11742	700	1.4413358	0.0925	0.2247009	5000	1.1932476	0.0833	0.27875406
100000000	0.10351	800	1.6472409	0.0745	0.1809753	6000	1.4318971	0.0682	0.22822361
1E+09	0.092533	1000	2.0590511	0.0483	0.1173303	8000	1.9091962	0.0418	0.13987899
1E+10	0.083653	1300	2.6767665	0.0283	0.0687463	10000	2.3864952	0.0254	0.08499824
1E+11	0.076324	1600	3.2944818	0.0132	0.0320654	13000	3.1024438	0.012	0.04015665
1E+12	0.070173	2000	4.1181023	0.0056	0.0136035	16000	3.8183923	0.0056	0.01873977
		3000	6.1771534	0.0006	0.0014575	20000	4.7729904	0.0021	0.00702741
						24000	5.7275885	0.0006	0.00200783
						30000	7.1594856	0.0002	0.00066928

Table D-6 Depletion Solutions Generalized for Figure 5.7 Continued

logterm	3.508311528			logterm	4.111404083		
c1c2	20238.97575	19273.92334		c1c2	94852.62108	90984.07317	
c1	4.039568498			c1	4.732637252		
fetkovich constants				fetkovich constants			
A/rw^2	31412.78494			A/rw^2	125660.5646		
c1	3.855170186			c1	4.548317367		
c2	4998.5			c2	19999.5		
reD=100	100			reD=200	200		
tD	tdD	qD	qdD	tD	tdD	qD	qdD
2000	0.09881923	0.2304	0.930718582	10000	0.105426712	0.1943	0.919551418
3000	0.148228845	0.2179	0.880221976	13000	0.137054726	0.186	0.880270529
4000	0.19763846	0.207	0.836190679	16000	0.16868274	0.182	0.86133998
5000	0.247048075	0.1967	0.794583124	20000	0.210853425	0.1742	0.824425409
6000	0.29845769	0.1869	0.754995353	24000	0.25302411	0.1668	0.789403894
8000	0.39527692	0.1686	0.681071249	30000	0.316280137	0.1562	0.739237939
10000	0.49409615	0.1536	0.620477722	40000	0.421706849	0.1401	0.663042479
13000	0.642324996	0.1304	0.526759732	50000	0.527133562	0.1236	0.584953964
16000	0.79055384	0.1118	0.451623758	60000	0.632560274	0.1126	0.532894955
20000	0.9881923	0.091	0.367600733	80000	0.843413699	0.0905	0.428303671
24000	1.18583076	0.0741	0.299332026	100000	1.054267124	0.0728	0.344535992
30000	1.482288451	0.0645	0.260552168	130000	1.370547261	0.0524	0.247990192
40000	1.976384601	0.0326	0.131689933	160000	1.686827398	0.0378	0.178893688
50000	2.470480751	0.0195	0.078771586	200000	2.108534247	0.0244	0.115476349
60000	2.964576901	0.0117	0.047262951	240000	2.530241097	0.0138	0.065310394
80000	3.952769201	0.0042	0.016966188	300000	3.162801371	0.0082	0.038807625
100000	4.940961502	0.0015	0.006059353	400000	4.217068495	0.0028	0.013251384
110000	5.435057652	0.0009	0.003635612	500000	5.271335619	0.0009	0.004259374

Table D-6 Depletion Solutions Generalized for Figure 5.7 Continued

logterm	4.907283231			logterm	5.509354525		
c1c2	707604.0659	683073.28		c1c2	3177681.198	3078874.561	
c1	5.648785238			c1	6.341817994		
fetkovich constants				fetkovich constants			
A/rw^2	785395.0218			A/rw^2	3141589 512		
c1	5.464608098			c1	6.157755279		
c2	124999.5			c2	499999.5		
reD=500	500			reD=1000	1000		
tD	tdD	qD	qdD	tD	tdD	qD	qdD
100000	0.141321969	0.1566	0.884599788	30000	0.009440846	0.1773	1.12440433
130000	0.18371856	0.1498	0.846188029	40000	0.012587795	0.1729	1.096500331
160000	0.226115151	0.1435	0.810600882	50000	0.015734744	0.1697	1 076206514
200000	0.282643938	0.1354	0.764845521	100000	0.031469488	0.1604	1.017227606
240000	0.339172726	0.1277	0.721349875	200000	0.062938976	0.1516	0.962687971
300000	0.423965908	0.117	0.660907873	300000	0.094408464	0 1464	0.928442154
400000	0.565287877	0.1012	0.571657086	400000	0.125877952	0 1416	0.898001428
500000	0.706609846	0.0875	0 494268708	500000	0.15734744	0.1371	0.869463247
600000	0.847931815	0.0756	0.427048164	600000	0.188816927	0.1327	0 841559248
800000	1.130575754	0.0565	0.319156366	700000	0.220286415	0.1285	0.814923612
1000000	1 413219692	0 0422	0.238378737	800000	0.251755903	0.1244	0.788922158
1300000	1 8371856	0.0273	0.154211837	900000	0.283225391	0.1204	0.763554886
1600000	2.261151507	0.0176	0.09941862	1000000	0.314694879	0.1166	0.739455978
2000000	2.826439384	0.0098	0.055358095	1400000	0.440572831	0.1024	0.649402163
2400000	3.391727261	0.0055	0.031068319	2000000	0.629389758	0.0844	0.535249439
3000000	4.239659076	0 0023	0.012992206	2400000	0.75526771	0.0741	0.469928713
4000000	5.652878768	0.0005	0.002824393	3000000	0.944084637	0.061	0.386850898
5000000	7 06609846	0.0001	0.000564879	4000000	1.258779516	0 0442	0.280308355
				5000000	1.573474395	0.032	0.202938176
				7000000	2.202864153	0.0167	0.10590836
				8400000	2.643436984	0.0106	0.067223271
				10000000	3.14694879	0.0063	0.039953453
				14000000	4.405728306	0.0017	0.010781091
				20000000	6.29389758	0.0004	0.002536727
				30000000	9.44084637	0.0001	0.000634182

Table D-6 Depletion Solutions Generalized for Figure 5.7 Continued

logterm	7.509354955			logterm	9.509354959		
c1c2	433124417.1	423017014.4		c1c2	54848038065	53814627319	
c1	8.644018489			c1	10.94621849		
fetkovich constants				fetkovich constants			
A/rw^2	314159262.2			A/rw^2	31415926533		
c1	8.460340372			c1	10.76292546		
c2	49999999.5			c2	5000000000		
reD=10000	10000			reD= 1e5 depletion	100000		
tD	tdD	qD	qdD	tD	tdD	qD	qdD
3000000	0.006926416	0.1263	1.091739535	140000000	0.002552507	0.1017	1.113230421
4000000	0.009235222	0.124	1.071858293	200000000	0.003646439	0.1	1.094621849
5000000	0.011544027	0.1222	1.056299059	240000000	0.004375726	0.099	1.083675631
6000000	0.013852832	0.121	1.045926237	300000000	0.005469658	0.098	1.072729412
8000000	0.018470443	0.1188	1.026909396	350000000	0.006381267	0.0971	1.062877816
10000000	0.023088054	0.1174	1.014807771	400000000	0.007292877	0.0966	1.057404706
12000000	0.027705665	0.1162	1.004434948	500000000	0.009116096	0.0956	1.046458488
14000000	0.032323276	0.1152	0.99579093	600000000	0.010939316	0.0948	1.037701513
16000000	0.036940887	0.1143	0.988011313	700000000	0.012762535	0.0941	1.03003916
18000000	0.041558497	0.1135	0.981096098	800000000	0.014585754	0.0935	1.023471429
20000000	0.046176108	0.1128	0.975045286	840000000	0.015315042	0.0933	1.021282185
24000000	0.05541133	0.1115	0.963808061	900000000	0.016408973	0.093	1.01799832
30000000	0.069264162	0.1098	0.94911323	1000000000	0.018232193	0.0925	1.012525211
40000000	0.092352217	0.1071	0.92577438	1400000000	0.02552507	0.0911	0.997200505
50000000	0.115440271	0.105	0.907621941	2000000000	0.036464385	0.0896	0.980781177
70000000	0.161616379	0.0998	0.862673045	3000000000	0.054696578	0.0877	0.959983362
80000000	0.184704433	0.0975	0.842791803	4000000000	0.072928771	0.0861	0.942469412
90000000	0.207792487	0.0952	0.82291056	5000000000	0.091160964	0.0845	0.924955463
100000000	0.230880542	0.093	0.803893719	6000000000	0.109393156	0.0829	0.907441513
120000000	0.27705665	0.0887	0.76672444	7000000000	0.127625349	0.0814	0.891022185
140000000	0.323232758	0.0846	0.731283984	8000000000	0.145857542	0.0799	0.874602858
170000000	0.392496921	0.0788	0.681148657	9000000000	0.164089734	0.0784	0.85818353
200000000	0.461761083	0.0734	0.634470957	10000000000	0.182321927	0.077	0.842858824
240000000	0.5541133	0.0668	0.577420435	13000000000	0.237018505	0.0728	0.796884706
300000000	0.692641625	0.058	0.501353072	16000000000	0.291715083	0.0689	0.754194454
400000000	0.923522166	0.0458	0.395896047	20000000000	0.364643854	0.0639	0.699463362
500000000	1.154402708	0.0362	0.312913469	24000000000	0.437572625	0.0594	0.650205379
600000000	1.38528325	0.0286	0.247218929	30000000000	0.546965781	0.0531	0.581244202
700000000	1.616163791	0.0226	0.195354818	40000000000	0.729287709	0.0441	0.482728236
800000000	1.847044333	0.0178	0.153863529	50000000000	0.911609636	0.0366	0.400631597
1000000000	2.308805416	0.0111	0.095948605	60000000000	1.093931563	0.0304	0.332765042
1400000000	3.232327583	0.0043	0.03716928	70000000000	1.27625349	0.0253	0.276939328
2000000000	4.617610832	0.0011	0.00950842	80000000000	1.458575417	0.021	0.229870588
3000000000	6.926416249	0.0001	0.000864402	90000000000	1.640897344	0.0174	0.190464202
				1E+11	1.823219271	0.0145	0.158720168
				1.3E+11	2.370185053	0.0083	0.090853613
				1.6E+11	2.917150834	0.0048	0.052541849

Table D-7 Depletion Solutions Generalized for Figure 5.8

New adaptation of Fetkovich for rectangular shape x:y=4:1 Figure 5.8

infinite values from infq.out, finite values from table c-5 Lee book

Depletion Region Stems Various Reservoir Sizes

CA	5.379	logterm	2.7188173			logterm	3.5158107		
		c1c2	625.69539	448.02359		c1c2	5067 3053	3950.94775	
		c1	3.1296306			c1	4.0468194		
		fetkovich constants				fetkovich constants			
	Equivalent	A/rw^2	1253.4955			A/rw^2	7850.84		
		c1	2.2457323			c1	3.162023		
		c2	199 5			c2	1249.5		
infinite		reD	20			reD =50 depletion	50		
tD	qD	tD	tdD	qD	qdD	tD	tdD	qD	qdD
0.01	6.1289	100	0.1598222	0.3394	1 0621966	600	0.1184061	0.2652	1.07321651
0.1	2.2488	130	0.2077688	0.3174	0 9933447	800	0.1578748	0.2915	1.17964786
1	0 98443	160	0.2557155	0.2975	0.9310651	1000	0.1973435	0.2393	0 96840389
10	0.53392	200	0 3196444	0.2728	0.8537632	1300	0.2565466	0.222	0.89839391
100	0.34556	240	0.3835732	0.2502	0.7830336	1600	0.3157497	0.206	0.8336448
1000	0.25096	300	0.4794665	0.2197	0.6875798	2000	0.3946871	0.1865	0.75473182
10000	0.19593	400	0.6392887	0.177	0.5539446	2400	0.4736245	0.1682	0.68067503
100000	0.16037	500	0.7991109	0.1426	0.4462853	3000	0.5920306	0.1543	0.62442424
1000000	0.13561	600	0.9589331	0.1148	0 3592816	4000	0.7893742	0.1133	0.45850464
10000000	0.11742	700	1 1187552	0.0925	0.2894908	5000	0.9867177	0.0833	0.33710006
100000000	0.10351	800	1 2785774	0.0745	0.2331575	6000	1 1840613	0 0682	0.27599308
1E+09	0.092533	1000	1 5982218	0.0483	0.1511612	8000	1.5787484	0.0418	0.16915705
1E+10	0.083653	1300	2.0776883	0.0283	0.0885685	10000	1 9734355	0.0254	0.10278921
1E+11	0 076324	1600	2.5571548	0 0132	0 0413111	13000	2.5654661	0 012	0.04856183
1E+12	0 070173	2000	3 1964435	0.0056	0 0175259	16000	3.1574968	0.0056	0.02266219
		3000	4 7946653	0.0006	0.0016778	20000	3.946871	0.0021	0.00849832
						24000	4 7362452	0.0006	0.00242809
						30000	5.9203065	0.0002	0.00080936

Table D-7 Depletion Solutions Generalized for Figure 5.8 Continued

logterm	4.117800969			logterm	4.719893534		
c1c2	23748.26893	19273.92334		c1c2	108890.8467	90964.07317	
c1	4.740000695			c1	5.433069447		
fetkovich constants				fetkovich constants			
A/rw^2	31412.78494			A/rw^2	125660.5646		
c1	3.855170186			c1	4.548317367		
c2	4999.5			c2	19999.5		
reD=100	100			reD=200	200		
tD	tdD	qD	qdD	tD	tdD	qD	qdD
2000	0.084216665	0.2304	1.09209616	10000	0.091835083	0.1943	1.055645394
3000	0.126324997	0.2179	1.032846151	13000	0.119385609	0.186	1.010550917
4000	0.168433329	0.207	0.981180144	16000	0.146936134	0.182	0.988818639
5000	0.210541662	0.1967	0.932358137	20000	0.183670167	0.1742	0.946440698
6000	0.252649994	0.1869	0.88590613	24000	0.2204042	0.1668	0.906235984
8000	0.336866658	0.1686	0.799164117	30000	0.27550525	0.1562	0.848645448
10000	0.421083323	0.1536	0.728064107	40000	0.367340334	0.1401	0.76117303
13000	0.54740832	0.1304	0.618096091	50000	0.459175417	0.1236	0.671527384
16000	0.673733317	0.1118	0.529932078	60000	0.551010501	0.1126	0.61176362
20000	0.842166646	0.091	0.431340063	80000	0.734680668	0.0905	0.491692785
24000	1.010599975	0.0741	0.351234052	100000	0.918350835	0.0728	0.395527456
30000	1.263249969	0.0645	0.305730045	130000	1.193856085	0.0524	0.284692839
40000	1.684333292	0.0326	0.154524023	160000	1.469361336	0.0378	0.205370025
50000	2.105416615	0.0195	0.092430014	200000	1.83670167	0.0244	0.132566895
60000	2.526499938	0.0117	0.055458008	240000	2.204042004	0.0138	0.074976358
80000	3.368666585	0.0042	0.019908003	300000	2.755052505	0.0082	0.044551169
100000	4.210833231	0.0015	0.007110001	400000	3.67340334	0.0028	0.015212594
110000	4.631916554	0.0009	0.004266001	500000	4.591754174	0.0009	0.004889763

Table D-7 Depletion Solutions Generalized for Figure 5.8 Continued

logterm	5.515782672			logterm	6.117843966		
c1c2	795344.8167	683073.28		c1c2	3528645.262	3078874.561	
c1	6.349217433			c1	7.042250189		
fetkovich constants				fetkovich constants			
A/rw^2	785395.0218			A/rw^2	3141589.512		
c1	5.464606098			c1	6.157755279		
c2	124999.5			c2	499999.5		
reD=500	500			reD=1000	1000		
tD	tdD	qD	qdD	tD	tdD	qD	qdD
100000	0.125731629	0.1566	0.99428745	30000	0.008501846	0.1773	1.248590959
130000	0.163451118	0.1498	0.951112772	40000	0.011335795	0.1729	1.217605058
160000	0.201170607	0.1435	0.911112702	50000	0.014169744	0.1697	1.195069857
200000	0.251463259	0.1354	0.85968404	100000	0.028339488	0.1604	1.12957693
240000	0.301755911	0.1277	0.810795066	200000	0.056678976	0.1518	1.069013579
300000	0.377194888	0.117	0.74285844	300000	0.085018464	0.1464	1.030985428
400000	0.502926518	0.1012	0.642540804	400000	0.113357952	0.1416	0.997182627
500000	0.628658147	0.0875	0.555558525	500000	0.14169744	0.1371	0.965492501
600000	0.754389776	0.0756	0.480000838	600000	0.170036928	0.1327	0.9345066
800000	1.005853035	0.0565	0.358730785	700000	0.198376416	0.1285	0.904929149
1000000	1.257316294	0.0422	0.267936976	800000	0.226715904	0.1244	0.876055924
1300000	1.634511182	0.0273	0.173333636	900000	0.255055392	0.1204	0.847886923
1600000	2.011705071	0.0176	0.111746227	1000000	0.28339488	0.1166	0.821126372
2000000	2.514632588	0.0098	0.062222331	1400000	0.396752832	0.1024	0.721126419
2400000	3.017559106	0.0055	0.034920696	2000000	0.56678976	0.0844	0.594365916
3000000	3.771948882	0.0023	0.0146032	2400000	0.680147712	0.0741	0.521830739
4000000	5.029265176	0.0005	0.003174609	3000000	0.85018464	0.061	0.429577262
5000000	6.28658147	0.0001	0.000634922	4000000	1.133579519	0.0442	0.311267458
				5000000	1.416974399	0.032	0.225352006
				7000000	1.983764159	0.0167	0.117605578
				8400000	2.380516991	0.0106	0.074647852
				10000000	2.833948798	0.0063	0.044366176
				14000000	3.967528318	0.0017	0.011971825
				20000000	5.667897597	0.0004	0.0028169
				30000000	8.501846395	0.0001	0.000704225

Table D-7 Depletion Solutions Generalized for Figure 5.8 Continued

logterm	8.117844396			logterm	10.1178444		
c1c2	468220858.2	423017014.4		c1c2	58357682217	53814827319	
c1	9.344450684			c1	11.64665069		
fetkovich constants				fetkovich constants			
A/rw^2	314159262.2			A/rw^2	31415926533		
c1	8.460340372			c1	10.76292546		
c2	49999999.5			c2	5000000000		
reD=10000	10000			reD= 1e5 depletion	100000		
tD	tdD	qD	qdD	tD	tdD	qD	qdD
3000000	0.006407233	0.1263	1.180204121	140000000	0.002398999	0.1017	1.184464375
4000000	0.008542977	0.124	1.158711885	200000000	0.003427141	0.1	1.164665069
5000000	0.010678721	0.1222	1.141891874	240000000	0.004112569	0.099	1.153018418
6000000	0.012814465	0.121	1.130678533	300000000	0.005140711	0.098	1.141371768
8000000	0.017085954	0.1188	1.110120741	350000000	0.005997497	0.0971	1.130889782
10000000	0.021357442	0.1174	1.09703851	400000000	0.006854282	0.0966	1.125068457
12000000	0.025628931	0.1162	1.085825169	500000000	0.008567852	0.0956	1.113419806
14000000	0.029900419	0.1152	1.076480719	600000000	0.010281423	0.0948	1.104102485
16000000	0.034171908	0.1143	1.068070713	700000000	0.011994993	0.0941	1.09594983
18000000	0.038443396	0.1135	1.060595153	800000000	0.013708564	0.0935	1.088961839
20000000	0.042714885	0.1128	1.054054037	840000000	0.014393992	0.0933	1.086632509
24000000	0.051257862	0.1115	1.041906251	900000000	0.015422134	0.093	1.083138514
30000000	0.064072327	0.1098	1.026020685	1000000000	0.017135705	0.0925	1.077315189
40000000	0.08542977	0.1071	1.000790688	1400000000	0.023989986	0.0911	1.061009878
50000000	0.106787212	0.105	0.981167322	2000000000	0.034271409	0.0896	1.043539902
70000000	0.149502097	0.0998	0.932576178	3000000000	0.051407114	0.0877	1.021411265
80000000	0.170859539	0.0975	0.911083942	4000000000	0.068542818	0.0861	1.002776624
90000000	0.192216981	0.0952	0.889591705	5000000000	0.085678523	0.0845	0.984141983
100000000	0.213574424	0.093	0.869033914	6000000000	0.102814227	0.0829	0.965507342
120000000	0.256289309	0.0887	0.828852776	7000000000	0.119949932	0.0814	0.948037366
140000000	0.299004193	0.0846	0.790540528	8000000000	0.137085636	0.0799	0.93056739
170000000	0.36307652	0.0788	0.736342714	9000000000	0.154221341	0.0784	0.913097414
200000000	0.427148848	0.0734	0.68588268	10000000000	0.171357045	0.077	0.896792103
240000000	0.512578617	0.0668	0.624209306	13000000000	0.222784159	0.0728	0.84787817
300000000	0.640723271	0.058	0.54197814	16000000000	0.274171273	0.0689	0.802454232
400000000	0.854297695	0.0458	0.427975841	20000000000	0.342714091	0.0639	0.744220979
500000000	1.067872119	0.0362	0.338269115	24000000000	0.411256909	0.0594	0.691811051
600000000	1.281446543	0.0286	0.26725129	30000000000	0.514071136	0.0531	0.618437152
700000000	1.495020966	0.0226	0.211184585	40000000000	0.685428182	0.0441	0.513617295
800000000	1.70859539	0.0178	0.166331222	50000000000	0.856785227	0.0366	0.426267415
1000000000	2.135744238	0.0111	0.103723403	60000000000	1.028142272	0.0304	0.354058181
1400000000	2.990041933	0.0043	0.040181138	70000000000	1.199499318	0.0253	0.294660262
2000000000	4.271488476	0.0011	0.010278896	80000000000	1.370856363	0.021	0.244579664
3000000000	6.407232713	0.0001	0.000934445	90000000000	1.542213408	0.0174	0.202651722
				1E+11	1.713570454	0.0145	0.168876435
				1.3E+11	2.22784159	0.0083	0.096667201
				1.6E+11	2.741712726	0.0048	0.055903923

Table D-8 Derivative Solutions for Type Curve

red		10		red		20		red		50	
c1		1.8025851		c1		2.49573227		c1		3.412023	
tD	qD'	qDd'	qDd'*tD	tD	qD'	qDd'	qDd'*tD	tD	qD'	qDd'	qDd'*tD
8.97E-05				6.03E-05				7.04E-05			
1.01E-04	29775.045	53672.053	5.41E+00	1.00E-04	13000.0852	32444.7321	3.26E+00	9.38E-05	5179.77644	17673.52	1.66E+00
1.12E-04	26155.886	47148.211	5.28E+00	1.21E-04	9826.41694	24524.1059	2.96E+00	1.17E-04	3675.76078	12541.78	1.47E+00
2.24E-04	10675.902	19244.222	4.31E+00	1.41E-04	7772.56857	19398.2502	2.73E+00	1.41E-04	2716.94699	9270.286	1.30E+00
3.36E-04	5241.0206	9447.3856	3.18E+00	1.61E-04	6350.64695	15849.5146	2.55E+00	1.64E-04	2222.341	7582.679	1.25E+00
4.48E-04	3299.2985	5947.2663	2.67E+00	1.81E-04	5319.76953	13276.7205	2.40E+00	1.88E-04	1928.57308	6580.336	1.23E+00
5.60E-04	2329.7772	4199.6217	2.35E+00	2.01E-04	4676.77476	11671.9777	2.34E+00	2.35E-04	1397.80868	4769.355	1.12E+00
6.72E-04	1760.9755	3174.3081	2.13E+00	4.02E-04	1923.1715	4799.72118	1.93E+00	4.69E-04	571.768351	1950.887	0.9152
7.85E-04	1392.8547	2510.7392	1.97E+00	6.03E-04	952.948696	2378.30481	1.43E+00	7.04E-04	290.444828	991.0044	0.69735
8.97E-04	1138.0668	2051.4622	1.84E+00	8.03E-04	604.881326	1509.62185	1.21E+00	9.38E-04	187.61149	640.1347	0.6006
1.01E-03	953.16004	1718.1521	1.73E+00	1.00E-03	429.33279	1071.4997	1.08E+00	1.17E-03	135.375153	461.9031	0.54172
1.12E-03	838.49914	1511.466	1.69E+00	1.21E-03	317.272174	791.826404	0.95423	1.41E-03	104.269374	355.7695	0.50071
2.24E-03	344.65141	621.2635	1.39E+00	1.41E-03	259.548272	647.762999	0.91069	1.64E-03	83.7849331	285.8761	0.46938
3.36E-03	170.74072	307.77467	1.03E+00	1.61E-03	225.261315	562.191934	0.90333	1.88E-03	69.4726752	237.0424	0.44481
4.48E-03	108.40747	195.41368	0.87602	2.01E-03	163.252198	407.433778	0.81829	2.11E-03	58.9800003	201.2411	0.42482
5.60E-03	76.949077	138.70726	0.77726	4.02E-03	66.7813323	166.668326	0.66949	2.35E-03	52.3375457	178.5769	0.41887
6.72E-03	56.875093	102.5222	0.68939	6.03E-03	33.9051566	84.6181933	0.50986	4.69E-03	22.9781905	78.40211	0.3678
7.85E-03	46.504391	83.828122	0.65764	8.03E-03	21.9055019	54.6702681	0.43921	7.04E-03	12.1825643	41.56719	0.2925
8.97E-03	40.377147	72.783243	0.65256	1.00E-02	15.8198759	39.4821749	0.39648	9.38E-03	8.08422472	27.58356	0.2588
1.12E-02	29.2601	52.743821	0.5911	1.21E-02	12.178453	30.3941582	0.36628	1.17E-02	5.94734046	20.29246	0.23799
2.24E-02	11.966644	21.570693	0.48349	1.41E-02	9.78553615	24.4220784	0.34335	1.41E-02	4.64819298	15.85974	0.22321
3.36E-02	6.0783893	10.956814	0.36839	1.61E-02	8.1091879	20.238362	0.32519	1.64E-02	3.78619075	12.91857	0.21211
4.48E-02	3.9279484	7.0804613	0.31741	1.81E-02	6.88429028	17.1813454	0.31057	1.88E-02	3.17368036	10.82867	0.2032
5.60E-02	2.8339864	5.1085017	0.28626	2.01E-02	6.11619673	15.2643896	0.30657	2.11E-02	2.71783929	9.27333	0.19576
6.72E-02	2.1828836	3.9348334	0.26459	4.02E-02	2.68426063	6.6991959	0.2691	2.35E-02	2.42889096	8.287432	0.19439
7.85E-02	1.7546986	3.1629935	0.24814	6.03E-02	1.42343802	3.55252021	0.21405	4.69E-02	1.1139237	3.800733	0.1783
8.97E-02	1.4533199	2.6197328	0.23488	8.03E-02	0.94712206	2.3637631	0.1899	7.04E-02	0.61879097	2.111329	0.14857
0.10087	1.2360667	2.2281154	0.22475	1.00E-01	0.70752129	1.76578371	0.17732	9.38E-02	0.43694797	1.490877	0.13988
0.11207	1.1052606	1.9923262	0.22328	0.12051	0.57221573	1.42809725	0.1721	1.17E-01	0.3537067	1.206855	0.14154
0.22414	0.5945577	1.0717409	0.24022	0.14059	0.49197007	1.22782559	0.17262	0.14074	0.31194808	1.064374	0.1498
0.33622	0.4441272	0.800577	0.26917	0.16068	0.44168005	1.10231516	0.17712	0.16419	0.28858303	0.984652	0.16167
				0.18076	0.40886349	1.02041381	0.18445	0.18765	0.27396421	0.934772	0.17541
				0.20084	0.38985093	0.97298355	0.19541	0.21111	0.26364958	0.899578	0.18991
				0.40169	0.29780231	0.74323483	0.29855	0.23456	0.25800878	0.873508	0.20489

Table D-8 Derivative Solutions For Type Curve Continued

red	100			red	200			red	1000		
c1	4.10517			c1	4.79831737			c1	6.407755		
tD	qD'	qDd'	qDd'*tD	tD	qD'	qDd'	qDd'*tD	tD	qD'	qDd'	qDd'*tD
3.41E-06				7.29E-06				6.24E-05			
3.90E-05	9286.604	38123.09	1.49E+00	8.34E-06	43418.727	208336.832	1.74E+00	9.36E-05	460.731	2952.252	0.27644
4.87E-05	6727.817	27618.83	1.35E+00	1.04E-05	31457.9456	150945.207	1.573	1.25E-04	312.7468	2004.005	0.2502
9.74E-05	2752.72	11300.39	1.10E+00	2.08E-05	8580.3808	41171.3902	1.2871	1.56E-04	234.0113	1499.487	0.23401
1.46E-04	1397.86	5738.455	0.83879	3.13E-05	4902.61508	23524.3031	0.98054	1.87E-04	185.2364	1186.949	0.22228
1.95E-04	903.1022	3707.388	0.72257	4.17E-05	3378.34906	16210.391	0.84461	2.18E-04	152.4824	977.0699	0.21348
2.44E-04	651.9838	2676.504	0.65205	5.21E-05	2539.956	12187.515	0.762	2.50E-04	128.7612	825.0701	0.20602
2.92E-04	501.9476	2060.58	0.60239	6.25E-05	2010.8371	9648.63457	0.70381	2.81E-04	111.2554	712.8974	0.20026
3.41E-04	403.1924	1655.173	0.56453	7.29E-05	1650.12662	7917.83122	0.66007	3.12E-04	100.2206	642.1889	0.20044
3.90E-04	334.4677	1373.047	0.5362	8.34E-05	1390.19073	6670.57632	0.6256	6.24E-04	47.32527	303.2488	0.1893
4.39E-04	283.963	1165.717	0.51119	9.38E-05	1194.04202	5729.39257	0.59706	9.36E-04	26.82487	171.8872	0.16096
4.87E-04	251.7544	1033.495	0.50356	1.04E-04	588.789801	2825.20033	0.5888	1.25E-03	18.51962	118.6692	0.1482
9.74E-04	103.1395	423.4053	0.4126	2.08E-04	344.86851	1654.78856	0.51732	1.56E-03	14.00108	89.71549	0.14001
1.46E-03	58.66818	240.8429	0.35204	3.13E-04	205.721436	987.116741	0.41145	1.87E-03	11.20354	71.78953	0.13439
1.95E-03	38.894	159.6665	0.31119	4.17E-04	145.600081	698.635395	0.36401	2.18E-03	9.299083	59.58625	0.13019
2.44E-03	28.62409	117.5068	0.28627	5.21E-04	111.5814	535.402972	0.33475	2.50E-03	7.900544	50.62475	0.12641
2.92E-03	22.39803	91.94773	0.2688	6.25E-04	89.7406875	430.604299	0.3141	2.81E-03	6.850546	43.89662	0.12331
3.41E-03	18.24733	74.90838	0.25549	7.29E-04	74.570808	357.814403	0.29819	3.12E-03	6.175035	39.56811	0.1235
3.90E-03	15.27353	62.70043	0.2444	8.33E-04	63.4652289	304.52631	0.2856	6.24E-03	2.997517	19.20736	0.1199
4.39E-03	13.073	53.66688	0.23534	9.38E-04	56.0684037	264.235678	0.27536	9.36E-03	1.732491	11.10138	0.10395
4.87E-03	11.69381	48.00509	0.2339	1.04E-03	27.3235267	131.106953	0.27324	1.25E-02	1.212513	7.769483	0.097
9.74E-03	5.359456	22.00148	0.2144	2.08E-03	16.7067767	80.1644169	0.25061	0.01561	0.925066	5.927592	0.09251
1.46E-02	2.952241	12.11945	0.17715	3.13E-03	10.3498207	49.6617245	0.207	0.01873	0.742454	4.757462	0.08909
1.95E-02	2.002131	8.219087	0.16019	4.17E-03	7.49579822	35.9672188	0.1674	0.02185	0.619929	3.972356	0.08679
2.44E-02	1.499848	6.15713	0.15	5.21E-03	5.84156548	28.0296851	0.17525	0.02497	0.530038	3.396356	0.08481
2.92E-02	1.187396	4.874461	0.1425	6.25E-03	4.74845662	22.7846019	0.1662	0.02809	0.455888	2.92122	0.08206
3.41E-02	0.977395	4.012373	0.13685	7.29E-03	3.99638277	19.1855095	0.15994	0.03121	0.415797	2.664328	0.08316
3.90E-02	0.82742	3.396701	0.1324	8.34E-03	3.43992207	16.5058378	0.1548	0.06242	0.224324	1.437412	0.08973
4.39E-02	0.712421	2.92461	0.12825	9.38E-03	2.99640432	14.3776989	0.14983	0.09364	0.164171	1.051967	0.0985
4.87E-02	0.641935	2.635252	0.1284	1.04E-02	1.49337413	7.16568303	0.14934	0.12485	0.149073	0.955226	0.11926
9.74E-02	0.336686	1.38207	0.13488	2.08E-02	0.94530184	4.53585823	0.1418	0.15606	0.142411	0.912534	0.14241
1.46E-01	0.245045	1.005952	0.14704	3.13E-02	0.60223957	2.88973658	0.12045	0.18727	0.137536	0.881294	0.16504
0.1949	0.220623	0.905695	0.17652	4.17E-02	0.44398805	2.13039556	0.111	0.21849	0.133111	0.852945	0.18636
0.24362	0.207549	0.852024	0.20757	5.21E-02	0.34359405	1.64867329	0.10572	0.2497	0.128836	0.825551	0.20614
0.29234	0.196924	0.808408	0.23633	6.25E-02	0.2940786	1.41108247	0.10308	0.28091	0.124811	0.799758	0.22466
0.34107	0.187101	0.768083	0.26197	7.29E-02	0.26199232	1.25712229	0.10293	0.31212	0.121126	0.776144	0.24225
0.38979	0.177627	0.729188	0.28423	8.34E-02	0.24066121	1.15476889	0.1048				
				9.38E-02	0.22896505	1.09864696	0.1063				
				0.10421	0.18522679	0.88877693	0.11449				
				0.20841	0.16387454	0.78632205	0.18523				
				0.31262	0.14694745	0.70510052	0.24582				
				0.41682			0.2939				

Table D-8 Derivative Solutions For Type Curve Continued

red		10000		red		100000	
c1		8.71034037		c1		11.0129255	
tD	qD'	qDd'	qDd'*tD	tD	qD'	qDd'	qDd'*tD
1.84E-05				7.26E-06			
2.07E-05	932.5598	8122.91314	0.16786	9.08E-06	1120.1	12335.8314	0.11201
2.30E-05	843.9079	7350.72514	0.16878	1.09E-05	905.11	9967.87812	0.10861
4.59E-05	407.5038	3549.49697	0.163	1.27E-05	757.52	8342.51101	0.10605
6.89E-05	235.4988	2051.27461	0.1413	1.45E-05	650.02	7158.59031	0.104
9.18E-05	164.4873	1432.73994	0.13159	1.63E-05	570.02	6277.53304	0.1026
1.15E-04	125.7357	1095.20077	0.12574	1.82E-05	516.56	5688.87665	0.10331
1.38E-04	101.0063	879.799668	0.12121	3.63E-05	256.75	2827.56532	0.1027
1.61E-04	84.25636	733.901574	0.11796	5.45E-05	152.25	1676.73134	0.09135
1.84E-04	72.00614	627.197997	0.11521	7.26E-05	107.75	1186.62757	0.0862
2.07E-04	62.75584	546.624728	0.11296	9.08E-05	83.255	916.886091	0.08326
2.30E-04	56.94053	495.97143	0.11388	1.09E-04	67.502	743.39207	0.081
4.59E-04	27.95026	243.458296	0.1118	1.27E-04	56.501	622.246696	0.0791
6.89E-04	16.39958	142.845944	0.0984	1.45E-04	48.751	536.894273	0.078
9.18E-04	11.54936	100.598835	0.0924	1.63E-04	48.095	529.66685	0.07695
1.15E-03	8.874297	77.2981448	0.08875	1.82E-04	42.941	472.901371	0.07729
1.38E-03	7.150359	62.2820643	0.08581	3.63E-04	38.901	428.40859	0.0778
1.61E-03	5.975302	52.046911	0.08366	5.45E-04	17.437	192.037684	0.06975
1.84E-03	5.150242	44.8603626	0.0824	7.26E-04	11.067	121.875516	0.0884
2.07E-03	4.500243	39.1986451	0.081	9.08E-04	8.0312	88.4474546	0.06425
2.30E-03	4.057488	35.3421018	0.08115	1.09E-03	6.2404	68.7253585	0.0624
4.59E-03	2.029994	17.6819389	0.0812	1.27E-03	5.1043	56.2132893	0.06125
6.89E-03	1.202477	10.4739853	0.07215	1.45E-03	4.3144	47.5141598	0.0604
9.18E-03	0.854949	7.44689422	0.0684	1.63E-03	3.7407	41.1963106	0.05985
1.15E-02	0.657448	5.72659176	0.06575	1.82E-03	3.3799	37.2222222	0.06084
1.38E-02	0.532531	4.63852796	0.06391	3.63E-03	3.05	33.5897577	0.061
1.61E-02	0.450024	3.91986561	0.063	5.45E-03	1.3762	15.156521	0.05505
1.84E-02	0.385018	3.35363928	0.0616	7.26E-03	0.8733	9.61803197	0.0624
2.07E-02	0.335018	2.91812243	0.0603	9.08E-03	0.6375	7.02114479	0.051
0.022961	0.304823	2.65511084	0.06096	1.09E-02	0.415	4.57075991	0.0498
0.045922	0.166899	1.45374766	0.06676	0.012712	0.35	3.85462555	0.049
0.068884	0.122848	1.07004529	0.07371	0.014528	0.3025	3.3314978	0.0484
0.091845	0.112067	0.97614459	0.08965	0.016344	0.265	2.9185022	0.0477
0.11481	0.107796	0.9389426	0.1078	0.01816	0.2419	2.66365639	0.04837
0.13777	0.105006	0.91464034	0.12601	0.036321	0.1324	1.4580821	0.05296
0.16073	0.102506	0.89286381	0.14351	0.054481	0.098	1.07955067	0.05882
0.18369	0.100056	0.87152267	0.16009	0.072642	0.0897	0.98758294	0.07174
0.20665	0.097776	0.85168159	0.176	0.090802	0.0866	0.95380058	0.08661
0.22961	0.095651	0.83315187	0.1913	0.10896	0.0848	0.93346182	0.10171
0.45922	0.076168	0.66345107	0.30467	0.12712	0.0832	0.9157489	0.11641
				0.14528	0.0816	0.89812775	0.13048
				0.16344	0.0801	0.88215859	0.14418
				0.1816	0.0788	0.86734581	0.15751
				0.36321	0.0657	0.72382368	0.2629
				0.54481	0.0546	0.60131056	0.3276
				0.72642	0.0454	0.49951819	0.36286
				0.90802	0.0377	0.4148587	0.3767
				1.09E+00	0.0313	0.34440162	0.37526

Table D-9 Arps Derivative Solutions For Type Curve

b values	0	0.1	0.2	0.3	0.4	0.5	0.6	0.7	0.8	0.9	1
tdD	qDd*tDd										
0.1	0.09048374	0.08963237	0.0888	0.08798	0.087173	0.086384	0.08561	0.084848	0.0841	0.08336591	0.08264
0.5	0.30326533	0.29233964	0.28224	0.27286	0.264141	0.256	0.24838	0.241238	0.234521	0.228194	0.22222
1	0.36787944	0.3504939	0.3349	0.32081	0.308001	0.296296	0.28555	0.275638	0.266463	0.25794088	0.25
1.5	0.33469524	0.32241483	0.31076	0.2998	0.289515	0.279883	0.27086	0.262407	0.254472	0.24701639	0.24
2	0.27067057	0.26917597	0.26582	0.26092	0.255609	0.25	0.24429	0.238594	0.232991	0.22752531	0.22222
2.5	0.2052125	0.21474836	0.21948	0.22119	0.220971	0.219479	0.21715	0.214284	0.211065	0.20783347	0.20408
3	0.14936121	0.16739573	0.17881	0.18586	0.189951	0.192	0.19262	0.192227	0.191115	0.18948912	0.1875
3.5	0.10569084	0.12894265	0.145	0.156	0.163429	0.168295	0.17131	0.172956	0.173602	0.17350014	0.17284
4	0.07326256	0.09877604	0.1178	0.13129	0.141141	0.148148	0.15303	0.15632	0.158396	0.15955285	0.16
4.5	0.04999048	0.07553783	0.09565	0.11098	0.122507	0.131088	0.13741	0.141984	0.145214	0.14739819	0.14876
5	0.03368973	0.0578061	0.07813	0.09431	0.108917	0.116818	0.12402	0.129598	0.133748	0.13676725	0.13889
5.5	0.02247724	0.04433166	0.06413	0.08059	0.093829	0.104296	0.11249	0.118847	0.12373	0.12742989	0.13018
6	0.01487251	0.03410605	0.05292	0.06926	0.082789	0.09375	0.10252	0.109468	0.114931	0.11918339	0.12245
6.5	0.00977235	0.02633844	0.04391	0.05984	0.073427	0.084673	0.09384	0.101238	0.10716	0.11186074	0.11556
7	0.00638317	0.0204249	0.03663	0.05198	0.065442	0.076818	0.08625	0.093979	0.100259	0.10532405	0.10938
7.5	0.00414813	0.01590899	0.03072	0.04538	0.058594	0.069981	0.07957	0.087541	0.0941	0.09945957	0.10381
8	0.0026837	0.0124478	0.0259	0.03981	0.052689	0.064	0.07367	0.081803	0.088577	0.09417322	0.09877
8.5	0.00172948	0.0097843	0.02194	0.03508	0.04757	0.058741	0.06842	0.076666	0.0836	0.08938689	0.09418
9	0.00111069	0.00772597	0.01868	0.03105	0.043111	0.054095	0.06374	0.072045	0.079097	0.08503536	0.09
9.50E+00	0.00071109	0.00612834	0.01597	0.02759	0.039208	0.049971	0.05955	0.067872	0.075007	0.08106392	0.08617
1.00E+01	0.000454	0.00488281	0.01372	0.02461	0.035777	0.046296	0.05577	0.064089	0.071278	0.07742637	0.08264
2.00E+01	4.1223E-08	0.0001129	0.00128	0.00435	0.009145	0.015026	0.0214	0.027849	0.034082	0.03994285	0.04535
3.00E+01	2.8073E-12	7.1526E-06	0.00025	0.00139	0.003787	0.007324	0.01167	0.01648	0.021466	0.02642469	0.03122
4.00E+01	1.6993E-16	8.192E-07	7.5E-05	0.0006	0.001975	0.004319	0.00749	0.011234	0.015325	0.01956194	0.0238
5.00E+01	9.6437E-21	1.3782E-07	2.8E-05	0.0003	0.001178	0.002845	0.00527	0.008308	0.011755	0.015442	0.01922
6.00E+01	5.2539E-25	3.0344E-08	1.2E-05	0.00017	0.000768	0.002014	0.00395	0.006474	0.009445	0.01270727	0.01612
7.00E+01	2.7828E-29	8.1491E-09	6.1E-06	0.00011	0.000533	0.0015	0.00308	0.005236	0.007841	0.01076593	0.01389
8.00E+01	1.4439E-33	2.5493E-09	3.3E-06	7E-05	0.000388	0.001161	0.00249	0.004353	0.006669	0.00931984	0.01219
9.00E+01	7.3746E-38	9E-10	1.9E-06	4.8E-05	0.000292	0.000925	0.00206	0.003697	0.005778	0.00820293	0.01087
1.00E+02	3.7201E-42	3.5049E-10	1.2E-06	3.4E-05	0.000227	0.000754	0.00173	0.003192	0.005081	0.00731553	0.0098
5.00E+02							0.00012	0.000329	0.000695	0.00124655	0.00199
1.00E+03							3.9E-05	0.000123	0.000293	0.00057843	0.001

APPENDIX E

DERIVATION OF GENERALIZED DECLINE CURVE EQUATIONS

Derivation of Generalized Decline Curve Equations

Fetkovich[3] (1980) presented a useful form of the solution of Tsarevich and Kuranov[11] (1966) to prepare type curves of dimensionless rate versus dimensionless time. Observation of the type curves shows that transition from the infinite acting transient to the PSS is instantaneous at t_{pss}. Irregular outer geometry will however affect the infinite acting period and postpone true pseudo-steady state production and cause a transition zone. This research will show how to extend and construct type curves to illustrate this phenomenon for various reservoir shape factors and well positions with in the reservoir.

Fetkovich prepared a type curve of dimensionless rate versus dimensionless time using the following relationship[4].

$$q_D = \frac{141.5 q \mu B}{kh(P_i - P_{wf})} \qquad \textbf{E1}$$

$$t_D = \frac{0.00634kt}{\phi \mu c_t r_{wa}^2} \qquad \textbf{E2}$$

$$r_{wa} = r_w e^{-S} \qquad \textbf{E3}$$

$$r_{wa} = \frac{x_f}{2} \qquad \textbf{E4}$$

An irregular outer geometry or off center well location can create a period of transition between transient and PSS production. This transition zone has not been the focus of much research but it may provide valuable information about the reservoir shape and permit more accurate curve fitting.

A general expression for PSS decline for constant pressure according to the analytical solution is:

$$q_D = Ae^{-Bt_D} \qquad \textbf{E5}$$

Where A and B are constants defined by the ratio r_e/r_{wa}. Fetkovich developed expressions for A and B which reflect different ratios of r_e/r_{wa}. The higher the ratio the larger is the time to pseudosteady state t_Dpss.

$$A = \frac{1}{\ln(r_e/r_{wa}) - 0.5} \qquad \textbf{E6}$$

$$B = \frac{2A}{(r_e/r_{wa})^2 - 1} \qquad \textbf{E7}$$

The expressions for A and B reflect the observation that different ratios of r_e/r_{wa} give different depletion stems. The higher the ratio of r_e/r_{wa} the larger the time to pseudosteady state t_Dpss and the lower is q_D at the start of depletion.

Exponential decline, according to the analytical solution, is substantiated by many field observations. The primary observation in Arp's[1] work (1945) suggested that all conventional depletion declines can be expressed by three types of: hyperbolic, exponential and harmonic.

Perhaps not well known, the Fetkovich Type Curves are based on a strictly radial system operating above the bubble point with the well centrally located. It is obviously desirable to derive a more general case that would apply to any particular reservoir drainage shape such as rectangular, triangular, and reservoirs in which the well is displaced from the reservoir center. It would also be desirable to modify the curves for cases below the bubble point. This method utilizes shape factors derived for these various conditions such as shown in Earlouger's Table C-1 in *Advances in Well Testing*. Application of these factors to the Fetkovich system is not straightforward. I have derived a system that will incorporate all reservoir shapes, positions and later will be applied to vertically fractured and horizontal wells using an equivalent well bore radius concept.

Based on the productivity and decline theory of the previous section Fetkovich defined q_{Dd} as:

$$q_{Dd} = \frac{q(t)}{q_{i\,max}} = \frac{141.3\mu B q(t)}{kh(P_i - P_{wf})}\left[\ln\frac{r_e}{r_w} - \frac{1}{2}\right] = q_D\left[\ln\frac{r_e}{r_w} - \frac{1}{2}\right] = q_D c_1 \qquad \textbf{E8}$$

Now instead of using the radial form let us begin with a more general equation such as that found on page 243 in Craft and Hawkins in terms of the shape factors and drainage area A so that:

$$q(i) = \frac{kh(P_i - P_{wf})}{162.6\mu B}\left[\log\frac{4A}{1.781C_A r_w^2}\right] = \frac{kh(P_i - P_{wf})}{141.3\mu B}\left[1.151\log\frac{4A}{1.781C_A r_w^2}\right] \qquad \textbf{E9}$$

Then applying the Fetkovich definition above and converting constants to Fetkovich's definitions of q_D:

$$q_{Dd} = \frac{q(t)}{q_i} = \frac{q(t)}{\dfrac{kh(p_i - p_{wf})}{141.3\mu B\left[1.151\log\dfrac{4A}{1.781C_A r_w^2}\right]}} \qquad \textbf{E10}$$

But since:

$$q_D = \frac{141.3\mu B q(t)}{kh(P_i - P_{wf})} \qquad \textbf{E11}$$

$$q_{Dd} = \frac{q(t)}{q_{i\,max}} = q_D\left[1.151\left[\log\frac{4A}{1.781C_A r_w^2}\right]\right] \qquad \textbf{E12}$$

Therefore we only need to adjust the dimensionless rate values of VanEverdingen and Hurst by the appropriate shape factors, well position and well radius. Since it is desirable to present the more general forms in terms of A/r_w^2 the equivalent radial solutions to q_D and t_D at the various $r_{eD}=r_e/r_w$ values can be obtained by finding equivalent expressions in terms of A/r_w^2 and the various shape factors using the following relationship:

$$\frac{A}{r_w^2} = \pi\left(\frac{r_e}{r_w}\right)^2 - \pi = \pi\left(\left(\frac{r_e}{r_w}\right)^2 - 1\right) \qquad \text{E13}$$

I have confirmed that when the circular shape factor is used, the above derivation is identical to the Fetkovich radial form. Compare Figures 5.6 with 5.2 in chapter 5.

In a similar manner the dimensionless time t_{Dd} was defined by Fetkovich as:

$$t_{Dd} = \left[\frac{q_{i\,max}}{N_{pi}}\right]t = D_i t =$$

$$\frac{0.00634kt}{\phi\mu c_t r_w^2}\left[\frac{1}{\frac{1}{2}\left[\left(\frac{r_e}{r_w}\right)^2 - 1\right]\left[\ln\left(\frac{r_e}{r_w}\right) - \frac{1}{2}\right]}\right] = t_D\left[\frac{1}{\frac{1}{2}\left[\left(\frac{r_e}{r_w}\right)^2 - 1\right]\left[\ln\left(\frac{r_e}{r_w}\right) - \frac{1}{2}\right]}\right] \qquad \text{E14}$$

or:

$$t_{dD} = t_D \frac{2}{c_1 c_2} \qquad \text{E15}$$

Likewise the more general dimensionless time decline can be derived in a manner similar to that of Fetkovich but in terms of the reservoir shape and drainage size factors:

$$t_{Dd} = \left[\frac{q_{i\max}}{N_{pi}}\right]t = D_i t \qquad \textbf{E16}$$

where :

$$q_{i\max} = \frac{khP_i}{162.6\mu B}\left[\frac{1}{\log\dfrac{4A}{1.781C_A r_w^2}}\right] \qquad \textbf{E17}$$

and :

$$N_i = \frac{A\phi c_t hP_i}{5.615B} \qquad \textbf{E18}$$

$$t_{Dd} = \frac{q_{i\max}}{N_i}t = \frac{\dfrac{khP_i}{162.6\mu B}\left[\dfrac{1}{\log\dfrac{4A}{1.781C_A r_w^2}}\right]}{\dfrac{A\phi c_t hP_i}{5.615B}}t \qquad \textbf{E19}$$

$$t_{Dd}=\frac{q_{i\max}}{N_i}t=\frac{0.00634kt}{\phi\mu c_t A}\left[\frac{5.44678}{\log\frac{4A}{1.781C_A r_w^2}}\right] \qquad \textbf{E20}$$

$$t_{Dd}=\frac{0.00634kt}{\phi\mu c_t r_w^2}\frac{r_w^2}{A}\left[\frac{5.44678}{\log\frac{4A}{1.781C_A r_w^2}}\right]=t_D\frac{r_w^2}{A}\left[\frac{5.44678}{\log\frac{4A}{1.781C_A r_w^2}}\right] \qquad \textbf{E21}$$

or putting in a similar arrangement to that of the Fetkovich radial form:

$$t_{Dd}=\frac{t_D}{\frac{A}{r_w^2}\frac{\log\frac{4A}{1.781C_A r_w^2}}{5.44678}}=\frac{t_D}{\frac{0.183594A}{r_w^2}\log\frac{4A}{1.781C_A r_w^2}}=\frac{t_D}{0.183594(c_1 c_2^{\cdot})} \qquad \textbf{E22}$$

Where $c_2^{\cdot}$ is:

$$c_2^{\cdot}=\frac{A}{r_w^2} \qquad \textbf{E23}$$

As compared to c_2 in the Fetkovich radial case:

$$c_2=\frac{r_e}{r_w^2}-1 \qquad \textbf{E24}$$

And:

$$c_1^{'} = \log \frac{4A}{1.781 C_A r_w^2} \qquad \textbf{E25}$$

Again comparing this to the Fetkovich equivalent forms one notes the similarities:

$$c_1 = \ln \frac{r_e}{r_w} - \frac{1}{2} \qquad \textbf{E25}$$

APPENDIX F

BACKGROUND OF EFFECTIVE WELLBORE RADIUS OF A HORIZONTAL WELL

Derivation of Effective Wellbore Radius Of A Horizontal Well

The effective wellbore radius is the theoretical well radius required matching the observed production rate. Thus stimulated wells will have effective wellbore radius greater than the drilled wellbore radius, and damaged wells will have an effective wellbore radius smaller than the drilled wellbore radius.

Due to the longer well length, for a given time period under similar operating conditions, a horizontal well would drain a larger reservoir area than a vertical well. Then each horizontal well would drain either a square of a circular drainage area with a rectangular drainage area at the center. This concept implies that the reservoir thickness is considerably less than the length of the sides of the drainage area. It is possible to calculate the drainage area of a horizontal well by assuming an elliptical drainage area in the horizontal plane with each end of the well as a foci of a drainage ellipse.

Slicter[31,41] showed that ellipses could represent constant pressure (constant porosity) curves (see Figures F-1, F-2) while the hyperbolas represent constant streamlines (constant potential) as:

$$w(z) = \phi + i\Psi = \cosh^{-1}(z/\Delta r) \qquad \mathbf{F1}$$

By definition z=x+iy. Substituting this into the equation and equation real and imaginary parts yields:

$$x=\Delta r \cosh \phi \cos \Psi \qquad \textbf{F2}$$

$$y=\Delta r \sinh \phi \sin \Psi \qquad \textbf{F3}$$

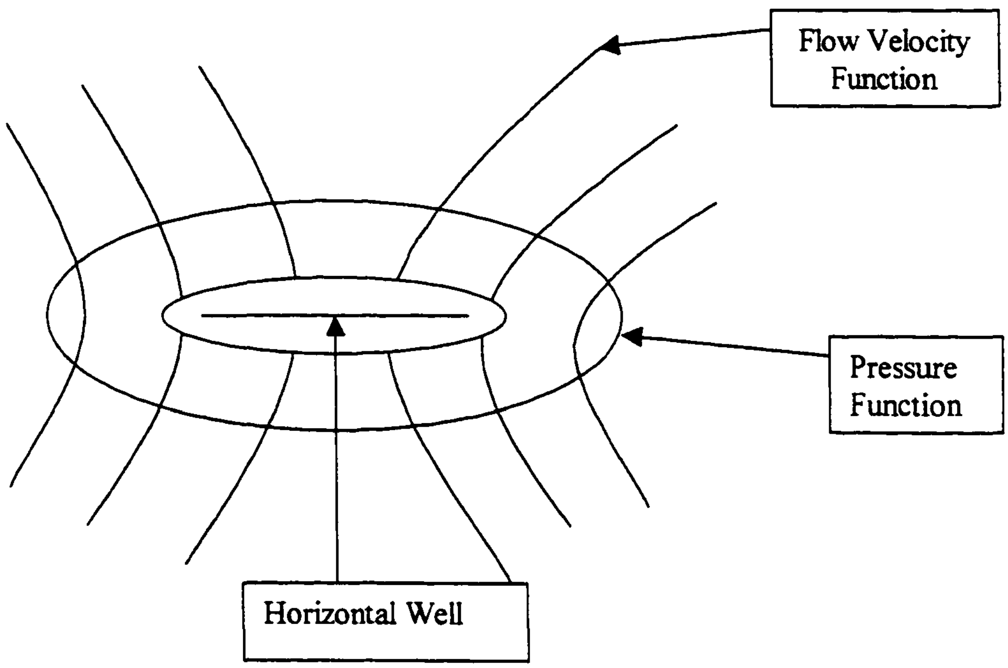

Figure F1 Potential Flow to a Horizontal Well-Horizontal plane

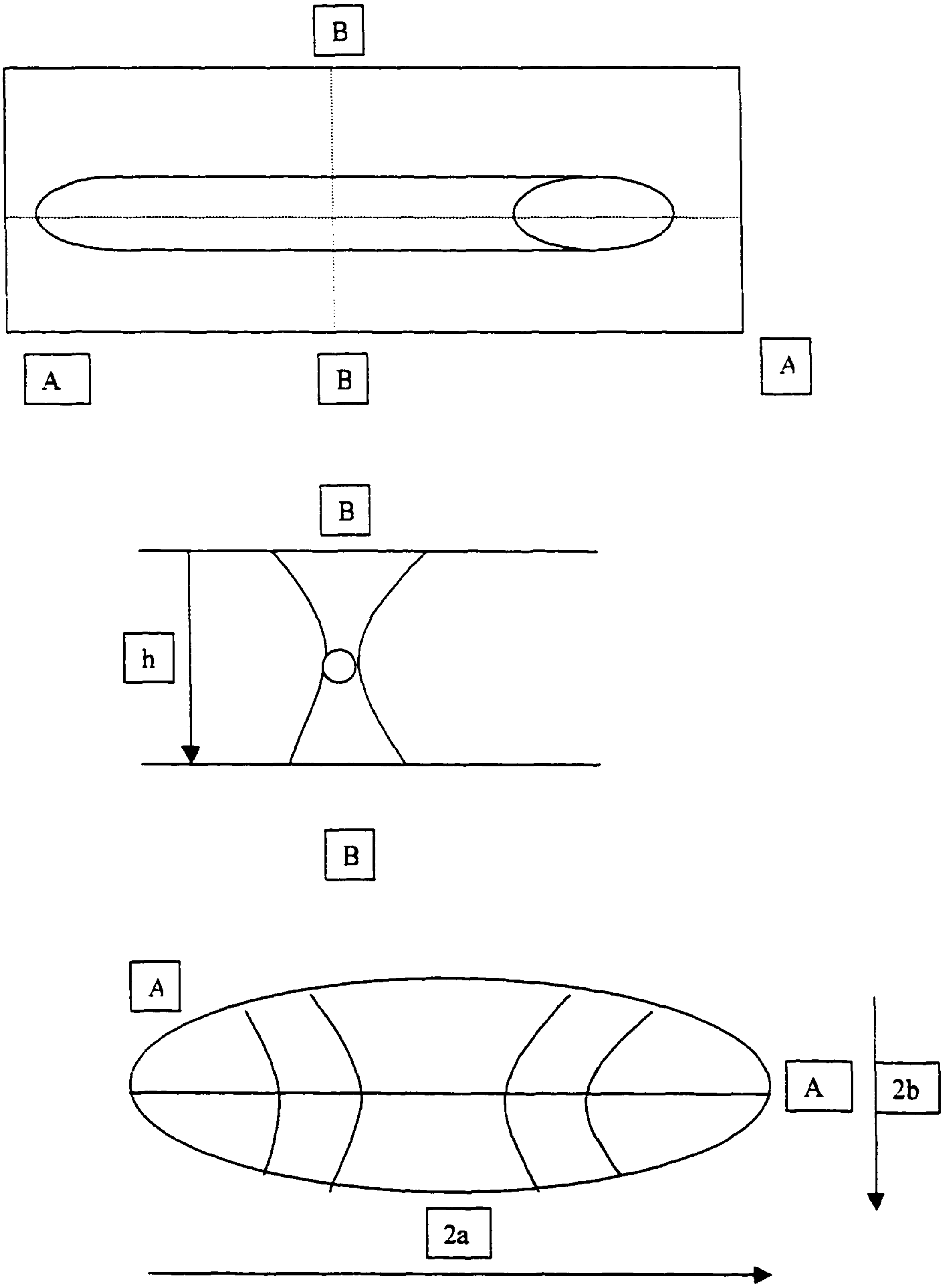

Figure F-2 Division of 3D Horizontal Well Into Two 2-D Problems

The equation with the hyperbolic function represents a classic equation of an ellipse, while the equation with the trigonometric functions represents the equation of the hyperbola. Therefore the above equations can be reformulated as

$$\phi = \cosh^{-1} H^{*}$$

$$\Psi = \cos^{-1} H^{*}$$

where:

$$H^{*} = \left[\frac{x^{2} + y^{2} + \Delta r^{2} \pm \sqrt{(x^{2} + y^{2} + \Delta r^{2})^{2} - 4\Delta r^{2} x^{2}}}{2\Delta r^{2}}\right]^{\frac{1}{2}} \qquad \textbf{F4}$$

The plus sign refers to ϕ and the minus sign refers to Ψ. The pressure drop between drainage boundary and well, Δp is the same as p_e because wellbore pressure is assumed to be zero. The potential function ϕ is the same as the pressure, p. At drainage radius r_{eH} , half the major and minor axes of the ellipse of constant pressure are a and b. Hence the pressure at the drainage boundary p_e is:

$$p_e = \cosh^{-1}\frac{a}{\Delta r} = \ln\frac{\left(a + \sqrt{a^{2} - \Delta r^{2}}\right)}{\Delta r} \qquad \textbf{F5}$$

Because wellbore pressure is assumed to be zero, the pressure drop between the drainage boundary and well, Δp , is the same as p_e defined above,. Substituting this into Darcy's porous medium equation yields:

$$q_1 = \frac{2\pi k_o \Delta p / \mu}{\ln\left(\frac{a+\sqrt{a^2 - \Delta r^2}}{\Delta r}\right)} \qquad \textbf{F6}$$

where Δr is the half length = L/2. Therefore this equation represents the flow to a horizontal well from a horizontal plane.

Since drainage radius in normally used in the calculations, the horizontal well drainage radius r_eH can be represented by equating the areas of a circle and ellipse which reduces to:

$$r_{eH} = \sqrt{ab} \qquad \textbf{F7}$$

where a and b are the major and minor axes of a drainage ellipse and +/- L/2 represent the foci of the drainage ellipse. Thus using the properties of an ellipse, b can be defined as:

$$b = \sqrt{a^2 - (L/2)^2} \qquad \textbf{F8}$$

which upon substituting into the radius equation above yields:

$$r_{eH} = a\left[1 - (l/2a)^2\right]^{\frac{1}{4}} \qquad \textbf{F9}$$

If L/2a is less than 0.5, the effective horizontal radius is approximately equal to a.The flow in the vertical plan can be calculated in a similar manner and yields:

$$q_2 = \frac{2\pi k \Delta p / \mu}{\ln(h / 2r_s)} \qquad \textbf{F10}$$

If we let k_H represent the horizontal permeability and K_V theoretical permeability in a reservoir of thickness h. then the influence of anisotropy in the horizontal versus vertical direction can be represented (Muscat) by the geometric mean of K_V and K_H. Therefore equation for q_1 can be modified to:

$$q_1 = \frac{2\pi\sqrt{K_V \cdot K_H}\, h\Delta p / (\mu / B_o)}{\ln\left(\dfrac{a + \sqrt{a^2 - (L/2)^2}}{L/2}\right)} \qquad \textbf{F11}$$

and for the vertical flow in a horizontal well of length L the vertical flow q_2 can be represented as:

$$q_2 = \frac{2\pi\sqrt{k_V \cdot k_H}\, \Delta p / (\mu / B_o)}{\ln(h / 2r_s)} \qquad \textbf{F12}$$

Now expressing q_1 and q_2 in terms of flow resistance and summing the results yields the flow of a horizontal well as:

$$q_H = \frac{2\pi k_h \Delta p / (\mu / B_o)}{\ln\left[\frac{a + \sqrt{a^2 - (L/2)^2}}{L/2}\right] + \frac{\beta^2 h}{L} \ln \frac{h}{2r_w}} \qquad \textbf{F13}$$

where :

$$\beta = \left(\frac{k_h}{k_v}\right)^{\frac{1}{2}} \qquad \textbf{F14}$$

The effective radius of a horizontal well can then be calculated by converting the productivity of a horizontal well into that of an equivalent vertical well. As demonstrated earlier the effective wellbore radius can be defined as:

$$r_w' = r_w e^{-s} \qquad \textbf{F15}$$

or as shown from type curve matching, it can be obtained from the infinite acting portion of the type curve by:

$$r_{wa} = \frac{r_e}{\left(\frac{r_e}{r_{wa}}\right)_{match}} \qquad \textbf{F16}$$

The following relationship equates the vertical well that is required to produce oil at the same rate as that of a horizontal well, assuming equal drainage volumes, equal actual well bore radii, and equal productivity indices, $(q/\Delta P)_h = (q/\Delta P)_v$.

$$\left[\frac{2\pi k_h}{\mu B \ln\left(\frac{r_e}{r_w^{'}}\right)}\right]_v = \left[\frac{2\pi k_h}{\ln\left[\frac{a+\sqrt{a^2-(L/2)^2}}{L/2}\right]+(h/L)\ln[h/(2r_w)]}\right]_h \quad \textbf{F17}$$

Solving for r_w' yields:

$$r_w^{'} = \frac{0.5 r_{eh} L}{a\left[1+\sqrt{1-\left[\frac{L}{2a}\right]^2}\right]\left[\frac{h}{2r_w}\right]^{\frac{h}{L}}} \quad \textbf{F18}$$

where:

$$a = 0.5L\left[0.5+\sqrt{0.25+\left(\frac{2r_{eh}}{L}\right)^4}\right]^{\frac{1}{2}} \quad \textbf{F19}$$

If the reservoir were anisotropic then the effective wellbore radius would be:

$$r_w^{'} = \frac{0.5 r_{eh} L}{a\left[1+\sqrt{1-\left[\frac{L}{2a}\right]^2}\right]\left[\frac{\beta h}{2r_w}\right]^{\frac{\beta h}{L}}} \quad \textbf{F20}$$

where :

$$\beta = \left(\frac{k_h}{k_v}\right)^{\frac{1}{2}} \quad \textbf{F21}$$

APPENDIX G
Fracture Model Tabular Experimental Results

Model Type1							
28 by 28	phimatrix	0.01	2Xe/L	8.5	ooip	3.373	
	w	0.036			(mmbo)		
	kmatrix	0.1	So	0.75			
	kfracture	1000					

delta t days	average pressure	cum oil mbo	oil rate bopd	gas rate mcf/d	cum gas mmcf	dt hours	dq	dp	q/dp	dp/q	q cum/dp	tp(days) q cum/q	qcum/dq
6	1932	8.61	460	594	8.026	144		68	6.7647	0.147826	129.559	19.15217	
8	1925	9.672	415	470	8.974	192	45	75	5.5333	0.180723	128.96	23.30602	214.93
10	1920	10.42	380	410	9.904	240	80	80	4.75	0.210526	130.25	27.42106	130.25
12	1914	11.16	367	376	10.67	288	93	86	4.2674	0.234332	129.767	30.40872	120
14	1910	11.89	363	340	11.37	336	97	90	4.0333	0.247934	132.111	32.75482	122.58
16	1906	12.61	360	318	12.01	384	100	94	3.8298	0.261111	134.149	35.02778	126.1
18	1902	13.33	358	302	12.63	432	102	98	3.6531	0.273743	136.02	37.23464	130.69
20	1899	14.04	356	290	13.21	480	104	101	3.5248	0.283708	139.01	39.4382	135
22	1895	14.75	353	281	13.78	528	107	105	3.3619	0.29745	140.476	41.7847	137.85
24	1892	15.45	349	274	14.33	576	111	108	3.2315	0.309456	143.056	44.26934	139.19
26	1889	16.14	344	268	14.87	624	116	111	3.0991	0.322674	145.405	46.9186	139.14
31	1880	17.65	332	249	16.7	744	128	120	2.7667	0.361446	147.083	53.16265	137.89
62	1841	27.31	309	167	23.22	1488	151	159	1.9434	0.514563	171.761	88.38188	180.86
123	1787	44.42	233	183	32.97	2952	227	213	1.0939	0.914163	208.545	190.6438	195.68
214	1728	64.6	203	116	44.52	5136	257	272	0.7463	1.339901	237.5	318.2266	251.36
395	1639	96.08	143	92	63.66	9480	317	361	0.3961	2.524476	266.15	671.8881	303.09
576	1572	120.9	125	85	79.8	13824	335	428	0.2921	3.424	282.477	967.2	360.9
942	1480	158.4	86	77	111.2	22608	374	520	0.1654	6.046512	304.615	1841.86	423.53
1308	1434	187.3	74	61	134.3	31392	386	566	0.1307	7.648649	330.919	2531.081	485.23
2304	1363	250	56	41	181.9	55296	404	637	0.0879	11.375	392.465	4464.286	618.81
3400	1306	303.4	40	33	223.3	81600	420	694	0.0576	17.35	437.176	7585	722.38
5996	1217	401.8	31	28	294.6	143904	429	783	0.0396	25.25806	513.155	12961.29	936.6
8592	1150	474.4	27	21	353.1	206208	433	850	0.0318	31.48148	558.118	17570.37	1095.6
11188	1093	536.1	21	19	406.6	268512	439	907	0.0232	43.19048	591.069	25528.57	1221.2
13784	1048	588.7	20	18	452.1	330816	440	952	0.021	47.6	618.382	29435	1338
16380	1005	634.9	16	16	497.3	393120	444	995	0.0161	62.1875	638.09	39681.25	1430
18976	968	675.7	15	15	537.6	455424	445	1032	0.0145	68.8	654.748	45046.67	1518.4
21572	933	712.9	13	15	577.3	517728	447	1067	0.0122	82.07692	668.135	54838.46	1594.9
24168	901	745.8	12	14	614.2	580032	448	1099	0.0109	91.58333	678.617	62150	1664.7

Table G-1 Model 1 Type 1 Fracture Simulation Output and Calculations

Model Type1

28 by 28

phimatrix 0.01

w 0.036

kmatrix 0.1

kfracture 1000

2Xe/L 8.5

Soi 0.75

delta t	cum oil			days/days		hours	
days	mbo	dq/q	dp/p	(tp+dt)/dt	sqrt dt	sqrt dt	d(dq/q)
6	8810	0	0.035197	4.192029	2.4494897	12	
8	9672	0.10843	0.038961	3.913253	2.8284271	13.85640646	
10	10420	0.21053	0.041667	3.742105	3.1622777	15.49193338	0.036243065
12	11160	0.25341	0.044932	3.53406	3.4641016	16.97056275	0.014172829
14	11890	0.26722	0.04712	3.33963	3.7416574	18.33030278	0.006092946
16	12610	0.27778	0.049318	3.189236	4	19.59591794	0.004424643
18	13330	0.28492	0.051525	3.068591	4.2426407	20.78460969	0.003589263
20	14040	0.29213	0.053186	2.97191	4.472136	21.9089023	0.004549967
22	14750	0.30312	0.055409	2.899305	4.6904158	22.97825059	0.006479186
24	15450	0.31805	0.057082	2.844556	4.8989795	24	0.008523289
26	16140	0.33721	0.058761	2.804562	5.0990195	24.97999199	0.009641513
31	17650	0.38554	0.06383	2.714924	5.5677644	27.27636339	0.004207329
62	27310	0.48867	0.086366	2.425514	7.8740079	38.57460304	0.006398987
123	44420	0.97425	0.119194	2.549949	11.090537	54.33231083	0.005114057
214	64600	1.26601	0.157407	2.48704	14.628739	71.66589147	0.004568141
395	96080	2.21678	0.220256	2.700983	19.874607	97.36529156	0.00390605
576	120900	2.68	0.272265	2.679167	24	117.5755077	0.003897722
942	158400	4.34884	0.351351	2.955266	30.692019	150.359669	0.003464776
1308	187300	5.21622	0.3947	2.935077	36.166283	177.1778767	0.002103854
2304	250000	7.21429	0.467351	2.937624	48	235.1510153	0.002525709
3400	303400	10.5	0.531394	3.230882	58.309519	285.6571371	0.001794264
5996	401800	13.8387	0.643385	3.161656	77.433843	379.346807	0.001066456
8592	474400	16.037	0.73913	3.044969	92.693042	454.1013103	0.00136095
11188	536100	20.9048	0.829826	3.281782	105.77334	518.1814354	0.001148491
13784	588700	22	0.908397	3.135447	117.40528	575.166063	0.00131842
16380	634900	27.75	0.99005	3.422543	127.98437	626.9928229	0.001476631
18976	675700	29.6667	1.086116	3.373876	137.7534	674.8510947	0.001277854
21572	712900	34.3846	1.143623	3.542113	146.8741	719.533182	0.001476631
24168	745800	37.3333	1.219756	3.571582	155.46061	761.5983193	

Table G-1 Model 1 Type 1 Fracture Simulation Output and Calculations -Continued

delta t	cum oil				The pressure decline can be compared with actual pressures as a function of time							
days	mbo	q*t	1/q*t	1/q'	q' (deriv)	q'alt	t*Q'	t*Q'alt	p'	p' alt	t*p'	t*p'alt
6	8810											
8	9672	2E+05	0.0004	0.00005	20000	20000	160000	160000	3	3	24	24
10	10420	1E+05	0.0008	8.33E-05	12000	12000	120000	120000	3	3	28	28
12	11160	51000	0.0028	0.000235	4250	4250	51000	51000	3	3	30	30
14	11890	24500	0.008	0.000571	1750	1750	24500	24500	2	2	28	28
16	12610	20000	0 0128	0.0008	1250	1250	20000	20000	2	2	32	32
18	13330	18000	0.018	0.001	1000	1000	18000	18000	2	2	32	32
20	14040	25000	0.016	0.0008	1250	1250	25000	25000	2	2	35	35
22	14750	38500	0.0126	0.000571	1750	1750	38500	38500	2	2	39	39
24	15450	54000	0.0107	0.000444	2250	2250	54000	54000	2	2	36	36
26	16140	64257	0.0105	0.000406	2428.6	2471	63143	64257	1 714286	1 58571	44.57143	41.229
31	17650	67261	0.0143	0.000461	972.22	2170	30139	67261	1.333333	1.72473	41.33333	53.467
62	27310	56529	0.068	0.001097	1076.1	911 8	66717	56529	1 01087	1 13244	62.67391	70.211
123	44420	1E+05	0.1401	0.001139	697 37	878.2	85776	108019	0.743421	0.79018	91.44079	97 192
214	64600	70680	0.6479	0.003028	330.88	330.3	70809	70680	0.544118	0.59695	116 4412	127 53
395	96080	85110	1 8332	0.004641	215.47	215.5	85110	85110	0.430939	0.43094	170.221	170.22
576	120900	58637	5 6581	0.009823	104.2	101 8	60022	58637	0.290676	0.33086	167 4296	190.57
942	158400	65631	13.52	0.014353	69.672	69.67	65631	65631	0.188525	0.18852	177 5902	177 59
1308	187300	37713	45.365	0.034683	22.026	28.83	28811	37713	0.085903	0.11107	112.3612	145.27
2304	250000	37828	140.33	0.060907	16.252	16.42	37446	37828	0.061185	0.06211	140.9713	143.09
3400	303400	38400	301.04	0.088542	6.7714	11 29	23023	38400	0.039545	0.04675	134.4529	158.94
5996	401800	15013	2394.7	0.399385	2.5039	2.504	15013	15013	0.030046	0.03005	180.1572	180.16
8592	474400	16549	4461	0.5192	1 926	1 926	16549	16549	0.023883	0.02388	205.2018	205.2
11188	536100	15084	8298.3	0.741714	1.3482	1.348	15084	15084	0 019646	0.01965	219.7951	219.8
13784	588700	13274	14313	1.0384	0.963	0.963	13274	13274	0.016949	0.01695	233.6271	233.63
16380	634900	15774	17009	1 0384	0.963	0.963	15774	15774	0.015408	0.01541	252.3883	252.39
18976	675700	10965	32841	1.730667	0.5778	0.578	10965	10965	0.013867	0.01387	263.1495	263.15
21572	712900	12465	37334	1 730667	0.5778	0.578	12465	12465	0.012904	0.0129	278.3752	278.38

Table G-1 Model 1 Type 1 Fracture Simulation Output and Calculations -Continued

delta t days	Q'smooth	Q' smooth	Q"smooth	Q"	Q"*t
6					
8	-403	403			
10	-372	372	8750	8750	87500
12	-368	368	2375	2375	28500
14	-363	363	1875	1875	26250
16	-360	360	1250	1250	20000
18	-358	358	1250	1250	22500
20	-355	355	1250	1250	25000
22	-353	353	1875	1875	41250
24	-348	348	4946	4946.429	118714.29
26	-333	333	6959	6309.268	164040.96
31	-303	303	5070	877.44	27200.64
62	-301	301	291	504.5003	31279.019
123	-257	257	660	627.4475	77176.045
214	-206	206	467	372.7803	79774.98
395	-156	156	221	221.2676	87400.695
576	-126	126	142	118.4908	68250.713
942	-91	91	70	69.66672	65626.052
1308	-75	75	37	25.35468	33163.927
2304	-56	56	14	13.93324	32102.196
3400	-46	46	8	6.295238	21403.809
5996	-33	33	4	3.7836	22686.466
8592	-26	26	2	2.10336	18072.072
11188	-22	22	1	1.316919	14733.687
13784	-19	19	1	1.012729	13959.458
16380	-17	17	1	0.771603	12638.859
18976	-15	15	3	3.227378	
21572					

Table G-1 Model 1 Type 1 Fracture Simulation Output and Calculations -Continued

Model Type 1h						
28 by 28	phimatrix	0.01	2Xe/L	8.5	ooip	3.373
	w	0.036			(mmbo)	
	kmatrix	0.1	Soi	0.75		
	kfracture	4000				

delta t days	average pressure	delta q cum oil mbo	oil rate bopd	gas rate mcf/d	cum gas mmcf	dt hours	dq	dp	q/dp	dp/q	q cum/dp	tp(days) q cum/q	qcum/dq
6	1927	9.151	475	662	8.183	144		73	6.5068	0.153684	125.356	19.26526	
8	1921	10.06	436	528	9.22	192	39	79	5.519	0.181193	127.342	23.07339	257.95
10	1916	10.9	426	435	10.16	240	49	84	5.0714	0.197183	129.762	25.58685	222.45
12	1911	11.73	419	391	11.04	288	56	89	4.7079	0.212411	131.798	27.99523	209.46
14	1907	12.54	416	362	11.84	336	59	93	4.4731	0.223558	134.839	30.14423	212.54
16	1902	13.35	414	343	12.58	384	61	98	4.2245	0.236715	136.224	32.24638	218.85
18	1899	14.16	412	330	13.3	432	63	101	4.0792	0.245146	140.198	34.36893	224.76
20	1895	14.96	408	322	14	480	67	105	3.8857	0.257353	142.476	36.66667	223.28
22	1891	15.76	403	317	14.67	528	72	109	3.6972	0.270471	144.587	39.1067	218.89
24	1888	16.54	396	313	15.34	576	79	112	3.5357	0.282828	147.679	41.76768	209.37
26	1885	17.31	389	308	15.98	624	86	115	3.3826	0.29563	150.522	44.49871	201.28
31	1876	19.1	394	237	17.82	744	81	124	3.1774	0.314721	154.032	48.47716	235.8
62	1837	30.54	353	230	25.31	1488	122	163	2.1656	0.461756	187.362	86.51558	250.33
123	1785	51.24	302	157	36.47	2952	173	215	1.4047	0.711921	238.326	169.6689	296.18
214	1728	76.34	243	140	49.81	5136	232	272	0.8934	1.119342	280.662	314.1564	329.05
395	1641	111.9	148	163	76.07	9480	327	359	0.4123	2.425676	311.698	756.0811	342.2
576	1576	135.1	113	101	98.96	13824	362	424	0.2665	3.752212	318.632	1195.575	373.2
942	1494	173.4	93	84	127.7	22608	382	506	0.1838	5.44086	342.688	1864.516	453.93
1308	1441	202.4	73	59	153.3	31392	402	559	0.1306	7.657534	362.075	2772.603	503.48
2304	1359	268.9	57	53	200	55296	418	641	0.0889	11.24561	419.501	4717.544	643.3
3400	1301	320.6	48	23	242.8	81600	427	699	0.0687	14.5625	458.655	6679.167	750.82
5996	1207	419.9	29	27	320.6	143904	446	793	0.0366	27.34483	529.508	14479.31	941.48
8592	1139	494.9	26	25	379.9	206208	449	861	0.0302	33.11538	574.797	19034.62	1102.2
11188	1083	553	22	18	433.3	268512	453	917	0.024	41.68182	603.053	25136.36	1220.8
13784	1035	607.2	18	19	482	330816	457	965	0.0187	53.61111	629.223	33733.33	1328.7
16380	994	651.3	17	16	526.7	393120	458	1006	0.0169	59.17647	647.416	38311.76	1422.1
18976	955	693.3	15	17	569.9	455424	460	1045	0.0144	69.66667	663.445	46220	1507.2
21572	919	728.6	13	15	610.4	517728	462	1081	0.012	83.15385	674.006	56046.15	1577.1
24168	886	761.8	12	15	648.9	580032	463	1114	0.0108	92.83333	683.842	63483.33	1645.4

Table G-2 Model 1 Type 1h Fracture Simulation Output and Calculations

Model Type 1h					
28 by 28	phimatrix 0.01	2Xe/L 8.5		ooip	3.373
	w 0.036			(mmbo)	
	kmatrix 0.1	Soi 0.75			
	kfracture 4000				

delta t	cum oil			days/days		hours		
days	mbo	dq/q	dp/p	(tp+dt)/dt	sqrt dt	sqrt dt	1/q	d(dq/q)
6	3151	0	0.037883	4.210877	2.4494897	12	0.002105263	
8	10060	0.08945	0.041124	3.884174	2.8284271	13.85640646	0.002293578	
10	10900	0.11502	0.043841	3.558685	3.1622777	15.49193338	0.002347418	0.011050503
12	11730	0.13365	0.046572	3.332936	3.4641016	16.97056275	0.002386635	0.006700862
14	12540	0.14183	0.048768	3.153159	3.7416574	18.33030278	0.002403846	0.003422861
16	13350	0.14734	0.051525	3.015399	4	19.59591794	0.002415459	0.002771425
18	14160	0.15291	0.053186	2.909385	4.2426407	20.78460969	0.002427184	0.004218173
20	14960	0.16422	0.055409	2.833333	4.472136	21.9089023	0.00245098	0.006436857
22	15760	0.17866	0.057641	2.777577	4.6904158	22.97825059	0.00248139	0.008819816
24	16540	0.19949	0.059322	2.74032	4.8989795	24	0.002525253	0.01060491
26	17310	0.22108	0.061008	2.711489	5.0990195	24.97999199	0.002570694	0.00086983
31	19100	0.20558	0.066098	2.563779	5.5677644	27.27636339	0.002538071	0.003459149
62	30540	0.34561	0.088732	2.395413	7.8740079	38.57460304	0.002832861	0.003991999
123	51240	0.57285	0.120448	2.379422	11.090537	54.33231083	0.003311258	0.004007391
214	76340	0.95473	0.157407	2.46802	14.628739	71.66589147	0.004115226	0.006016955
395	111900	2.20946	0.218769	2.914129	19.874607	97.36529156	0.006756757	0.006212175
576	135100	3.20354	0.269036	3.075651	24	117.5755077	0.008849558	0.003469959
942	173400	4.10753	0.338688	2.979316	30.692019	150.359569	0.010752688	0.003146598
1308	202400	5.50685	0.387925	3.119727	36.166283	177.1778767	0.01369863	0.002368434
2304	268900	7.33333	0.47167	3.047545	48	235.1510153	0.01754386	0.001619973
3400	320600	8.89583	0.537279	2.984461	58.309519	285.6571371	0.020833333	0.0021793
5996	419900	15.3793	0.657001	3.414828	77.433843	379.346807	0.034482759	0.00161275
8592	494900	17.2692	0.755926	3.215388	92.693042	454.1013103	0.038461538	0.001003775
11188	553000	20.5909	0.846722	3.246725	105.77334	518.1814354	0.045454545	0.001563879
13784	607200	25.3889	0.932367	3.447282	117.40528	575.166063	0.055555556	0.001223087
16380	651300	26.9412	1.012072	3.338936	127.98437	626.9928229	0.058823529	0.001016521
18976	693300	30.6667	1.094241	3.435708	137.7534	674.8510947	0.066666667	0.001655872
21572	728600	35.5385	1.176279	3.598097	146.8741	719.533182	0.076923077	0.001524782
24168	761800	38.5833	1.257336	3.626752	155.46061	761.5963193	0.083333333	

Table G-2 Model 1 Type 1h Fracture Simulation Output and Calculations - Continued

delta t	cum oil	the pressure decline can be compared with actual pressures as a function of time									
days	mbo	1/q'*t	1/q'	q' (deriv)	q'alt	t*Q'	t*Q'alt	p'	p' alt	t*p'	t*p'alt
6	9151										
8	10060	0.0007	8.16E-05	12250	12250	98000	98000	3	3	22	22
10	10900	0.0024	0.000235	4250	4250	42500	42500	3	3	25	25
12	11730	0.0048	0.0004	2500	2500	30000	30000	2	2	27	27
14	12540	0.0112	0.0008	1250	1250	17500	17500	2	2	32	32
16	13350	0.016	0.001	1000	1000	16000	16000	2	2	32	32
18	14160	0.012	0.000667	1500	1500	27000	27000	2	2	32	32
20	14960	0.0089	0.000444	2250	2250	45000	45000	2	2	40	40
22	15760	0.0073	0.000333	3000	3000	66000	66000	2	2	39	39
24	16540	0.0069	0.000286	3500	3500	84000	84000	2	2	36	36
26	17310	0.0117	0.000452	285.71	2214	7428.6	57571	1.714286	1.58571	44.57143	41.229
31	19100	-0.046	-0.00148	1000	-677	31000	-21000	1.333333	1.72473	41.33333	53.467
62	30540	0.0535	0.000863	1000	1159	62000	71836	0.98913	1.12139	61.32609	69.526
123	51240	0.1617	0.001315	723.68	760.7	89013	93570	0.717105	0.76173	88.20395	93.692
214	76340	0.3525	0.001647	566.18	607	121162	129906	0.529412	0.57762	113.2941	123.61
395	111900	1.0999	0.002785	359.12	359.1	141851	141851	0.41989	0.41989	165.8564	165.86
576	135100	3.906	0.006781	100.55	147.5	57916	84941	0.268739	0.31442	154.7934	181.11
942	173400	17.239	0.0183	54.645	54.64	51475	51475	0.184426	0.18443	173.7295	173.73
1308	202400	29.541	0.022585	26.432	44.28	34573	57915	0.099119	0.12802	129.6476	167.45
2304	268900	186.93	0.081132	11.95	12.33	27533	28398	0.066922	0.06833	154.1874	157.43
3400	320600	427.85	0.125839	7.584	7.947	25785	27019	0.04117	0.04796	139.9783	163.06
5996	419900	1415.1	0.236	4.2373	4.237	25407	25407	0.031202	0.0312	187.0863	187.09
8592	494900	6372.8	0.741714	1.3482	1.348	11584	11584	0.023883	0.02388	205.2018	205.2
11188	553000	7261	0.649	1.5408	1.541	17239	17239	0.020031	0.02003	224.1048	224.1
13784	607200	14313	1.0384	0.963	0.963	13274	13274	0.017142	0.01714	236.282	236.28
16380	651300	28348	1.730667	0.5778	0.578	9464.6	9464.6	0.015408	0.01541	252.3883	252.39
18976	693300	24631	1.298	0.7704	0.77	14619	14619	0.014445	0.01445	274.114	274.11
21572	728600	37334	1.730667	0.5778	0.578	12465	12465	0.01329	0.01329	286.6849	286.68

Table G-2 Model 1 Type 1h Fracture Simulation Output and Calculations - Continued

delta t days	Q'smooth	Q' smooth	Q"smooth	Q"
6				
8	-437	437		
10	-418	418	6813	6812.5
12	-410	410	3125	3125
14	-405	405	1250	1250
16	-405	405	625	625
18	-403	403	1250	1250
20	-400	400	1875	1875
22	-395	395	3125	3125
24	-388	388	4429	4428.571
26	-377	377	4662	3995.392
31	-360	360	3080	507.1394
62	-359	359	260	498.5175
123	-314	314	728	722.0733
214	-249	249	633	557.1037
395	-162	162	356	356.0315
576	-120	120	181	128.6665
942	-92	92	61	60.79999
1308	-76	76	37	25.33205
2304	-57	57	15	14.99098
3400	-45	45	10	6.464455
5996	-34	34	4	3.637876
8592	-26	26	2	2.299971
11188	-22	22	1	1.290951
13784	-19	19	1	0.971923
16380	-17	17	1	0.779022
18976	-15	15	1	0.652895
21572	-13	13		

Table G-2 Model 1 Type 1h Fracture Simulation Output and Calculations - Continued

Table G-3 Model 1 Type 1a Fracture Simulation Output and Calculations

model Type1n | kfracture 1000

28 by 28 | phimatrix 0.009 | 2Xe/L 8.5 | ooip 3.373 | w 0.146 | kmatrix 0.1 | Soi 0.75

delta t days	average pressure	cum oil mbo	oil rate bopd	gas rate mcf/d	cum gas mmcf	dt hours	dq	dp	q/dp	dp/q	q cum/dp	tp(days) q cum/q	qcum/dq
6	1821	10.6	814			144		79	10.304	0.097052	134.177	13.02211	
8	1912	12.13	739			192	75	88	8.3977	0.11908	137.841	16.41407	161.73
10	1905	13.47	644			240	170	95	6.7789	0.147516	141.789	20.91615	79.235
12	1898	14.63	560			288	254	102	5.4902	0.182143	143.431	26.125	57.598
14	1893	15.62	476			336	338	107	4.4486	0.22479	145.981	32.81513	46.213
16	1887	16.49	422			384	392	113	3.7345	0.267773	145.929	39.07583	42.066
18	1881	17.3	402			432	412	119	3.3782	0.29602	145.378	43.03483	41.99
20	1876	18.08	389			480	425	124	3.1371	0.318766	145.806	46.47815	42.541
22	1871	18.85	383			528	431	129	2.969	0.336815	146.124	49.21671	43.735
24	1866	19.61	382			576	432	134	2.8507	0.350785	146.343	51.33508	45.394
26	1862	20.38	380			624	434	138	2.7536	0.363158	147.681	53.63158	46.959
37	1844	24.51	373			888	441	156	2.391	0.418231	157.115	65.71046	55.578
48	1828	28.56	366			1152	448	172	2.1279	0.469945	166.047	78.03279	63.75
59	1815	32.61	369			1416	445	185	1.9946	0.501355	176.27	88.37398	73.281
70	1803	36.67	368			1680	446	197	1.868	0.535326	186.142	99.64674	82.22
81	1792	40.65	357			1944	457	208	1.7163	0.582633	195.433	113.8655	88.95
92	1781	44.5	344			2208	470	219	1.5708	0.636628	203.196	129.3605	94.681
103	1771	48.22	335			2472	479	229	1.4629	0.683582	210.568	143.9403	100.67
114	1762	51.86	328			2736	486	238	1.3782	0.72561	217.899	158.1098	106.71
125	1753	55.43	323			3000	491	247	1.3077	0.764706	224.413	171.6099	112.89
136	1744	58.95	318			3264	496	256	1.2422	0.805031	230.273	185.3774	118.85
147	1736	62.42	313			3528	501	264	1.1856	0.84345	236.439	199.4249	124.59
158	1728	65.82	307			3792	507	272	1.1287	0.885993	241.985	214.3974	129.82
169	1720	69.17	302			4056	512	280	1.0786	0.927152	247.036	229.0397	135.1
180	1713	72.45	296			4320	518	287	1.0314	0.969595	252.439	244.7635	139.86
191	1705	75.67	290			4584	524	295	0.9831	1.017241	256.508	260.931	144.41
222	1686	84.45	277			5328	537	314	0.8822	1.133574	268.949	304.8736	157.26
253	1669	92.81	260			6072	554	331	0.7855	1.273077	280.393	356.9615	167.53
284	1652	100.5	243			6816	571	348	0.6983	1.432099	288.793	413.5802	176.01
345	1621	114.8	216.4			8280	597.6	379	0.571	1.751386	302.902	530.4991	192.1
406	1593	127.6	206.3			9744	607.7	407	0.5069	1.972856	313.514	618.5167	209.97
772	1472	189.2	141.6			18528	672.4	528	0.2682	3.728814	358.333	1336.158	281.38
1138	1407	234.5	111			27312	703	593	0.1872	5.342342	395.447	2112.613	333.57
1504	1365	270.4	85			36096	729	635	0.1339	7.470588	425.827	3181.176	370.92
1870	1326	297.9	64.7			44880	749.3	674	0.096	10.41731	441.988	4604.328	397.57
2236	1293	319.1	52			53664	762	707	0.0736	13.59615	451.344	6136.538	418.77
2602	1265	336.6	44.5			62448	769.5	735	0.0605	16.51685	457.959	7564.045	437.43
3698	1202	379.3	35.1			88752	778.9	798	0.044	22.73504	475.313	10806.27	486.97
4794	1157	414.9	31			115056	783	843	0.0368	27.19355	492.171	13383.87	529.89
5890	1122	448.3	30			141360	784	878	0.0342	29.26667	510.592	14943.33	571.81
6986	1091	479.3	27			167664	787	909	0.0297	33.66667	527.283	17751.85	609.02
8082	1064	507.1	24.6			193968	789.4	936	0.0263	38.04878	541.774	20613.82	642.39
9178	1039	533.7	23.9			220272	790.1	961	0.0249	40.20921	555.359	22330.54	675.48
10274	1015	556.9	22			246576	792	985	0.0223	44.77273	567.411	25404.55	705.68

	model Type1n		kfracture 1000		kmatrix 0.1		
	28 by 28		phimatrix 0.0089		2Xe/L 8.5		ooip 3.373
delta t	cum oil			days/days		hours	w 0.146
days	mbo	dq/q	dp/p	(tp+dt)/dt	sqrt dt	sqrt dt	
6	10600	0	0.041124	3.170352	2.4494897	12	
8	12130	0.10149	0.046025	3.051758	2.8284271	13.856406	
10	13470	0.26398	0.049869	3.091615	3.1622777	15.491933	
12	14630	0.45357	0.053741	3.177083	3.4641016	16.970563	
14	15620	0.71008	0.056524	3.343938	3.7416574	18.330303	
16	16490	0.92891	0.059683	3.442239	4	19.595918	
18	17300	1.02488	0.063264	3.390824	4.2426407	20.78461	
20	18080	1.09254	0.066098	3.323907	4.472136	21.908902	
22	18850	1.12533	0.068947	3.237123	4.6904158	22.978251	
24	19610	1.13089	0.071811	3.138962	4.8989795	24	
26	20380	1.14211	0.074114	3.062753	5.0990195	24.979992	
37	24510	1.18231	0.084599	2.775958	6.0827625	29.799329	
48	28560	1.22404	0.094092	2.625683	6.9282032	33.941125	
59	32610	1.20596	0.101928	2.497864	7.6811457	37.629775	
70	36670	1.21196	0.109262	2.423525	8.3666003	40.987803	
81	40650	1.28011	0.116071	2.405747	9	44.090815	
92	44500	1.36628	0.122965	2.406092	9.591663	46.98936	
103	48220	1.42985	0.129305	2.397479	10.148892	49.719212	
114	51860	1.48171	0.135074	2.386928	10.677078	52.306787	
125	55430	1.52012	0.140901	2.372879	11.18034	54.772256	
136	58950	1.55975	0.146789	2.363069	11.661904	57.131427	
147	62420	1.60064	0.152074	2.356632	12.124356	59.39697	
158	65820	1.65147	0.157407	2.356946	12.569805	61.579217	
169	69170	1.69536	0.162791	2.355265	13	63.686733	
180	72450	1.75	0.167542	2.359797	13.416408	65.726707	
191	75670	1.8069	0.173021	2.366131	13.820275	67.705244	
222	84450	1.93863	0.18624	2.373305	14.899664	72.99315	
253	92810	2.13077	0.198322	2.410915	15.905974	77.923039	
284	100500	2.34979	0.210654	2.456268	16.8523	82.55907	
345	114800	2.76155	0.233806	2.537678	18.574176	90.994505	
406	127600	2.94571	0.255493	2.52344	20.149442	98.711701	
772	189200	4.74859	0.358696	2.730775	27.784888	136.1176	
1138	234500	6.33333	0.421464	2.858426	33.734256	165.26343	
1504	270400	8.57647	0.465201	3.115144	38.781439	189.98947	
1870	297900	11.5811	0.508296	3.462207	43.243497	211.849	
2236	319100	14.6538	0.54679	3.744427	47.286362	231.65492	
2602	336600	17.2921	0.581028	3.907012	51.009803	249.89598	
3698	379300	22.1909	0.663694	3.922192	60.811183	297.91274	
4794	414900	25.2581	0.728608	3.791796	69.238717	339.19906	
5890	448300	26.1333	0.782531	3.537068	76.746335	375.97872	
6986	479300	29.1481	0.833181	3.541061	83.582295	409.46795	
8082	507100	32.0894	0.879699	3.550584	89.899944	440.41798	
9178	533700	33.0586	0.924928	3.433051	95.801879	469.33144	
10274	558900	36	0.970443	3.472702	101.36074	496.5642	

Table G-3 Model 1 Type 1n Fracture Simulation Output and Calculations - Continued

Table G-3 Model 1 Type 1n Fracture Simulation Output and Calculations - Continued

delta t	cum oil				the pressure decline can be compared with actual pressures as a function of time							
days	mbo	q'*t	1/q'*t	1/q'	q' (deriv)	q'alt	t*q'	t*q'alt	p'	p' alt	t*p'	t*p'alt
6	10600											
8	12130	3E+05	0.0002	2.35E-05	42500	42500	340000	340000	4	4	32	32
10	13470	4E+05	0.0002	2.23E-05	44750	44750	447500	447500	4	4	35	35
12	14630	5E+05	0.0003	2.38E-05	42000	42000	504000	504000	3	3	36	36
14	15620	5E+05	0.0004	2.9E-05	34500	34500	483000	483000	3	3	39	39
16	16490	3E+05	0.0009	5.41E-05	18500	18500	296000	296000	3	3	48	48
18	17300	1E+05	0.0022	0.000121	8250	8250	148500	148500	3	3	50	50
20	18080	95000	0.0042	0.000211	4750	4750	95000	95000	3	3	50	50
22	18850	38500	0.0126	0.000571	1750	1750	38500	38500	3	3	55	55
24	19610	18000	0.032	0.001333	750	750	18000	18000	2	2	54	54
26	20380	24545	0.0275	0.001059	692.31	944.1	18000	24545	1.692308	1.94406	44	50.545
37	24510	23545	0.0581	0.001571	636.36	636.4	23545	23545	1.545455	1.54545	57.18182	57.182
48	28560	8727	0.264	0.0055	181.82	181.8	8727.3	8727.3	1.318182	1.31818	63.27273	63.273
59	32610	-5364	-0.849	-0.011	-90.91	-90.9	-5364	-5363.6	1.136364	1.13636	67.04545	67.045
70	36670	38182	0.1283	0.001833	545.45	545.5	38182	38182	1.045455	1.04545	73.18182	73.182
81	40650	88364	0.0742	0.000917	1090.9	1091	88364	88364	1	1	81	81
92	44500	92000	0.092	0.001	1000	1000	92000	92000	0.954545	0.95455	87.81818	87.818
103	48220	74909	0.1416	0.001375	727.27	727.3	74909	74909	0.863636	0.86364	88.95455	88.955
114	51860	62182	0.209	0.001833	545.45	545.5	62182	62182	0.818182	0.81818	93.27273	93.273
125	55430	56818	0.275	0.0022	454.55	454.5	56818	56818	0.818182	0.81818	102.2727	102.27
136	58950	61818	0.2992	0.0022	454.55	454.5	61818	61818	0.772727	0.77273	105.0909	105.09
147	62420	73500	0.294	0.002	500	500	73500	73500	0.727273	0.72727	106.9091	106.91
158	65820	79000	0.316	0.002	500	500	79000	79000	0.727273	0.72727	114.9091	114.91
169	69170	84500	0.338	0.002	500	500	84500	84500	0.681818	0.68182	115.2273	115.23
180	72450	98182	0.33	0.001833	545.45	545.5	98182	98182	0.681818	0.68182	122.7273	122.73
191	75670	97874	0.3727	0.001961	452.38	512.4	86405	97874	0.642857	0.69732	122.7857	133.19
222	84450	1E+05	0.4588	0.002067	483.87	483.9	107419	107419	0.580645	0.58065	128.9032	128.9
253	92810	1E+05	0.4614	0.001824	548.39	548.4	138742	138742	0.548387	0.54839	138.7419	138.74
284	100500	1E+05	0.5563	0.001959	473.91	510.5	134591	144993	0.521739	0.53484	148.1739	151.9
345	114800	1E+05	1.1469	0.003324	300.82	300.8	103783	103783	0.483607	0.48361	166.8443	166.84
406	127600	67873	2.4286	0.005982	175.18	167.2	71121	67873	0.348946	0.44067	141.6721	178.91
772	189200	1E+05	5.9297	0.007681	130.19	130.2	100508	100508	0.254098	0.2541	196.1639	196.16
1138	234500	87993	14.718	0.012933	77.322	77.32	87993	87993	0.146175	0.14617	166.347	166.35
1504	270400	95130	23.778	0.01581	63.251	63.25	95130	95130	0.110656	0.11066	166.4262	166.43
1870	297900	84303	41.48	0.022182	45.082	45.08	84303	84303	0.098361	0.09836	183.9344	183.93
2236	319100	61704	81.027	0.036238	27.596	27.6	61704	61704	0.083333	0.08333	186.3333	186.33
2602	336600	45558	148.61	0.057114	11.56	17.51	30078	45558	0.062244	0.07174	161.9576	186.67
3698	379300	22775	600.45	0.16237	6.1588	6.159	22775	22775	0.04927	0.04927	182.2007	182.2
4794	414900	11154	2060.5	0.429804	2.3266	2.327	11154	11154	0.036496	0.0365	174.9635	174.96
5890	448300	10748	3227.7	0.548	1.8248	1.825	10748	10748	0.030109	0.03011	177.3449	177.34
6986	479300	17210	2835.8	0.405926	2.4635	2.464	17210	17210	0.02646	0.02646	184.8485	184.85
8082	507100	11430	5714.8	0.707097	1.4142	1.414	11430	11430	0.023723	0.02372	191.7283	191.73
9178	533700	10886	7737.8	0.843077	1.1861	1.186	10886	10886	0.022354	0.02235	205.1651	205.17

delta t	cum				2 smooths	
days	Q' smooth	-Q'smooth	Q"	Q"	Q" smooth	Q"*t
6						
8	-718	718				
10	-625	625	-45000	45000	45000	450000
12	-538	538	-40000	40000	40000	480000
14	-465	465	-29375	29375	29375	411250
16	-420	420	-16875	16875	16875	270000
18	-398	398	-8125	8125	8125	146250
20	-388	388	-3750	3750	3750	75000
22	-383	383	-1250	1250	1250	27500
24	-383	383	257.8671	-257.8671	-258	-6188.8112
26	-384	384	-821.678	821.6783	-273	21363.636
37	-372	372	-697.711	697.7114	698	25815.321
48	-368	368	-144.628	144.6281	145	6942.1488
59	-369	369	-123.967	123.9669	124	7314.0496
70	-365	365	-578.512	578.5124	579	40495.868
81	-356	356	-971.074	971.0744	971	78657.025
92	-344	344	-971.074	971.0744	971	89338.843
103	-335	335	-743.802	743.8017	744	76611.57
114	-328	328	-557.851	557.8512	558	63595.041
125	-322	322	-454.545	454.5455	455	56818.182
136	-318	318	-454.545	454.5455	455	61818.182
147	-312	312	-495.868	495.8678	496	72892.562
158	-307	307	-495.868	495.8678	496	78347.107
169	-301	301	-516.529	516.5289	517	87293.388
180	-295	295	-505.675	505.6747	506	91021.442
191	-290	290	-452.451	452.4508	466	86418.098
222	-276	276	-505.933	505.9327	506	112317.05
253	-259	259	-531.978	531.9775	532	134590.31
284	-243	243	-399.346	399.3459	447	113414.23
345	-222	222	-324.31	324.3099	324	111886.91
406	-204	204	-178.204	178.2035	279	72350.623
772	-146	146	-127.014	127.014	127	98054.798
1138	-111	111	-81.1834	81.18337	81	92386.679
1504	-87	87	-60.6542	60.65424	61	91223.984
1870	-67	67	-46.0972	46.09723	46	86201.813
2236	-53	53	-28.5963	28.59626	29	63941.241
2602	-46	46	-11.7292	11.72917	17	30519.306
3698	-36	36	-6.44137	6.441373	6	23820.196
4794	-31	31	-2.8929	2.892902	3	13868.572
5890	-29	29	-2.12285	2.122849	2	12503.58
6986	-27	27	-2.08122	2.081224	2	14539.433
8082	-25	25	-1.45686	1.456857	1	11774.319
9178	-24	24	-1.33198	1.331984	1	12224.945

Table G-3 Model 1 Type 1a Fracture Simulation Output and Calculations - Continued

Table G-4 Model 1 Type 1nh Fracture Simulation Output and Calculations

model Type1nh										kfracture 4000			
28 by 28		phimatrix 0.009		2Xe/L 8.5		ooip 3.373		w 0.146		kmatrix 0.1		So 0.75	
delta t days	average pressure	cum oil mbo	oil rate bopd	gas rate mcf/d	cum gas mmcf	dt hours	dq	dp	q/dp	dp/q	q cum/dp	tp(days) q cum/q	qcum/dq
6	1909	11.24	920			144		91	10.11	0.098913	123.516	12.21739	
8	1900	12.98	833			192	87	100	8.33	0.120048	129.8	15.58223	149.2
10	1893	14.45	708			240	212	107	6.6168	0.15113	135.047	20.4096	68.16
12	1887	15.69	592			288	328	113	5.2389	0.190878	138.85	26.50338	47.835
14	1882	16.73	491			336	429	118	4.161	0.240326	141.78	34.07332	38.998
16	1876	17.62	440			384	480	124	3.5484	0.281818	142.097	40.04545	36.708
18	1871	18.48	428			432	492	129	3.3178	0.301402	143.256	43.17757	37.561
20	1866	19.33	425			480	495	134	3.1716	0.315294	144.254	45.48235	39.051
22	1862	20.18	424			528	496	138	3.0725	0.325472	146.232	47.59434	40.685
24	1858	21.03	423			576	497	142	2.9789	0.335697	148.099	49.71631	42.314
26	1855	21.87	422			624	498	145	2.9103	0.343602	150.828	51.82464	43.916
37	1836	26.47	414			888	506	164	2.5244	0.398135	161.402	63.9372	52.312
48	1821	30.99	410			1152	510	179	2.2905	0.436585	173.128	75.58537	60.765
59	1808	35.51	413			1416	507	192	2.151	0.464891	184.948	85.98063	70.039
70	1795	40.07	413			1680	507	205	2.0146	0.496368	195.463	97.02179	79.034
81	1784	44.54	402			1944	518	216	1.8611	0.537313	206.204	110.796	85.985
92	1773	48.88	389			2208	531	227	1.7137	0.583548	215.33	125.6555	92.053
103	1762	53.1	380			2472	540	238	1.5966	0.626316	223.109	139.7368	98.333
114	1753	57.24	373			2736	547	247	1.5101	0.662198	231.741	153.4584	104.64
125	1744	61.32	368			3000	552	256	1.4375	0.695652	239.531	166.6304	111.09
136	1734	65.34	363			3264	557	266	1.3647	0.732782	245.639	180	117.31
147	1726	69.31	358			3528	562	274	1.3066	0.765363	252.956	193.6034	123.33
158	1718	73.22	353			3792	567	282	1.2518	0.798867	259.645	207.4221	129.14
169	1710	77.06	347			4056	573	290	1.1966	0.835735	265.724	222.0749	134.49
180	1702	80.84	341			4320	579	298	1.1443	0.8739	271.275	237.0674	139.62
191	1694	84.55	335			4584	585	306	1.0948	0.913433	276.307	252.3881	144.53
222	1674	94.71	322			5328	598	326	0.9877	1.012422	290.521	294.1304	158.38
253	1655	104.5	309			6072	611	345	0.8957	1.116505	302.899	338.1877	171.03
284	1638	113.9	298.4			6816	621.6	362	0.8243	1.213137	314.641	381.7024	183.24
345	1606	131.5	281			8280	639	394	0.7132	1.402135	333.756	467.9715	205.79
406	1578	147.9	274			9744	646	422	0.6493	1.540146	350.474	539.781	228.95
772	1450	222.8	160			18528	760	550	0.2909	3.4375	405.091	1392.5	293.16
1138	1372	266.3	88			27312	832	628	0.1401	7.136364	424.045	3026.136	320.07
1504	1320	292.8	62			36096	858	680	0.0912	10.96774	430.588	4722.581	341.26
1870	1281	312.6	48			44880	872	719	0.0668	14.97917	434.771	6512.5	358.49
2236	1251	329.2	44			53664	876	749	0.0587	17.02273	439.519	7481.818	375.8
2602	1226	344.8	41			62448	879	774	0.053	18.87805	445.478	8409.756	392.26
3698	1172	384.6	33.8			88752	886.2	828	0.0408	24.49704	464.493	11378.7	433.99
4794	1133	423	35.4			115056	884.6	867	0.0408	24.49153	487.889	11949.15	478.18
5890	1098	458.4	29.3			141360	890.7	902	0.0325	30.78498	508.204	15645.05	514.65
6986	1068	488.5	26.7			167664	893.3	932	0.0286	34.90637	524.142	18295.88	546.85
8082	1041	517.9	26.4			193968	893.6	959	0.0275	36.32576	540.042	19617.42	579.57
9178	1016	546.3	23.4			220272	896.6	984	0.0238	42.05128	554.167	23303.42	608.19
10274	993	569.4	21			246576	899	1007	0.0209	47.95238	565.442	27114.29	633.37

model Type1nh			w 0.146		kfracture 4000		kmatrix 0.1
28 by 28			phimatrix 0.0089		2Xe/L 8.5		ooip 3.373
delta t	cum oil			days/days		hours	
days	mbo	dq/q	dp/p	(tp+dt)/dt	sqrt dt	sqrt dt	1/q
6	11240	0	0.047669	3.036232	2.4494897	12	0.001086957
8	12980	0.10444	0.052632	2.947779	2.8284271	13.85640646	0.00120048
10	14450	0.29944	0.058524	3.04096	3.1622777	15.49193338	0.001412429
12	15690	0.55405	0.059883	3.208615	3.4641016	16.97056275	0.001689189
14	16730	0.87373	0.062699	3.433809	3.7416574	18.33030278	0.00203666
16	17620	1.09091	0.066098	3.502841	4	19.59591794	0.002272727
18	18480	1.14853	0.068947	3.398754	4.2426407	20.78460969	0.002336449
20	19330	1.16471	0.071811	3.274118	4.472136	21.9089023	0.002352941
22	20180	1.16981	0.074114	3.163379	4.6904158	22.97825059	0.002358491
24	21030	1.17494	0.076426	3.071513	4.8989795	24	0.002364066
26	21870	1.18009	0.078167	2.993256	5.0990195	24.97999199	0.002369668
37	26470	1.22222	0.089325	2.728032	6.0827625	29.79932885	0.002415459
48	30990	1.2439	0.098298	2.574685	6.9282032	33.9411255	0.002439024
59	35510	1.2276	0.106195	2.457299	7.6811457	37.62977544	0.002421308
70	40070	1.2276	0.114206	2.386026	8.3666003	40.98780306	0.002421308
81	44540	1.28856	0.121076	2.367852	9	44.09081537	0.002487562
92	48880	1.36504	0.128032	2.365821	9.591663	46.9893605	0.002570694
103	53100	1.42105	0.135074	2.356668	10.148892	49.71921158	0.002631579
114	57240	1.46649	0.140901	2.346127	10.677078	52.30678732	0.002680965
125	61320	1.5	0.146789	2.333043	11.18034	54.77225575	0.002717391
136	65340	1.53444	0.153403	2.323529	11.661904	57.13142743	0.002754821
147	69310	1.56983	0.158749	2.31703	12.124356	59.39696962	0.002793296
158	73220	1.60623	0.164144	2.312798	12.569805	61.57921727	0.002832861
169	77060	1.6513	0.169591	2.314053	13	63.68673331	0.002881844
180	80840	1.69795	0.175088	2.317041	13.416408	65.7267069	0.002932551
191	84550	1.74627	0.180638	2.321403	13.820275	67.70524352	0.002985075
222	94710	1.85714	0.194743	2.324912	14.899664	72.99315036	0.00310559
253	104500	1.97735	0.208459	2.33671	15.905974	77.92303898	0.003236246
284	113900	2.08311	0.221001	2.344023	16.8523	82.55906976	0.003351206
345	131500	2.27402	0.24533	2.358439	18.574176	90.99450533	0.003558719
406	147900	2.35766	0.267427	2.32951	20.149442	98.71170143	0.003649635
772	222800	4.75	0.37931	2.803756	27.784888	136.1175962	0.00625
1138	266300	9.45455	0.457726	3.659171	33.734256	165.2634261	0.011363636
1504	292800	13.8387	0.515152	4.140014	38.781439	189.9894734	0.016129032
1870	312600	18.1667	0.56128	4.48262	43.243497	211.8490028	0.020833333
2236	329200	19.9091	0.598721	4.346073	47.286362	231.6549158	0.022727273
2602	344800	21.439	0.631321	4.232035	51.009803	249.8959784	0.024390244
3698	384600	26.2189	0.706485	4.076987	60.811183	297.9127389	0.029585799
4794	423000	24.9887	0.765225	3.492522	69.238717	339.1990586	0.028248588
5890	458400	30.3993	0.821494	3.656206	76.746335	376.9787228	0.034129693
6986	488500	33.4569	0.872659	3.618935	83.582295	409.4679475	0.037453184
8082	517900	33.8485	0.92123	3.427298	89.899944	440.4179833	0.037878788
9178	545300	38.3162	0.968504	3.539052	95.801879	469.3314394	0.042735043
10274	569400	42.8095	1.014099	3.639117	101.36074	496.5841952	0.047619048

Table G-4 Model 1 Type 1nh Fracture Simulation Output and Calculations - Continued

Table G-4 Model 1 Type 1nh Fracture Simulation Output and Calculations - Continued

delta t	cum oil			the pressure decline can be compared with actual pressures as a function of time							
days	mbo	1/q'*t	1/q'	q' (deriv)	q'alt	t*Q'	t*Q'alt	p'	p' alt	t*p'	t*p'alt
6	11240										
8	12980	0.0002	1 89E-05	53000	53000	424000	424000	4	4	32	32
10	14450	0.0002	1.66E-05	60250	60250	602500	602500	3	3	33	33
12	15690	0.0002	1 84E-05	54250	54250	651000	651000	3	3	33	33
14	16730	0.0004	2.63E-05	38000	38000	532000	532000	3	3	39	39
16	17620	0.001	6.35E-05	15750	15750	252000	252000	3	3	44	44
18	18480	0.0048	0.000267	3750	3750	67500	67500	3	3	45	45
20	19330	0.02	0.001	1000	1000	20000	20000	2	2	45	45
22	20180	0.044	0.002	500	500	11000	11000	2	2	44	44
24	21030	0.048	0.002	500	500	12000	12000	2	2	42	42
26	21870	0.0376	0.001444	692.31	535	18000	13909	1.692308	1.53497	44	39.909
37	26470	0.0678	0.001833	545.45	545.5	20182	20182	1.545455	1.54545	57.18182	57.182
48	30990	1.066	0.022	45.455	45.45	2181.8	2181.8	1.272727	1.27273	61.09091	61.091
59	35510	-0.433	-0.00733	-136.4	-136	-8045	-8045.5	1.181818	1.18182	69.72727	69.727
70	40070	0.14	0.002	500	500	35000	35000	1.090909	1.09091	76.36364	76.364
81	44540	0.0743	0.000917	1090.9	1091	88364	88364	1	1	81	81
92	48880	0.092	0.001	1000	1000	92000	92000	1	1	92	92
103	53100	0.1416	0.001375	727.27	727.3	74909	74909	0.909091	0.90909	93.63636	93.636
114	57240	0.209	0.001833	545.45	545.5	62182	62182	0.818182	0.81818	93.27273	93.273
125	61320	0.275	0.0022	454.55	454.5	56818	56818	0.863636	0.86364	107.9545	107.95
136	65340	0.2992	0.0022	454.55	454.5	61818	61818	0.818182	0.81818	111.2727	111.27
147	69310	0.3234	0.0022	454.55	454.5	66818	66818	0.727273	0.72727	106.9091	106.91
158	73220	0.316	0.002	500	500	79000	79000	0.727273	0.72727	114.9091	114.91
169	77060	0.3098	0.001833	545.45	545.5	92182	92182	0.727273	0.72727	122.9091	122.91
180	80840	0.33	0.001833	545.45	545.5	98182	98182	0.727273	0.72727	130.9091	130.91
191	84550	0.4222	0.002211	452.38	512.4	86405	97874	0.666667	0.70577	127.3333	134.8
222	94710	0.5294	0.002385	419.35	419.4	93097	93097	0.629032	0.62903	139.6452	139.65
253	104500	0.6647	0.002627	380.65	380.6	96303	96303	0.580645	0.58065	146.9032	146.9
284	113900	0.9331	0.003286	304.35	322.8	86435	91685	0.532609	0.54037	151.2609	153.46
345	131500	1.725	0.005	200	200	69000	69000	0.491803	0.4918	169.6721	169.67
406	147900	1.4327	0.003529	283.37	142.9	115049	58000	0.36534	0.4434	148.3279	180.02
772	222800	3.0382	0.003935	254.1	254.1	196164	196164	0.281421	0.28142	217.2568	217.26
1138	266300	8.5002	0.007469	133.88	133.9	152365	152365	0.177596	0.1776	202.1038	202.1
1504	292800	27.523	0.0183	54.645	54.64	82186	82186	0.124317	0.12432	186.9727	186.97
1870	312600	76.047	0.040667	24.59	24.59	45984	45984	0.094262	0.09426	176.2705	176.27
2236	329200	233.82	0.104571	9.5628	9.563	21383	21383	0.075137	0.07514	168.0055	168.01
2602	344800	372.95	0.143333	6.9767	7.789	18153	20268	0.054036	0.06354	140.6005	165.33
3698	384600	1447.5	0.391429	2.5547	2.555	9447.4	9447.4	0.042427	0.04243	156.8951	156.9
4794	423000	2335.2	0.487111	2.0529	2.053	9841.7	9841.7	0.033759	0.03376	161.8412	161.84
5890	458400	1484	0.251954	3.969	3.969	23377	23377	0.029653	0.02965	174.6578	174.66
6986	488500	5280.5	0.755862	1.323	1.323	9242.4	9242.4	0.026004	0.026	181.6615	181.66
8082	517900	5368.4	0.664242	1.5055	1.505	12167	12167	0.023723	0.02372	191.7263	191.73
9178	545300	3725.6	0.405926	2.4635	2.464	22610	22610	0.021898	0.0219	200.9781	200.98

delta t	cum				2 smooths
days	Q' smooth	-Q'smooth	Q"	Q"	Q" smooth
6					
8	-803	803			
10	-678	678	-58125	58125	58125
12	-570	570	-48750	48750	48750
14	-483	483	-33125	33125	33125
16	-438	438	-13750	13750	13750
18	-428	428	-3125	3125	3125
20	-425	425	-625	625	625
22	-425	425	-625	625	625
24	-423	423	-1319.93	1319.93	1320
26	-420	420	-611.888	611.8881	1248
37	-415	415	-400.509	400.5086	401
48	-411	411	-82.6446	82.64463	83
59	-413	413	-20.6612	20.66116	21
70	-410	410	-557.851	557.8512	558
81	-400	400	-971.074	971.0744	971
92	-389	389	-929.752	929.7521	930
103	-380	380	-702.479	702.4793	702
114	-374	374	-537.19	537.1901	537
125	-368	368	-475.207	475.2066	475
136	-363	363	-454.545	454.5455	455
147	-358	358	-495.868	495.8678	496
158	-352	352	-537.19	537.1901	537
169	-346	346	-537.19	537.1901	537
180	-340	340	-526.685	526.6849	527
191	-335	335	-444.77	444.7703	491
222	-322	322	-407.426	407.4264	407
253	-310	310	-379.065	379.0654	379
284	-298	298	-335.083	335.0827	349
345	-279	279	-316.329	316.3295	316
406	-260	260	-273.864	273.8639	305
772	-162	162	-224.114	224.1141	224
1138	-96	96	-134.559	134.5591	135
1504	-63	63	-62.7072	62.70716	63
1870	-50	50	-26.3146	26.31461	26
2236	-44	44	-11.8624	11.86237	12
2602	-41	41	-5.68665	5.686654	7
3698	-36	36	-3.3648	3.364799	3
4794	-34	34	-2.64315	2.643155	3
5890	-30	30	-2.97615	2.976151	3
6986	-27	27	-1.81067	1.810665	2
8082	-26	26	-1.66498	1.664979	2
9178	-23	23	-2.16447	2.164473	2

Table G-4 Model 1 Type 1nh Fracture Simulation Output and Calculations - Continued

model Type2							
28 by 28	phimatrix	0.11	2Xe/L	8.5	ooip(mm bo)	3.373
	w	0.007				
	kmatrix	0.1	Soi	0.75		
	kfracture	1000				

delta t days	average pressure	delta q cum oil mbo	oil rate bopd	gas rate mcf/d	cum gas mmcf	dt hours	dq	dp	q/dp	dp/q	q cum/dp	tp(days) q cum/q	qcum/dq
6	1863	13.18	1548	808	9.345	144		137	11.299	0.088501	96.2044	8.514212	
8	1838	16.19	1444	974	11.15	192	104	162	8.9136	0.112188	99.9383	11.21191	155.67
10	1814	18.95	1321	950	13.12	240	227	186	7.1022	0.140802	101.882	14.34519	83.48
12	1792	21.55	1289	804	14.72	288	259	208	6.1971	0.161365	103.606	16.71839	83.205
14	1771	24.1	1253	824	16.33	336	295	229	5.4716	0.182761	105.24	19.23384	81.695
16	1751	26.55	1220	727	17.89	384	328	249	4.8996	0.204098	106.627	21.7623	80.945
18	1732	28.93	1163	744	19.41	432	385	268	4.3396	0.230439	107.948	24.87532	75.143
20	1714	31.23	1183	499	20.7	480	365	286	4.1364	0.241758	109.196	26.39899	85.562
22	1698	33.55	1152	631	21.9	528	396	302	3.8146	0.262153	111.093	29.12326	84.722
24	1682	35.82	1163	556	22.98	576	385	318	3.6572	0.273431	112.642	30.79966	93.039
26	1667	37.95	1064	630	24.32	624	484	333	3.1952	0.31297	113.964	35.66729	78.409
31	1634	43.14	1055	545	27.7	744	493	366	2.8825	0.346919	117.869	40.891	87.505
62	1541	70.68	793	459	43.55	1488	755	459	1.7277	0.578815	153.987	89.12989	93.616
123	1483	114.6	697	331	67.49	2952	851	517	1.3482	0.74175	221.663	164.4189	134.67
214	1430	171.8	591	300	96.56	5136	957	570	1.0368	0.964467	301.404	290.6937	179.52
395	1355	268.4	481	212	143.9	9480	1067	645	0.7457	1.340956	416.124	558.0042	251.55
576	1297	351.8	439	214	184.8	13824	1109	703	0.6245	1.601367	500.427	801.3667	317.22
942	1203	494.2	349	168	256.5	22608	1199	797	0.4379	2.283668	620.075	1416.046	412.18
1308	1129	611.8	290	153	319.5	31392	1258	871	0.333	3.003448	702.411	2109.655	486.33
2304	969	845.8	179	216	498.3	55296	1369	1031	0.1736	5.759777	820.369	4725.14	617.82
3400	812	1007	111	224	719.7	81600	1437	1188	0.0934	10.7027	847.643	9072.072	700.77
5996	511	1179	38	128	1161	143904	1510	1489	0.0255	39.18421	791.807	31026.32	780.79
8592	362	1244	17	54	1371	206208	1531	1638	0.0104	96.35294	759.463	73176.47	812.54
11188	298	1276	9.2	34	1486	268512	1539	1702	0.0054	185	749.706	138695.7	829.22
13784	266	1295	6	22	1556	330816	1542	1734	0.0035	289	746.828	215833.3	839.82
16380	254	1309	4.8	17.2	1606	393120	1543	1746	0.0027	363.75	749.714	272708.3	848.24
18976	246	1320	4	14.3	1647	455424	1544	1754	0.0023	438.5	752.566	330000	854.92
21572	239	1330	3.3	11.9	1681	517728	1545	1761	0.0019	533.6364	755.253	403030.3	861.01
24168	233	1337	2.8	10.2	1709	580032	1545	1767	0.0016	631.0714	756.65	477500	865.26

Table G-5 Model 2 Type 2 Fracture Simulation Output and Calculations

model Type2

28 by 28 | phimatrix 0.11 | 2Xe/L 8.5 | ooip(mmbo) 3.373

w 0.007

kmatrix 0.1 | Soi 0.75

kfracture 1000

delta t	cum oil			days/days		hours	
days	mbo	dq/q	dp/p	(tp+dt)/dt	sqrt dt	sqrt dt	d(dq/q)
6	13180	0	0.073537	2.419035	2.4494897	12	
8	16190	0.07202	0.088139	2.401489	2.8284271	13.85640646	
10	18950	0.17184	0.102536	2.434519	3.1622777	15.49193338	0.032227198
12	21550	0.20093	0.116071	2.393199	3.4641016	16.97056275	0.01589886
14	24100	0.23543	0.129305	2.373846	3.7416574	18.33030278	0.016980376
16	26550	0.26885	0.142204	2.360143	4	19.59591794	0.023901364
18	28930	0.33104	0.154734	2.381962	4.2426407	20.78460969	0.009921289
20	31230	0.30854	0.166861	2.319949	4.472136	21.9089023	0.003177397
22	33550	0.34375	0.177856	2.323785	4.6904158	22.97825059	0.005625699
24	35820	0.33104	0.189061	2.283319	4.8989795	24	0.027784305
26	37950	0.45489	0.19976	2.371819	5.0990195	24.97999199	0.019465452
31	43140	0.4673	0.22399	2.319064	5.5677644	27.27636339	0.01381093
62	70680	0.95208	0.297859	2.437579	7.8740079	38.57460304	0.00819183
123	114600	1.22095	0.348618	2.336739	11.090537	54.33231083	0.00438953
214	171800	1.61929	0.398601	2.358382	14.628739	71.66589147	0.003686722
395	268400	2.2183	0.476015	2.412669	19.874607	97.36529156	0.002505267
576	351800	2.5262	0.54202	2.391262	24	117.5755077	0.002225292
942	494200	3.43553	0.68251	2.503233	30.692019	150.359569	0.002475048
1308	611800	4.33793	0.771479	2.612886	36.166283	177.1778767	0.003092889
2304	845800	7.64804	1.063983	3.050842	48	235.1510153	0.00411473
3400	1007000	12.9459	1.463054	3.668256	58.309519	285.6571371	0.00869144
5996	1179000	39.7368	2.913894	6.174502	77.433843	379.346807	0.014852249
8592	1244000	90.0588	4.524862	9.516815	92.693042	454.1013103	0.024561639
11188	1276000	167.261	5.711409	13.39682	105.77334	518.1814354	0.032153539
13784	1296000	257	6.518797	16.65825	117.40528	575.166063	0.029707074
16380	1309000	321.5	6.874016	17.64886	127.98437	626.9928229	0.024845917
18976	1320000	386	7.130081	18.39039	137.7534	674.8510947	0.028233996
21572	1330000	468.091	7.368201	19.68303	146.8741	719.533182	0.03194475
24168	1337000	551.857	7.583691	20.75753	155.46061	761.5983193	

Table G-5 Model 2 Type 2 Fracture Simulation Output and Calculations - Continued

delta t	cum oil	the pressure decline can be compared with actual pressures as a function of time									
days	mbo	1/q''t	1/q'	q' (deriv)	q'alt	t*Q'	t*Q'alt	p'	p' alt	t*p'	t*p'alt
6	13180										
8	16190	0.0001	1.76E-05	56750	56750	454000	454000	12	12	98	98
10	18950	0.0003	2.58E-05	38750	38750	387500	387500	12	12	115	115
12	21550	0.0007	5.88E-05	17000	17000	204000	204000	11	11	129	129
14	24100	0.0008	5.8E-05	17250	17250	241500	241500	10	10	144	144
16	26550	0.0007	4.44E-05	22500	22500	360000	360000	10	10	156	156
18	28930	0.0019	0.000108	9250	9250	166500	166500	9	9	167	167
20	31230	0.0073	0.000364	2750	2750	55000	55000	9	9	170	170
22	33550	0.0044	0.0002	5000	5000	110000	110000	8	8	176	176
24	35820	0.0011	4.55E-05	22000	22000	528000	528000	8	8	186	186
26	37950	0.0017	6.48E-05	15429	35871	401143	932657	6.857143	7.24286	178.2857	188.31
31	43140	0.0041	0.000133	7527.8	2724	233361	84439	3.5	6.1	108.5	189.1
62	70680	0.0159	0.000257	3891.3	6134	241261	380313	1.641304	2.30952	101.7609	143.19
123	114600	0.0926	0.000752	1328.9	1410	163461	173388	0.730263	0.80297	89.82237	98.766
214	171800	0.2695	0.001259	794.12	978.5	169941	209389	0.470588	0.52619	100.7059	112.61
395	268400	0.9407	0.002382	419.89	419.9	165856	165856	0.367403	0.3674	145.1243	145.12
576	351800	2.3869	0.004144	241.32	236.6	138998	136299	0.277879	0.29939	160.0585	172.45
942	494200	4.6278	0.004913	203.55	203.6	191746	191746	0.229508	0.22951	216.1967	216.2
1308	611800	10.479	0.008012	124.82	147.8	163260	193364	0.171806	0.19102	224.7225	249.86
2304	845800	26.927	0.011687	85.564	87.93	197140	202580	0.15153	0.15236	349.1243	351.04
3400	1E+06	89.027	0.026184	38.191	51.97	129848	176709	0.124052	0.13514	421.7768	459.49
5996	1E+06	331.18	0.055234	18.105	18.1	108556	108556	0.086672	0.08667	519.6841	519.68
8592	1E+06	1548.9	0.180278	5.547	5.547	47660	47660	0.041025	0.04102	352.4838	352.48
11188	1E+06	5280.7	0.472	2.1186	2.119	23703	23703	0.01849	0.01849	206.8659	206.87
13784	1E+06	16265	1.18	0.8475	0.847	11681	11681	0.008475	0.00847	116.8136	116.81
16380	1E+06	42522	2.596	0.3852	0.385	6309.7	6309.7	0.003852	0.00385	63.09707	63.097
18976	1E+06	65682	3.461333	0.2889	0.289	5482.3	5482.3	0.002889	0.00289	54.8228	54.823
21572	1E+06	93335	4.326667	0.2311	0.231	4985.8	4985.8	0.002504	0.0025	54.0131	54.013

Table G-5 Model 2 Type 2 Fracture Simulation Output and Calculations - Continued

delta t				2 smooths	
days	Q' smooth	Q'smooth	Q"	Q" smooth	Q"*t
6					
8	-1443	1443			
10	-1340	1340	38750	38750	387500
12	-1288	1288	22500	22500	270000
14	-1250	1250	20000	20000	280000
16	-1208	1208	20000	20000	320000
18	-1170	1170	13125	13125	236250
20	-1155	1155	5625	5625	112500
22	-1148	1148	13750	13750	302500
24	-1100	1100	22554	22554	541285.71
26	-1057	1057	11826	17545	307466.97
31	-1017	1017	6268	7732	194299.17
62	-832	832	3629	4789	225027.76
123	-683	683	1545	1837	190015.62
214	-597	597	684	816	146393.86
395	-497	497	441	441	174350.45
576	-437	437	260	297	149577.1
942	-355	355	190	190	178807.54
1308	-298	298	119	142	155655.21
2304	-193	193	84	86	192750.27
3400	-123	123	40	54	135799.95
5996	-46	46	20	20	120571.68
8592	-19	19	7	7	59284.047
11188	-10	10	2	2	26562.14
13784	-6	6	1	1	13294.722
16380	-5	5	0	0	
18976	-4	4	1	1	
21572					

Table G-5 Model 2 Type 2 Fracture Simulation Output and Calculations - Continued

model Type2h

28 by 28 | phimatrix 0.11 | 2Xe/L 8.5 | ooip 3.373 (mmbo)

w 0.007

kmatrix 10.1 | Soi 0.75

kfracture 4000

delta t days	average pressure	delta q cum oil mbo	oil rate bopd	gas rate mcf/d	cum gas mmcf	dt hours	dq	dp	q/dp	dp/q	q cum/dp	tp(days) q cum/q	qcum/dq
6	1840	14.84	1780	1165	10.23	144		160	11.125	0.089888	92.75	8.337079	
8	1810	18.27	1676	1226	12.73	192	104	190	8.8211	0.113365	96.1579	10.90095	175.67
10	1782	21.52	1611	1152	15.1	240	169	218	7.3899	0.13532	98.7156	13.35816	127.34
12	1756	24.77	1605	1077	17.16	288	175	244	6.5779	0.152025	101.516	15.43302	141.54
14	1733	27.91	1548	982	19.17	336	232	267	5.7978	0.172481	104.532	18.02972	120.3
16	1711	30.97	1511	898	21.2	384	269	289	5.2284	0.191264	107.163	20.49636	115.13
18	1691	33.94	1494	856	22.95	432	286	309	4.835	0.206827	109.838	22.71754	118.67
20	1673	36.88	1453	883	24.81	480	327	327	4.4434	0.225052	112.783	25.38197	112.78
22	1656	39.67	1373	959	26.73	528	407	344	3.9913	0.250546	115.32	28.89294	97.469
24	1640	42.44	1375	851	28.38	576	405	360	3.8194	0.261818	117.889	30.86545	104.79
26	1626	45.16	1344	796	29.95	624	436	374	3.5936	0.278274	120.749	33.60119	103.58
31	1594	51.2	1246	798	34.41	744	534	406	3.069	0.325843	126.108	41.09149	95.88
62	1520	86.03	1006	621	54.54	1488	774	480	2.0958	0.477137	179.229	85.5169	111.15
123	1457	142.4	882	475	86.74	2952	898	543	1.6243	0.615646	262.247	161.4512	158.57
214	1397	216	751	432	124.6	5136	1029	603	1.2454	0.802929	358.209	287.6165	209.91
395	1310	339.8	642	299	186.1	9480	1138	690	0.9304	1.074766	492.464	529.2835	298.59
576	1242	444.2	540	265	238.2	13824	1240	758	0.7124	1.403704	586.016	822.5926	358.23
942	1132	612.1	386	284	334.5	22608	1394	868	0.4447	2.248705	705.184	1585.751	439.1
1308	1040	736.9	301	278	433.6	31392	1479	960	0.3135	3.189369	767.604	2448.173	498.24
2304	841	959.6	170	259	696.9	55296	1610	1159	0.1467	6.817647	827.955	5644.706	596.02
3400	661	1099	90	235	983.8	81600	1690	1339	0.0672	14.87778	820.762	12211.11	650.3
5996	391	1230	28	92	1343	143904	1752	1609	0.0174	57.46429	764.45	43928.57	702.05
8592	297	1277	12.3	43	1499	206208	1768	1703	0.0072	138.4553	749.853	103821.1	722.41
11188	262	1302	7.6	28.3	1584	268512	1772	1738	0.0044	228.6842	749.137	171315.8	734.6
13784	248	1319	5.7	20	1643	330816	1774	1752	0.0033	307.3684	752.854	231403.5	743.39
16380	240	1332	4.6	16.1	1689	393120	1775	1760	0.0026	382.6087	756.818	289565.2	750.25
18976	233	1343	3.7	13.2	1727	455424	1776	1767	0.0021	477.5676	760.045	362973	756.07
21572	228	1352	3	10.8	1758	517728	1777	1772	0.0017	590.6667	762.98	450666.7	760.83
24168	224	1359	2.6	9.4	1784	580032	1777	1776	0.0015	683.0769	765.203	522692.3	764.6

Table G-6 Model 2 Type 2h Fracture Simulation Output and Calculations

model Type2h					
28 by 28	phimatrix 0.11	2Xe/L 8.5	ooip 3.373
	w 0.007		(mmbo)
	kmatrix 10.1	Soi 0.75	
	kfracture 4000		

delta t	cum oil			days/days		hours	
days	mbo	dq/q	dp/p	(tp+dt)/dt	sqrt dt	sqrt dt	1/q'
6	14840	0	0.086957	2.389513	2.4494897	12	0.000561798
8	18270	0.06205	0.104972	2.362619	2.8284271	13.85640646	0.000596659
10	21520	0.1049	0.122334	2.335816	3.1622777	15.49193338	0.000620732
12	24770	0.10903	0.138952	2.286085	3.4641016	16.97056275	0.000623053
14	27910	0.14987	0.154068	2.287637	3.7416574	18.33030278	0.000645995
16	30970	0.17803	0.168907	2.281023	4	19.59591794	0.000661813
18	33940	0.19143	0.182732	2.262085	4.2426407	20.78460969	0.000669344
20	36880	0.22505	0.195457	2.269098	4.472136	21.9089023	0.000688231
22	39670	0.29643	0.207729	2.313315	4.6904158	22.97825059	0.000728332
24	42440	0.29455	0.219512	2.286061	4.8989795	24	0.000727273
26	45160	0.3244	0.230012	2.292353	5.0990195	24.97999199	0.000744048
31	51200	0.42857	0.254705	2.325532	5.5677644	27.27636339	0.000802568
62	86030	0.76938	0.315789	2.379305	7.8740079	38.57460304	0.000984036
123	142400	1.01814	0.372684	2.312612	11.090537	54.33231083	0.001133787
214	216000	1.37017	0.431639	2.344002	14.628739	71.66589147	0.001331558
395	339800	1.77259	0.526718	2.339958	19.874607	97.36529156	0.001557632
576	444200	2.2963	0.610306	2.428112	24	117.5755077	0.001851852
942	612100	3.6114	0.766784	2.683388	30.692019	150.358569	0.002590674
1308	736900	4.91362	0.923077	2.871692	36.166283	177.1778767	0.003322259
2304	959600	9.47059	1.378121	3.449959	48	235.1510153	0.005882353
3400	1099000	18.7778	2.025719	4.591503	58.309519	285.6571371	0.011111111
5996	1230000	62.5714	4.11509	8.326313	77.433843	379.346807	0.035714286
8592	1277000	143.715	5.734007	13.08347	92.693042	454.1013103	0.081300813
11188	1302000	233.211	6.633588	16.31246	105.77334	518.1814354	0.131578947
13784	1319000	311.281	7.064516	17.78783	117.40528	575.166063	0.175438596
16380	1332000	385.957	7.333333	18.67797	127.98437	626.9928229	0.217391304
18976	1343000	480.081	7.583691	20.128	137.7534	674.8510947	0.27027027
21572	1352000	592.333	7.77193	21.89128	146.8741	719.533182	0.333333333
24168	1359000	683.615	7.928571	22.62745	155.46061	761.5983193	0.384615385

Table G-6 Model 2 Type 2h Fracture Simulation Output and Calculations - Continued

delta t	cum oil	the pressure decline can be compared with actual pressures as a function of time									
days	mbo	1/q"t	1/q'	q' (deriv)	q'alt	t*Q'	t*Q'alt	p'	p' alt	t*p'	t*p'alt
6	14840										
8	18270	0.0002	2.37E-05	42250	42250	338000	338000	15	15	116	116
10	21520	0.0006	5.63E-05	17750	17750	177500	177500	14	14	135	135
12	24770	0.0008	6.35E-05	15750	15750	189000	189000	12	12	147	147
14	27910	0.0006	4.26E-05	23500	23500	329000	329000	11	11	158	158
16	30970	0.0012	7.41E-05	13500	13500	216000	216000	11	11	168	168
18	33940	0.0012	6.9E-05	14500	14500	261000	261000	10	10	171	171
20	36880	0.0007	3.31E-05	30250	30250	605000	605000	9	9	175	175
22	39670	0.0011	5.13E-05	19500	19500	429000	429000	8	8	182	182
24	42440	0.0033	0.000138	7250	7250	174000	174000	8	8	180	180
26	45160	0.0016	6E-05	18429	16671	479143	433457	6.571429	6.82857	170.8571	177.54
31	51200	0.0017	5.57E-05	9388.9	17953	291056	556544	2.944444	5.84265	91.27778	181.12
62	86030	0.0107	0.000172	3956.5	5818	245304	360728	1.48913	1.93075	92.32609	119.71
123	142400	0.0685	0.000557	1677.6	1795	206349	220750	0.809211	0.88292	99.53289	108.6
214	216000	0.1846	0.000863	882.35	1159	188824	248115	0.540441	0.59956	115.6544	128.31
395	339800	0.6777	0.001716	582.87	582.9	230235	230235	0.428177	0.42818	169.1298	169.13
576	444200	1.1156	0.001937	468.01	516.3	269572	297385	0.325411	0.35083	187.4369	202.08
942	612100	2.8851	0.003063	326.5	326.5	307566	307566	0.275956	0.27596	259.9508	259.95
1308	736900	6.375	0.004874	158.59	205.2	207436	268371	0.213656	0.23751	279.4626	310.66
2304	959600	22.227	0.009647	100.86	103.7	232382	238829	0.181166	0.18287	417.4073	421.32
3400	1E+06	58.205	0.017119	38.462	58.41	130769	198608	0.121885	0.14635	414.4095	497.61
5996	1E+06	400.66	0.066821	14.965	14.97	89732	89732	0.070108	0.07011	420.3667	420.37
8592	1E+06	2186.7	0.25451	3.9291	3.929	33759	33759	0.024846	0.02485	213.4761	213.48
11188	1E+06	8801.2	0.786667	1.2712	1.271	14222	14222	0.009438	0.00944	105.5878	105.59
13784	1E+06	23856	1.730667	0.5778	0.578	7964.6	7964.6	0.004237	0.00424	58.40678	58.407
16380	1E+06	42522	2.596	0.3852	0.385	6309.7	6309.7	0.002889	0.00289	47.3228	47.323
18976	1E+06	61577	3.245	0.3082	0.308	5847.8	5847.8	0.002311	0.00231	43.85824	43.858
21572	1E+06	101820	4.72	0.2119	0.212	4570.3	4570.3	0.001733	0.00173	37.39368	37.394

Table G-6 Model 2 Type 2h Fracture Simulation Output and Calculations - Continued

delta t				2 smooths	
days	Q' smooth	Q'smooth	Q"	Q" smooth	Q"*t
6					
8	-1670	1670			
10	-1625	1625	18125	18125	181250
12	-1598	1598	18750	18750	225000
14	-1550	1550	22500	22500	315000
16	-1508	1508	18125	18125	290000
18	-1478	1478	18750	18750	337500
20	-1433	1433	21875	21875	437500
22	-1390	1390	15000	15000	330000
24	-1373	1373	18357	18357	440571.43
26	-1317	1317	25176	26849	654566.31
31	-1196	1196	7229	21345	224086.11
62	-1056	1056	3461	3879	214605.47
123	-878	878	1903	2241	234111.55
214	-767	767	910	1063	194674.73
395	-630	630	633	633	250204.44
576	-538	538	421	467	242744.88
942	-400	400	312	312	293788.25
1308	-309	309	163	216	213358.79
2304	-178	178	98	101	225802.89
3400	-104	104	39	55	132070.19
5996	-34	34	17	17	104566.34
8592	-14	14	5	5	43347.475
11188	-8	8	2	2	17431.404
13784	-6	6	1	1	9204.038
16380	-5	5	0	0	
18976	-4	4	1	1	
21572					

Table G-6 Model 2 Type 2h Fracture Simulation Output and Calculations - Continued

model Type3

28 by 28	phimatrix 0.11	2Xe/L 8.5	ooip 3.373	
	w 0.007		(mmbo)	
	kmatrix 0.1	Soi 0.75		
	kfracture 1000			

delta t days	average pressure	delta q cum oil mbo	oil rate bopd	gas rate mcf/d	cum gas mmcf	dt hours	dq	dp	q/dp	dp/q	q cum/dp	tp(days) q cum/q	qcum/dq
6	1935	7.57	365	592	7.922	144		65	5.6154	0.178082	116.462	20.73973	
8	1931	8.242	322	420	8.843	192	43	69	4.6667	0.214286	119.449	25.59627	191.67
10	1928	8.866	278	351	9.5	240	87	72	3.8611	0.258993	123.139	31.89209	101.91
14	1923	10.01	264	239	10.53	336	101	77	3.4286	0.291667	130	37.91667	99.109
16	1921	10.53	254	219	10.96	384	111	79	3.2152	0.311024	133.291	41.45669	94.865
18	1919	11.05	232	254	11.34	432	133	81	2.8642	0.349138	136.42	47.62931	83.083
20	1916	11.53	238	194	11.72	480	127	84	2.8333	0.352941	137.262	48.44538	90.787
22	1915	12	218	202	12.07	528	147	85	2.5647	0.389908	141.176	55.04587	81.633
24	1913	12.48	225	166	12.35	576	140	87	2.5862	0.386667	143.448	55.46667	89.143
26	1911	12.94	213	183	12.64	624	152	89	2.3933	0.41784	145.393	60.75117	85.132
31	1906	13.63	209	145	12.76	744	156	94	2.2234	0.449761	147.128	66.17225	88.654
62	1885	19.45	168	96	17.4	1488	197	115	1.4609	0.684524	169.13	115.7738	98.731
123	1854	28.68	146	71	22.54	2952	219	146	1	1	196.438	196.4384	130.96
214	1820	40.41	121	65	28.75	5136	244	180	0.6722	1.487603	224.5	333.9669	165.61
395	1769	59.03	88	56	39.41	9480	277	231	0.381	2.625	255.541	670.7955	213.1
576	1729	73.47	70	49	48.98	13824	295	271	0.2583	3.871429	271.107	1049.571	249.05
942	1666	96.83	54	41	63.07	22608	311	334	0.1617	6.185185	289.91	1793.148	311.35
1308	1617	116.3	51	31	74.13	31392	314	383	0.1332	7.509804	303.655	2280.392	370.38
2304	1527	155.3	38	25	103.6	55296	327	473	0.0803	12.44737	328.33	4086.842	474.92
3400	1469	190	30	17	124.1	81600	335	531	0.0565	17.7	357.815	6333.333	567.16
5996	1381	254.3	20	16	170.6	143904	345	619	0.0323	30.95	410.824	12715	737.1
8592	1329	302.8	18.6	9.8	202.8	206208	346.4	671	0.0277	36.07527	451.267	16279.57	874.13
11188	1289	347.8	15.3	13.3	232.4	268512	349.7	711	0.0215	46.47059	489.17	22732.03	994.57
13784	1252	382.7	12.6	8.6	262.3	330816	352.4	748	0.0168	59.36508	511.631	30373.02	1086
16380	1222	413.9	11.7	8.7	286.3	393120	353.3	778	0.015	66.49573	532.005	35376.07	1171.5
18976	1196	444.5	11.8	8.8	307.5	455424	353.2	804	0.0147	68.13559	552.861	37669.49	1258.5
21572	1169	473.1	10	9.1	330.5	517728	355	831	0.012	83.1	569.314	47310	1332.7
24168	1145	497.3	8.9	8.1	352.2	580032	356.1	856	0.0104	96.06742	581.637	56876.4	1396.5

Table G-7 Model 3 Type 3 Fracture Simulation Output and Calculations

model Type3

28 by 28 | phimatrix 0.11 | 2Xe/L 8.5 | ooip 3.373 (mmbo)

w 0.007

kmatrix 0.1 | Soi 0.75

kfracture 1000

delta t days	cum oil mbo	dq/q	dp/p	days/days (tp+dt)/dt	sqrt dt	hours sqrt dt	d(dq/q)dt
6	7570	0	0.033592	4.456621	2.4494897	12	
8	8242	0.13354	0.035733	4.199534	2.8284271	13.85640646	
10	8866	0.31295	0.037344	4.189209	3.1622777	15.49193338	0.041505897
14	10010	0.38258	0.040042	3.708333	3.7416574	18.33030278	0.020676372
16	10530	0.43701	0.041124	3.591043	4	19.59591794	0.047675026
18	11050	0.57328	0.042209	3.646073	4.2426407	20.78460969	0.024151393
20	11530	0.53361	0.043841	3.422269	4.472136	21.9089023	0.025259016
22	12000	0.67431	0.044386	3.502085	4.6904158	22.97825059	0.022152194
24	12480	0.62222	0.045478	3.311111	4.8989795	24	0.009825774
26	12940	0.71362	0.046572	3.336584	5.0990195	24.97999199	0.017741323
31	13830	0.74641	0.049318	3.134589	5.5677644	27.27636339	0.012750112
62	19450	1.17262	0.061006	2.86732	7.8740079	38.57460304	0.00819118
123	28680	1.5	0.078749	2.59706	11.090537	54.33231083	0.005552039
214	40410	2.01653	0.098901	2.560593	14.628739	71.66589147	0.006057821
395	59030	3.14773	0.130582	2.698216	19.874607	97.36529156	0.006071151
576	73470	4.21429	0.156738	2.822173	24	117.5755077	0.004774282
942	96830	5.75926	0.20048	2.903554	30.692019	150.359569	0.002653794
1308	116300	6.15686	0.236858	2.743419	36.166283	177.1778767	0.002089577
2304	155300	8.60526	0.309758	2.773803	48	235.1510153	0.002394744
3400	190000	11.1667	0.36147	2.862745	58.309519	285.6571371	0.002341478
5996	254300	17.25	0.448226	3.12058	77.433843	379.346807	0.001436246
8592	302800	18.6237	0.504891	2.894736	92.693042	454.1013103	0.001079778
11188	347800	22.8562	0.55159	3.031822	105.77334	518.1814354	0.001799807
13784	382700	27.9683	0.597444	3.203498	117.40528	575.166063	0.001413785
16380	413900	30.1966	0.636661	3.159711	127.98437	626.9928229	0.000378265
18976	444500	29.9322	0.672241	2.985112	137.7534	674.8510947	0.00102146
21572	473100	36.5	0.710864	3.193121	146.8741	719.533182	0.001941262
24168	497300	40.0112	0.746725	3.312	155.46061	761.5983193	

Table G-7 Model 3 Type 3 Fracture Simulation Output and Calculations - Continued

delta t	cum oil	the pressure decline can be compared with actual pressures as a function of time									
days	mbo	1/q'*t	1/q'	q' (deriv)	q'alt	t*Q'	t*Q'alt	p'	p' alt	t*p'	t*p'alt
6	7570										
8	8242	0.0004	4.6E-05	21750	21750	174000	174000	2	2	14	14
10	8866	0.001	0.000103	9667	15833	96667	158333	1	1	13	14
14	10010	0.0035	0.00025	4000	4500	56000	63000	1	1	16	15
16	10530	0.002	0.000125	8000	8000	128000	128000	1	1	16	16
18	11050	0.0045	0.00025	4000	4000	72000	72000	1	1	23	23
20	11530	0.0057	0.000286	3500	3500	70000	70000	1	1	20	20
22	12000	0.0068	0.000308	3250	3250	71500	71500	1	1	17	17
24	12480	0.0192	0.0008	1250	1250	30000	30000	1	1	24	24
26	12940	0.0114	0.000438	2285.7	4514	59429	117371	1	1	26	26
31	13830	0.0248	0.0008	1250	872.6	38750	27050	0.722222	0.9552	22.38889	29.611
62	19450	0.0905	0.00146	684.78	998.5	42457	61904	0.565217	0.6204	35.04348	38.465
123	28680	0.3978	0.003234	309.21	326.2	38033	40119	0.427632	0.45419	52.59868	55.866
214	40410	1.0036	0.00469	213.24	243.8	45632	52175	0.3125	0.34289	66.875	73.379
395	59030	2.8037	0.007098	140.88	140.9	55649	55649	0.251381	0.25138	99.29558	99.296
576	73470	9.2668	0.016088	62.157	81.01	35803	46660	0.1883	0.20483	108.4607	117.98
942	96830	36.292	0.038526	25.956	25.96	24451	24451	0.153005	0.15301	144.1311	144.13
1308	116300	111.34	0.085125	11.747	9.501	15366	12426	0.102056	0.12219	133.489	159.82
2304	155300	229.52	0.099619	10.038	10.31	23128	23762	0.070746	0.07254	162.9981	167.12
3400	190000	697.38	0.205111	4.8754	6.276	16576	21338	0.039545	0.04727	134.4529	160.73
5996	254300	2730.8	0.455439	2.1957	2.196	13165	13165	0.026965	0.02696	161.6795	161.66
8592	302800	9491.4	1.104681	0.9052	0.905	7777.8	7777.8	0.01772	0.01772	152.2465	152.25
11188	347800	9681.3	0.865333	1.1556	1.156	12929	12929	0.014831	0.01483	165.9237	165.92
13784	382700	19880	1.442222	0.6934	0.693	9557.5	9557.5	0.012904	0.0129	177.8752	177.88
16380	413900	106306	6.49	0.1541	0.154	2523.9	2523.9	0.010786	0.01079	176.6718	176.67
18976	444500	57965	3.054118	0.3274	0.327	6213.3	6213.3	0.010208	0.01021	193.7072	193.71
21572	473100	38621	1.790345	0.5586	0.559	12049	12049	0.009823	0.00982	211.8975	211.9

Table G-7 Model 3 Type 3 Fracture Simulation Output and Calculations - Continued

delta t				2 smooths	
days	Q' smooth	Q'smooth	Q"	Q" smooth	Q"*t
6					
8	-324	324			
10	-303	303	9222	9778	92222.222
14	-269	269	7222	5778	101111.11
16	-260	260	4667	4667	74666.667
18	-250	250	5625	5625	101250
20	-238	238	3125	3125	62500
22	-238	238	625	625	13750
24	-235	235	5589	5589	134142.86
26	-215	215	8078	9188	210016.9
31	-178	178	1221	6351	37849.366
62	-171	171	393	315	24354.646
123	-142	142	335	381	41266.184
214	-120	120	187	215	40118.604
395	-91	91	126	126	49658.61
576	-74	74	60	77	34554.775
942	-59	59	34	34	32270.07
1308	-49	49	17	22	22014.316
2304	-36	36	9	10	21816.532
3400	-30	30	4	5	12765.686
5996	-22	22	2	2	13403.52
8592	-18	18	1	1	10486.264
11188	-15	15	1	1	11371.916
13784	-13	13	1	1	9255.1715
16380	-12	12	0	0	4192.6984
18976	-11	11	0	0	6335.455
21572	-10	10	2	2	47374.294

Table G-7 Model 3 Type 3 Fracture Simulation Output and Calculations - Continued

model Type 3h					
28 by 28	phimatrix	0.11	2Xe/L 8.5		ooip 3.373
	w	0.007			(mmbo)
	kmatrix	0.1	Soi 0.75		
	kfracture	4000			

delta t days	average pressure	delta q cum oil mbo	oil rate bopd	gas rate mcf/d	cum gas mmcf	dt hours	dq	dp	q/dp	dp/q	q cum/dp	tp(days) q cum/q	qcum/dq
6	1934	7 897	378	734	8 043	144		56	5.7273	0.174603	119 652	20.89153	
8	1930	8.659	365	470	9.059	192	13	70	5.2143	0.191781	123.7	23.72329	666.08
10	1927	9.393	303	453	9.8	240	75	73	4.1507	0.240924	128.671	31	125.24
14	1921	10.81	303	273	10.9	336	75	79	3.8354	0.260726	136 835	35.67657	144 13
16	1918	11.41	297	258	11 42	384	81	82	3.622	0.276094	139 146	38.41751	140.86
18	1916	11.99	288	251	11.92	432	90	84	3.4286	0.291667	142.738	41 63194	133.22
20	1914	12.6	284	232	12.36	480	94	86	3.3023	0.302817	146.512	44.3662	134.04
22	1912	13.17	279	221	12.79	528	99	88	3.1705	0.315412	149 659	47.2043	133 03
24	1910	13 72	278	209	13.22	576	100	90	3.0889	0 323741	152 444	49.35252	137 2
26	1908	14.29	282	182	13.6	624	96	92	3.0652	0.326241	155.326	50.67376	148.85
31	1903	15.5	256	188	14 68	744	122	97	2.6392	0.378906	159.794	60.54688	127 05
62	1881	22.64	205	141	19.39	1488	173	119	1 7227	0.580488	190.252	110.439	130.87
123	1850	33 56	148	114	26.39	2952	230	150	0.9867	1 013514	223.733	226.7568	145.91
214	1815	46.5	128	78	33.38	5136	250	185	0.6919	1 445313	251.351	363.2813	186
395	1761	64.74	81	65	47 82	9480	297	239	0.3389	2.950617	270 879	799.2593	217 98
576	1721	79.04	77	43	56.48	13824	301	279	0.276	3.623377	283.297	1026.494	262.59
942	1658	103.7	59	34	69 62	22608	319	342	0.1725	5.79661	303.216	1757 627	325.08
1308	1608	123.4	44	45	84 12	31392	334	392	0.1122	8.909091	314.796	2804.545	369.46
2304	1519	160.8	34	21	113.6	55296	344	481	0.0707	14.14706	334.304	4729.412	467 44
3400	1462	196.8	26	29	133.9	81600	352	538	0.0483	20.69231	365 799	7569.231	559.09
5996	1372	259	20	15	183.1	143904	358	628	0.0318	31.4	412.42	12950	723.46
8592	1322	309	18.4	11 9	214.3	206208	359 6	678	0.0271	36.84783	455.752	16793.48	859.29
11188	1279	353.2	14.5	13	248.1	268512	363.5	721	0.0201	49.72414	489.875	24358.62	971 66
13784	1243	387	12.4	10.2	277 5	330816	365.6	757	0.0164	61 04839	511.229	31209.68	1058.5
16380	1213	418.3	12 1	8.3	299.9	393120	365.9	787	0.0154	65.04132	531.512	34570.25	1143.2
18976	1186	449.9	10.8	11.1	322	455424	367.2	814	0.0133	75.37037	552.703	41657 41	1225.2
21572	1160	477 1	10.3	7 6	345.4	517728	367.7	840	0.0123	81.5534	567 976	46320.39	1297 5
24168	1137	500.9	8.6	7 4	366.2	580032	369.4	863	0.01	100.3488	580.417	58244.19	1356

Table G-8 Model 3 Type 3h Fracture Simulation Output and Calculations

model Type 3h			
28 by 28	phimatrix 0.11	2Xe/L 8.5	ooip 3.373
	w 0.007		(mmbo)
	kmatrix 0.1	Soi 0.75	
	kfracture 4000		

delta t days	cum oil mbo	dq/q	dp/p	days/days (tp+dt)/dt	sqrt dt	hours sqrt dt	1/q
6	7897	0	0.034126	4.481922	2.4494897	12	0.002645503
8	8659	0.03562	0.036269	3.965411	2.8284271	13.85640646	0.002739726
10	9393	0.24752	0.037883	4.1	3.1622777	15.49193338	0.00330033
14	10610	0.24752	0.041124	3.548326	3.7416574	18.33030278	0.00330033
16	11410	0.27273	0.042753	3.401094	4	19.59591794	0.003367003
18	11990	0.3125	0.043841	3.312886	4.2426407	20.78460969	0.003472222
20	12600	0.33099	0.044932	3.21831	4.472136	21.9089023	0.003521127
22	13170	0.35484	0.046025	3.14565	4.6904158	22.97825059	0.003584229
24	13720	0.35971	0.04712	3.056355	4.8989795	24	0.003597122
26	14290	0.34043	0.048218	2.948991	5.0990195	24.97999199	0.003546099
31	15500	0.47656	0.050972	2.953125	5.5677644	27.27636339	0.00390625
62	22640	0.8439	0.063264	2.781275	7.8740079	38.57460304	0.004878049
123	33560	1.55405	0.081081	2.843551	11.090537	54.33231083	0.006756757
214	46500	1.95313	0.101928	2.697576	14.628739	71.66589147	0.0078125
395	64740	3.66667	0.135718	3.023441	19.874607	97.36529156	0.012345679
576	79040	3.90909	0.162115	2.782107	24	117.5755077	0.012987013
942	103700	5.40678	0.206273	2.865846	30.692019	150.359569	0.016949153
1308	123400	7.59091	0.243781	3.144148	36.166283	177.1778767	0.022727273
2304	160800	10.1176	0.316656	3.052696	48	235.1510153	0.029411765
3400	196800	13.5385	0.367989	3.226244	58.309519	285.6571371	0.038461538
5996	259000	17.9	0.457726	3.159773	77.433843	379.346807	0.05
8592	309000	19.5435	0.512859	2.954548	92.693042	454.1013103	0.054347826
11188	353200	25.069	0.563722	3.17721	105.77334	518.1814354	0.068965517
13784	387000	29.4839	0.60901	3.264196	117.40528	575.166063	0.080645161
16380	418300	30.2397	0.648805	3.110516	127.98437	626.9928229	0.082644628
18976	449900	34	0.686341	3.195268	137.7534	674.8510947	0.092592593
21572	477100	35.099	0.724138	3.147246	146.8741	719.533182	0.097087379
24168	500900	42.9535	0.759015	3.409971	155.46061	761.5963193	0.11627907

Table G-8 Model 3 Type 3h Fracture Simulation Output and Calculations - Continued

delta t	cum oil	the pressure decline can be compared with actual pressures as a function of time									
days	mbo	1/q'*t	1/q'	q' (deriv)	q'alt	t*Q'	t*Q'alt	p'	p' alt	t*p'	t*p'alt
6	7897										
8	8659	0.0004	5.33E-05	18750	18750	150000	150000	2	2	14	14
10	9383	0.0005	4.84E-05	10333	20667	103333	206667	2	2	15	15
14	10610	0.007	0.0005	1000	2000	14000	28000	2	2	21	21
16	11410	0.0043	0.000267	3750	3750	60000	60000	1	1	20	20
18	11990	0.0055	0.000308	3250	3250	58500	58500	1	1	18	18
20	12600	0.0089	0.000444	2250	2250	45000	45000	1	1	20	20
22	13170	0.0147	0.000667	1500	1500	33000	33000	1	1	22	22
24	13720	-0.032	-0.00133	-750	-750	-18000	-18000	1	1	24	24
26	14290	0.455	0.0175	3142.9	57.14	81714	1485.7	1	1	26	26
31	15500	0.0066	0.000212	2138.9	4706	66306	145894	0.75	0.95968	23.25	29.75
62	22640	0.0441	0.000711	1173.9	1406	72783	87152	0.576087	0.64179	35.71739	39.791
123	33580	0.1899	0.001544	506.58	647.6	62309	79658	0.434211	0.4586	53.40789	56.408
214	46500	0.918	0.00429	246.32	233.1	52713	49889	0.327206	0.35575	70.02206	76.131
395	64740	2.8037	0.007098	140.88	140.9	55649	55649	0.259669	0.25967	102.5691	102.57
576	79040	18.545	0.032195	40.219	31.06	23166	17891	0.1883	0.20483	108.4607	117.98
942	103700	20.895	0.022182	45.082	45.08	42467	42467	0.154372	0.15437	145.418	145.42
1306	123400	40.039	0.030611	18.355	32.67	24009	42730	0.102056	0.12391	133.489	162.08
2304	160800	263.76	0.114479	8.6042	8.735	19824	20126	0.06979	0.07158	160.7954	164.91
3400	196800	584.34	0.171665	3.792	5.819	12893	19783	0.039816	0.04686	135.3738	159.32
5996	259000	4096.2	0.683158	1.4638	1.464	8776.9	8776.9	0.026965	0.02696	161.6795	161.68
8592	309000	8110.8	0.944	1.0593	1.059	9101.7	9101.7	0.017912	0.01791	153.9014	153.9
11188	353200	9681.3	0.865333	1.1556	1.156	12929	12929	0.015216	0.01522	170.2334	170.23
13784	387000	29819	2.163333	0.4622	0.462	6371.6	6371.6	0.012712	0.01271	175.2203	175.22
16380	418300	53153	3.245	0.3082	0.308	5047.8	5047.8	0.010978	0.01098	179.8267	179.83
18976	449900	54735	2.884444	0.3467	0.347	6578.7	6578.7	0.010208	0.01021	193.7072	193.71
21572	477100	50910	2.36	0.4237	0.424	9140.7	9140.7	0.009438	0.00944	203.5878	203.59

Table G-8 Model 3 Type 3b Fracture Simulation Output and Calculations - Continued

delta t				2 smooths
days	Q' smooth	Q'smooth	Q"	Q" smooth
6				
8	-374	374		
10	-363	363	9319	7472
14	-318	318	11292	11417
16	-295	295	5146	5146
18	-298	298	0	0
20	-295	295	4375	4375
22	-280	280	3750	3750
24	-280	280	1821	1821
26	-273	273	5860	4450
31	-240	240	1658	5682
62	-213	213	828	854
123	-164	164	557	637
214	-128	128	273	334
396	-90	90	147	147
578	-75	75	54	68
942	-61	61	35	35
1308	-49	49	19	26
2304	-35	35	9	10
3400	-30	30	4	4
5996	-22	22	2	2
8592	-18	18	1	1
11188	-15	15	1	1
13784	-13	13	1	1
16380	-12	12	0	0
18976	-11	11	0	0
21572	-10	10	2	2

Table G-8 Model 3 Type 3h Fracture Simulation Output and Calculations - Continued

model Type4h													
28 by 28		phimatrix 0.11		2Xe/L 8.5		ooip 3.373							
		w 0.007				(mmbo)							
		kmatrix 10.1		Soi 0.75									
		kfracture 4000											
		k partitions											

delta t days	average pressure	delta q cum oil mbo	oil rate bopd	gas rate mcf/d	cum gas mmcf	dt hours	dq	dp	q/dp	dp/q	q cum/dp	tp(days) q cum/q	qcum/dq
6	1842	14.78	1773	1141	10.2	144		158	11.222	0.089114	93.5443	8.336153	
8	1812	16.19	1666	1223	12.68	192	107	188	8.8617	0.112845	96.7553	10.91837	170
10	1784	21.41	1586	1185	15.06	240	187	216	7.3426	0.136192	99.1204	13.49937	114.49
12	1759	24.66	1607	1036	17.08	288	166	241	6.668	0.149969	102.324	15.34536	148.55
14	1735	27.76	1513	1091	19.2	336	260	265	5.7094	0.175149	104.755	18.34765	106.77
16	1713	30.77	1513	868	21.19	384	260	287	5.2718	0.189689	107.213	20.33708	118.35
18	1693	33.79	1496	908	22.92	432	277	307	4.873	0.205214	110.065	22.5869	121.99
20	1675	36.73	1453	921	24.69	480	320	325	4.4708	0.223675	113.015	25.27873	114.78
22	1658	39.53	1410	677	26.49	528	363	342	4.1228	0.242553	115.585	28.03546	108.9
24	1642	42.28	1411	591	28.06	576	362	358	3.9413	0.253721	118.101	29.96456	116.8
26	1629	45.07	1392	666	29.24	624	381	371	3.752	0.266523	121.482	32.37787	118.29
31	1597	51.35	1245	803	34.01	744	528	403	3.0893	0.323695	127.419	41.24498	97.254
62	1521	86.02	1007	604	54.07	1488	766	479	2.1023	0.47567	179.582	85.42205	112.3
123	1458	142	867	458	85.98	2952	906	542	1.5996	0.625144	261.993	163.7832	156.73
214	1398	215.1	758	360	123.5	5136	1015	602	1.2591	0.794195	357.309	283.7731	211.92
386	1312	337.9	610	330	185	9480	1163	688	0.8866	1.127869	491.134	553.9344	290.54
576	1244	440.9	536	283	236.9	13824	1237	756	0.709	1.410448	583.201	822.5746	356.43
942	1135	606.2	388	280	333	22608	1385	865	0.4486	2.229381	700.809	1562.371	437.69
1308	1045	730.9	300	271	427.5	31392	1473	956	0.3141	3.183333	765.34	2436.333	496.2
2304	848	955.1	173	260	685.2	55296	1600	1152	0.1502	6.65896	829.08	5520.809	596.94
3400	689	1095	92	234	950.5	81600	1681	1331	0.0691	14.46739	822.69	11902.17	651.4
5996	396	1228	29	95	1346	143904	1744	1604	0.0181	55.31034	765.586	42344.83	704.13
8592	299	1277	12.6	43.6	1508	206208	1760	1701	0.0074	135	750.735	101349.2	725.4
11188	263	1302	7.6	26.6	1594	268512	1765	1737	0.0044	228.5526	749.568	171315.8	737.51
13784	249	1319	5.7	20.1	1653	330816	1767	1751	0.0033	307.193	753.284	231403.5	746.34
16380	241	1332	4.6	16.2	1700	393120	1768	1759	0.0026	382.3913	757.248	289565.2	753.22
18976	234	1343	3.7	13.4	1738	455424	1769	1766	0.0021	477.2973	760.476	362973	759.06
21572	228	1351	3	10.9	1770	517728	1770	1772	0.0017	590.6667	762.415	450333.3	763.28
24168	224	1358	2.6	9.4	1796	580032	1770	1776	0.0015	683.0769	764.64	522307.7	767.06

Table G-9 Model 4 Type 4h Fracture Simulation Output and Calculations

model Type4h						
28 by 28		phimatrix 0.11		2Xe/L 8.5		ooip 3.373
		w 0.007				(mmbo)
		kmatrix 10.1		Soi 0.75		
		kfracture 4000				
		k partitions				

delta t days	cum oil mbo	dq/q	dp/p	days/days (tp+dt)/dt	sqrt dt	hours sqrt dt
6	14780	0	0.085776	2.389359	2.4494897	12
8	18190	0.06423	0.103753	2.364798	2.8284271	13.85640646
10	21410	0.11791	0.121076	2.349937	3.1622777	15.49193338
12	24660	0.1033	0.13701	2.27878	3.4641016	16.97056275
14	27760	0.17184	0.152738	2.310547	3.7416574	18.33030278
16	30770	0.17184	0.167542	2.271067	4	19.59591794
18	33790	0.18516	0.181335	2.254828	4.2426407	20.78460969
20	36730	0.22023	0.19403	2.263937	4.472136	21.9089023
22	39530	0.25745	0.206273	2.274339	4.6904158	22.97825059
24	42280	0.25656	0.218027	2.248524	4.8989795	24
26	45070	0.27371	0.227747	2.245303	5.0990195	24.97999199
31	51350	0.4241	0.252348	2.330483	5.5677644	27.27636339
62	86020	0.76068	0.314924	2.377775	7.8740079	38.57460304
123	142000	1.04498	0.371742	2.33157	11.090537	54.33231083
214	215100	1.33905	0.430615	2.326042	14.628739	71.66589147
395	337900	1.90656	0.52439	2.402366	19.874607	97.36529156
576	440900	2.30784	0.607717	2.428081	24	117.5755077
942	606200	3.56959	0.762115	2.658568	30.692019	150.359569
1308	730900	4.91	0.913876	2.86264	36.166283	177.1778767
2304	955100	9.24855	1.358491	3.396185	48	235.1510153
3400	1095000	18.2717	1.989537	4.500639	58.309519	285.6571371
5996	1228000	60.1379	4.050505	8.062179	77.433843	379.346807
8592	1277000	139.714	5.688963	12.79576	92.693042	454.1013103
11188	1302000	232.289	6.604563	16.31246	105.77334	518.1814354
13784	1319000	310.053	7.032129	17.78783	117.40628	575.166063
16380	1332000	384.435	7.298755	18.67797	127.98437	626.9928229
18976	1343000	478.189	7.547009	20.128	137.7534	674.8510947
21572	1351000	590	7.77193	21.87583	146.8741	719.533182
24168	1358000	680.923	7.928571	22.61154	155.46061	761.5983193

Table G-9 Model 4 Type 4h Fracture Simulation Output and Calculations - Continued

delta t	cum oil	the pressure decline can be compared with actual pressures as a function of time									
days	mbo	1/q"t	1/q'	q' (deriv)	q'alt	t*Q'	t*Q'alt	p'	p' alt	t*p'	t*p'alt
6	14780										
8	18190	0.0002	2.14E-05	46750	46750	374000	374000	15	15	116	116
10	21410	0.0007	6.78E-05	14750	14750	147500	147500	13	13	133	133
12	24660	0.0007	5.48E-05	18250	18250	219000	219000	12	12	147	147
14	27760	0.0006	4.26E-05	23500	23500	329000	329000	12	12	161	161
16	30770	0.0038	0.000235	4250	4250	68000	68000	11	11	168	168
18	33790	0.0012	6.67E-05	15000	15000	270000	270000	10	10	171	171
20	36730	0.0009	4.65E-05	21500	21500	430000	430000	9	9	175	175
22	39630	0.0021	9.52E-05	10500	10500	231000	231000	8	8	182	182
24	42280	0.0053	0.000222	4500	4500	108000	108000	7	7	174	174
26	45070	0.0017	6.59E-05	23714	15186	616571	394829	6.428571	6.47143	167.1429	168.26
31	51350	0.0012	3.79E-05	10694	26383	331528	817872	3	5.85161	93	181.4
62	86020	0.0106	0.000171	4108.7	5864	254739	363556	1.51087	1.97353	93.67391	122.36
123	142000	0.0663	0.000539	1638.2	1855	201493	228131	0.809211	0.88292	99.53289	108.6
214	215100	0.1999	0.000934	944.85	1071	202199	229115	0.536765	0.59771	114.8676	127.91
395	337900	0.6441	0.001631	613.26	613.3	242238	242238	0.425414	0.42541	168.0387	168.04
576	440900	1.414	0.002455	405.85	407.4	233770	234640	0.323583	0.34992	186.3839	201.55
942	606200	2.9218	0.003102	322.4	322.4	303705	303705	0.271858	0.27186	256.0902	256.09
1308	730900	6.2259	0.00476	157.86	210.1	206476	274799	0.21072	0.23297	275.6211	304.73
2304	955100	22.591	0.009805	99.426	102	229078	234982	0.179732	0.18138	414.1033	417.9
3400	1E+06	57.462	0.0169	39.003	59.17	132611	201178	0.122427	0.14606	416.2514	496.59
5996	1E+06	392.08	0.06539	15.293	15.29	91695	91695	0.071263	0.07126	427.2958	427.3
8592	1E+06	2084.6	0.242617	4.1217	4.122	35414	35414	0.025616	0.02562	220.0955	220.1
11188	1E+06	8418.6	0.752464	1.329	1.329	14868	14868	0.00963	0.00963	107.7427	107.74
13784	1E+06	23856	1.730667	0.5778	0.578	7964.6	7964.6	0.004237	0.00424	58.40678	58.407
16380	1E+06	42522	2.595	0.3852	0.385	6309.7	6309.7	0.002889	0.00289	47.3228	47.323
18976	1E+06	61577	3.245	0.3082	0.308	5847.8	5847.8	0.002504	0.0025	47.5131	47.513
21572	1E+06	101820	4.72	0.2119	0.212	4570.3	4570.3	0.001926	0.00193	41.54854	41.549

Table G-9 Model 4 Type 4h Fracture Simulation Output and Calculations - Continued

delta t days	Q' smooth	Q'smooth	Q"	2 smooths Q" smooth	Q"*t
6					
8	-1658	1658			
10	-1618	1618	17500	17500	175000
12	-1588	1588	22500	22500	270000
14	-1528	1528	20000	20000	280000
16	-1508	1508	9375	9375	150000
18	-1490	1490	18125	18125	326250
20	-1435	1435	25625	25625	512500
22	-1388	1388	12500	12500	275000
24	-1385	1385	8054	8064	193285.71
26	-1355	1355	21159	17378	550133.64
31	-1237	1237	8459	21225	262225.37
62	-1051	1051	3968	4969	246042.96
123	-872	872	1903	2243	234053.44
214	-762	762	912	1061	195144.55
395	-624	624	639	639	252410.06
576	-530	530	416	467	239647.64
942	-396	396	301	301	283839.44
1308	-310	310	160	208	208850.2
2304	-179	179	98	101	225423.39
3400	-105	105	39	55	132287.33
5996	-35	35	17	17	104756.05
8592	-14	14	5	5	44622.401
11188	-8	8	2	2	18261.471
13784	-6	6	1	1	9204.038
16380	-5	5	0	0	6684.0119
18976	-4	4	1	1	
21572					

Table G-9 Model 4 Type 4h Fracture Simulation Output and Calculations - Continued